Author:
Charlton, Rosemary Anne

Title:
An investigation into the effect of lateral hillslope inputs on floodplain hydraulic model predictions

AN INVESTIGATION INTO THE EFFECT OF LATERAL HILLSLOPE INPUTS ON FLOODPLAIN HYDRAULIC MODEL PREDICTIONS

Rosemary Anne Charlton

A thesis submitted to the University of Bristol in accordance with the requirements for the degree of Ph.D in the Faculty of Science

September 1995

SYNOPSIS

In recent years there has been a growing interest in the contemporary floodplain environment which has come from a number of fields including civil engineering, hydrology, geomorphology and ecology. A major advance in civil engineering has been the development of two-dimensional hydraulic models capable of a high degree of spatial representation. These models were originally developed for engineering applications although recent developments, such as their application to longer reach lengths, mean that these models are very powerful predictive tools with potential for application in many different fields. Two-dimensional floodplain hydraulic models can be viewed as a platform for further development through the incorporation of additional components to represent specific processes. For the case of the application of these models in hydrology, whilst the models provide a good representation of floodplain processes in a hydraulic context, catchment hydrology is essentially treated as a black box. The only input to the system is the upstream input hydrograph (occasionally rainfall over the floodplain surface and tributary inflows are included) and output only occurs at the downstream boundary. The floodplain is assumed to be impermeable and any input from the hillslopes bordering the reach is ignored.

This investigation examines the significance of contributions to the floodplain from the hillslopes bordering the reach. In order to do this, the zero flux boundary condition at the hillslope-floodplain interface is relaxed. A two-dimensional floodplain inundation model, RMA-2, is set up for a 14 km reach of the River Culm in Devon. A distributed hillslope hydrology model, VSAS3 is set up for a section of the hillslopes bordering the reach. This model is coupled to RMA-2 using a simple external coupling mechanism whereby water produced by VSAS3 is applied to elements along the edge of the RMA-2 finite element mesh. A sensitivity analysis is carried out using this coupled scheme to identify some of the range of hillslope environments which may contribute a significant volume of lateral inflow to the floodplain. Five key hillslope parameters are selected and altered over a range of values. It has been shown that hillslope inflows can have a significant effect on the predictions made by RMA-2, both in terms of changes to the predicted output hydrograph and localised changes in depth and inundation extent. It has also been shown that the timing of the hillslope inflow peak relative to the arrival of the floodwave from upstream is of great importance. The addition of inflows has also been found to affect the calibration of the floodplain inundation model.

ACKNOWLEDGEMENTS

I am obviously grateful to NERC for providing financial support to allow me to undertake this research.

Firstly I would like to thank Malcolm for all his supervision, support and encouragement particularly in the later stages of writing up.

I would also like to extend my gratitude to Ed Thomas for his help with computing, Paul Bates for guidance in familiarising myself with RMA-2, the principles of river hydraulics and hydraulic modelling and also to Tim Davie and Katie Fawcett, both of whom provided useful advice and support when setting up VSAS3. I am very grateful to Anne-Marie, Rich, Neil, Sal and Helen for helping with figure labelling, page numbering and printing at the end. Also in the department I would like to thank Sue, Fiona and Dom for helping me to keep things in perspective.

Rainfall data was provided by the NRA South Western Region.

The support of many friends has been invaluable, and I would particularly like to thank Ben as well as H, Paul, Tony, Vic, Elaine, Andy F., Andy B., Mark, Helen, Rob, Katherine and Phil for cheering me up when things weren't going well and for ensuring that I spent some enjoyable times away from work.

Finally and by no means least, I would like to thank my parents who have always been supportive and given me encouragement in everything I do.

This thesis is the original work of the candidate except where acknowledgement is given and has not been submitted for a higher degree in this or any other university.

SUMMARY CONTENTS

CONTENTS

Chapter Four: Modelling hillslope hydrology

Chapter Five: Coupling and running the models

Chapter Six: Analysing the results

Chapter Seven: The calibration issue

Chapter Eight: Conclusions

References

Appendices

LIST OF FIGURES

LIST OF TABLES

Chapter One

INTRODUCTION

1.1 INTRODUCTION: THE FLOODPLAIN ENVIRONMENT AND THE NEED FOR HYDRAULIC MODELS OF FLOODPLAIN PROCESSES

Despite the frequency of flooding, civilisation has always been located alongside rivers. Rivers have many uses and the floodplain provides a preferred site for human habitation due to the proximity of a fresh water supply, a possible source of power and fertile land for agriculture (Marriot, 1992). The floodplain is defined by Bhowmick and Demissie (1982) as a land area adjoining a river, stream, watercourse, bay or lake which is likely to be flooded during times of high water. Since the floodplain is basically a conveyance channel for flood water there are many hazards, both in terms of human and economic losses, associated with locating settlements on the floodplain. Floodplains are typically used to their fullest extent and hence the understanding of flood processes in sedimental, geomorphological and engineering terms is essential. As a result of this, a considerable quantity of research has been conducted by workers in a number of fields.

In engineering terms, the cost-benefit ratio is a major factor in the design of most flood alleviation works. This has led to a considerable amount of research by civil engineers into the hydraulics of flood channels. The importance of designing efficient flood alleviation schemes is indicated by the fact that an average of £73 million per annum has been spent on flood protection by water authorities in England and Wales over the past six years (Hollinrake, 1987). Interest in the contemporary floodplain environment has come from a number of other fields including geomorphology, hydrology and ecology, leading to an increasing demand for data for floodplain inundation events with a high spatial resolution. For example, in a geomorphological context, well-developed floodplains provide an important sink for suspended sediment during periods of inundation (Walling et al. 1986). The alluvium which forms the floodplain comes from two sources; overbank deposition which occurs at the time of flooding and from channel deposits. Several studies have been carried out to investigate long term patterns of sedimentation, which is a function of the climatic history, changes in base level and human activity, although little is understood about contemporary floodplain sediment dynamics. Walling et al (1986, 1992) report recent advances in techniques for

interpreting rates of floodplain deposition by examining the spatial distribution of Caesium-137 content in floodplain soils. In order to effectively interpret this data, detailed information is required on the depth and velocity distribution of flow over the floodplain surface. Demand for such data also arises from other areas, for example when assessing the timing and extent of inundation for flood prediction or the need for information on depths and flow field behaviour for determining habitat suitability indices. There are many practical difficulties in obtaining this data in the field due to the unpredictable occurrence of flood events, the extensive network of measuring sites required and the fact that measurements should be taken over a wide range of event magnitudes. In order to obtain an improved knowledge of flood processes, an increased understanding of the dynamic morphology of floodplain systems in the context of floodplain flow and sedimentation is required. This has been aided by the recent development of numerical algorithms which are capable of simulating hydraulic processes and has led to the development of numerical hydraulic models. Numeric models have been developed for a variety of different applications to increase understanding of floodplain hydraulics and to make predictions by solving the equations of unsteady fluid flow.

This chapter introduces the need for hydraulic models of floodplain inundation. Current understanding of the processes of overbank flow is outlined together with the equations of unsteady fluid flow, since various forms of these equations provide the basis for the numerical solution schemes used. A description of the various modelling strategies which have been developed to solve these equations is made before considering the problem that current state-of-the-art floodplain models consider the catchment hydrology as a black box. A parallel problem associated with catchment-scale hydrology models, where representation of the floodplain element is often simplified, is also discussed. Attention is then focused on the potential importance of contributions to the floodplain from the adjacent hillslopes, which is the subject of this research, in the context of the range of different hillslope-floodplain environments.

1.2 THE PHYSICAL PROCESSES OF OVERBANK FLOW

In order to model floodplain hydraulics an understanding is required of the processes of overbank flow. Current understanding of these processes is now summarised. The discussion in sections 1.2.1 and 1.2.2 was based on texts by Richards (1982), Knighton (1984), Shaw (1988), Bathurst (1993) and Beven and Wood (1993).

1.2.1 *Laminar and turbulent flow*

A number of theoretical models exist for open channel flow which involve simplifying assumptions concerning the spatial and temporal characteristics of the flow properties. Flow classifications can also be made at a more detailed level based on the energy, momentum, inertia and viscosity.

The spatial characteristics of flow can be defined by the pressure distribution, which in turn reflects the streamline pattern. When the flow is *uniform*, the depth is constant from section to section; the bed, water surface, energy grade line and all streamlines are parallel and the pressure distribution is everywhere hydrostatic. At any point, the pressure is dependent upon the depth beneath the free surface. *Gradually varied* flow occurs where the streamlines are not parallel because the channel cross section, depth and velocity vary along the length of the reach. The bed, surface and energy gradients are not necessarily equal and the divergence and convergence of flow lines causes acceleration and deceleration so the pressure distribution is not isostatic. For example, at a meander bend, the downward acting centrifugal force acting in conjunction with the gravitational force leads to pressures greater than hydrostatic. However, streamline curvature is sufficiently slow with distance along a reach that when a short channel reach is being considered, flow may be considered uniform. *Rapidly varied* flow involves hydraulic jumps and drops, the sudden changes in water level normally reflecting contractions and expansions of the cross sectional geometry. In natural rivers, flow is normally gradually varied.

When considering the temporal aspects of flow, a division can be made into *steady* and *unsteady* flow. *Steady* flow involves constant discharges and therefore constant depths and velocities through time at each section. For example:

$$Q = A1{+}v1 = A2{+}v2 = A3{+}v3 \qquad 1.1$$

Where:

A = cross sectional area

v = velocity

Unsteady flow is associated with a temporally changing discharge, depth and velocity for example during the passage of a flood wave. Since the water surface slope changes as a flood wave passes a section, uniform unsteady flow is impossible. Natural channels normally show unsteady, gradually varied flow.

At a more detailed level, *stream power* is defined as the rate of work done by water in overcoming bed and internal flow resistance and in transporting sediment. Since the momentum of flowing water is the product of its mass and velocity, the momentum per unit time of water passing a section can be defined as density x discharge. For a small volume of water within the main body of flow, the momentum is the product of the unit mass and velocity of that small body of water. Dividing by the width of flow gives:

$$\rho_W Q/w = \rho_W w\, dv/w = \rho_W dv \qquad 1.2$$

where:

ρ_W = the density of water

Q = discharge

w = section width

v = velocity

Water is a typical Newtonian viscous fluid; when it is subjected to stress, the rate of strain or deformation of the fluid increases linearly with the applied stress. The gradient of this curve is the dynamic viscosity (μ) which is the inertia of the flow per unit width per unit time. The dynamic viscosity measures the force per unit area (stress) required to maintain a unit difference of velocity (strain rate) between two parallel layers separated by a unit distance. The kinematic viscosity (v) is a measure of the interference between adjacent layers of fluid; $v = \mu/\rho_W$.

The state of flow can be determined by a dimensionless number, the Reynold's Number (Re). This distinguishes between laminar and turbulent flow on the basis of the ratio between the inertial and viscous forces.

$$\mathrm{Re} = \frac{\rho_w \upsilon L}{\mu} \qquad 1.3$$

Or:

$$\mathrm{Re} = \frac{\rho_w \upsilon R}{\mu} = \frac{\upsilon R}{\upsilon} \qquad 1.4$$

Where:

L = a "characteristic length" taken as the hydraulic radius (R) in *ii*) to give the Reynold's number of the total flow.

The numerator in equation 1.4 is the inertia per unit width per unit time.

In the case of laminar flow which has smooth, linear streamlines, the viscous forces are significant and Re is normally less than 500. When flow becomes turbulent, the inertial forces predominate and the value of Re exceeds 2000.

1.2.2 *Boundary layer theory and velocity distribution*

Water flowing in a channel is retarded by the resistance of the bed and banks. A very thin layer of water adjacent to the solid boundary is slowed to a stop. However the shear resistance between the adjacent fluid layers is less effective and this retardation is diminished away from the boundary. Fluid remote from the boundary has a greater momentum per unit volume ($\rho_w \upsilon$) than fluid close to the boundary although momentum transfer occurs from 'layers' of high momentum to those of low momentum. The amount of retardation caused by this momentum transfer reflects the degree of interference between the layers. During the occurrence of laminar flow, the layers glide over each other and momentum exchange occurs at a molecular level where molecules move between layers increasing the momentum of slower layers and decreasing that of faster layers.

The rate of momentum exchange is measured by the kinematic viscosity, v. The shear stress at any point is determined by the overlying water depth. It can be shown that the velocity profile in laminar flow is an approximate parabolic function of the distance from a solid boundary. When turbulent flow is considered, momentum exchange between layers is brought about by eddies which act over distances far beyond the molecular scale. Thus the high momentum of the upper flow can be transferred close to the bed resulting in a rapid increase in momentum above the bed. The opposite effect also occurs, where the low momentum of layers close to the bed is carried to the upper layers. This means that the rate of increase in momentum immediately below the water surface is less than that for laminar flow.

The shear stress at any point in the profile is:

$$\tau = (\upsilon + \varepsilon)\frac{d(\rho_w \upsilon)}{dy} \equiv \varepsilon \rho_w \frac{d\upsilon}{dy} \qquad 1.5$$

The molecular viscosity may be neglected since it is insignificant relative to the 'eddy viscosity' ε.

Analysis of the velocity profile in turbulent flow is complicated since the eddy viscosity is not constant but varies with distance from the boundary. The complete profile is composed of three elements:

1) The laminar sub-layer

2) The buffer zone

3) The main turbulent profile

The laminar sub-layer is the layer closest to the bed where viscous forces are the most significant in the same way as for laminar flow. This layer is thinner under conditions of high bed shear stress because the turbulence penetrates closer to the bed. The momentum transfer which occurs in turbulent flow is now considered in further detail, with particular reference to the exchange which takes place between the channel and floodplain during overbank flow.

1.2.3 Momentum transfer

There are four physical mechanisms by which linear momentum can be transported perpendicular to the direction of flow. These were ranked in order of their effectiveness by Wright and Carstens (1970).

i) Transverse circulation stresses (secondary currents)

ii) Eddies generated in the mixing zones of stream tubes of differing velocities

iii) Eddies generated by flow along a boundary

iv) Molecular motion

Erivine and Ellis (1987) identified the first two of these processes as important although did not account for the other two processes. It is not known which of the processes is dominant in two-stage channels. Baird and Anderson (1990) suggested that eddies generated by the mixing of differing velocity tubes must be greater in two-stage channels than in a single channel system because of the greater cross-sectional velocity gradient. In addition, they suggested that secondary flows in the main channel may be suppressed by the head of water when overbank flow occurs.

Figure 1.1 shows a representation of the processes of momentum exchange and shear stress distribution in a two-stage channel. From this it can be seen that the eddies generated by flow along a boundary are contained within the main channel and that the eddies generated by mixing zones are at the main channel/floodplain interface.

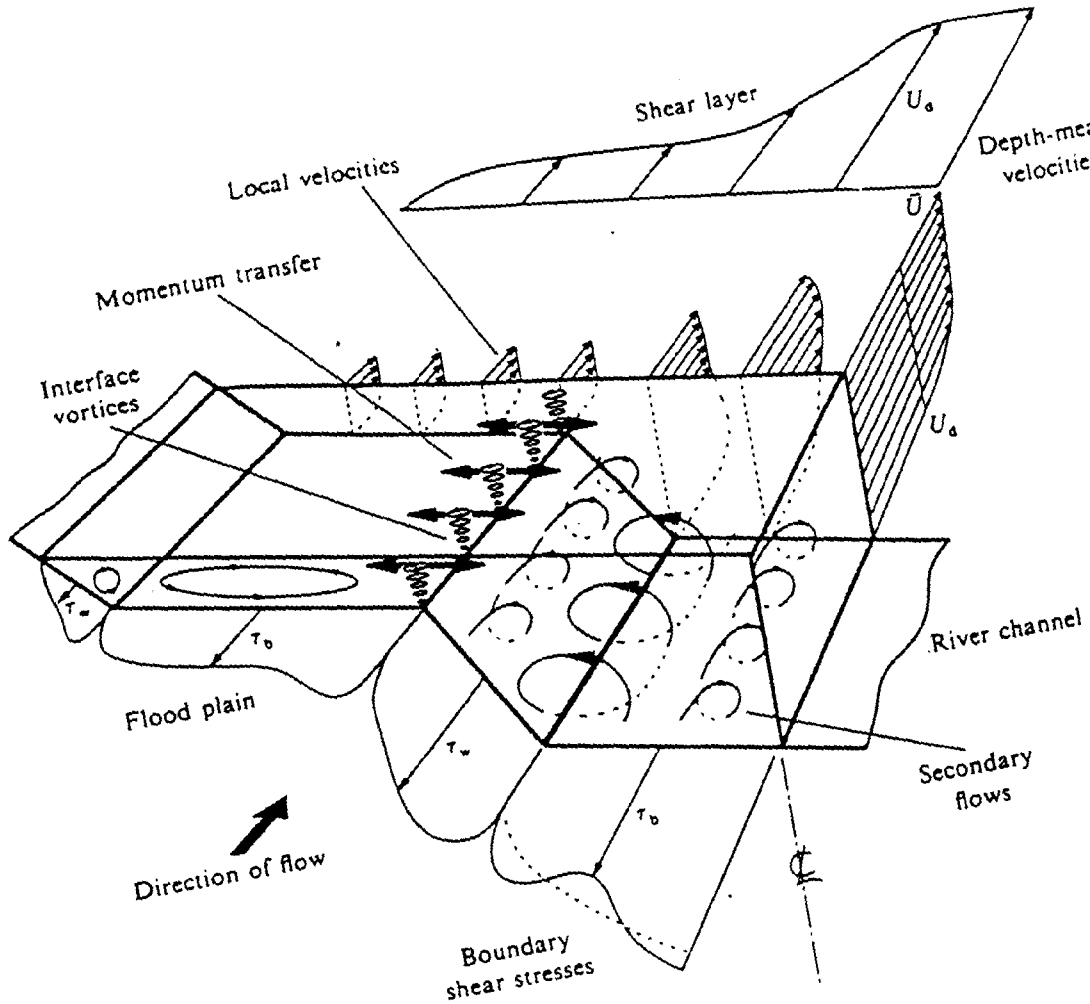

Figure 1.1: **Hydraulic aspects of overbank flow (after Knight, 1989)**

The processes of secondary currents and momentum exchange in a two-stage channel are now considered in more detail.

1.2.3.1 Secondary currents

Flow has a three-dimensional nature and is influenced by secondary flows. Secondary currents are generated in a meandering main channel when the centrifugal forces in a meander bend cause flow to be drawn to the outer bank of the main channel. This generates a cell orthogonal to the longitudinal flow. A second cell near the outer bank may also develop. Each cell returns flow along the bed towards the channel centre line where it meets the return flow from opposite corner. The direction of circulation within these secondary cells varies according to the relative position of the cells within a meander wavelength. Cells diverge at the surface in a riffle section and converge at the surface in a pool section (Keller and Melhorn, 1973). Figure 1.2 shows a generalised three-dimensional model of flow structure within successive meander bends at bankfull discharges. Einstein and Shen (1964) suggested that the secondary flow system is initiated by shear, possibly along a rough bank. Secondary flows are directed upwards at the centre line, normally away from the bed. Isovels are therefore more spaced out in this region and the local bed shear stress is reduced (Tracy, 1965; Naot and Rodi, 1982; Odgaard, 1984; Knight and Patel, 1985a). An important consequence of this three-dimensional flow is that, even in straight smooth prismatic channels, the classical logarithmic distribution laws of velocity with distance from the channel bed apply only close to the channel boundary and not over the whole cross-section. In rough channels this effect is diminished. The logarithmic law is hard to apply because information such as the bed datum is not known and it is difficult to measure these values over a short distance. Also, a straight filament of maximum velocity may no longer occur at the centreline of the channel free surface but will probably be depressed below the surface (Knight et al, 1984). Changes in plan form geometry may also enhance secondary flows and distort the isovel pattern further. These effects make the accurate prediction of velocity in natural channels very difficult. In terms of momentum exchange, secondary flows convect high momentum fluid in the direction of the channel walls to the edges of the channel.

1.2.3.2 Momentum exchange in two stage channels

When overbank flow occurs, there is an exchange of momentum between the faster moving water in the channel and the slower moving water on the floodplain. In two-stage channels the irregular cross-sectional geometry of the deep channel and its

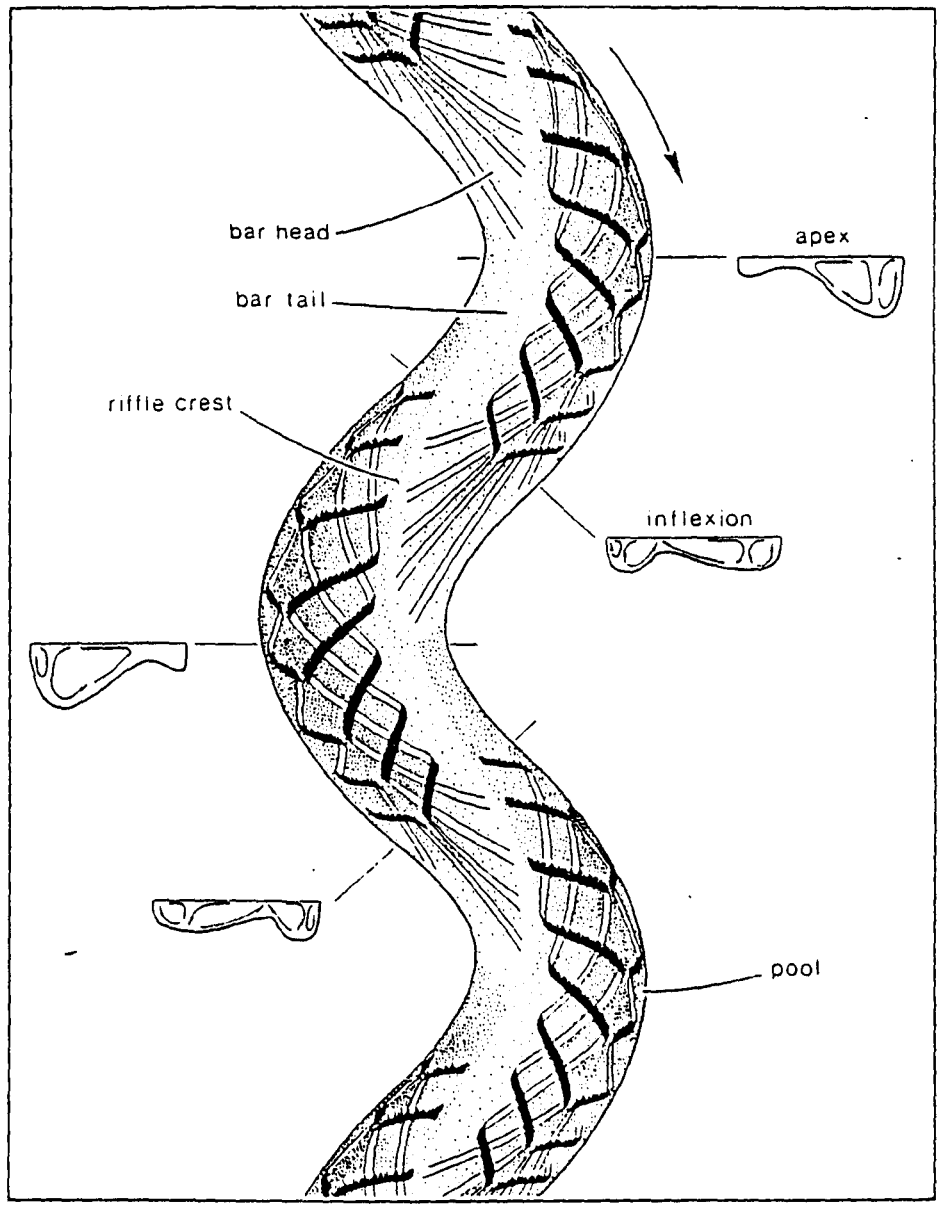

Figure 1.2: **Model of flow structure in meandering channels (after Thompson, 1985)**

associated shallow floodplains generate higher velocities in the main channel. This is because the channel has a greater depth and smaller wetted perimeter than the floodplain. Figure 1.3 shows velocity isovels (lines of equal velocity) for a two stage flume experiment conducted by Knight et al. (1984). The isovels are dimensionless parameters because the observed values are divided by the mean velocity for the cross-section; where V=Q/A. They found that the maximum main channel velocities were at least 25% greater than the mean for the section whereas average floodplain velocities were as low as 70% of this mean. From Figure 1.3, it can be seen that the maximum channel velocity was observed in the centre of the channel, away from the influence of the floodplain. This is in contrast to the maximum velocities on the floodplain which occurred close to the main channel, with a decrease in velocity with increasing distance away from the channel. The reason for these effects is the difference in flow velocities between the main channel and floodplain which causes a transfer of longitudinal momentum, generally from the main channel to the floodplain. Sellin (1964) was the first to identify turbulence at the interface between the main channel and floodplain by photographing vortices in a flume based study. A considerable amount of work has subsequently been carried out on the transfer of momentum in two stage channels. Zheleznyakov found in flume (1965) and field (1971) experiments that the momentum transfer mechanism decreased the overall rate of discharge for floodplain depths of just over bankfull. Radojkovic (1976) identified the dependence of the shear stress on the velocity profile in two-stage channels. This can be seen from the results of flume based experiments carried out by Knight and Lai (1985) to investigate the distribution of shear stress across a section of a two-stage channel. Analysis of the distribution shown in Figure 1.4 reveals that an interface can be imagined acting along the velocity gradient between the main channel and floodplain. The position of this interface is marked by a concentration of shear stresses. The shear stresses acting on this imaginary interface between channel and floodplain are generally known as 'apparent shear stresses' to distinguish them from the shear stresses that act on the physical boundary between the main channel and floodplain.

1.2.4 Behaviour of downstream two-stage channel flow

In two-stage channels the downstream reach length of a relatively sinuous main channel may be up to 30% longer than the straighter floodplain flows (Baird and Anderson, 1990). The sinuosity of the main channel was found by Ervine and Ellis

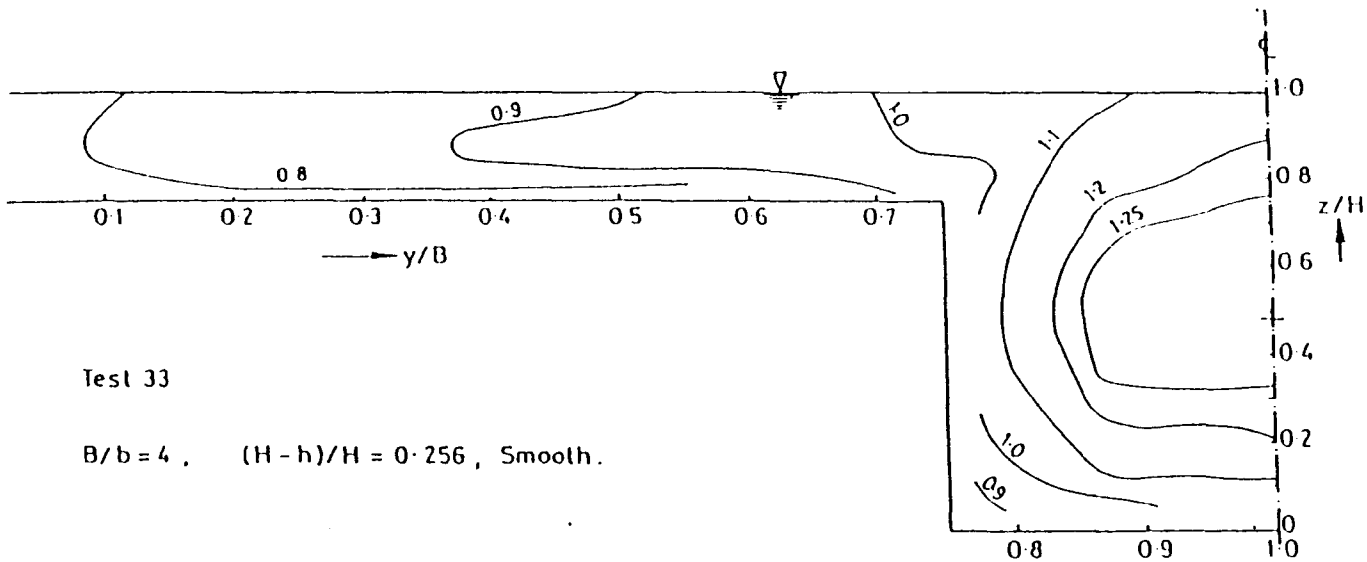

Figure 1.3: **Velocity isovels generated from a two-stage channel experiment conducted by Knight et al. (1984)**

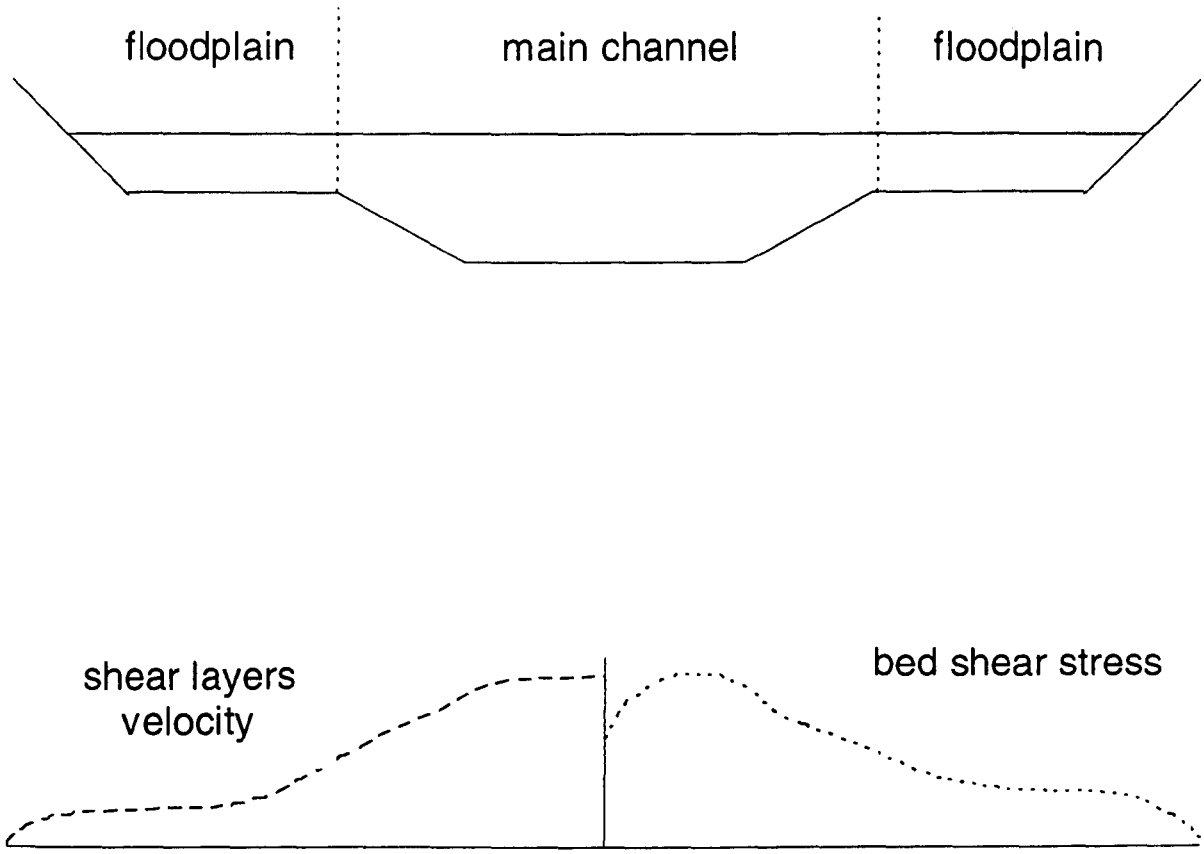

Figure 1.4: Distribution of shear stresses in a two-stage channel (after Knight and Lai, 1985)

(1987) to be important in determining the length of the downstream or longitudinal flow path.

Water on the floodplain may return to the channel either as overland flow or as throughflow. Water ponded by the topographic pattern of floodplain can only return to the channel by throughflow whilst flowing water can either go straight back to the channel or be routed downslope, over the floodplain surface, before rejoining the main channel. Under bankfull conditions, the floodplain flows may cross and re-cross the sinuous main channel beneath them with only relatively small amounts of momentum exchange occurring.

It is possible for floodplain flow to 'short circuit' the generally more sinuous route taken by the main channel, taking a more direct route (Fread 1976). The accelerating effects of the shorter path length and greater slope on the velocity of floodplain flows are, however, reduced by the effects of boundary friction. Floodplain boundary roughnesses are higher because of vegetation and obstructions such as hedges and man-made structures.

Overall, velocities on the floodplain tend to be lower than those in the main channel because of the relatively greater frictions. However the travel time of the *floodwave* tends to be faster over the floodplain because of the shorter reach length. The faster travel time of the floodwave over the floodplain creates complications when modelling two-stage flow. For a sinuous reach, where the floodwave is travelling faster downstream over the floodplain than the floodwave in the channel, the transfer of momentum may from the floodplain to channel.

1.3 EQUATIONS OF FLOW: CONTINUITY, MOMENTUM AND MASS TRANSPORT

The derivations of these equations are for a general three-dimensional fluid volume at an arbitrary location in a fluid body of infinite extent.

1.3.1.1 The continuity equation

For a fixed volume of water, the change in mass over time is equal to the difference between the inflow and outflow from the volume during that time. Changes in velocity and fluid density with respect to the space co-ordinates also need to be taken into account. The fluid mass entering one side of the fluid body is the product of the density, velocity, area and time interval. Since the velocity and density fields are not

constant, the equation can be expanded to incorporate these. The sum of the density terms is zero because the individual particles do not undergo changes in density.

$$\frac{\partial u}{\partial x}+\frac{\partial v}{\partial y}+\frac{\partial w}{\partial z}=0 \qquad 1.6$$

This is the volumetric continuity equation for an incompressible fluid.

1.3.1.2 The momentum equations

The momentum equations result from Newton's second law to an elemental fluid mass. Simply expressed this states that for an elemental fluid volume the inertial forces (mass x acceleration) are equal to the applied forces (pressure , gravity and friction due to fluid viscosity).

Inertial forces

The mathematical expression for the inertial force is found by formulating the basic definition that inertial force = mass x acceleration. Thus the mass of an elemental unit volume with density ρ, may be expressed as:

$$M = \rho\, dxdydz \qquad 1.7$$

Acceleration along the X axis can be expressed as *du/dt* where *u* is the velocity component in the X direction. Thus the inertial force F_I , along the X axis can be stated as:

$$F_I = \frac{\rho du}{dt} dxdydz \qquad 1.8$$

If the total differential *du/dt* is restated in terms of its components the final expression for the inertial force in the x direction is obtained:

$$F_I = \rho\left(\frac{\partial u}{\partial t}+u\frac{\partial u}{\partial x}+v\frac{\partial u}{\partial y}+w\frac{\partial u}{\partial z}\right)dxdydz \qquad 1.9$$

Equation 1.9 is the final expression for the inertial force in the X direction

Pressure forces

Pressure forces result from the normal components of molecular forces near the boundary of the elemental fluid volume. Pressure is a scalar force quantity and acts in all directions with equal magnitude. The case of the pressure force acting on an elemental fluid volume is shown in Figure 1.5.

The pressure acting on face ABCD acts in the opposite direction to that on face EFGH and is written:

$$-\left(p+\frac{\partial \rho}{\partial x}dx\right)\times EFGH=-\left(p+\frac{\partial \rho}{\partial x}dx\right)dydz \qquad 1.10$$

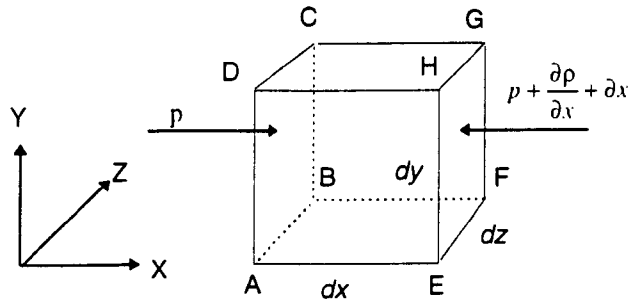

Figure 1.5: Diagram showing an elemental fluid volume to define the notation used in the equation for the pressure force

The net pressure force F_P, per unit volume is the difference in these opposing forces and is given by:

$$F_P = pdydz-\left(p+\frac{\partial \rho}{\partial x}dx\right)dydz=-\frac{\partial p}{\partial x}dxdydz \qquad 1.11$$

The Gravity force

The gravity force is the force exerted on the elemental fluid volume by the earth's gravitational field. This is a force equal to the weight of the particle in the vertical Z direction and zero in the horizontal X and Y directions. The gravitational force per unit volume in the vertical direction is given by:

$$F_G = -\rho g\ dxdydz \qquad 1.12$$

Viscous forces

Fluid viscosity causes the development of shear stresses, and the effective resistance to fluid movement is caused by the transfer of molecular momentum within the fluid body. Figure 1.6 shows the effects of viscous friction for a two dimensional fluid element.

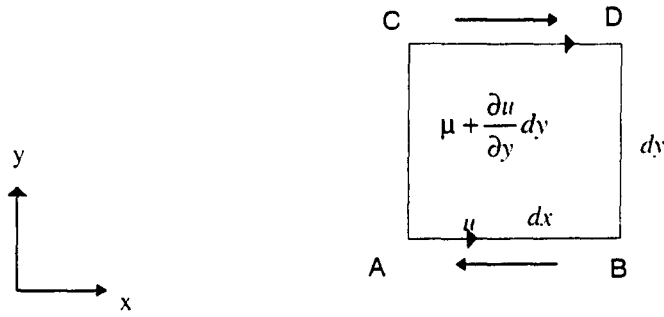

Figure 1.6: Diagram showing the notation used in the two-dimensional viscosity equations

The shear stress τ along the X axis is equal to $\mu\, \partial u/\partial y$. The total friction force along side AB is:

$$\tau dx dz = \mu \frac{\partial u}{\partial y} dx dz \qquad 1.13$$

These forces operate in opposite directions and the net viscous friction force, F_v over the area is found by the difference in the forces at AB and CD. If this type of derivation is used for all sides of the three dimensional fluid volume it is possible to demonstrate that the total viscous friction force in the X direction is given by:

$$F_v = \mu \left(\frac{\partial^2 u}{\partial x^2} + \frac{\partial^2 u}{\partial y^2} + \frac{\partial^2 u}{\partial z^2} \right) dx dy dz \qquad 1.14$$

Complete form

If the inertial forces are equated to the applied forces, there results the following set of equations:

$$\rho \left(\frac{\partial u}{\partial t} + u \frac{\partial u}{\partial x} + v \frac{\partial u}{\partial y} + w \frac{\partial u}{\partial z} \right) = -\frac{\partial p}{\partial x} + \mu \left(\frac{\partial^2 u}{\partial x^2} + \frac{\partial^2 u}{\partial y^2} + \frac{\partial^2 u}{\partial z^2} \right) \qquad 1.15$$

$$\rho \left(\frac{\partial v}{\partial t} + u \frac{\partial v}{\partial x} + v \frac{\partial v}{\partial y} + w \frac{\partial v}{\partial z} \right) = -\frac{\partial p}{\partial y} - \rho g + \mu \left(\frac{\partial^2 v}{\partial x^2} + \frac{\partial^2 v}{\partial y^2} + \frac{\partial^2 v}{\partial z^2} \right) \qquad 1.16$$

$$\rho \left(\frac{\partial w}{\partial t} + u \frac{\partial w}{\partial x} + v \frac{\partial w}{\partial y} + w \frac{\partial w}{\partial z} \right) = -\frac{\partial p}{\partial z} + \mu \left(\frac{\partial^2 w}{\partial x^2} + \frac{\partial^2 w}{\partial y^2} + \frac{\partial^2 w}{\partial z^2} \right) \qquad 1.17$$

These are the Navier-Stokes Equations along the X, Y and Z axes, respectively. They are second order differential equations because of the viscous friction terms and quadratic because of the inertial terms.

1.3.2 *The turbulent analogy of the flow equations*

The Navier-Stokes equations discussed above are only applicable to laminar flow. In order to apply these equations to the turbulent model, it is necessary to consider the components of turbulent flow. Turbulent motion can be considered to have two components; an instantaneous, fluctuating, disorderly motion and a mean motion. At any time the resultant motion is a function of the mean and fluctuating components. The fine scale detail of turbulent flow is a major research area in advanced fluid dynamics. However, for most engineering applications, it is only necessary to analyse turbulent flow for its average and longer term effects. The pressure, viscosity and velocity components consist of an instantaneous component and a mean component. This can be expressed mathematically as shown below:

$$\begin{aligned} u &= \overline{u} + u' \\ v &= \overline{v} + v' \\ w &= \overline{w} + w' \\ p &= \overline{p} + p' \\ \rho &= \overline{\rho} + \rho' \end{aligned} \qquad 1.18 - 1.22$$

Where:

u,v,w	=	Instantaneous velocity components in the X, Y and Z directions
p	=	Instantaneous value of pressure
ρ	=	Instantaneous value of density
$\overline{u}, \overline{v}, \overline{w}$	=	The mean velocity in the X, Y and Z directions over some time interval Δt
$\overline{p}, \overline{\rho}$	=	The mean pressure and density over Δt
u', v', w'	=	The velocity fluctuations with respect to the mean values in the X, Y and Z directions respectively
p', ρ'	=	The fluctuations in pressure and density

The following definitions clarify the statistical description which is made by considering turbulent motion as a superposition of a mean motion and a fluctuating and disorderly motion which is random in nature and can only be described in terms of statistical values.

$$\overline{u} = \frac{1}{\Delta t}\int_0^{\Delta t} u dt \qquad 1.23$$

$$\overline{v} = \frac{1}{\Delta t}\int_0^{\Delta t} v dt \qquad 1.24$$

$$\overline{w} = \frac{1}{\Delta t}\int_0^{\Delta t} w dt \qquad 1.25$$

$$\overline{p} = \frac{1}{\Delta t}\int_0^{\Delta t} p\,dt \qquad 1.26$$

$$\overline{\rho} = \frac{1}{\Delta t}\int_0^{\Delta t} \rho\,dt \qquad 1.26$$

$$\overline{u'} = \frac{1}{\Delta t}\int_0^{\Delta t} u'\,dt = 0 \qquad 1.27$$

$$\overline{v'} = \frac{1}{\Delta t}\int_0^{\Delta t} v'\,dt = 0 \qquad 1.28$$

$$\overline{w'} = \frac{1}{\Delta t}\int_0^{\Delta t} w'\,dt = 0 \qquad 1.29$$

$$\overline{p'} = \frac{1}{\Delta t}\int_0^{\Delta t} p'\,dt = 0 \qquad 1.30$$

$$\overline{\rho'} = \frac{1}{\Delta t}\int_0^{\Delta t} \rho'\,dt = 0 \qquad 1.31$$

1.3.2.1 The turbulent analogy of the continuity equation

The expression of the relationship shown in equation 1.6 as a function of the mean values in a turbulent flow has the form:

$$\frac{\partial \overline{u}}{\partial x} + \frac{\partial \overline{v}}{\partial y} + \frac{\partial \overline{w}}{\partial z} + \frac{\partial u'}{\partial x} + \frac{\partial v'}{\partial y} + \frac{\partial w'}{\partial z} = 0 \qquad 1.32$$

If the following examples are considered, the averaging process as it relates to the various terms of equation 1.6 can be evaluated:

$$\overline{\frac{\partial \overline{u}}{\partial x}} = \frac{1}{\Delta t}\int_0^{\Delta t} \frac{\partial \overline{u}}{\partial x}\,dt = \frac{\partial}{\partial x}\frac{1}{\Delta t}\int_0^{\Delta t} \overline{u}\,dt = \frac{\partial \overline{u}}{\partial x} \qquad 1.33$$

$$\overline{\frac{\partial \overline{u'}}{\partial x}} = \frac{1}{\Delta t}\int_0^{\Delta t} \frac{\partial u'}{\partial x}\,dt = \frac{\partial}{\partial x}\frac{1}{\Delta t}\int_0^{\Delta t} u'\,dt = 0 \qquad 1.34$$

Thus the continuity equation for mean motion in a turbulent flow becomes

$$\frac{\partial \overline{u}}{\partial x} + \frac{\partial \overline{v}}{\partial y} + \frac{\partial \overline{w}}{\partial z} = 0 \qquad 1.35$$

1.3.2.2 The turbulent analogy of the momentum equations

If mean value approximations introduced into the Navier-Stokes Equations there results a set of general momentum equations for turbulent flow.

$$\bar{\rho}\left(\frac{\partial \bar{u}}{\partial t}+\bar{u}\frac{\partial \bar{u}}{\partial x}+\bar{v}\frac{\partial \bar{u}}{\partial y}+\bar{w}\frac{\partial \bar{u}}{\partial z}\right)=-\frac{\partial \bar{p}}{\partial x}+\mu\left(\frac{\partial^2 \bar{u}}{\partial x^2}+\frac{\partial^2 \bar{u}}{\partial y^2}+\frac{\partial^2 \bar{u}}{\partial z^2}\right)-\bar{\rho}\left(\frac{\partial \overline{u'u'}}{\partial x}+\frac{\partial \overline{u'v'}}{\partial y}+\frac{\partial \overline{u'w'}}{\partial z}\right) \quad 1.36$$

$$\bar{\rho}\left(\frac{\partial \bar{v}}{\partial t}+\bar{u}\frac{\partial \bar{v}}{\partial x}+\bar{v}\frac{\partial \bar{v}}{\partial y}+\bar{w}\frac{\partial \bar{v}}{\partial z}\right)=-\frac{\partial \bar{p}}{\partial y}+\rho g+\mu\left(\frac{\partial^2 \bar{v}}{\partial x^2}+\frac{\partial^2 \bar{v}}{\partial y^2}+\frac{\partial^2 \bar{v}}{\partial z^2}\right)-\bar{\rho}\left(\frac{\partial \overline{u'v'}}{\partial x}+\frac{\partial \overline{v'v'}}{\partial y}+\frac{\partial \overline{v'w'}}{\partial z}\right) 1.37$$

$$\bar{\rho}\left(\frac{\partial \bar{w}}{\partial t}+\bar{u}\frac{\partial \bar{w}}{\partial x}+\bar{v}\frac{\partial \bar{w}}{\partial y}+\bar{w}\frac{\partial \bar{w}}{\partial z}\right)=-\frac{\partial \bar{p}}{\partial z}+\mu\left(\frac{\partial^2 \bar{w}}{\partial x^2}+\frac{\partial^2 \bar{w}}{\partial y^2}+\frac{\partial^2 \bar{w}}{\partial z^2}\right)-\bar{\rho}\left(\frac{\partial \overline{u'w'}}{\partial x}+\frac{\partial \overline{v'w'}}{\partial y}+\frac{\partial \overline{w'w'}}{\partial z}\right) 1.38$$

These are the so-called Reynold's equations. they are similar to the Navier-Stokes equations with the exceptions that an additional term has been added to the viscous forces due to the turbulent fluctuations and that the other forces are now expressed in terms of mean values. The turbulent fluctuation forces, which are the final terms on the right hand side of the Reynold's equations are the "Reynold's Stresses" and are the subject of a considerable amount of research in advanced fluid mechanics.

1.4 HYDRAULIC MODELS OF FLOODPLAIN PROCESSES

A number of physical and numeric models exist to represent the floodplain environment. These have been developed for a wide range of applications in many fields. Physical models are scaled models of a particular reach and have been used for various applications; for example to develop empirical relationships or to examine the impact of engineering structures. These models do have some disadvantages in that they may be unique to a particular reach or alternatively may not incorporate the reach characteristics. There are also problems of scaling. Numeric models, which are the subject of this investigation, have also been developed to solve the equations of unsteady fluid flow in their 1, 2 and 3 dimensional forms. These range from linear-conceptual models which replace the momentum equation with an empirical storage equation (Meyer, 1941) to highly complicated numerical techniques to solve the complete non-linear hydrodynamic equations.

One and two-dimensional models are now examined. Three-dimensional models have also been developed and applied to understand the pattern of secondary flow cells and

the structure of the shear layer. They are applied to short reaches and involve the integration of the full 3-dimensional equations of flow. Although these models are highly accurate, they require a large number of empirical constants and are extremely intensive in terms of computer time (Shiono and Knight 1991). At present they are not appropriate for engineering design purposes or large reach scale applications although they are very useful for small scale flow physics research.

1.4.1 One-dimensional schemes

For most flow routing cases, the full three-dimensional Navier-Stokes equations are too complex and models using a one-dimensional gradually-varied flow version are frequently used. The propagation of floodwaves along a river is determined by storage and conveyance averaged between pairs of surveyed cross sections and controlled at discrete locations. The St. Venant equations form the basis of most one-dimensional channel flow models and are a two-dimensional form of the Reynold's equations. In their full form, the St. Venant equations are non-linear and have no known general analytical solution. Hydraulic channel models have been widely developed to approximate the St. Venant equations using a kinematic or diffusion wave scheme. The form of these equations is discussed in Section 1.7.3. For the numerical simulation of free surface flows in compound channels for this set of flow problems, a number of solutions are available including one-dimensional finite difference methods (Cunge et al., 1980; Fread, 1985). Currently, many engineering applications use one-dimensional finite difference codes (Samuels, 1990).

Problems associated with these models are mainly caused by the simplifying assumptions made and poor schematization of topographic features. For example, there is currently no allowance made for the effects of lateral momentum exchange in one-dimensional routing models for unsteady flow (Bathurst 1988) although empirical relationships have been derived for steady flow. Another problem associated with these models is that the cross sections are assumed to be laterally aligned in a downstream direction. This means that features such as a meandering channel and non-uniform floodplain topography between cross sections cannot be adequately represented. The channel-floodplain cross-section is treated as a single system and the boundary roughness and velocity differences are averaged between flow segments. In addition, assumptions have to be made regarding the routes of flow paths across the floodplain since these have to be pre-defined. The floodplain is often treated as a storage area only.

1.4.2 2-dimensional schemes

Two-dimensional reach models use depth-averaged parameters to enable a lateral description of velocity and boundary shear stress components to be included. Such models have the obvious advantage over one-dimensional schemes in that a greater representation of floodplain topography and longitudinal channel form is possible. In addition, these models usually include a representation of momentum exchange.

These models solve the Reynold's equations using the Finite Difference (Zeike and Urban, 1981; O'Brien et al., 1993) or Finite Element (Feldhaus et al., 1992; Samuels, 1985) techniques to compute fluxes between segments of flow. These are numerical solution techniques which are applied to sets of equations describing non-steady state situations. The system being modelled is divided spatially into a number of smaller discrete elements. After the inclusion of boundary conditions, which define the domain within which the system operates, the governing equations are solved numerically to provide an approximation of spatially distributed values for the unknown parameters. The discretisation is extended to include the time dimension to produce these spatial results at a series of different times. These two techniques are described in more detail in Chapters Three (Finite Element Method) and Four (Finite Difference Method). The basic difference between them is that the finite difference method provides solutions for points either at the corners or at the centre of elements while the finite element method integrates the equations to provide a solution for the whole area of each element. Due to its nature, the finite element method allows elements to have irregular shapes. This means that a more detailed representation of the floodplain surface is possible than when applying the finite difference method, which places considerably greater constraints on the shape and size of elements. Models which are two-dimensional in cross section also exist such the model developed by Shiono and Knight using data from the SERC flood channel facility (1988, 1991). This includes the effects of secondary flow and has also been applied to natural river channels.

Until recently, the application of two-dimensional finite element methods to free surface flows was confined to certain classes of problems. These included the analysis of detailed flow patterns near structures (Tseng, 1975; King and Norton, 1978) and river confluence studies (Niemeyer, 1979; Su, 1980). Due to their continued development, two-dimensional finite element codes can now provide a viable alternative to one-dimensional schemes (Hervouet and Janin, 1994) and a number of

hydraulic model two-dimensional codes are now available for river channel-floodplain problems (Hervouet, 1993; Akanbi and Katopodes, 1988).

1.5 THE PROBLEM

A definition of channel flow and the components of flow contributing to it was defined by Freeze (1972a):

> The flow at the downstream end of any reach of channel is termed the channel flow (streamflow). Channel flow is the sum of the channel inflow to the reach, and the channel precipitation along the reach. According to the source from which it is derived the lateral inflow may consist of overland flow, subsurface stormflow, and base flow.

The hydraulic models considered so far do not consider all these components of flow. The representation of the floodplain by these models can be visualised as a mathematical flume; the only inputs to the system are the upstream reach input hydrograph, precipitation inputs over the area of the floodplain and channel and any tributary inflows. The only output from the system is the downstream hydrograph. Thus catchment hydrology is essentially treated as a black box. The floodplain is assumed to be an impermeable surface and any contributions from the hillslopes bordering the floodplain are ignored. These could potentially contribute a significant volume of water. To date, no work has been carried out to assess the importance of this contribution, relative to the floodwave arriving from upstream, following a precipitation input to the catchment. It is therefore not known if an important input to the channel-floodplain system is being ignored by these models and if so, under what circumstances this lateral inflow is important.

There are many factors which could have an influence on the relative contributions made by lateral inflows and the floodwave entering at the upstream end of a given reach. These have an influence on the comparative volumes contributed to the floodplain from both sources during a given time period. For example, this time period might correspond to the time over which a model simulation is carried out for a particular inundation event. The mechanisms of water delivery to the floodplain are highly complex. As stated by Freeze (1972a), inflow to the channel-floodplain system may be from overland flow, throughflow and base flow. Moreover, aquifer-channel interactions mean that water may also be contributed *from* the channel by percolation through the channel boundary and floodplain surface, to recharge the groundwater. There is therefore a need to further examine two-dimensional hydraulic floodplain

flow and to develop methods of relaxing initially the current zero flux boundary at the floodplain / hillslope interface.

1.6 THE RANGE OF HILLSLOPE - FLOODPLAIN ENVIRONMENTS

There is a wide range of hillslope-floodplain environments and it is possible that inflows may be significant for only some of these. There are several factors to be considered:

- **Hillslope parameters.** Soil parameters, slope angle, soil depth, vegetation and land use as well as the geometry and area of the slope will all affect the hydrological response of the hillslopes, both those in the headwaters of the catchment and those adjacent to the reach. In turn, the relative volumes and timing of the reach upstream hydrograph and lateral hillslope contributions will be affected.
- **Rainfall distribution.** Rainfall is generally greater in the upland headwater areas of a catchment due to orographic effects. The result of this is probably to augment the volume of water arriving from upstream and to lessen the volume contributed from adjacent hillslopes. Alternatively, the occurrence of a localised convective storm with its centre over the lower reaches of the catchment could increase the importance of these lateral contributions.
- **Event return period.** Events with a very large return period may cause part or all of the floodplain to become completely inundated, meaning that inflows do not influence floodplain inundation extent. The effect of hillslope inflows on inundation patterns is probably most apparent for events with smaller return periods.
- **Relative timing of floodplain and hillslope hydrograph peaks.** Again this is a function of the relative position of the floodplain within the catchment. Travel times are obviously greater if the water has further to travel from the source areas to the upstream end of the reach under consideration. Water from hillslopes adjacent to the floodplain has a relatively short distance to travel and it is quite possible that the lateral hillslope hydrograph peak could occur prior to the arrival of the flood peak from upstream. The exact timing of the lag between these peaks obviously depends upon the relative distances travelled as well as other factors such as the speed at which the processes of water delivery to the floodplain operate for a particular reach. If the peak hillslope contribution occurs concurrently with the

main floodwave peak it could potentially yield a significant volume of water relative to the upstream hydrograph. If the route to be taken by hillslope contributions is long and tortuous and the floodplain very wide, the bulk of the hillslope contribution could arrive after the passage of the floodwave. A significant hillslope contribution after the main floodwave could have an effect on the recession limb characteristics of the reach outflow hydrograph and increase floodplain storage times, although water from adjacent hillslopes may only contribute to baseflow in this case. If most of the water from the lateral hillslopes arrives at the floodplain before the flood peak from upstream, it is possible it would have only a minor effect, since the volume of water being delivered during the hillslope recession limb is probably a relatively insignificant proportion of the volume of water arriving from upstream. However, this contribution may be important in 'priming' the floodplain and making it more saturated than it would otherwise have been, reducing infiltration rates. It may also affect the rising limb of the reach outflow hydrograph.

- **Proportion of catchment upstream of reach and length of reach considered.** The area of the catchment upstream from the floodplain reach influences the volume of water entering the reach at the upstream end. If this area is considerably larger than the area of the bordering hillslopes, hillslope inflows are unlikely to form a significant percentage of the total volume of water reaching the floodplain. If an upland catchment is considered, the area of the catchment contributing along the edges of the floodplain is probably relatively greater, forming a larger percentage of the total volume delivered to the floodplain. The length of the reach along which inflows are contributed from the adjacent hillslopes, and therefore the area of hillslopes contributing to lateral inflows, also affects this percentage volume.

- **Floodplain width.** To some extent, this is a function of the location of the reach within the catchment; steep narrow floodplains generally being associated with upland reaches and wide floodplains with lowland areas. In association with this, wide lowland floodplains are often bordered by shallow hillslopes with deep soils whereas upland reaches are more likely to be bordered by steep hillslopes. This is not always the case, for example, well developed floodplains can occur in upland or mountainous areas. The width of the floodplain in relation to its topography and the volume of water being delivered to it will have a substantial influence on the extent and pattern of inundation. A wide floodplain may only be fully inundated during very major events and might never become completely inundated whereas a

narrow floodplain could become completely inundated during events with a relatively small return period. In terms of inundation patterns, lateral hillslope inflows probably have a greater influence for wide floodplains although the time taken for water to be transported from the hillslopes to the floodplain might mean that these contributions are to base flow only. The effect on water depths and flow field behaviour is likely to be greater for the case of narrow reaches.

In general terms upland floodplains are typically narrow, indeed a floodplain as such may not exist, with a steep longitudinal gradient and are often bordered by steep hillslopes. Since the distance between the upstream source areas and the floodplain is relatively short, there is not likely to be much of a lag between the reach hydrograph peak and that of the hillslope inflows. This, in conjunction with a relatively high rainfall over the lateral hillslopes means that the percentage contribution of water from those hillslopes is probably quite high in volumetric terms.

1.7 REPRESENTATION OF THE CHANNEL-FLOODPLAIN COMPONENT IN MODELS OF CATCHMENT HYDROLOGY

As a starting point to this discussion, a description is provided outlining current understanding of runoff mechanisms. This is for the dual purposes of describing the mechanisms by which the inflows to the floodplain are generated as well as understanding the basic structure of catchment hydrology models. Catchment hydrology models have been developed for many different applications, although attention here will focus on the representation of the channel component by physically based distributed models.

1.7.1 Runoff pathways and development of the Variable Source Area Concept

Under natural conditions a river usually receives water from within the bounds of its own drainage basin. A catchment can be regarded as a system which converts an input in the form of precipitation to outputs of evaporation and streamflow. In all but the driest areas, outputs from the system are continuous although precipitation inputs form discrete blocks separated in time. Generally, the speed of streamflow response to the precipitation input which is observed indicates that a percentage of the precipitation input is rapidly translated into streamflow (quickflow). This component is termed direct runoff and it occurs over an arbitrary time period. The fact that

streams continue to flow during periods of no precipitation is due to the slowflow or baseflow component of runoff.

The speed at which precipitation inputs are delivered from the hillslopes to the channel-floodplain system is dependent on the pathway taken. There are four main pathways which are illustrated in Figure 1.7.

i) Channel precipitation (Q_p), this is the term for precipitation which falls directly into the channel. Clearly this is the quickest route.

ii) Overland flow (Q_o), water flowing over the surface of the soil is a rapid transport mechanism and several conditions can cause its occurrence.

iii) Throughflow (Q_i), this is the term used for water flowing through the soil in micropores and channels or as a mass.

iv) Groundwater flow (Q_g), water entering the bedrock flows very slowly through fissures and pores, the rate varies with rock type.

Water reaching the channel can have taken any number of these pathways and the time taken by a particular 'parcel' of water delivered at a point A within a catchment to the channel outlet at B is obviously highly dependent upon the exact route taken.

Horton (1933) proposed that the soil surface divides precipitation inputs into two parts, the first draining overland to the channel network and the other infiltrating into the soil, from there either seeping slowly to the channel or evaporating to the atmosphere. The process is controlled by the infiltration capacity. If the rainfall intensity is less than the infiltration rate, no overland flow will occur. However, once the rainfall intensity exceeds the infiltration rate, overland flow will occur. Horton observed that the infiltration capacity changes with time as the storm progresses, starting with a maximum value and decreasing as cracks in the soil close due to the swelling of the soil particles.

This concept was qualitatively supported by other workers including Betson (1964) who worked on the assumption of the Hortonian mechanism of saturation from above. He indicated that due to the spatial variation of infiltration capacity throughout a catchment, only certain areas will yield overland flow with storm runoff usually originating from small but relatively consistent fixed source areas. The location of these areas was proposed as being a function of the spatial variation in soil moisture storage and rainfall intensity in the catchment. Although Hortonian overland flow does occur on impermeable surfaces, such as roads and areas denuded of vegetation,

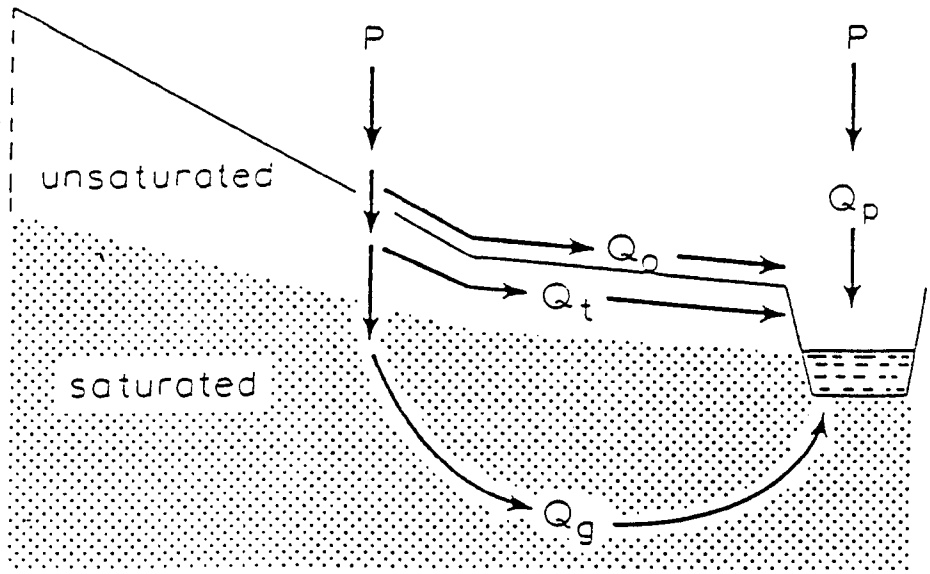

Figure 1.7: Flow paths of the sources of streamflow: Q_p is direct precipitation onto the water surface, Q_o is overland flow, Q_t is throughflow and Q_g is groundwater flow (after Ward and Robinson, 1990)

doubts were expressed by several hydrologists who had failed to observe overland flow over vegetated catchments. Much important work was carried out by US Forest Service hydrologists working in Coweeta. Hursh (1944) referred to the significant contribution of throughflow to total streamflow and observed that stormflow hydrographs were produced in forested catchments without the occurrence of Hortonian overland flow. Of particular importance was work carried out by Hewlett and co-workers, which remained unpublished until the 1960s. Hortonian overland flow had not been observed in the Coweeta watersheds, even during events with very intense precipitation and rapid streamflow response. The Hewlett hypothesis (Hewlett and Hibbert 1963, 1967) proposes that even during prolonged and intense precipitation, infiltration occurs over much of the catchment. Precipitation inputs travel downslope, through the combined processes of infiltration and throughflow. As the cumulative throughflow input to areas adjacent to the channel network increases, the shallow water table associated with these areas rises to the surface causing surface saturation. Any precipitation then falling onto these areas is then transmitted as saturated overland flow (Figure 1.8). These areas act as a source of quickflow and are of variable size, expanding as rainfall proceeds. They are spatially and temporally variable and act as a "rapid extension of the channel system" (Hewlett and Hibbert, 1967).

Contributing areas may be found at locations other than adjacent to the channel and are associated with zones of convergence. Various zones of flow convergence, where surface saturation is likely to occur, have been suggested. Kirkby and Chorley (1967) specified four areas of flow convergence. The first three areas are; slope concavities in plan, slope concavities in section and areas of thin or less permeable soils. The fourth type of flow convergence occurs as water percolates vertically downwards through the soil profile. The rate of vertical percolation generally decreases with depth. This results in the formation of a saturated layer in the soil profile. Normally, the hydraulic gradient is sufficient for the water in this layer to run downslope before the occurrence of surface saturation. However on shallow slopes, or where rainfall intensity is high, there will be a build up of water which may result in surface saturation. This is particularly likely where a relatively impermeable soil horizon occurs near the top of the soil profile. Betson and Marius (1967) suggested that saturated areas would occur where the A horizon was thin. Anderson and Burt (1978) studied a hollow and two adjacent spurs on the valley side of a catchment in the Quantock Hills, Somerset to examine the effect of contour curvature on flow convergence. They observed the

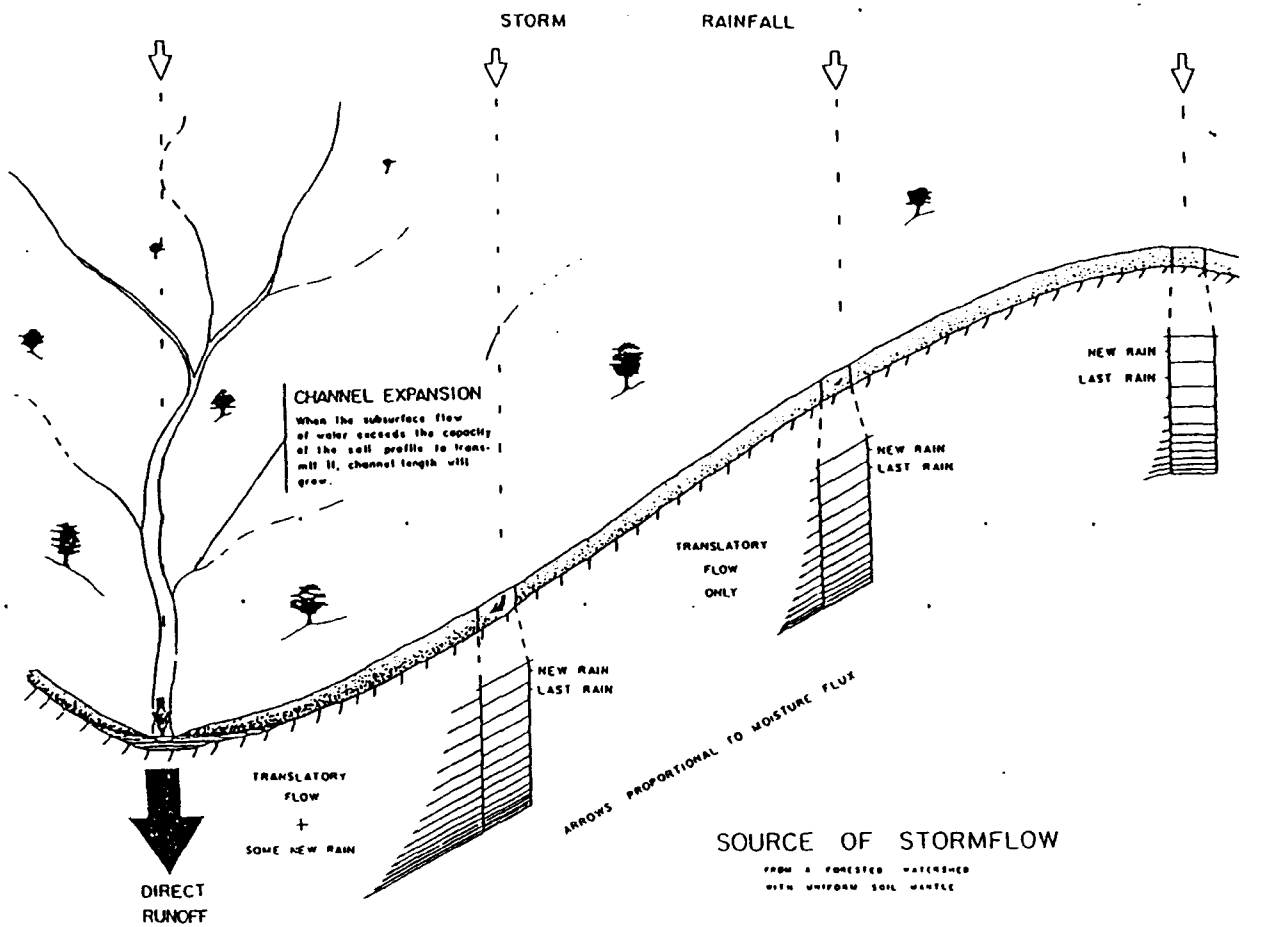

Figure 1.8: **The relative contributions of rainfall to streamflow (after Hewlett and Hibbert, 1967)**

formation of a saturated wedge in the hollow, due to the three dimensional convergence of water both from the freely draining spurs and from upslope. Contributing areas at locations remote from the saturated slope base can still make significant contributions to the volume of storm runoff if a suitable transport mechanism exists. For example, Jones (1979, 1988) found that soil pipes formed by hydraulic and hydrologic processes may increase the contributing area as much as two or even five times the area identified by surface contours.

However, field experiments carried out in a number of different environments using natural isotope tracers support the view of Hewlett that water stored in the catchment prior to the storm event dominates the storm hydrograph (Sklash et al., 1986, Pearce et al., 1987). Hewlett and Troendle (1975) suggested that in view of the anisotropic nature of the soil profile, a vertical flow path was unlikely to dominate and that instead "water responds to changing hydraulic gradients and flows more or less parallel to the slope surface, depending on local moisture contents, soil conductivities and the steepness of gradients.

1.7.2 The range of catchment hydrology models

Catchment hydrology models aim to predict the catchment response to an input of rainfall and have been developed for many different applications. The simplest macroscopic (black box) models simulate the relationship between input (rainfall) and output (stream runoff) from the system (the drainage basin). A transfer function is used to predict future runoffs from a given rainfall. These vary in complexity from simple regression models to more sophisticated multiple regression models which take several catchment characteristics into account such as the model described in the Natural Environment Research Council Flood Studies Report (NERC, 1975). However, this approach cannot be used to predict the catchment response to conditions outside the range of the observed data, such as the response to climate change or land use change within the catchment. In order to do this, it is necessary to provide a representation of the processes operating within the catchment. This requirement has led to the development of conceptual and subsequently physically based distributed models.

Conceptual models represent the basin by a series of interlinked processes and stages and are spatially lumped. One of first lumped conceptual models was the Stanford Watershed Model. Continuous development of this model has resulted in the Hydrologic Simulation Program. The catchment processes are described

mathematically, with each storage component consisting of a non-linear reservoir for which a budget is kept. However, in lumping catchment parameters and processes in this way, the spatial variation which occurs within a catchment cannot be represented.

In the late 1970's a semi-distributed physically-based model, TOPMODEL, was developed (Beven, 1977a; Beven and Kirkby, 1979). TOPMODEL combines the spatial variability of hydrological source areas with a lumped approach to the average response of soil-water storage within the basin. The spatial variation within the catchment is represented through the use of a topographic index to divide the catchment into hydrologically similar areas which are then modelled separately. This reduces the number of model parameters and thus the amount of fieldwork required. It is also less computer-intensive compared to fully distributed models and as such provides a compromise between lumped conceptual models and physically based distributed models.

Work carried out by Freeze in the early 1970's provided a foundation for the development of physically-based distributed models (Freeze, 1972a, 1972b). One of the original aims in developing these models was to apply them to ungauged catchments or to situations where catchment change had or was occurring. Beven and O'Connell (1982) identified four major areas of application for these models:

i) monitoring the effect of land use change
ii) forecasting the effects of spatially variable inputs and outputs
iii) modelling the movement of pollutants and sediments
iv) predicting the hydrological response of ungauged catchments

They are distributed because they can explicitly represent the spatial distribution of catchment properties rather than treating the catchment as a lumped unit. The term 'physically based' is applied because these models use equations derived from the physics of water transport, although Beven (1989) is among those who discuss this issue pointing out that the equations are drawn from small scale physics and there is no sound theoretical basis for scaling them up to the grid scale of catchment models. Although small-scale physical equations may still apply at the model grid scale, additional processes arising at this scale such as macropore flow, are currently not adequately represented by these models. Fawcett et al. (1994) suggest that 'physically based' can be used to describe a type of model and its objectives but does not necessarily mean that a satisfactory physical representation has been achieved.

These models use finite element or finite difference methods to solve the governing equations, which exist in varying forms of complexity. The spatial discretization is carried out using either a grid-based overlay such as that used by the Système Hydrologique Européen (SHE) (Abbott et al., 1986; Bathurst, 1986) and illustrated in Figure 1.9 (a) or a catchment segmentation as used by the Variable Source Area Simulator (VSAS) (Hewlett and Troendle, 1975; Bernier, 1985) which divides the catchment into a series of hillslope units or elements as shown in Figure 1.9 (b). A similar catchment sub-division is used by the Institute of Hydrology Distributed Model (IHDM) (Morris, 1980; Calver, 1988). Beven (1987) concluded that this element structure gave more flexibility in representing near-channel features, in particular the extent of the hydrologically significant variable source area. Models such as the IHDM and VSAS represent the expansion and contraction of the contributing area by means of a finer spatial discretisation at the base of the slope. The subsurface flow component is either simulated using one dimensional vertical solutions of subsurface flow at points on the hillslope planes, or by using an infiltration equation. Beven (1985) suggested these models should only be applied to systems dominated by surface flows.

A different approach is required where catchments dominated by subsurface flow are considered, or where the subsurface contours and divides are markedly different from the surface topography. This requirement has led to the development of the basin scale model, SHE. The underlying aims behind the development of SHE were centred around the prediction of the effects of human interference on the hydrological cycle. Each of the primary processes of the land phase of the hydrological cycle is modelled in a separate component. These components are run in parallel with information exchanges occurring between them. The overall control of this parallel running is managed by a FRAME component. A modular structure was used so that improvements or additional components such as water quality and sediment yield could be added in the future. In the next section, attention will be focused on the channel-floodplain component of this model in addition to considering the treatment of this component in models developed for catchments dominated by surface flows.

1.7.3 *The representation of the channel-floodplain component by these models*

Various approaches are used in modelling the channel-floodplain component of catchment hydrology models. These vary in complexity from a simple lagging function to finite difference solutions of the one-dimensional form of the St. Venant

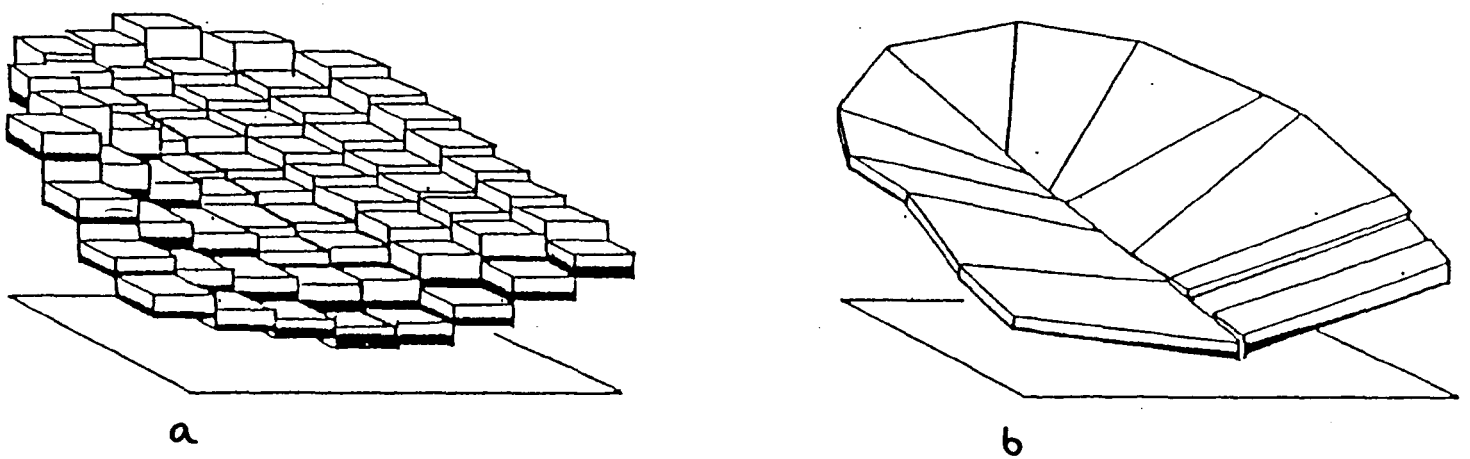

Figure 1.9: **Comparison of topographic representation between the (a) SHE and (b) VSAS modelling schemes (after Davie, 1992)**

equations. Some of the methods by which lateral inflows from the hillslopes are applied to the channel system are also considered.

The equations describing one-dimensional free surface overland or channel flow are subject to the following simplifying assumptions (Beven, 1985):

a) the flow is gradually varied in a wide, regular, approximately rectangular channel;
b) the slope of the bed is small and the bed is fixed;
c) the streamlines are essentially straight and the flow can be represented by cross-sectional averages of discharge, Q; velocity, v and depth, h;
d) the fluid is incompressible and of constant viscosity;
e) the pressure distribution is approximately hydrostatic; and the momentum due to lateral inflows is negligible.

These assumptions can be relaxed, resulting in more complex models. Alternatively, if they are made more restrictive, the models can be simplified. For example, VSAS uses a simple lagging function where flows are lagged according to the estimated time of travel from each catchment segment to the basin outlet. This involves passing a certain proportion of a given hour's flow to the following hour. Flows from each segment simulation are accumulated to form the final outflow hydrograph.

The form of the equations used to represent the channel flow component of most process based distributed models is now considered. The equation of continuity of mass at a point is defined as:

$$\frac{\partial Q}{\partial x}+\frac{\partial A}{\partial t}=i \qquad 1.39$$

Where:

A = the cross-sectional area of flow

i = is the lateral inflow rate per unit length of channel

x = the distance along the channel

t = time

The equation contains the unknown variables Q and A and a second equation is necessary to describe the flow. This may be based on the conservation of momentum at a point, under the assumptions listed above, as:

$$\frac{\partial Q}{\partial t}+Q\frac{\partial}{\partial x}\left(\frac{Q}{A}\right)=gA(S-S_f)-\frac{g}{B}\frac{\partial A}{\partial x}-i\frac{QB}{A} \qquad 1.40$$

Where:

g = the gravitational acceleration

B = the channel width

S = the bedslope of the channel

S_f = the friction slope

Equations 1.39 and 1.40 are the St. Venant equations. The system remains incomplete in that the friction slope S_f must be defined. This is usually done by assuming the flow is quasi-uniform so that the friction slope can be related to flow velocity by one of the empirical flow equations such as the Manning, Chezy or Darcy-Weisbach equations.

Under certain conditions it may be valid to use simplified forms of equations 1.39 and 1.40. For example if it is assumed that inertial effects are negligible in the development of 1.40, a 'diffusion analogy' equation can be derived:

$$\frac{\partial Q}{\partial t} + c\frac{\partial Q}{\partial x} = D\frac{\partial^2 Q}{\partial x^2} + ic \qquad 1.41$$

Where for a rectangular channel:

$$c = \frac{dQ}{dA} \qquad D = \frac{Q}{2BS}$$

The SHE model uses a one-dimensional solution based on the diffusion wave approximation of the St. Venant equations (Abbott et al., 1986).

By making the further assumption that both inertial and diffusive effects are negligible, equation 1.40 reduces to:

$$S_f = S \qquad 1.42$$

Substituting an appropriate relationship for S_f into equation 1.39 gives a 'kinematic wave' equation:

$$\frac{\partial Q}{\partial t} + c\frac{\partial Q}{\partial x} = ic \qquad 1.43$$

Channel flow (and any overland flow occurring on the hillslopes) is represented in a one-dimensional sense using a kinematic wave equation by the IHDM (Calver, 1988). The model uses a four-point implicit finite difference scheme and requires the channel slope, width, roughness and initial upstream and downstream discharges as inputs. Beven (1985) summarised the limitations associated with this technique. For example, kinematic flow assumptions cannot predict 'looped' rating curves and cannot predict the backwater effects due to downstream disturbances that may be important in

forecasting areas of flooding. Kinematic wave solutions may also be subject to 'kinematic shocks' due to disturbances travelling downstream at fast wave speeds and overtaking slower waves. These are of mathematical rather than physical origin and in the real world would be obscured by the diffusive and inertial effects that have been neglected in the kinematic wave formation. Beven concluded that the kinematic wave formation was most appropriate on steep slopes or in steep channels.

Any appropriate relationship, based directly on field measurements of velocities rather than estimated 'roughness coefficients' can be used (Beven 1979). TOPMODEL was developed originally for small to medium sized basins. Channel processes have been found to be highly non-linear in small, steep, rough and very irregular streams. In TOPMODEL a simple non-linear convolution routing algorithm is used, based on the at-a-station velocity relationship:

$$c(t) = CHA \bullet Q(t)^{CHB} \qquad 1.44$$

Where:

$Q(t)$ = Outflow discharge for the whole catchment at time t

CHA and *CHB* are constants

$c(t)$ = An average kinematic wave velocity for the channel network, which is assumes to be spatially constant.

This routing procedure takes into account the distribution of predicted sub-catchment inflows with distance along the channel network.

The methods described above assume that once water has entered the channel, it does not leave the channel, and do not therefore account for aquifer-channel interactions. The models described were developed for small catchments and are appropriate only for systems dominated by surface flows (Beven, 1985). A different approach is required in modelling catchments with a major groundwater component. The first to do this was Freeze (1972a). Previous to this, any coupling existed only between the surface flow components (overland and channel flow), subsurface flows were either ignored or specified as some simple external function to represent loss by infiltration or gain by base flow (Wooding, 1965; Chen and Chow, 1968). The groundwater response of watersheds had been vastly underrated in most studies of watershed behaviour. Freeze examined the mechanism of base flow generation and the nature of watershed response in base flow dominant systems using a deterministic mathematical model that coupled three-dimensional, transient, saturated-unsaturated subsurface flow and one-dimensional gradually varied, unsteady channel flow. The

full St. Venant equations were solved for the reasons that they are better suited to short, smooth reaches with low slopes and high rates of lateral inflow. In addition the shock wave phenomena associated with the kinematic solutions was avoided. The lateral inflow function is shown in Figure 1.10. The three possible sources of lateral inflow are rainfall on the stream (r), overland flow (q_s) and subsurface flow (q_g). The energy slope, S_i is defined by the Manning equation.

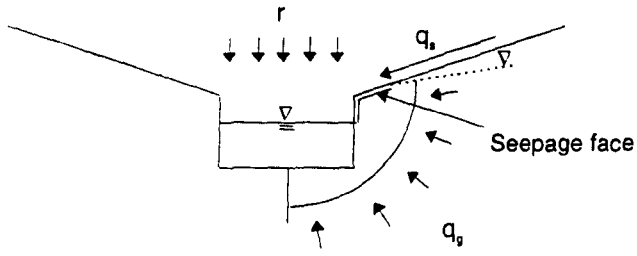

Figure 1.10: Cross-section showing the lateral inflow component of the one-dimensional flow model used by Freeze (1971)

An implicit coupling mechanism was implemented; that is, the internal boundary conditions of each model were satisfied at each time step. Stream depth was used as the convergence quantity. The subsurface model was solved at each time step by using the stream depth from the previous time step as the specified head condition at the stream boundary. The calculated outflow from the subsurface system became the lateral inflow to the streamflow model for that time step and the new stream depth profile calculated. This new profile then replaced the old profile to set the heads for the second subsurface cycle. This alternating cycle was continued until the stream depth and specified head boundary values converged to within a predefined tolerance. The inflow function to the groundwater model was through infiltration on the watershed under constant head or constant flux conditions. Outflow from the model was through base flow to the stream which occurred under constant head or fluctuating head boundary conditions at the stream and as seepage from a freely fluctuating seepage face on the stream bank. In this study, the source of river rise was lateral inflow itself. Discharge was applied at the upstream end for a number of time steps. The occurrence of sub-surface storm flow was found to be feasible only where convex hillslopes feed steeply incised channels and was also governed by a threshold saturated hydraulic conductivity below which subsurface storm flow cannot be important (Freeze, 1972b).

The SHE model also incorporates an implicit coupling mechanism between the channel and aquifer to allow for seepage losses and groundwater input. The overland and channel flow component uses topographic, channel shape and flow resistance parameters to route surface water as overland and channel flow. A 1-d diffusion wave approximation of St. Venant equations is used and the Strickler/Manning equation is applied to determine the relationship between velocities and flow depths. The channel system is represented on the boundaries of the grid squares. The depth of surface water available as runoff is determined from net rainfall and evaporation rates supplied by the interception/evapotranspiration component and from the soil infiltration rate determined by the unsaturated zone component (figure 1.11).

Stream aquifer interaction is simulated for the following cases:

a) phreatic surface in direct contact with a flowing stream
b) phreatic surface in direct contact with a dry stream
c) phreatic surface lying below a flowing stream
d) phreatic surface lying below a dry stream.

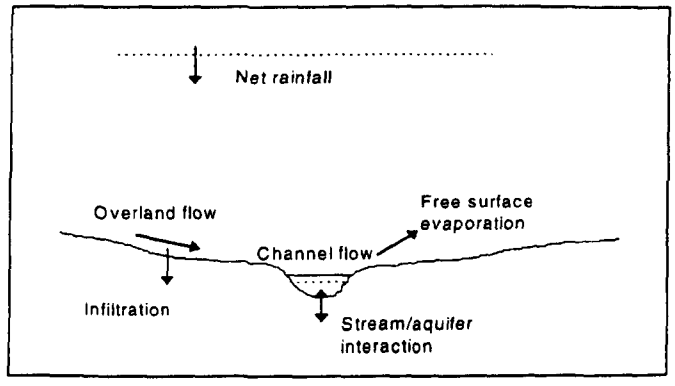

Figure 1.11: Schematic representation of the processes modelled in the overland and channel flow component of the SHE model (After Abbott et al., 1986)

The channel boundary can be assigned a hydraulic conductivity different from that of the surrounding aquifer. This is to account for the higher or lower conductivities which may characterise the sediments in the immediate vicinity of the channel.

From the previous discussion it can be seen that the approach used when applying a hydrology model to a catchment is dependent upon the processes perceived to be important within that catchment. The representation of the channel-floodplain component also varies in complexity. For example, in the case of steep upland catchments dominated by surface flows, the kinematic wave approximation is the most appropriate representation of the channel flow component (Beven, 1985). However,

for channels with shallow gradients and high rates of inflow, the one-dimensional form of the St. Venant equations is suggested to be most appropriate (Freeze, 1972a). In addition, parallel processing may be appropriate where there is a major baseflow contribution to storm runoff. It is suggested that under certain circumstances, in the light of the recent advances in floodplain modelling presented in Section 1.4.2, it may in future be possible to implement a 2-dimensional channel-floodplain scheme to improve this element of models such as the SHE. Such a development is beyond the scope of this investigation, although it is possible that some of the issues associated with it may be considered during the course of this research.

1.8 DEVELOPMENT OF RESEARCH OBJECTIVES

In the previous discussion, the problem has been identified; that current hydraulic models of floodplain processes do not consider the interaction of the hillslopes bordering the floodplain reach with the channel-floodplain system. A theoretical examination of the range of hillslope-floodplain environments which exist indicates that under certain circumstances the contribution from hillslopes bordering the reach could be an important additional input which is currently ignored.

Inflow to the channel consists of three components; overland flow, throughflow and baseflow. The mechanisms by which lateral inflows may be contributed to the channel-floodplain system have been examined together with a summary of the approaches used in catchment hydrology modelling. Physically based distributed models have been developed to simulate the runoff response for a catchment. The channel is thus an integral part of the catchment and contributions to channel flow as hillslope inflows are therefore simulated by these models. In addition, since the headwaters of the catchment are included, the major runoff producing areas are incorporated in the simulation. Floodplain inundation models are generally applied to lowland reaches. Instead of simulating the production of runoff, they use an observed hydrograph as the upstream input and any inflows from hillslopes bordering the reach are not included. The importance of hillslope inflows relative to the floodwave arriving from upstream has not been examined.

In examining this issue, it is possible that hillslope inflows to a floodplain reach may only be significant under certain circumstances. For example, a wide lowland floodplain in a relatively flat topographic area would be unlikely to receive a large volume of water as lateral inflows during the course of a flood event. At the other

extreme, it may not be appropriate to apply a two-dimensional inundation model to a steep upland catchment, although it is in upland areas that the main runoff producing areas occur and high rates of lateral inflow to the channel are observed. However, between these extremes is a range of environments where floodplain reaches are bordered by hillslopes which could produce significant lateral inflow volumes.

It is proposed to examine the significance of this additional input. This will be done by selecting and setting up a two-dimensional floodplain inundation model for a suitable floodplain reach, bordered by hillslopes, and to apply inflows to elements at the edge of the simulated reach. If this additional input is found to have an influence on model predictions, an examination will be made of the range of environments where hillslope inflows may be important in the context of two-dimensional floodplain modelling. The method proposed is to set up a hillslope hydrology model, using the bordering hillslopes as a geometric template, to apply inflows to the floodplain model. A sensitivity analysis of the floodplain model to changes in selected hillslope parameters could then be carried out. While it will not be possible to conduct a full investigation into every possible circumstance where inflows should be considered as an additional input, it is hoped that some insight will be gained into this issue.

In using lateral inflows generated by the hillslope model as an additional input to the floodplain model, consideration must be given to the coupling mechanism used to effect the transfer. The coupling mechanism is important in determining the relative timing of lateral inflow contributions to the floodplain. The relative timing is an important consideration because of the relatively short period over which floodplain inundation models are run to simulate a flood event. If the hillslopes inflows are delivered to the channel as baseflow some time after the flood wave has travelled down the reach they would not be important in this context. It could be argued that hillslope and channel models have already been coupled through the development of some process based distributed models. However, these models have been developed for small to medium sized catchments, are less sophisticated in their two-dimensional channel representation and are usually applied to upland environments. Although there has been a move towards large scale basin modelling, such as the SHE model, the relative importance of hillslope inflows has not been examined and a hillslope hydrology model has not previously been coupled to a two-dimensional floodplain inundation model.

The aims of this research are therefore:

- To find out if lateral hillslope contributions are likely to have a significant effect on the predictions made by floodplain inundation models.
- To set up a coupled hillslope hydrology - floodplain inundation modelling scheme
- To use this scheme to carry out a sensitivity analysis to identify the range of environments where inflows are significant
- To examine the impact this additional input has on the calibration of the floodplain model.

1.9 CONCLUSION

The need for floodplain inundation models has been identified and the current modelling approaches have been examined. A number of hydraulic model exist which provide a good representation of the floodplain in a hydraulic context but essentially treat catchment hydrology as a black box. The problem that these models do not currently incorporate hillslope hydrology could be important. A consideration of the range of hillslope-floodplain environments has revealed that there is a limitation on the environments to which two-dimensional floodplain models can be applied and within this sub set, inflows may only be significant in some cases. Attention was then turned to catchment hydrology and the processes of lateral inflow generation. Catchment hydrology models have been developed to simulate these processes and differ from the floodplain models in that the whole catchment is modelled including all the runoff producing areas and the channel is an integral part of this system. They are usually applied to upland catchments. Although there has been a move towards basin scale modelling and hillslope and channel components have been coupled, no investigation has been made of the relative importance of lateral inflows to the channel relative to the flood wave arriving upstream for floodplain reaches.

Chapter Two now describes the research design proposed to achieve the aims of this first pass investigation into the importance of lateral inflows.

Chapter Two
RESEARCH DESIGN

2.1 INTRODUCTION: AIMS OF RESEARCH AND RESEARCH OUTLINE

Chapter One identified and discussed the problem associated with current floodplain inundation models; that although the representation of floodplain processes is often very sophisticated in a hydraulic context, catchment hydrology is essentially treated as a black box. Usually the only input to the system is the observed upstream hydrograph with output generally only occurring at the downstream end of the reach. Floodplain inundation models currently ignore any contributions to the system from the hillslopes bordering the reach. Lateral hillslopes could potentially contribute a significant volume of water. Currently any volumetric discrepancies between predicted and observed downstream reach hydrographs are corrected for during the calibration procedure which is carried out during the set-up of these models. It is therefore not known if an important input to the floodplain system is being ignored and if so, the circumstances in which applying this additional input could improve predictions made by current floodplain inundation models. The main aims of this research are therefore:

- To find out if lateral hillslope contributions are likely to have a significant effect on the predictions made by floodplain inundation models.
- To set up a coupled hillslope hydrology - floodplain inundation modelling scheme to explore this issue further
- To use this scheme to carry out a sensitivity analysis to identify some of the environments where inflows are significant
- To examine the impact this additional input has on the calibration of the floodplain model.

In order to achieve these aims, the investigation falls into several stages. The proposed programme of research is illustrated in Figure 2.1 and is discussed more fully in the following sections. The initial stage involves the selection of a floodplain inundation model, the selection of the study reach to which it is applied and the set up of the model. The first stage of the actual investigation is to carry out a pilot investigation to find out if contributions from the hillslopes bordering a floodplain reach are

significant. This involves carrying out model simulations with water added along the edges of the floodplain at various rates observed in the field. If the results of this pilot study indicate that a significant difference results from the addition of hillslope inflows, the problem can be studied further by examining the range of environments where hillslope contributions are important. This can be done by setting up a hillslope hydrology model and altering some of the input parameters to represent a range of hillslope types. The output from this model will then be used as an additional input to the floodplain inundation model. Using this coupled modelling scheme it will be possible to identify the circumstances where contributions from lateral hillslopes have a significant impact on floodplain inundation and to address some of the modelling issues concerned with applying an additional model input in this way.

2.2 INITIAL STAGE (SET-UP)

2.2.1 Introduction

This involves selecting the application reach and choosing and setting up a suitable floodplain inundation model.

In selecting a suitable reach several factors need to be taken into consideration in terms of the specific demands of the application. For this application a suitable reach would have a well developed floodplain bordered by hillslopes, which will eventually be used as a template for setting up the hillslope hydrology model. The reach length would ideally be in the order of 10-20 km. Since it is desirable that a lowland reach is selected, the cumulative effect of inflows applied along the edges of a reach of this length would allow the effect of inflows on the downstream predicted hydrograph to be examined. In order to set up a floodplain inundation model there will be a need for topographic data, land use information and observed hydrographs at the upstream and downstream ends of the reach for several flood events. Also, data on previous inundation extents will be useful for model validation.

Figure 2.1: SCHEMATIC REPRESENTATION OF PROPOSED RESEARCH

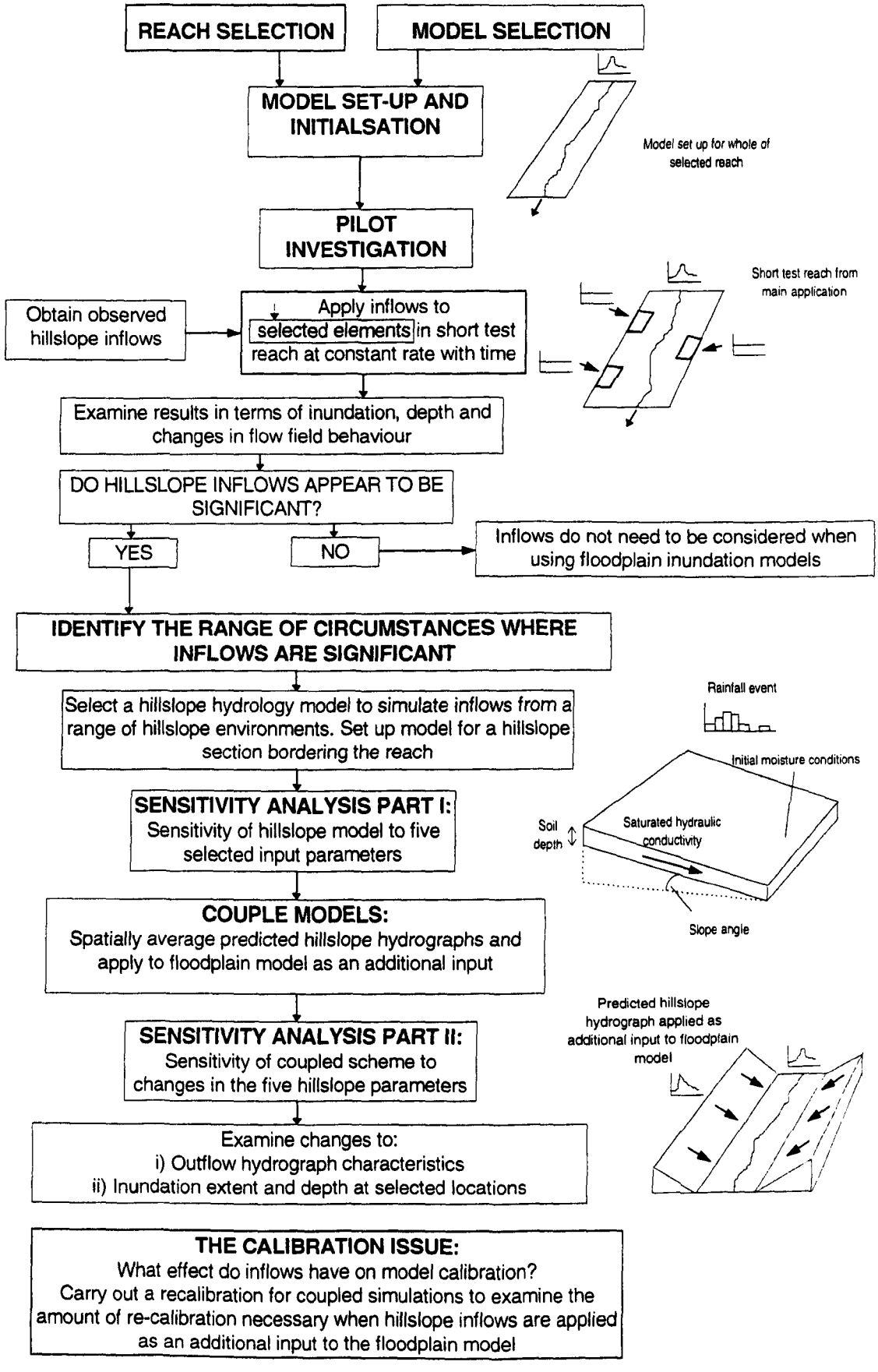

Once the reach has been selected, the model will be chosen. In doing this, there are several factors which must be taken into consideration. This application makes specific requirements such as the need to predict inundation extent, depth and flow field behaviour at as fine a resolution as possible for the proposed reach length. Traded off against this is the need for sufficient computer power to run the model, bearing in mind that a number of simulations are to be carried out. In addition, factors such as the type, quantity, quality and availability of data required to set up and validate the model have to be considered in light of the data available for the chosen reach. A very important consideration is how easy it will be to include inflows as an additional model input. The factors considered in selection of the floodplain inundation model are discussed in further detail in Section 2.2.3.

The specifics of setting up the model for this reach will be covered in Chapter Three where the selection and set-up of the model is described. In general terms the set-up will fall into several stages. Initially the physical environment within which the system will operate has to be defined. This will include the geometry and roughness characteristics of the floodplain providing a representation of its extent, topographic and land use characteristics and the location of river channels. Once this stage has been completed, a certain amount of mesh refinement may be necessary to ensure a stable numerical solution before the model is calibrated for that particular reach. Calibrating the model will involve carrying out several model simulations, changing certain input parameters such as floodplain roughness until the predicted hydrograph and inundation extent are as close as possible to those observed for the event being simulated.

2.2.2 *Selecting the application reach*

There are several attributes that a suitable reach will posses. These pertain both to the physical nature of the reach and the data available for it.

i) Nature of the reach

First, it is important that the reach has a well developed floodplain which is regularly inundated. For a populated lowland floodplain with a significant history of inundation, it is very likely that there will be records of inundation extents and previous flood levels. Secondly, the capabilities of the type of model chosen should be considered; the reach gradient should be within the limits of most floodplain inundation models and the reach itself not too complex in nature. The reach length is also important since for a short lowland reach (of for example 1-2 km) the volumetric

contribution from the hillslopes bordering the reach might be very small compared to the volume of water entering from upstream. The length of the reach will be restricted somewhat by the available computing power since the time for each simulation would be greater for a longer reach. Finally, in light of the fact that this investigation involves an examination of the impact of side inflows on floodplain inundation, there is also a need for hillslopes bordering the floodplain reach. These will be used as a geometric template for setting up the hillslope hydrology model.

ii) Topographic information required

2-dimensional models require height information across the surface of the floodplain and channel. This can be obtained from contours, although contour spacing over the surface of floodplains is generally too great to be of much use for this purpose. Spot heights can also be used, the height of a particular location being obtained through interpolation. Surveyed sections can be made to supplement this information.

iii) Hydrometric information

At the upstream and downstream ends of the reach, hydrographs are required for a number of events of different return periods. The upstream hydrograph provides the upstream input to the hydraulic model whereas the downstream hydrograph is used in model validation. In order to develop the downstream boundary condition, a rating curve based on the stage-discharge relationship is required. Rainfall data, for input to the hillslope hydrology model, is also needed from rain gauges sited either on the bordering hillslopes or as near to them as possible. This will be for the events corresponding to the observed hydrographs for the hillslopes or close to them and be on an hourly basis.

iv) Information on previous inundation extents

Any information on previous inundation extents is useful, both during the model set-up stage and for internal model validation. The exact ways in which this data can be used will be discussed in later sections. This information can comprise any or all of the following; aerial photographs of flood events, maps of previous inundation extents, sediment data and information on previous flood levels.

2.2.3 *Factors considered in the selection of a floodplain inundation model*

In selecting a suitable floodplain inundation model for this application, the data requirements of the model and the suitability of the model to the selected reach will be considered. The desired attributes of the model are now considered.

i) Model prediction products

The model must also be able to provide a good spatial representation, in addition to predictions at the downstream end of the reach, so that any changes in depth and inundation extent produced by the addition of inflows can be observed. Therefore a model which provides depth and velocity predictions for a number of locations over the surface of the floodplain at each time step is essential and for this reason a two-dimensional model will be chosen. Another factor to be taken into consideration is the resolution of the representation of the flow boundary for examining changes in inundation extent. Finally, the ease with which this information can be extracted is important, since data will be extracted for a number of time steps and at many locations over the surface of the floodplain.

ii) Range of environments to which the model can be applied

There is a range of application environments to which a given hydraulic model can be applied which is determined by factors such as the steepness of the floodplain (both laterally and longitudinally), channel complexity and floodplain topography. The model capabilities must be taken into account since if the chosen reach falls outside this range of capabilities an unstable numerical solution may well result. In some cases a compromise can be sought, for example by simplifying the channel complexity, or increasing the spatial resolution in the case of a steep floodplain environment, although this may not be an ideal solution in every case. Model capabilities must be taken into account both at this stage and when selecting the floodplain model and the reach to which the model is applied.

iii) Data Requirements

In order to set up and run a floodplain inundation model, there are various data requirements. These include upstream and downstream hydrographs for a number of events. The upstream hydrograph provides the model input while the downstream hydrograph is used both for both model calibration and validation. Topographic information is required for setting up the network of solution points and can be obtained from maps (contours and spot heights) and aerial photographs of previous inundation events from which the edge of the floodplain and areas of higher land can be identified. This information can be supplemented with surveyed cross sections. Aerial photographs, sediment data and maps of previous inundation extents are all useful for internal model calibration

iv) *Implementation of side inflows*

It will be vital to be able to implement side inflows or be relatively simple to adapt the model to accept inflows as an additional input. In view of the model requirements discussed above, it will be argued in Chapter 3 that a two-dimensional finite element model is most appropriate for this investigation. These models provide a good spatial representation of floodplain topography and longitudinal channel form and use depth-averaged parameters to enable a lateral description of velocity and boundary shear stress components to be included. They provide predictions of depths and velocities for a number of discrete locations over the surface of the floodplain. From these predictions it will not only be possible to examine the effect of hillslope inflows on the reach outflow hydrograph but in addition to investigate any localised effects on predictions such as changes to inundation extent, depth and flow field behaviour.

2.2.4 *Setting up the floodplain inundation model*

The set-up of the model will fall into several stages which are outlined here. The specific details of each stage will be discussed in Chapter Three once the floodplain model and study reach have been selected.

i) Mesh set-up

The spatial and topographic characteristics of a reach are defined in finite element models by a number of nodes bounding discrete elements. The finite element technique allows elements to vary in shape using quadrilateral, triangular or a mixture of both element shapes to represent complex topography accurately. The first stage of setting up a floodplain model is to define the location of the nodes defining these elements.

To start with, the locations of the channel and the edge of the floodplain will be defined. In some places, the channel geometry may have to be simplified for the reasons discussed in the previous section. In determining the position of the edge of the floodplain, topographic information and aerial photographs of previous extents will be used. Once these locations have been defined, the floodplain will be represented, taking into account the maximum desirable density of nodes to represent such features as variations in topography and man made structures. The size and shape of elements is influenced by floodplain features, topographic variation, the type of mesh used by the model and model-specific rules relating to mesh set-up. Once the nodes have been located, each node will be assigned a height value. These are obtained from surveyed cross sections and can also be interpolated from spot heights

and contours. Variations in roughness over the surface of the floodplain will also be defined. Once the finite element mesh (FEM) has been set up it will probably require a certain amount of refinement to enable a stable model solution. After checking that the data has been correctly entered into the database, initial conditions for the model will be developed to see if any instabilities occur at that stage. If problems do occur, it may be necessary to carry out a certain amount of mesh refinement.

ii) Model calibration and validation

Model calibration will involve carrying out several simulations using an observed upstream hydrograph as an input to the reach. The predicted downstream hydrograph will then be compared with the observed downstream hydrograph in terms of the closeness of fit with regard to the timing of the flood peak, the volume of water and the shape of the hydrograph. If, for example, the predicted hydrograph peak occurs before the observed hydrograph peak, it can be inferred that the model does not predict sufficient storage over the floodplain. The process of calibration involves changing the value of one or more parameters to which the model is sensitive in order to change the characteristics of the predicted hydrograph in an attempt to improve the fit of this hydrograph to the observed downstream hydrograph. There are many possible combinations of parameter values and several of these may provide a close fit. Optimisation procedures are often used to find the best fit although it is unlikely that any one of these combinations of parameter values is the correct one. More than one storm event can be calibrated in this way.

The process of validation involves running the model for events outside the range of those used during the calibration procedure. The closeness of fit between the observed and predicted hydrographs can be examined and quantified to assess the performance of the model. A certain amount of internal validation can also be carried out by examining areas of inundation observed from previous events and comparing these to model predictions for those areas. Measurements of velocities and flow field behaviour are difficult to obtain in the field during flood events so it is likely that internal validation will be carried out on the basis of depths and inundation extents, although data on the movement of sediment and observations on the alignment of vegetation such as grass immediately after an event can be used for this purpose if it is available.

2.3 PILOT INVESTIGATION

2.3.1 *Introduction*

The purpose of this pilot investigation is to determine whether hillslope contributions have a significant effect on floodplain inundation. First it is necessary to define 'significant' in this context. The addition of water to the floodplain might be expected to be manifested in several ways:

- Changes in the characteristics of the outflow hydrograph
- Volumetric changes to the outflow hydrograph
- Changes in inundation extent
- Changes in depth and flow field behaviour at selected sites - a small change in depth over the surface of the floodplain could involve a significant volume of water.

Working down this list, it can be seen that these effects become more and more localised although all can be described as significant. Changes to the outflow hydrograph will probably only be brought about when the total volume of water contributed by the lateral hillslopes is relatively large compared to the total volume of water entering at the upstream end of the reach. However, the more localised changes could have significant secondary effects such as changes in sediment distribution, local groundwater behaviour and influences on floodplain ecology. Currently, any volumetric discrepancy in model predictions caused by ignoring inflows as a model input is accounted for during the model calibration phase by altering model parameters to change the volume of water stored on the floodplain.

It is proposed therefore to use inflows as an additional model input and examine the changes, if any, to model predictions in terms of the factors listed above. Hillslope outflows measured in the field for another catchment will be obtained from the literature and used as an additional input to represent hillslope inflows at the edge of the floodplain. These will be converted to a form suitable for input to the model and applied at a constant rate with respect to time in order to examine any localised effects caused. In doing this, the method of water delivery to the floodplain must be considered. It is important to seek a compromise between physical representation and model complexity. As discussed in Chapter One, little is understood about the processes of water delivery to the floodplain from the bordering hillslopes. Since the significance of hillslope inflows is not known at this stage, it is felt to be inappropriate

to attempt to model the delivery of water to the floodplain in as physically realistic way as possible. In addition, this would increase the complexity of the modelling scheme, increasing the potential for error in model predictions, perhaps unnecessarily.

2.3.2 *Data selection*

Very few data exist for outflows along the base of hillslopes; observations which have been carried out for isolated hillslopes usually relate to measurements of soil water status. It may be possible to find some suitable data for an individual hillslope, although it is unlikely that this will be within the same catchment as the selected floodplain reach. However, at this stage in the investigation, data from another catchment will probably be sufficient to determine whether inflows are likely to have an impact on floodplain inundation.

2.3.3 *Implementation*

A short (approximately 1 km) test reach will be used for the pilot study. The primary reason for this is that it is not known quite what impact this additional input of water will have on the stability of the chosen floodplain model. If water is added to selected elements along the edge of a short test reach, the total volumetric input will form a very small proportion of the volume of water entering the reach at the upstream end and is unlikely to cause instability. It will still be possible to observe any localised effects resulting from the addition of inflows in terms of changes in depth and flow field behaviour. A significant change in these will indicate that it is worth extending the study. In order to simplify this initial investigation, the effect of temporal variations will not be considered, inflows being applied at a constant rate with respect to time.

2.3.4 *Analysis of results*

Since only a short test reach is being used and water is not being applied to all the elements along the edge of the reach, it is unlikely that applying inflows to selected elements will have much impact on the downstream hydrograph. Analysis of the results will thus concentrate on changes in depth and flow field behaviour. This will involve extracting depth and velocity information for selected nodes across the surface of the floodplain for certain time steps. Nodes will be selected at varying distances from the elements to which the inflows are added to examine the effect of increasing distance from the source of input. It is hoped that this will give some indication of

how localised the effects of inflows are. By comparing the results of these simulations with the control (no inflows) some idea can be obtained of how important inflows are likely to be. The observation of significant changes in depth and flow field behaviour will indicate whether it is worth continuing the investigation to examine the range of circumstances where inflows are important.

Assuming the pilot study indicates that inflows from hillslopes bordering the floodplain are an important input to the floodplain system, the next stage will be to identify the range of circumstances for which this is the case and to examine the varying impact different inflows have through carrying out a sensitivity analysis.

2.3.5 *Extending the study*

In order to extend this investigation to examine the circumstances under which hillslope contributions are important, data is required for outflows from the base of several distinct hillslope types and for events with different return periods. There are several ways in which this data could be obtained. Field measurements could be made during storm events for a wide range of hillslope types. This would obviously be time-consuming, since a number of events with different return periods would have to be observed, and is thus inappropriate within the available time frame. Few published data exist for outflows measured at the base of hillslopes, most measured observations from upland catchments are at catchment outflows. It would be difficult to use such data because inflows are required as a flow per unit length whereas the outflow hydrograph from a catchment is measured at a point. This could be converted to a flow per unit area but would probably provide a misrepresentation of the outflow from typical hillslopes within the catchment since channel flow processes would have an influence on the catchment response. The third approach proposed involves modelling the inflows, carrying out a sensitivity analysis using selected model input parameters to examine the sensitivity of the floodplain inundation model to these parameters. Using the slopes bordering the selected study reach as a template for the set up of this model, a semi-theoretical approach would be adopted, using the geometry of a slope bordering the reach as a template and altering selected parameters during the sensitivity analysis to represent a wide range of hillslope environments.

For the reasons discussed, it is felt the best approach is to model the hillslope inflows rather than use field measurements. It is proposed to set up the model for a 1 km wide section of the hillslopes bordering the floodplain reach and carry out a sensitivity analysis for the hillslope hydrology model using this slope as a template and changing

selected parameters. The output from this model will then be spatially averaged and used along the entire reach of the floodplain model. The first reason for using a hillslope section is due to the semi-theoretical approach being adopted; if the hillslope model was applied to the whole length of bordering hillslopes it would become too site-specific during the sensitivity analysis. Also during the sensitivity analysis, several simulations will be carried out. The use of a hillslope section enables considerably faster model simulations and easier interpretations of the results

2.4 THE SELECTION AND SENSITIVITY ANALYSIS OF A HILLSLOPE HYDROLOGY MODEL TO SELECTED INPUT PARAMETERS

2.4.1 Selection and set-up of the hillslope hydrology model

This particular application has specific requirements which mean that the hillslope model is required to have attributes which would not normally be necessary when setting up a hillslope model for a whole catchment. Since the model is being applied to a section of hillslope rather than a whole catchment, the model should allow the catchment to be split into sub-units. Another requirement is that the model should be able to provide a spatially distributed output along the base of the modelled slope rather than a point output such as at the catchment outlet. Finally, because no observed hydrograph is available, the model should not rely on calibration procedures for parameterisation.

Once selected, the set up of a hillslope hydrology model will involve several stages. The starting point will be to define the hillslope topography through dividing the hillslope up into smaller sub-units. Exactly how this is done will be dependent upon the model selected and may involve dividing the catchment up on the basis of some factor such as different soil types or flow lines. Alternatively a regular grid might be used. Following on from this there will be a need to parameterise the model to provide a description of the hydrological characteristics of each sub-unit. Since this investigation adopts the semi-theoretical approach discussed, the model will be parameterised using typical values for certain parameters published in the literature. The reason for this is that the hillslope section is being used as a template; i.e. the actual slope itself is not being modelled. Thus typical values can be assigned to the hillslope parameters which are altered during the sensitivity analysis. As a corollary to this, the errors inherent in the sampling strategies used to obtain a point value for parameters with a large degree of spatial variation can be avoided using this approach.

Rainfall input is usually derived from observed events for the catchment. In this case, the events used will correspond to the flood events applied at the upstream end of the floodplain reach. Depending on the location of rain gauges in the catchment, some spatial interpolation may be necessary to estimate the rainfall input to the hillslope section at the time interval required by the hillslope model.

In the probable absence of any hillslope outflow data for the reach, it will not be possible to calibrate and validate the model in the manner described in Section 2.2.4 for the floodplain inundation model, although some checks can be made to ensure that it is running stably and that the volume of water produced at the base of the hillslope appears to be a reasonable proportion of the rainfall input.

2.4.2 *Sensitivity analysis of the hillslope hydrology model*

Ideally, to clearly delineate the appropriate range of application environments, it would be desirable to run the coupled model many times to establish the effect of varying all the possible parameters in relation to each other over a wide range of values. However, this method of combinatorial model runs is greatly constrained by time. To illustrate this point, a series of model simulations could be considered involving ten values for each of five parameters. If each hillslope parameter was varied relative to all the others, the resultant number of model simulations would be 10^5. If each coupled model simulation took 24 hours, the total run time would be 274 years. Even if each parameter only had 3 values the resultant run time would be 243 days and it would take a considerable amount of additional time to analyse the results. It is clear therefore that a compromise must be sought by carrying out a number of simulations using the hillslope hydrology model and then selecting a representative sample of these for the coupled model runs. This will be done by identifying key parameters and varying each parameter whilst holding the others constant. Whilst this method will not define a clear threshold, it will be possible to determine the importance of hillslope inflows under some circumstances and will also show any areas of uncertainty where there is a need to carry out more experimental model runs.

For the identification of the broad area of interest, it is proposed initially to set up 11 hillslope model runs. Within the given time frame this is felt to be appropriate, looking at a range of values for each parameter and examining the sensitivity of the model to each of these. This will provide the information required for the next stage in the investigation such as whether further hillslope model runs are required for certain

parameters to more clearly delineate the variation which occurs as a result of altering the value of a given parameter.

2.4.2.1 Selection of key parameters

There are several model parameters within both the hillslope and the floodplain models which could affect side inflows. These fall into three broad categories.

1) Geometric parameters

- slope angle (a function of slope length and slope height)
- slope plan (convergence / divergence)
- floodplain width
- floodplain steepness
- floodplain roughness

2) Soil parameters

- hydraulic conductivity
- soil depth
- soil type distribution
- soil structure
- vegetation cover

3) Dynamic parameters

- storm characteristics
- initial moisture conditions
- rainfall distribution over the catchment

Five key parameters have been selected to represent these classes. The parameters which were felt to have the greatest influence on hillslope response were selected. The selected parameters are illustrated in Figure 2.2 and are:

i) Slope angle
ii) Antecedent conditions
iii) Soil depth
iv) Hydraulic conductivity
v) Rainfall event

The proposed model simulations are shown in Table 2.1.

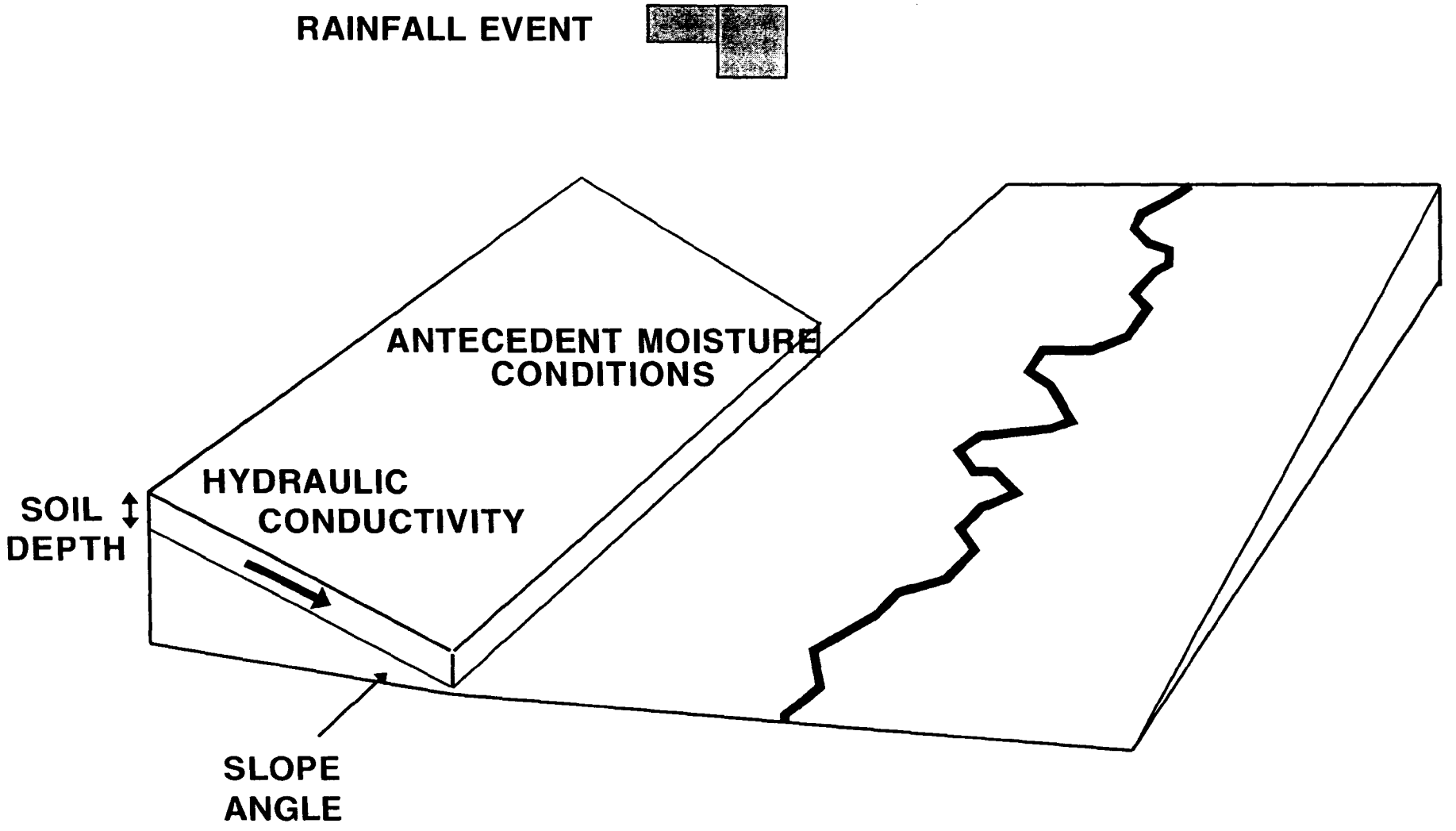

Figure 2.2: The input parameters altered during the sensitivity analysis

Simulation	Slope angle	Saturated hydraulic conductivity	Soil depth	Initial moisture conditions	Rainfall event
1	6°	loam	0.5	saturated	1 in 1 y
2	6°	loam	0.5	saturated	1 in 5 y
3	6°	loam	0.5	saturated	1 in 12 y
4	6°	clay loam	0.5	saturated	1 in 1 y
5	6°	sand	0.5	saturated	1 in 1 y
6	6°	loam	0.1	saturated	1 in 1 y
7	6°	loam	1.0	saturated	1 in 1 y
8	6°	loam	0.5	dry	1 in 1 y
9	6°	loam	0.5	semi-dry	1 in 1 y
10	12°	loam	0.5	saturated	1 in 1 y
11	45°	loam	0.5	saturated	1 in 1 y

* values used for hydraulic conductivities
loam - 5.56×10^{-6} m s^{-1}
sand - 1.00×10^{-4} m s^{-1}
clay loam - 1.39×10^{-6} m s^{-1}

Table 2.1: Parameter values for proposed model runs

2.4.3 *Selection of events for coupled model runs*

When the hillslope hydrology model simulations are carried out, a number of results files containing information on hillslope outflow and soil moisture status will be produced for each time step. Some of the changed hillslope parameters will probably have a greater effect on model predictions than others and it may be necessary to carry out further simulations in order to gain a greater understanding of the model's sensitivity to certain parameters. The sensitivity of the model to each change made to a given input parameter value may be expressed as a percentage change in, for example, the total volume of runoff produced for the event. When these outflows are applied to the floodplain model, they may in turn produce a significant percentage change to the reach outflow hydrograph. Alternatively the effects may only be seen at a more localised scale. Clearly, there is little point carrying out coupled model runs for every simulation if the difference between certain of the hillslope hydrology model predictions is negligible or if observed differences are only apparent in terms of changes in soil moisture status.

2.5 SENSITIVITY ANALYSIS FOR THE COUPLED SCHEME

2.5.1 *Coupling the models*

The second stage in the sensitivity analysis is to analyse the sensitivity of the floodplain model to the different hillslope inflows produced during the first stage. As

previously outlined, the first stage involves examining the effect certain selected input parameters have on the outflow hydrograph produced by the hillslope model. Before this second sensitivity analysis can be carried out, the hillslope hydrology model must be coupled to the floodplain model. In order to apply the predicted hillslope inflows along the length of the reach, the predicted hydrograph for the base of the hillslope will be spatially averaged. This will be done by dividing the hillslope discharge for each time-step by the length of the hillslope to produce an inflow per unit length. The methods considered to simulate the actual delivery of this water to the floodplain and the argument for selecting the method used will be discussed in Chapter Five. Computer programs will be written to convert the output data from the hillslope model into a suitable "inflows" input to the floodplain model. These programs will carry out the spatial averaging procedure and the process of distributing water at each time-step to appropriate elements within the mesh of the floodplain model; exactly how this is done will be dependant on the mechanism selected to represent the transfer of water from the hillslopes to the floodplain.

2.5.2 *Running the coupled scheme*

Once the volume of water to be delivered to each element at each time step has been calculated, the input file containing data such as the upstream input hydrograph will be adapted to incorporate this data. Since a number of coupled simulations are to be carried out, a program will be written to adapt the input file accordingly. Any other adaptations which have to be made to the model input files will be made at this stage, before actually running the model. The fact that programs will have been written means that should it be necessary to carry out further simulations, the whole process can be repeated. Once the input files are in order, the model can be run as normal with the results files produced being stored for later analysis. A control simulation (no inflows) will be carried out for each of the events used. The actual simulations carried out will be described in Chapter Five.

2.5.3 *Analysing the results*

Analysis of the of the results will be in terms of hydrograph characteristics which can be easily quantified, such as the total predicted discharge at the downstream end of the reach, the peak discharge, the timing of the hydrograph peak as well as an examination of more localised effects. Changes to inundation extent and depth at selected calculation nodes will also be examined. In order to analyse the results of the

sensitivity analysis, output data which is easily quantified for the purpose of comparison will be used; the sensitivity of the coupled scheme to a particular hillslope model input parameter being expressed as a resultant change in, say, the total volume of discharge produced for different values of that parameter.

2.6 THE CALIBRATION ISSUE

During the course of this investigation the floodplain model will be calibrated during the initial stage, without the additional input of inflows. It is not known what effect inflows will have upon the calibration of the model although it is quite possible that if there is a sizeable contribution to the reach outflow hydrograph the model may have to be re-calibrated for any future applications using hillslope inflows.

In order to explore this issue, it is proposed to examine the effect (if any) of re-calibrating selected coupled simulations. For each set of re-calibration simulations the same upstream and hillslope input files used for the original coupled simulation will be used although changes will be made to the parameter or parameters which are used in the calibration process. The degree of change made to these parameters when repeating the calibration process will indicate the effect a particular inflows hydrograph has on the calibration of the model. In addition, the degree of re-calibration necessary following the addition of inflows applied at various rates could also be used as a means of quantifying the relative effect of inflows simulated for different hillslope environments.

2.7 CONCLUSION

In this chapter the problem has been identified and a programme of research has been designed to examine the importance of contributions to floodplain inundation from the bordering hillslopes. This involves setting up a suitable two-dimensional finite element model for a floodplain reach selected on the basis of certain requirements made by this application. Following this, observed hillslope outflows will be applied during simulations using a short test reach taken from the main application reach . The effect of this additional input will be examined in terms of localised changes in depth and inundation predictions. If inflows do influence model predictions in this way the study will be continued by carrying out a sensitivity analysis, applying inflows at different rates along the entire modelled reach. These will be obtained by using a hillslope section bordering the reach as a geometric template to set up a

hillslope hydrology model. Several simulations will be carried out using this model and altering five selected parameters over a series of typical values to represent a range of hillslope environments. The sensitivity of the hillslope model to changes in each of these values will be assessed. Following this, the output from the hillslope model will be converted into a form suitable for input to the floodplain inundation model thus coupling the two models. A series of coupled simulations will be carried out in order to conduct the second part of the sensitivity analysis; the sensitivity of the floodplain model to the different hillslope inflow hydrographs resulting from changes made to the selected hillslope parameters. The final part of the investigation will examine the effect of this additional input from the hillslopes bordering the floodplain lateral hillslopes on the calibration of the floodplain model.

Chapter Three now describes the set up of the floodplain model and the pilot investigation carried out to find out if the addition of hillslope inflows has an effect on the predictions made by the model. Chapter Four goes on to discuss selecting and setting up the hillslope hydrology model in order to carry out the first part of the sensitivity analysis. The process by which this hillslope model is coupled to the floodplain inundation model is explained in Chapter Five. Chapter Six presents the results of the second part of the sensitivity analysis. In Chapter Seven the calibration issue is explored. In Chapter Eight conclusions are made together with a critique of the work carried out and suggestions for further work.

Chapter Three

MODELLING FLOODPLAIN INUNDATION

3.1. INTRODUCTION

Chapter Two identified the main aims of the research and developed the research design proposed to achieve these aims. This chapter outlines the reasons underlying the selection of the study reach and the hydraulic model which was applied to it. The set-up of the chosen model for the reach and the initial simulations carried out are described prior to an account of the pilot study carried out to examine possible effects of using hillslope inflows as an additional model input.

This chapter is divided into five main sections. The first of these describes the reasons underlying the choice of the study reach, through the examination of factors such as the physical nature of the reach, data availability and inundation history. Following this, the selection of a suitable floodplain inundation model is considered in terms of the requirements of this particular application. The set-up of this model is also described. The fourth section describes the observed backing up of water at the downstream end of the modelled reach. For this reason it was decided to extend the modelled reach in a downstream direction, beyond the downstream gauging station. Through the description of this model extension, the methods used for setting up and initialising the floodplain model are described. In the final section, the pilot study carried out to examine the effects of applying inflows to the reach is described. This investigation involved adding inflows, at a rate observed in the field, to selected elements along the edge of the reach. The results of this first-pass investigation into the significance of contributions to the floodplain from the bordering hillslopes are presented at the end of the chapter.

3.2. SELECTION OF THE STUDY REACH AND SITE DESCRIPTION

3.2.1 *Required reach attributes*

For the purposes of this investigation, a floodplain reach meeting several criteria was selected, these are now outlined. To start with, a reach with a history of previous inundation events was essential. In addition, a certain amount of information was required to set up a floodplain inundation model for the reach and in order to

parameterise the model there was a requirement for detailed topographic information and data from gauging stations (at the upstream and downstream ends of the reach) to provide the boundary conditions. Upstream and downstream boundary conditions generally comprise an observed input hydrograph for the upstream end and a stage-discharge relationship at the downstream end. For model validation, an observed downstream hydrograph would also be useful together with data on previous flood inundation extents, depths and flow field behaviour, where available, for internal model validation. A further consideration made in selecting a suitable reach was the reach length; inflows applied along the edges of a relatively short reach, say of the order of 1-2 km, would only contribute a small percentage of the total outflow hydrograph for a coupled simulation. Inflows applied at the same rate but to a longer reach, would form a considerably greater percentage of this volume. With this in mind, a reach length of 10-20 km was felt to be appropriate. The final consideration concerned the fact that a hillslope hydrology model was to be applied to a hillslope section bordering the reach. As discussed in Chapter Two, a hillslope section bordering the selected reach was to be used as a geometric template for the hillslope model during the sensitivity analysis. To enable the set-up of this hillslope model, it was important that rainfall data was available for the hillslopes bordering the reach. In light of these requirements, a suitable reach was selected and is described in the following sections.

3.2.2 *The River Culm reach*

3.2.2.1 *Site description*

The River Culm (Figure 3.1) is a tributary of the River Exe and joins the main river 3 km north of Exeter. The Culm has a total catchment area of 276 km^2. In the lower reaches between Cullumpton and Stoke Cannon, there is a well developed floodplain which averages 450m width. The meandering channel is approximately 12m wide and has a gravel bed and banks composed of fine alluvial material with a height of approximately 1m. There is a substantial inundation record, with overbank flooding occurring relatively frequently during the winter months with considerable floodplain inundation occurring on average six times a year. Inundation depths over the floodplain surface in the middle reaches vary from 40 cm for the mean annual flood to 70 cm for a 50 year event. Land use on the floodplain reflects the frequent occurrence of inundation and is mainly permanent pasture for cattle grazing, which is restricted to the summer months, together with hay and silage production. The National Rivers

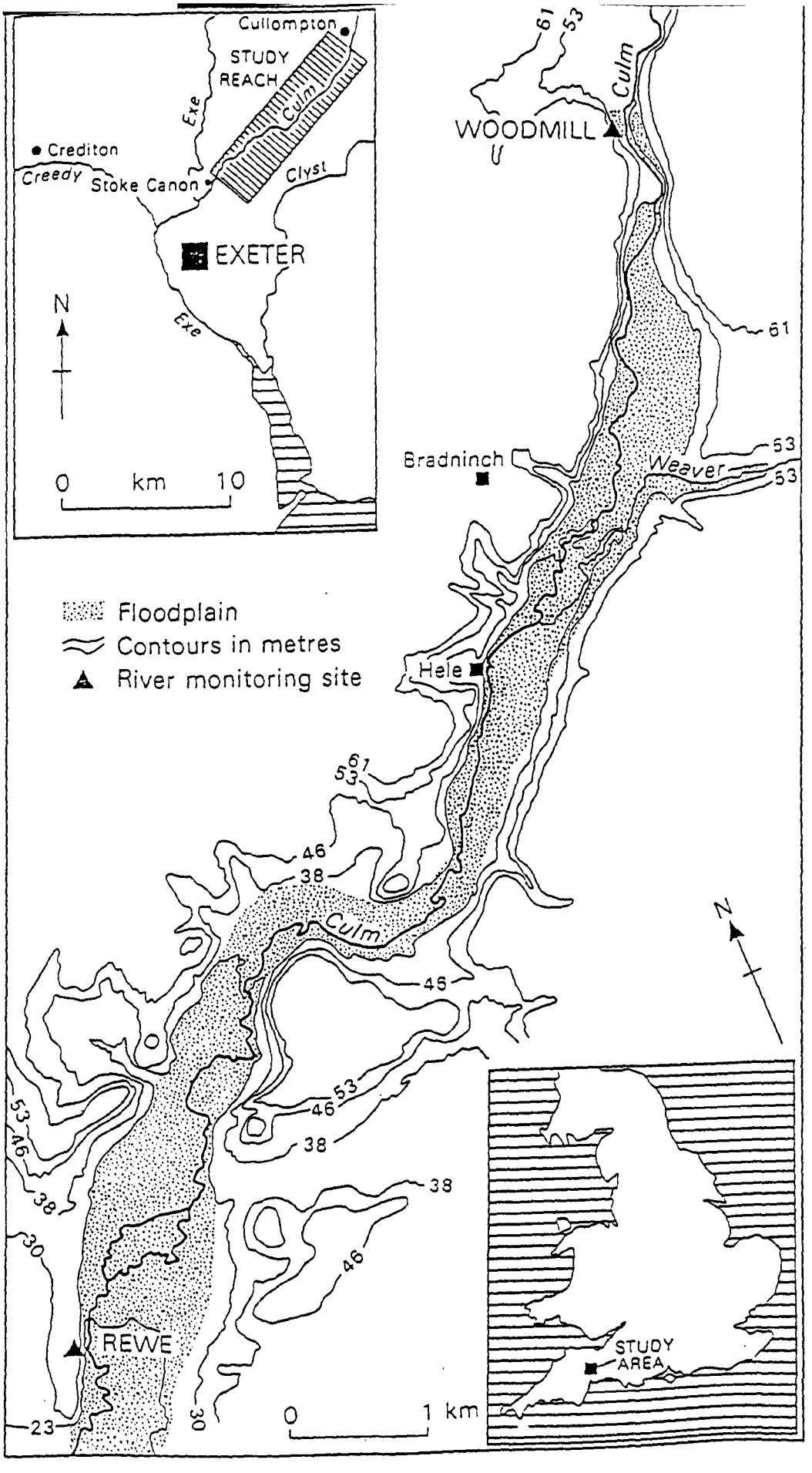

Figure 3.1: **Location of the River Culm study reach, Devon, UK**

Authority has gauging stations sited at Woodmill (upstream) and Rewe (downstream), the reach length between them is 11 km.

3.2.2.2 Data availability

The required topographic data was available from small scale topographic maps; 1:2500 and 1:25 000 scale maps were available for the area covered by the reach. In addition to this, a map of the probable maximum flood inundation was available together with air and ground photographs for selected events.

The water stage recorders at the two stations were capable of providing data at 0.25 hourly intervals. Stage-discharge conversion was based on the use of an empirically-derived rating curve at both sites. Since out-of-bank inundation was to be considered in this investigation, it was important that the full compound channel rating curve was available. A multi-function rating curve had been established by the NRA for the whole cross-section at Woodmill and has been found by Bates et al. (1992) to be reasonably accurate. They established a new stage-discharge relationship for the gauge at Rewe in addition to the original single-function rating curve which was found to be applicable only to in-bank flows. The new curve was established by linearly extrapolating the channel component of the flow and estimating the flows associated with floodplain inundation then adding these to the extrapolated rating curve for in-channel flows. The floodplain flows were estimated from detailed topographic surveys and the Manning formulae using the slope-area technique. The final form of the rating curve is shown together with the original in Figure 3.2 and consists of three parts, each with a specific equation developed for it. Due to the low gradient of the flow line, it was suggested that this rating curve was likely to be only approximate and could involve errors of $\pm 20\%$. Data exist for several events with different return periods.

In addition, a number of detailed investigations of floodplain sedimentation have been carried out for the reach (e.g.: Walling and Bradley, 1989; Walling et al., 1991). Suspended sediment concentrations are continuously monitored at the upstream and downstream ends of the reach. Comparison of the suspended sediment loads passing the upstream and downstream gauging stations allowed the conveyance losses during individual flood events to be examined. In addition, deposition rates on the floodplain have been monitored directly using sediment traps and Caesium-137 inventories of floodplain sediments (Walling et al., 1991). Such information was useful for internally validating the model.

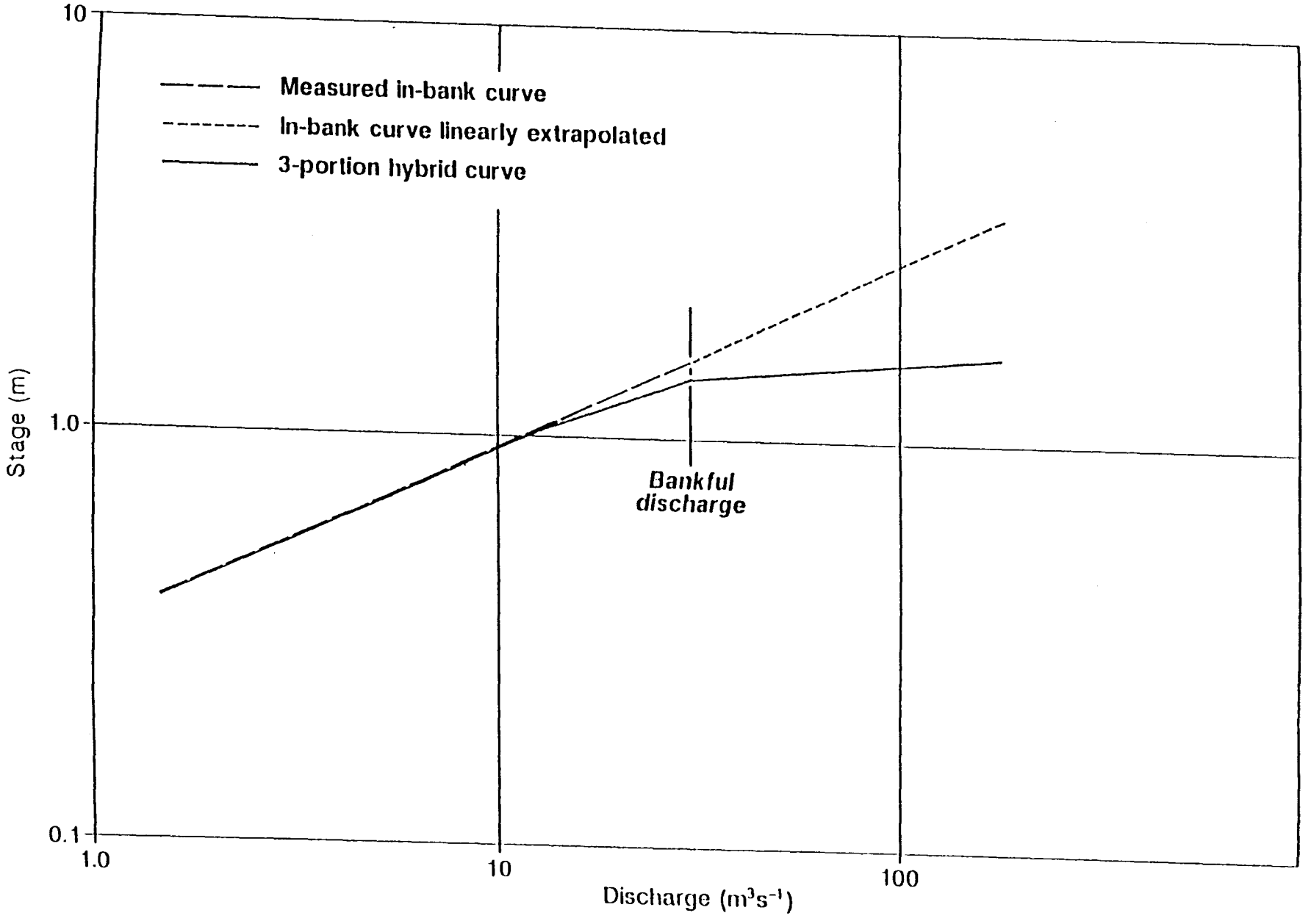

Figure 3.2: Stage-discharge rating curves derived for the River Culm gauging station at Rewe (after Bates at al., 1992)

Rainfall data is available for several hourly and daily gauges sited within the Culm catchment for the events for which flow data is available. The two nearest gauges are sited at Hemyock and Kentisbeare although neither of these are sited within the area of the hillslopes bordering the study reach. The use of the available rainfall data as an input to the hillslope hydrology model is described in Chapter Four.

3.3. MODEL SELECTION AND DESCRIPTION OF THE RMA-2 FINITE ELEMENT MODEL

3.3.1 Required model attributes

For this application there were a number of characteristics which the floodplain inundation model was required to fulfil. First because the model was to be used in coupled simulations it was desirable that the addition of inflows along the edge of the reach should be relatively easy to implement and not involve major changes to the model structure. Another required attribute concerned the range of reach lengths to which the model could be applied. In view of the fact that the Culm reach was 11 km long, a fundamental demand made by the application was the suitability of the model for longer reach lengths. Ideally a model which had previously been applied to a longer reach would be selected. A further issue concerned the degree of spatial representation over the surface of the floodplain. As part of the investigation, the effect of hillslope inflows on water depths at individual nodes and changes in inundation extents was examined. With these requirements in mind a model capable of producing predictions of depth and flow field behaviour over the surface of the floodplain was needed. Related to this was the issue of the representation of the inundation flow boundary. In Chapter Two the reasons for selecting a 2-dimensional floodplain inundation model were discussed. The inundation boundary is represented in several ways by 2-dimensional models. The simplest methods utilise a deformable grid from which elements which are not fully saturated are excluded. This means that the resolution of the flow boundary representation is only as fine as the element resolution. This can be increased by using narrow elements for areas close to the channel. More sophisticated methods use an interpolation function and allow partially inundated elements to remain within the solution. Since part of the sensitivity analysis was to involve examining changes in the inundation extent, a method of representing this boundary which allowed as fine a resolution as possible was needed. The final requirement made by the application was for a model which

could be applied to a complex reach such as the Culm which has a varied floodplain topography and includes a bifurcation section, a mill race and a railway embankment. The next section describes the features of the 2-dimensional finite element model of floodplain inundation, RMA-2. From the following discussion it will become apparent that previous developments made this model ideally suited to the requirements of this application. Features of the model include the ability to accept input along the edge of the FEM, the high resolution used for flow boundary representation and the fact that the model has successfully been applied to longer reach lengths.

3.3.2 *The RMA-2 finite element model*

RMA-2 was originally developed for the US Army Corps of Engineers to study circulation in lakes, reservoirs and estuaries (Norton et al., 1973; King et al., 1975; King, 1977). A set of mathematical models was devised that would simulate within acceptable and demonstrated limits of accuracy the hydrodynamic behaviour of an operating impoundment such as that created by the Lower Granite Lock and Dam in California. The models were capable of use under a wide range of operating policies and hydrological conditions and were conceived and formulated in such a way that they would provide the hydrodynamic information necessary for the subsequent water quality investigations carried out for the Lower Granite Reservoir.

The model solves the depth integrated Reynold's equations for two-dimensional free-surface flow in the horizontal plane using the finite element technique. It can be applied to steady and unsteady flows. The finite element formulation of RMA-2 allows boundary roughness and solution resolution to vary spatially to accurately reflect topography. King and Norton (1978) describe the application of RMA-2 to the convergent-divergent flow occurring for the Tallahalla Creek in Mississippi. Here the floodplain was constricted by a bridge crossing and elements with curved sides were used and were found to greatly improve the model predictions. These features make the model ideally suited to the complex nature of the Culm reach. The model also provides for a wide variety of boundary conditions, including stage hydrographs, discharge hydrographs and rating curves.

RMA-2 has been applied to a variety of different situations, mainly to large estuaries (King and Roig, 1988; McAnally et al., 1984a, 1984b; McArthur et al., 1987) or to the prediction of local flow patterns near structures (Gee and Wilcox, 1985). More recent developments have included the modification of the shallow water equations to reflect partially wet or fully dry conditions over an element allowing an improved

representation of the flow boundary (King and Roig, 1988) and application of the model to longer reach lengths (Gee et al., 1990). These are described in the following sections.

3.3.2.1 Previous model developments I: The RMA-2 side inflow capability

This facility is a feature originally created within the RMA-2 framework to model tributary flows along the banks of a river (King, pers. comm. 1992). The application used a finite element mesh composed of one-dimensional elements to which inflows were applied as a flow per unit length along the length of the elements. For example, if a flow of 'q' was entered for an element of length 'l' the total inflow applied was 'l*q' and was uniformly distributed along the length of that element. Inflows were also applied by King to two dimensional elements where the corresponding units became flow per unit area. In this case, when flow was specified as 'p' for an element of area 'a' a total inflow of 'a*p' was applied in a uniformly distributed fashion to the element. The actual units of 'p' are $m^3/sec/m^2$ which works out to be m s^{-1}. This side flow is analogous to rainfall on the surface of the element and was also used for a case where there was a requirement to assume rainfall for two dimensional elements. The side inflow capability allows side inflows to vary from element to element as well as from time step to time step. Although the option has been tested, it has not previously been used to apply inflows produced by hillslopes bordering the reach.

3.3.2.2 Previous model developments II: Improved representation of the flow boundary

Applications of RMA-2 using a fixed boundary were found to be unsatisfactory for shallow areas that were alternately flooded and exposed during simulation. To alleviate this, King et al. (1986) proposed an 'element elimination' procedure for simulating the inundation and evacuation process which was implemented through the use of a deformable grid. Within this solution technique, an element was dropped from the finite element grid when the water depth at one node in the element fell below a minimum depth. Elements re-entered the solution when every node associated with that element was at the minimum depth. Convergent solutions were obtained by this method although mass conservation was not consistent from iteration to iteration or from time step to time step. Using this procedure, the residual water volume on a drying element was abruptly removed from total system volume. Similarly when a dry element became wet again, a sufficient volume of water was added to the system to ensure all the nodes achieved the minimum depth. The disadvantages of the method were minimised by defining small elements that

followed the bathymetric contours. However, when this method was applied to closed estuaries, significant mass conservation errors were observed. When this method was applied to steady state simulations, a different error occurred. Mass was conserved although the elimination of the gradually sloping elements defining the banks caused computed velocities to be higher than those observed in the prototype model.

An improved representation of the flow boundary enabled by the 'Marsh Element Parameter' was developed by Roig and King (1988) and allows elements to slowly change between the wet and dry states. Partially dry elements are thus permitted to remain within the computational grid until all the nodes of a given element are dry, thus minimising changes in mass continuity as dry elements are removed from the solution. Dry elements re-enter the computation as soon as one node associated with an element meets a minimum depth criterion. This method has been found to be useful for gently sloping tidal flats and dissected marshes where the marsh channel dimensions are much smaller than main estuary channels.

The marsh element parameter is implemented by maintaining an artificial water depth over the surface of an element. A coefficient is used to scale this simulated flow volume to the true water volume residing on a partially wet element during each time step. This coefficient is conceptually similar to the porosity in Darcy flow through porous media. In Darcy flow, the porosity represents the proportion of the flow domain available for fluid flow. In this case, the elemental volume coefficient reflects the proportion of the simulated flow domain available for flow over the partially wet element. Whilst a completely dry element will remain part of the continuum, in practice these elements are removed from the computation scheme. The user is required to specify a bottom elevation below the lowest possible water surface elevation and control the flowing section by pre-defining the volume coefficient. This coefficient is then a function of the water surface elevation. The volume coefficient is now a nodal variable. In this case, the coefficient is always less than 1 within the de-watering element during the simulation period and equal to 1 in elements where the area is completely inundated during the simulation. Figure 3.3 shows this concept schematically with a typical distribution for the volume coefficient.

3.3.2.3 *Previous model developments III: Application to longer reach lengths*

There has been a general lack of attention to large scale floodplain flow modelling (for reaches of the order of 16-32 km). Gee et al. (1990) describe an application to a 24 km

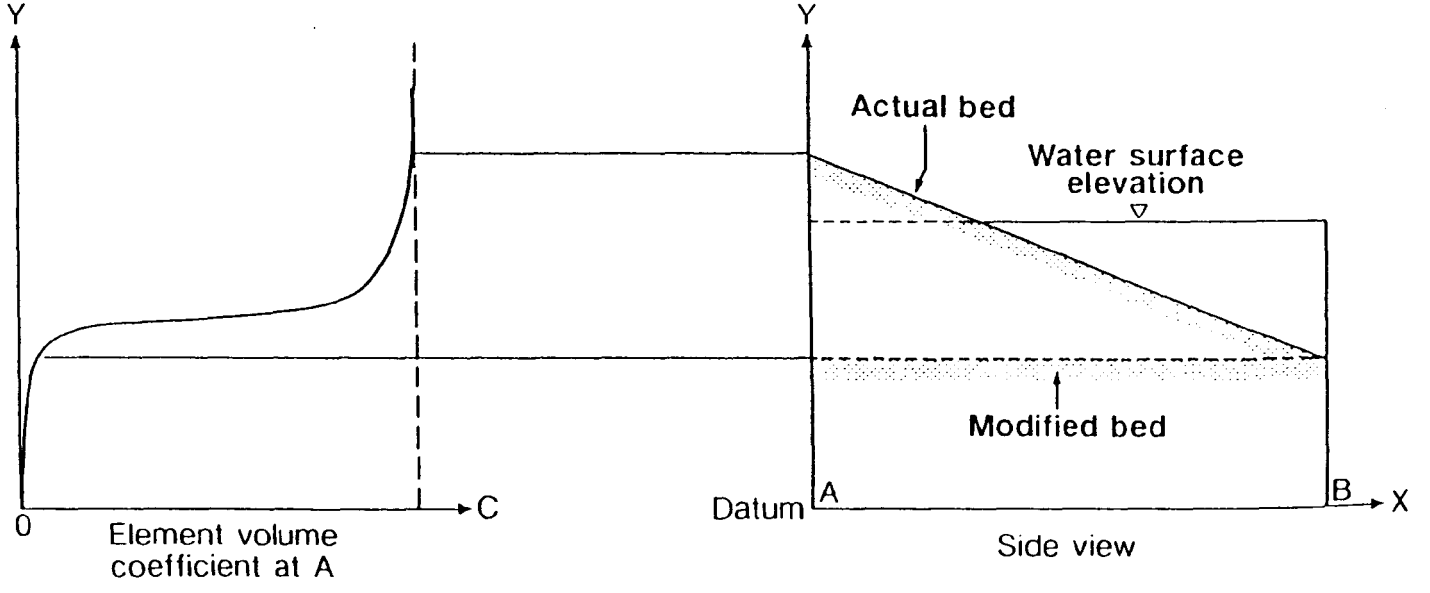

Figure 3.3: Description of the element volume coefficient (after Gee et al., 1990)

reach of the River Fulda in West Germany. This was selected because of high quality flood inundation data, rating curve and flow records. A finite element mesh was set up for the reach. This comprised 2660 nodes defining 860 triangular and quadrilateral elements with the channel represented by a strip 2 elements wide. The investigation showed that RMA-2 may be used successfully for estimating the depth and lateral extent of inundation at this scale. The stability of solutions for wetting and drying of large areas was greatly improved by use of the 'marsh' element option discussed in the previous section.

3.4. STRUCTURE OF THE RMA-2 FINITE ELEMENT MODEL

3.4.1 Governing equations

Three sets of equations are formed and solved simultaneously by RMA-2 for unsteady fluid flow. These are the turbulent analogy of the Navier-Stokes equations (known as the phenomonologic motion equations), the continuity equation and the convection-diffusion equation. All these equations include appropriate friction terms (bottom and wind) plus Coriolis effects.

Continuity Equation

In Chapter One, the derivation of the volumetric continuity equation for mean turbulent flow was described. The equation ensures continuity of mass and was found to have the form:

$$\frac{\partial \bar{u}}{\partial x}+\frac{\partial \bar{v}}{\partial y}+\frac{\partial \bar{w}}{\partial z}=0 \qquad 3.1$$

The bar notation indicates the averaging process.

Momentum Equations

The Reynold's equations are shown below; an outline of their derivation was given in Chapter One:

$$\bar{\rho}\left(\frac{\partial \bar{u}}{\partial t}+\bar{u}\frac{\partial \bar{u}}{\partial x}+\bar{v}\frac{\partial \bar{u}}{\partial y}+\bar{w}\frac{\partial \bar{u}}{\partial z}\right)=-\frac{\partial \bar{p}}{\partial x}+\mu\left(\frac{\partial^2 \bar{u}}{\partial x^2}+\frac{\partial^2 \bar{u}}{\partial y^2}+\frac{\partial^2 \bar{u}}{\partial z^2}\right)-\bar{\rho}\left(\frac{\partial \overline{u'u'}}{\partial x}+\frac{\partial \overline{u'v'}}{\partial y}+\frac{\partial \overline{u'w'}}{\partial z}\right) \quad 3.2$$

$$\bar{\rho}\left(\frac{\partial \bar{v}}{\partial t}+\bar{u}\frac{\partial \bar{v}}{\partial x}+\bar{v}\frac{\partial \bar{v}}{\partial y}+\bar{w}\frac{\partial \bar{v}}{\partial z}\right)=-\frac{\partial \bar{p}}{\partial y}+\rho g+\mu\left(\frac{\partial^2 \bar{v}}{\partial x^2}+\frac{\partial^2 \bar{v}}{\partial y^2}+\frac{\partial^2 \bar{v}}{\partial z^2}\right)-\bar{\rho}\left(\frac{\partial \overline{u'v'}}{\partial x}+\frac{\partial \overline{v'v'}}{\partial y}+\frac{\partial \overline{v'w'}}{\partial z}\right) \quad 3.3$$

$$\bar{\rho}\left(\frac{\partial \bar{w}}{\partial t}+\bar{u}\frac{\partial \bar{w}}{\partial x}+\bar{v}\frac{\partial \bar{w}}{\partial y}+\bar{w}\frac{\partial \bar{w}}{\partial z}\right)=-\frac{\partial \bar{p}}{\partial z}+\mu\left(\frac{\partial^2 \bar{w}}{\partial x^2}+\frac{\partial^2 \bar{w}}{\partial y^2}+\frac{\partial^2 \bar{w}}{\partial z^2}\right)-\bar{\rho}\left(\frac{\partial \overline{u'w'}}{\partial x}+\frac{\partial \overline{v'w'}}{\partial y}+\frac{\partial \overline{w'w'}}{\partial z}\right) \quad 3.4$$

These equations are similar to the Navier-Stokes equations, also discussed in Chapter One, with the exceptions that an additional term has been included to the viscous forces due to the turbulent fluctuations and that the other forces are expressed in terms of their mean values. The turbulent fluctuation forces (the final terms on the right hand side of the Reynold's Equations) are often referred to as the "Reynold's stresses" and are the subject of much research in advanced fluid mechanics. A simplified approach to the evaluation of the Reynold's stresses, the Boussinesq approximation, has been incorporated into the RMA-2 structure. Boussinesq has introduced the concept of a turbulent exchange coefficient, ε, which is dimensionally equal to the coefficient of viscosity, μ. In the case of uniform flow in X direction, this exchange coefficient is defined by:

$$\overline{\rho u'v'}=-\varepsilon\frac{\partial \bar{u}}{\partial y} \quad 3.5$$

Using this definition, the fluid shear stress becomes:

$$\tau=(\mu+\varepsilon)\frac{\partial \bar{u}}{\partial y} \quad 3.6$$

From this definition, it can be seen that the Reynold's stress terms would act similarly to the viscous friction term with their effect being added linearly. Experimental data has shown that μ and ε are of different orders of magnitude and in general $\varepsilon >>> \mu$. Thus for engineering purposes it is possible to make the approximation:

$$\tau=\varepsilon\frac{\partial \bar{u}}{\partial y} \quad 3.7$$

When this approximation is inserted into the Reynold's equations, the resultant form is the basic form of the general momentum equations which are sometimes referred to as the phemonologic motion equations. These equations have been incorporated into the RMA computer models with the addition of terms to describe the effects of wind

and bottom stress and the Coriolis Force. These additional terms were included since the equations were derived for an elemental fluid volume which was assumed to be contained within a much larger fluid mass. In order to make a realistic application of these equations, additional terms must be added to reflect the additional constraints of the real, opposed to the ideal world. The complete form of the equations incorporated in the RMA-2 structure is shown below. For reasons of clarity, the bar average notation has been dropped although the values of the independent variables represent their mean condition.

$$\rho\left(\frac{\partial u}{\partial t}+u\frac{\partial u}{\partial x}+u\frac{\partial u}{\partial y}+w\frac{\partial w}{\partial z}\right)=-\frac{\partial p}{\partial x}+\varepsilon_x\left(\frac{\partial^2 u}{\partial x^2}+\frac{\partial^2 u}{\partial y^2}+\frac{\partial^2 u}{\partial z^2}\right)-\rho\Omega w-F_{s_x}+F_{b_x}=0 \qquad 3.8$$

$$\rho\left(\frac{\partial v}{\partial t}+u\frac{\partial v}{\partial x}+v\frac{\partial v}{\partial y}+w\frac{\partial v}{\partial z}\right)=-\frac{\partial p}{\partial y}-\rho g+\varepsilon_y\left(\frac{\partial^2 v}{\partial x^2}+\frac{\partial^2 v}{\partial y^2}+\frac{\partial^2 v}{\partial z^2}\right)+F_{b_y}=0 \qquad 3.9$$

$$\rho\left(\frac{\partial w}{\partial t}+u\frac{\partial w}{\partial x}+v\frac{\partial w}{\partial y}+w\frac{\partial w}{\partial z}\right)=-\frac{\partial p}{\partial z}+\varepsilon_z\left(\frac{\partial^2 w}{\partial x^2}+\frac{\partial^2 w}{\partial y^2}+\frac{\partial^2 w}{\partial z^2}\right)+\rho\Omega u-F_{s_z}+F_{b_z}=0 \qquad 3.10$$

Where:

ε_x, ε_y and ε_z = The turbulent exchange coefficients in the X, Y and Z directions

$-\rho\Omega\overline{w}$ = Coriolis acceleration in the X direction

$+\rho\Omega\overline{u}$ = Coriolis acceleration in the Z direction

$F_{s_x}, F_{s_y}, F_{s_z}$ = Surface force due to wind stress at fluid-air interface in X, Y and Z directions[1]:

$F_{b_x}, F_{b_y}, F_{b_z}$ = Force due to the bottom stress caused by friction developed at the boundary between the moving fluid and the fixed boundary[2].

---

[1] $F_s = \tau_s A_s$

where: A_s = the area over which the wind stress is effective

and $\tau_s = \zeta V_a^2$

where: ζ = an empirical constant

V_a = the surface wind speed

[2] The effective force, F_b, has the form:

$$F_b = \tau_b A_b$$

where: A_b = the area over which the bottom stress is effective

and along the X axis, the bottom stress, τ_b, is:

$$\tau_b = \rho g C^{-2}\overline{u}|\overline{u}|$$

where: C = Chezy's coefficient

Convection-Diffusion equation

The continuity equation shown earlier in this section is valid for laminar and mean turbulent flow as long as the fluid is incompressible and there is no change in fluid density due to changes in fluid pressure. The derivations are therefore based on volume continuity. The type of applications for which RMA-2 was developed require that the fluid density be variable in both space and time, although the basic medium is always treated as incompressible fluid. To develop the movement of the density field the *Mass continuity* or *convection-diffusion* equation was applied. The derivation of the equation for laminar mass continuity is identical to that for the *volumetric* continuity equation for laminar flow except that the term β has been added to account for any changes in the fluid density resulting from internal or external influences such as external heating or internal chemical or biological activity and is restated in slightly modified form as:

$$\frac{\partial \rho}{\partial t} + \frac{\partial(\rho u)}{\partial x} + \frac{\partial(\rho v)}{\partial y} + \frac{\partial(\rho w)}{\partial z} + \beta = 0 \qquad 3.11$$

The average flow and average definition of the fluctuating component becomes:

$$\frac{\partial \rho}{\partial t} + \overline{u}\frac{\partial \rho}{\partial x} + \overline{v}\frac{\partial \rho}{\partial y} + \overline{w}\frac{\partial \rho}{\partial z} + \frac{\partial}{\partial x}(\overline{\rho' u'}) + \frac{\partial}{\partial y}(\overline{\rho' v'}) + \frac{\partial}{\partial z}(\overline{\rho' w'}) + \overline{\beta} = 0 \qquad 3.12$$

Cross product terms such as ρu represent the flux of mass due to turbulent fluctuations. This is assumed to be proportional to the concentration gradient meaning that the following can be substituted:

$$\overline{\rho' u'} = -D_x \frac{\partial \rho}{\partial x} \qquad 3.13$$

$$\overline{\rho' v'} = -D_y \frac{\partial \rho}{\partial y} \qquad 3.14$$

$$\overline{\rho' w'} = -D_z \frac{\partial \rho}{\partial z} \qquad 3.15$$

Where:

Dx, Dy, Dz = coefficients of turbulent mass transfer (turbulent diffusion) in the X Y and Z directions.

When these are introduced, the resultant final form is:

$$\frac{\partial \bar{\rho}}{\partial t} + \bar{u}\frac{\partial \bar{\rho}}{\partial x} + \bar{v}\frac{\partial \bar{\rho}}{\partial y} + \bar{w}\frac{\partial \bar{\rho}}{\partial z} - \frac{\partial}{\partial x}\left(D_x \frac{\partial \bar{\rho}}{\partial x}\right) - \frac{\partial}{\partial y}\left(D_y \frac{\partial \bar{\rho}}{\partial y}\right) - \frac{\partial}{\partial z}\left(D_z \frac{\partial \bar{\rho}}{\partial z}\right) + \beta = 0 \quad 3.16$$

This is the convection-diffusion equation for turbulent flow and is the form used by RMA-2.

3.4.2 *The RMA-2 solution scheme*

RMA-2 uses the finite element method. This is a numerical solution technique which is applied to sets of equations describing non-steady state situations. It was originally developed by structural analysts seeking the solution to the complex problems of stress analysis of a continuum. In the 1950s the concept of finite elements, a series of discrete polygons each interconnected at a finite number of locations, was introduced. The system being modelled is divided spatially into a number of smaller discrete elements and equations are derived from the governing partial differential equations to represent the entire region of each element. In doing this it is assumed that the unknown function varies within each element in a manner described by an interpolation function which may have a linear, quadratic or higher degree polynomial form. This technique does not place any restriction on the size or shape of elements so they may be used to represent complex shapes accurately. In the case under consideration, a detailed topographic representation of the floodplain is possible using a finite element network composed of triangles and quadrilateral elements. The elements representing the channel are relatively small, whilst for overbank areas elements are considerably larger. Ground elevations are defined at the corner nodes of each element and are assumed to vary linearly between nodes. After the inclusion of boundary conditions defining the domain within which the physical system operates, RMA-2 uses the Galerkin method of weighted residuals to solve the governing equations and provide spatially distributed values for velocity vectors and depth. The discretisation is extended by performing these calculations at a series of time steps to include the time dimension to produce these spatial results at a series of different times.

The present model formulation includes all the linear and non-linear terms usually found in the motion equations and the mathematical problem statement results in a set of unsymmetrical, non-linear equations. This set of equations is solved by the

Galerkin method of weighted residuals. The Galerkin method assumes the dependent variables vary in a prescribed manner over the surface of an element (linearly in the case of depth and quadratically for velocity). These functions are used as weighting factors to restate the governing equations in terms of specific shape functions that satisfy both the boundary conditions and the interpolation functions. The discrepancy between the true solution and that approximated by the shape functions are defined as a residual, R. The final step then forces this to zero in an average sense. This results in the development of a single equation for each node representing the sum of contributions from all the adjacent elements. These local equations are then collected into a global matrix which can be solved simultaneously using numerical integration. Due to the extreme non-linearity of the governing equations, this is achieved iteratively using the Newton-Raphson technique which has proved convergent for all problems that show reasonable answers in the initial step. To represent non steady system states, the spatially discretised finite element method needs an independent discretization of the time derivative. For this, the Crank-Nicholson finite difference procedure assumes acceleration varies linearly between time steps. The accuracy of the method depends on how well this assumption represents the physical system, although it is reasonable for problems involving gradually varied unsteady flow.

3.4.3 *Model Parameterisation*

All the model parameters, with the exception of wind velocity, are physical constants or in cases such as the turbulent eddy viscosity can be calculated automatically. In order to establish a finite element mesh for a given reach there are several data requirements; topographic data is required for the construction of the finite element mesh together with the data required to define the boundary conditions for the mathematical solution. The required topographic data can be derived from small scale topographic maps supplemented by surveyed cross-sections at upstream and downstream ends of the mesh to precisely determine the elevations of these locations. This represents the minimum level of data required to construct the mesh to an operational tolerance but additional ground surveys may be necessary in areas of insufficient topographic data. Data required to establish the upstream and downstream boundary conditions consist of an observed hydrograph at the upstream end of the reach and a stage-discharge relationship at the downstream mesh boundary of the form:

$$Q = A + B(H) \qquad 3.17$$

Where:

Q = discharge

H = stage

A = correction factor

B and C = dimensionless coefficients

Rating curves are normally already established for gauging stations, but if the section consists of more than one segment or is in some way inadequate then a single function curve can be constructed from the surveyed downstream cross-section using an appropriate technique.

A friction value is required for each element together with an element volume coefficient to determine the possible wetting and drying processes occurring over and element. The friction coefficient used is Manning's n. Each finite element is assigned to one of 10 classes of n varying between, for example, 0.03 for clear channel to 0.055 for wooded floodplain. In order to define the elemental volume coefficient, the model requires a minimum value to be set such that the depth of water maintained over each element is as small as possible and therefore a closer approximation to reality.

3.5. THE CULM APPLICATION

RMA-2 had previously been set up for the reach from Woodmill to Rewe (Bates et. al 1991). The finite element mesh for this reach was composed of 3655 nodes defining 1090 elements (Figure 3.4). In constructing the finite element mesh a number of guide lines were adhered to. The surface of the floodplain was defined by a number of irregular triangular and quadrilateral elements. Each element was defined by three or four nodes. Since the finite element method allows for irregularly shaped elements these were used to represent complex topography accurately. The channel was defined by a number of smaller elements. In the application by Gee et al. (1990), the channel cross-section was defined by two elements. In this later application, a trapezoidal section comprising 6 elements was used since the triangular section was found to produce unrealistically high channel velocities. In addition, a strip of narrow elements running each side of the channel was added to incorporate the effects of bankside roughness. The channel cross-sections used by Gee et al. and Bates et al. are shown in Figure 3.5. The FEM for the Culm included several physical features

Figure 3.4: Finite element mesh constructed for the River Culm study reach. 1 = Hele Mill; 2 = railway embankment; 3 = Silverton Mill; 4 = Channel bifurcation (after Bates et al., 1992)

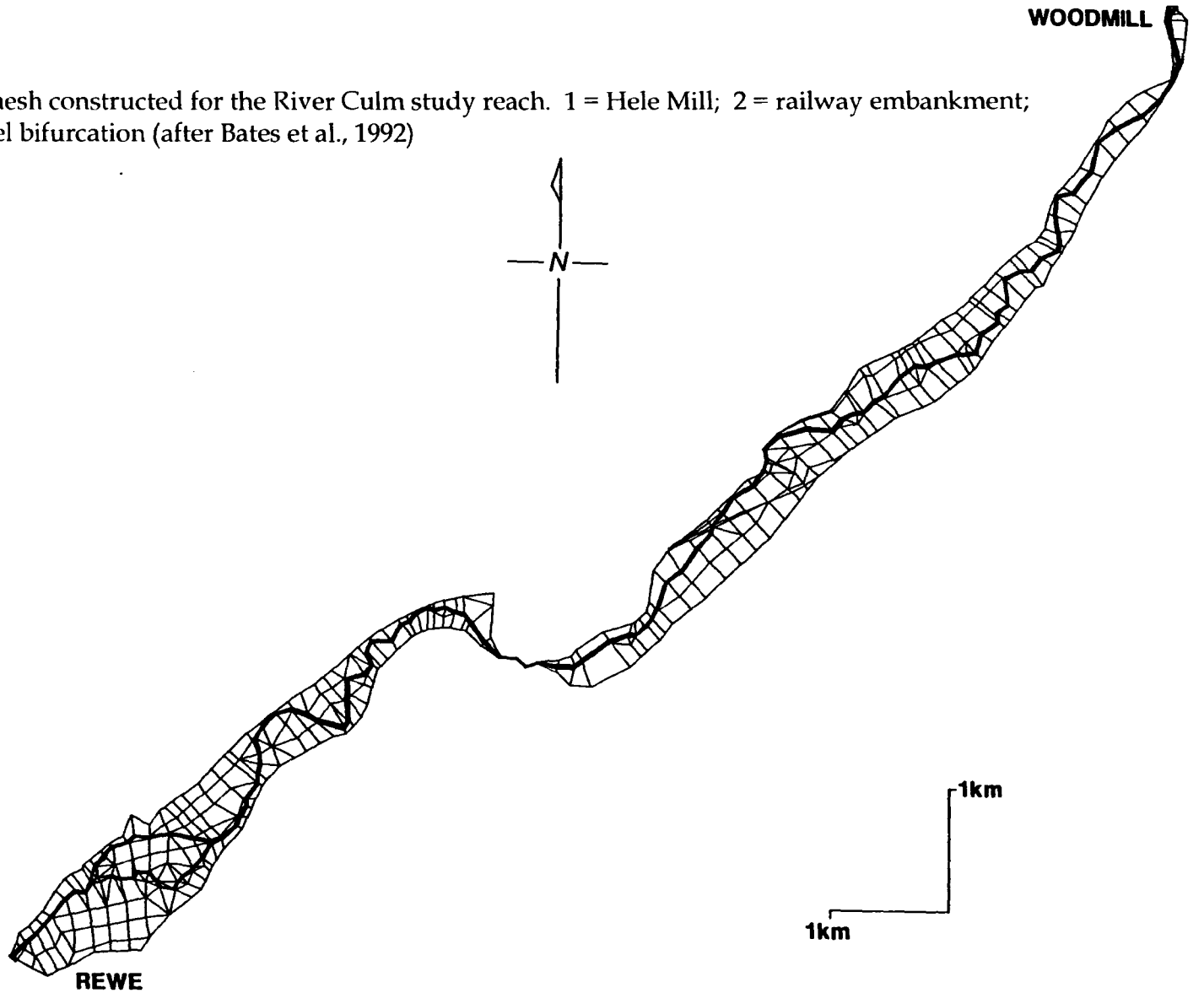

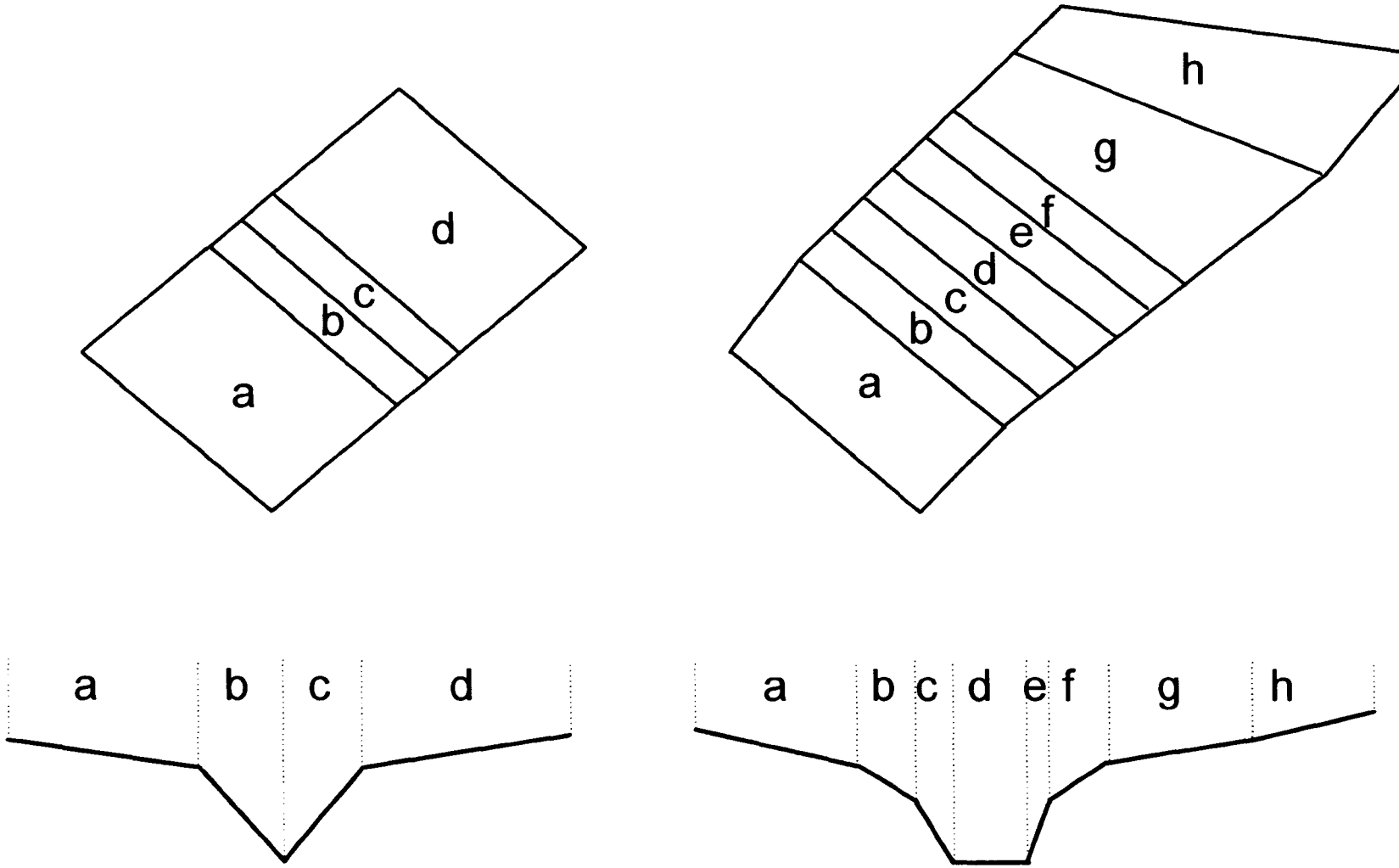

Figure 3.5: Conceptual mesh cross-sections used in RMA-2 applications. (a) Triangular channel used by Gee et al., 1990. (b) Trapezoidal formulation used by Bates et al. (1992) to enhance channel representation (after Bates et al., 1992)

including two mill races, represented as chanelised reaches. For example, the flow at Silverton was contained entirely within the channel and no floodplain elements were used. The railway embankment where the railway crosses the floodplain was modelled as a barrier across the floodplain, though was breachable by high flows. At the downstream end of the reach, within the 1 km long bifurcation section, flow was assumed to be equally divided between the two parts of the channel which flow around a topographically complex island.

A maximum element size of 150 by 150 m was set, representing a compromise between the mesh resolution required for this complex reach while maintaining acceptable computing requirements. The channel was represented by a trapezoidal section and the mesh was configured so that its longitudinal lines tended to run parallel to the channel, ensuring that the advance and retreat of floodwater occurred in a smooth fashion. A further property of the Culm mesh were lateral lines set up to cross the reach in a straight line perpendicular to the long axis to minimise the front width used in calculations which made the solution more efficient. Each element was then assigned to one of 10 roughness classes based on Manning's n. Typical values of Manning's n were derived for the whole reach using the photographic definition of roughness type established by Chow (1959).

After developing initial conditions, a dynamic model simulation was carried out using an observed input hydrograph. The model was calibrated by altering the roughness of the floodplain elements. Increasing the roughness of the floodplain elements slowed the passage of the flood wave. This was increased when the roughness of these elements was decreased. In this way, the predicted downstream hydrograph was altered until the timing of the peak was the same as the observed hydrograph at Rewe for that event.

3.6. PILOT INVESTIGATION TO EXAMINE THE EFFECT OF INFLOWS APPLIED AS AN ADDITIONAL MODEL INPUT

The pilot study involved examining the effect of inflows on a selected part of the modelled reach to find out if hillslope inflows were likely to have any impact on model predictions in terms of changes in depth and flow field behaviour. In addition, inflows were added to the reach at different rates in order to examine the potential sensitivity of the model to variation in hillslope contributions. Changes in volumetric output were not examined since, due to the shortness of the test reach, the volume of inflows applied was a very small percentage of that input at the upstream end of the

reach. It was decided first to find out if any localised effects occurred before extending the study to examine volumetric changes when inflows were applied along the whole reach from Woodmill to Rewe.

3.6.1 *Setting up and running the simulations carried out for the investigation*

3.6.1.1 *Selection of a test reach*

It was decided to examine the effects of side inflows on a short (1 km) test reach extracted from the 11 km Culm application. A short reach was favoured since this would allow several simulations to be carried out in a relatively short time period whilst it would be possible to observe any localised changes occurring as a result of the addition of inflows over the length of this reach. The 1 km long bifurcation section shown in Figure 3.6 was selected since it was a wide section of the reach where the floodplain was not always fully inundated. This allowed for the observation of any attenuation effect away from the inflow source at the edge of the reach. A special input file was set up for this test reach and using this a control simulation (no side inflows) was carried for comparison with later simulations.

3.6.1.2 *Selection of hillslope inflow data*

Hillslope output hydrographs produced by a hillslopes environment similar to that bordering the Culm reach were used to provide the input to elements along the edge of the FEM. It was decided to obtain this data from the literature rather than carry out a field measurement program as information was required for more than one event in order to compare the effect of different inflow rates. It would have been difficult and time-consuming to collect the data required for a hillslope bordering the Culm reach. It was felt that for this initial investigation using these hillslope inflows as an input to RMA-2 FEM would give a sufficient indication as to whether a more in-depth study was merited.

Few data exist in the literature for outflows along the base of hillslopes although a study carried out in 1978 by Anderson and Burt contained some suitable data. This work centred on the catchment of the Bicknoller Coombe, a small west facing valley in the Quantocks, Somerset. Unlike the Culm reach, this is an upland catchment with slope angles between 20^{o} and 30^{o} degrees compared to those of the Culm which are 8-12^{o}. The soils are freely drained brown earths 1-2m deep lying on impermeable Devonian old red sandstone. An automatic tensiometer system was used to continuously monitor the soil moisture status of a single hollow and adjacent spurs to

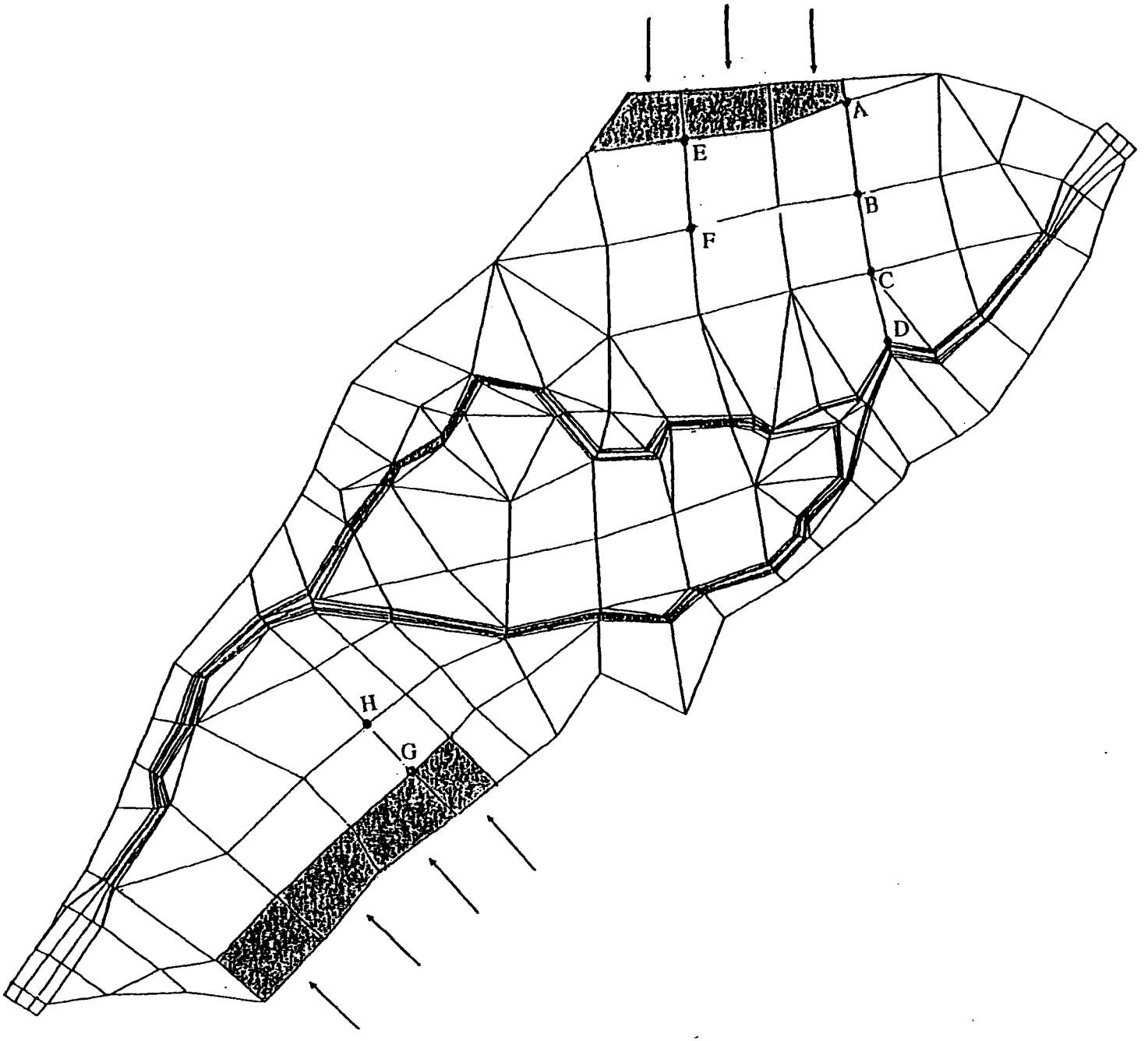

Figure 3.6: **The test reach used in the assessment of lateral hillslope contributions to floodplain flow. The shaded areas refer to those elements for which such *inflows were specified***

evaluate the role of topography in controlling throughflow generation. The results of these investigations are shown in Table 3.1.

	15.10.76	4.11.76
Total hollow reach input (l s^{-1})	16.34	2.78
Total hollow reach length (m)	190	190
Hollow discharge input per metre of channel length (cc min^{-1})	86	14.6
Total spur reach input (l s^{-1})	11.66	1.47
Total spur reach length (m)	360	360
Spur discharge input per metre of channel length (cc min^{-1})	32.4	4.1

Table 3.1: Total hollow and spur reach inputs for two storms in the Bicknoller Coombe catchment, Somerset, UK. (From Anderson and Burt 1978)

The actual inflows applied to the RMA- 2 scheme were calculated from the observed hollow and spur discharges per metre of channel length. Since only a mean discharge value was available, the inflows were applied at a constant discharge with respect to time. The nature of the Bicknoller catchment compared to the Culm hillslopes meant that these values were larger than might be expected for the Culm hillslopes. However this observed data did provide a range of inflow values which provided a useful starting point for this first pass study.

3.6.1.3 Converting the data for input to RMA-2

In order to include inflows as an input to RMA-2 simulations, it was necessary to make changes to the RMA-2 input files. These involved specifying the number of elements to which inflows were to be applied at each time step together with the dynamic simulation data for that time step. Following the data for each time step, the identifying numbers for each element were displayed together with the corresponding inflow values for individual elements in ft s^{-1}.

Seven elements at the edge of the test reach were selected and are shown shaded in Figure 3.6. Since RMA-2 required inflows expressed in feet per second, the Bicknoller data, in cc min^{-1} per metre of channel length was converted to a discharge in ft^3 s^{-1} per foot of the edge of the FEM (corresponding to the edge of the channel for the Bicknoller data). In order to distribute input between the selected elements, the discharge per unit length was multiplied by the length of each element side (these were measured from the original plot). Finally, since RMA-2 required that inputs to 2-

dimensional elements were expressed over the surface of the elements, the discharge to be applied to each element was divided by the element area.

3.6.1.4 Model simulations carried out

The mean inflow volume applied to each of the elements for the spur and hollow discharges for the two events are shown in Table 3.2.

Model simulation	SPUR/ HOLLOW	Event	Inflow volume (m s-1)
P01	N/A	N/A	0 (control)
P02	SPUR	4.11.76	0.0000015
P03	HOLLOW	4.11.76	0.0000044
P04	SPUR	15.10.76	0.0000097
P05	HOLLOW	15.10.76	0.000026

Table 3.2: Inflow volumes used in the initial investigation into hillslope inflows

These mean inflow volumes were calculated as the mean of the inflow volumes applied to the individual elements. These inflows were applied to RMA-2 by altering the input file in the manner described earlier in this section. For each of the five simulations, a new RMA-2 input file was created using the control input file as a template. The control simulation used a 1 in 1 year event which occurred between 27/1/90 and 29/1/90. The input hydrograph for this event was used as the upstream input for all five simulations.

3.6.2 Results of the initial investigation

In order to gain an insight into the effect of adding inflows to selected elements, data was extracted from the RMA-2 results file for the nodes (A-G) shown in Figure 3.6. Nodes A to D were selected to examine the attenuation effect away from the inflows source across the floodplain. Nodes E and F and G and H were also chosen. At these locations, the water depths observed in the control simulation (no inflows) were found to be consistently deeper for nodes G and H than for nodes E and F.

Localised changes in depth, inundation extent and flow field behaviour were examined from the predicted depth and flow field behaviour at these nodes. For each of the five simulations shown in Table 3.2, at the selected nodes and at each time step, the water depth and resultant velocity were extracted from the RMA-2 results file. Depth hydrographs for nodes E, F, G and H were plotted for each of the five simulations and are shown in Figure 3.7. Specific flow hydrographs plotted for nodes

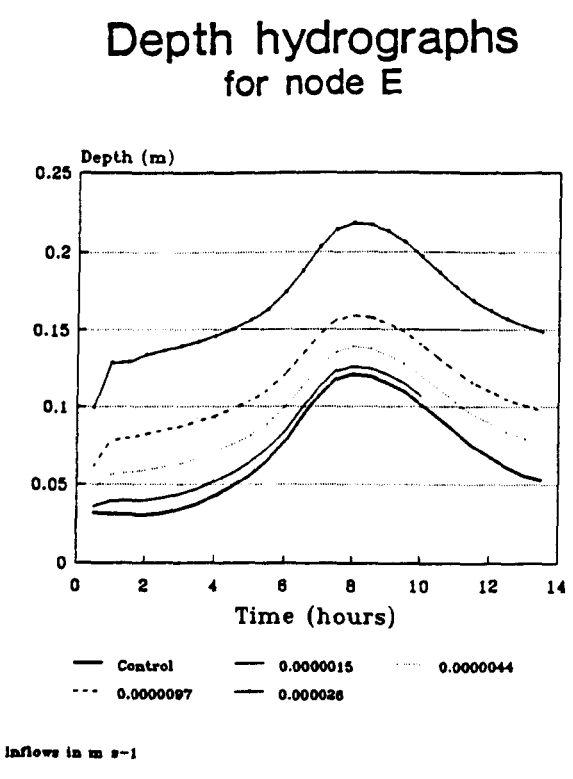

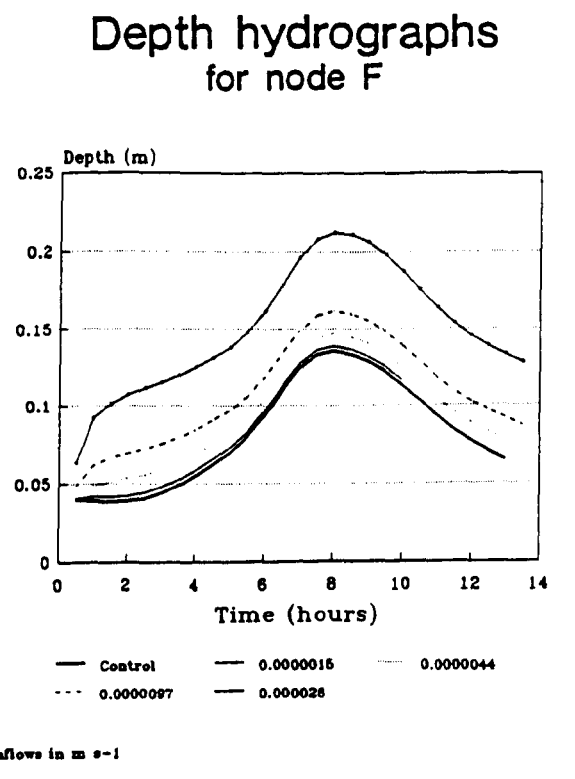

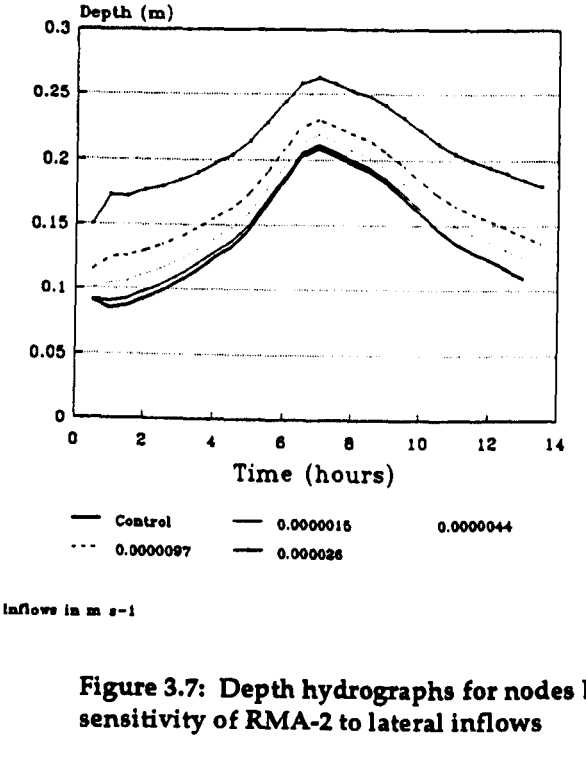

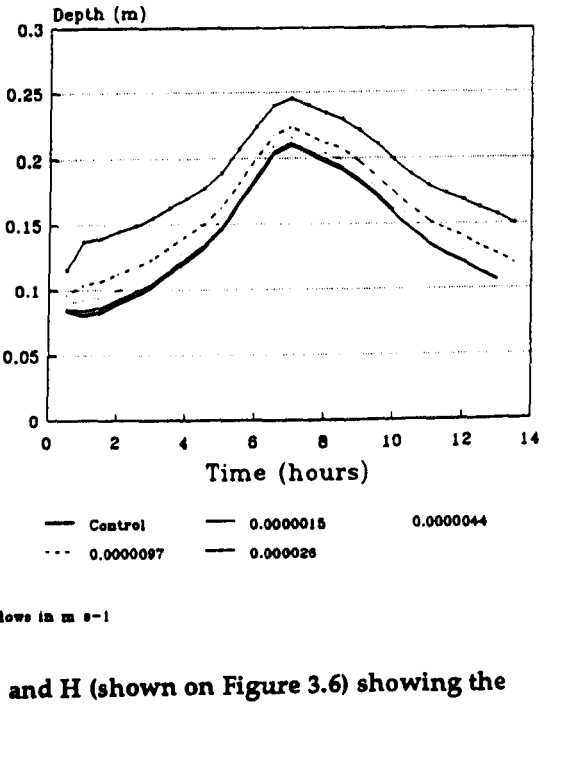

Figure 3.7: Depth hydrographs for nodes E, F, G and H (shown on Figure 3.6) showing the sensitivity of RMA-2 to lateral inflows

A, B, C and D are shown in Figure 3.8. The specific flow at a given time step for a particular node is the product of the depth and resultant velocity calculated for that node. This value gives a good indication of the flow field behaviour.

Examination of the depth and specific flow hydrographs showed that the timing of the hydrograph peak at all these nodes was unaffected by the addition of inflows. In addition the hydrograph shape was only slightly altered, besides the obvious upward transposition. Comparison of the depth hydrographs for nodes E and F and nodes H and G showed that the effect of inflows was greater for elements which had initially shallower water depths over their surface. This could also have been due to the fact that nodes E and F were downstream of two elements to which inflows were applied compared to only one for the case of G and H. From the specific flow hydrographs for nodes A, B, C and D it can be seen that adding inflows at the edge of the mesh had a significant effect. This was attenuated away from where the flow was added towards the direction of the channel.

3.6.3 Arguments for continuing the investigation

In this feasibility study, the RMA-2 side inflow capability was implemented to allow for the addition of lateral hillslope inflows as an additional input to RMA-2. Also some of the initial questions regarding the significance of this extra input have been answered. During the course of the pilot investigation the addition of inflows to the seven selected elements was not found to cause any model instability. The results from these model simulations have shown that a significant localised effect was caused by inflows in terms of depth, inundation and flow field behaviour. Whilst many questions remain unanswered at this stage, this initial study has shown that under certain circumstances hillslope inflows probably have an important impact on the extent and depth of floodplain inundation.

In this pilot investigation, inflows were added only to selected elements at the edge of the reach. This did not allow for an examination to be made of the effect inflows had on the outflow volume at the downstream end of the reach. Even had inflows been applied along the edges of the test reach, the total volume applied would have only formed a very small percentage of the volume entering the upstream end of the reach. If the whole reach from Woodmill to Rewe was considered, the volume of water contributed as inflows could potentially form a significant percentage of the reach inflow hydrograph. The initial results have demonstrated that inflows can have a localised effect on the depth and flow field behaviour of inundation water on the

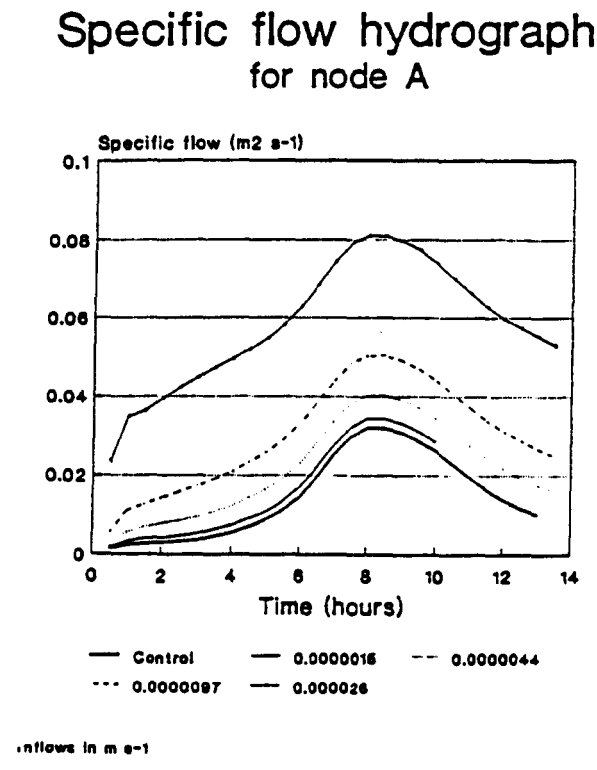

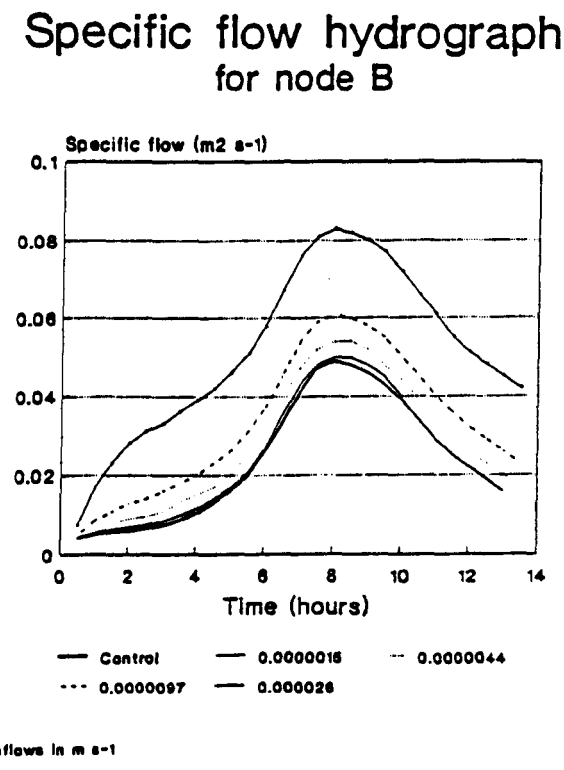

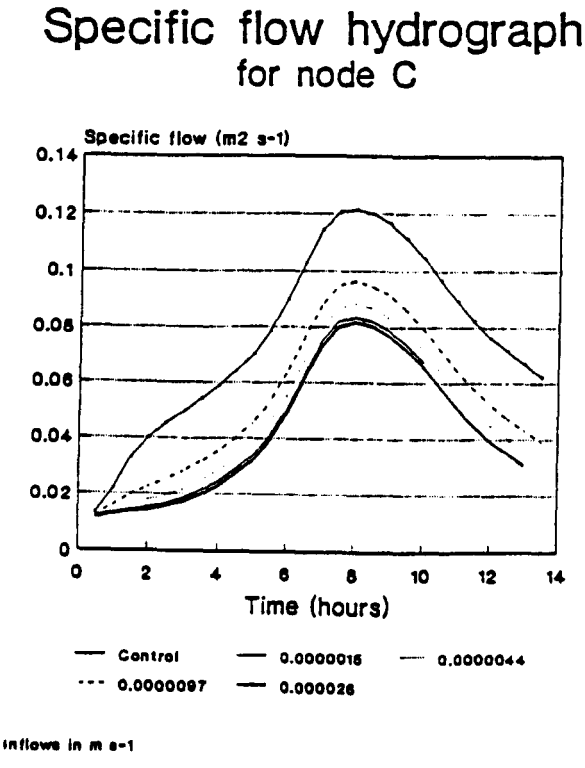

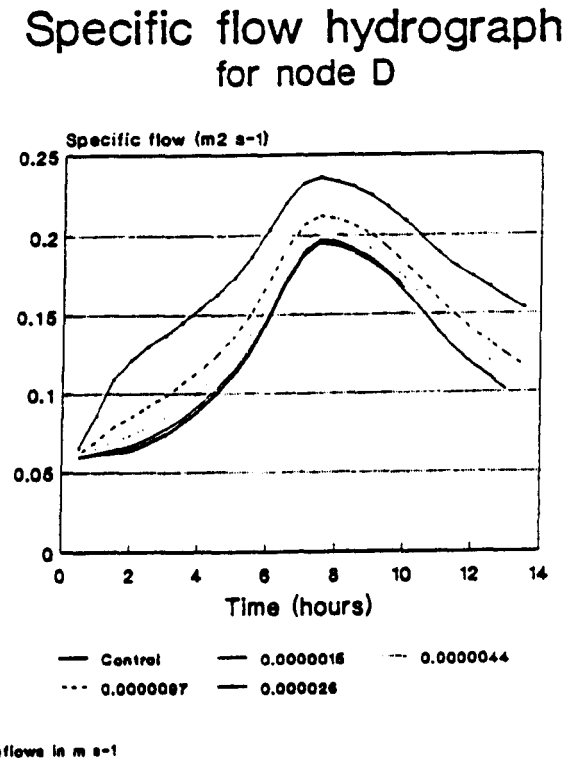

Figure 3.8: Specific flow hydrographs for nodes A, B, C and D showing the sensitivity of RMA-2 to lateral inflows

floodplain. There is a need to examine these effects in further detail through looking at changes in inundation patterns and water depth over the whole reach.

The importance of temporal variability and timing of inflow contributions is also not known since the inflows were applied at a constant rate with respect to time. Although a range of different inflow values were applied to the test reach it was not yet known how these different inflow rates relate to the range of hillslope-floodplain environments which might be expected to occur.

3.7. EXTENDING THE FINITE ELEMENT MESH

3.7.1 The reason for extending the application reach downstream

A problem associated with the RMA-2 application to the Woodmill to Rewe reach was the backing up of water observed at the downstream end of the reach.

Figure 3.9 shows a UNIRAS plot of the water depths observed at the downstream end of the reach at peak outflow discharge. The length of reach shown is approximately 1 km long and includes the bifurcation section. From this, it can be seen that a backing up of water occurred at the downstream end of the modelled reach. The boundary condition at the downstream end of the modelled reach was determined by the stage-discharge relationship provided for the Rewe gauge. The discharge exiting the reach at each time step was determined by the predicted stage at that time step using this relationship. The fact that during RMA-2 simulations water was backing up at the downstream end of the reach could have been caused by an error in the stage-discharge relationship. In other words, the discharge predicted using this relationship for a given stage may have been lower than that which would actually be observed. This would result in a backing up of water at the downstream end of the reach. In the absence of a more accurate stage-discharge relationship it was decided to extend the reach downstream, establishing a boundary condition at the new downstream end of the reach. In this way, the predictions made at Rewe could be examined in the absence of a backing up effect at that point. From the plot it can be seen that effect does not extend very far back upstream. The finite element mesh was therefore extended a further 3 km downstream to Stoke Cannon (see inset of Figure 3.1) to ensure the backing up effect was removed at the Rewe gauge. A new downstream boundary condition was established at Stoke Cannon although validation of the model

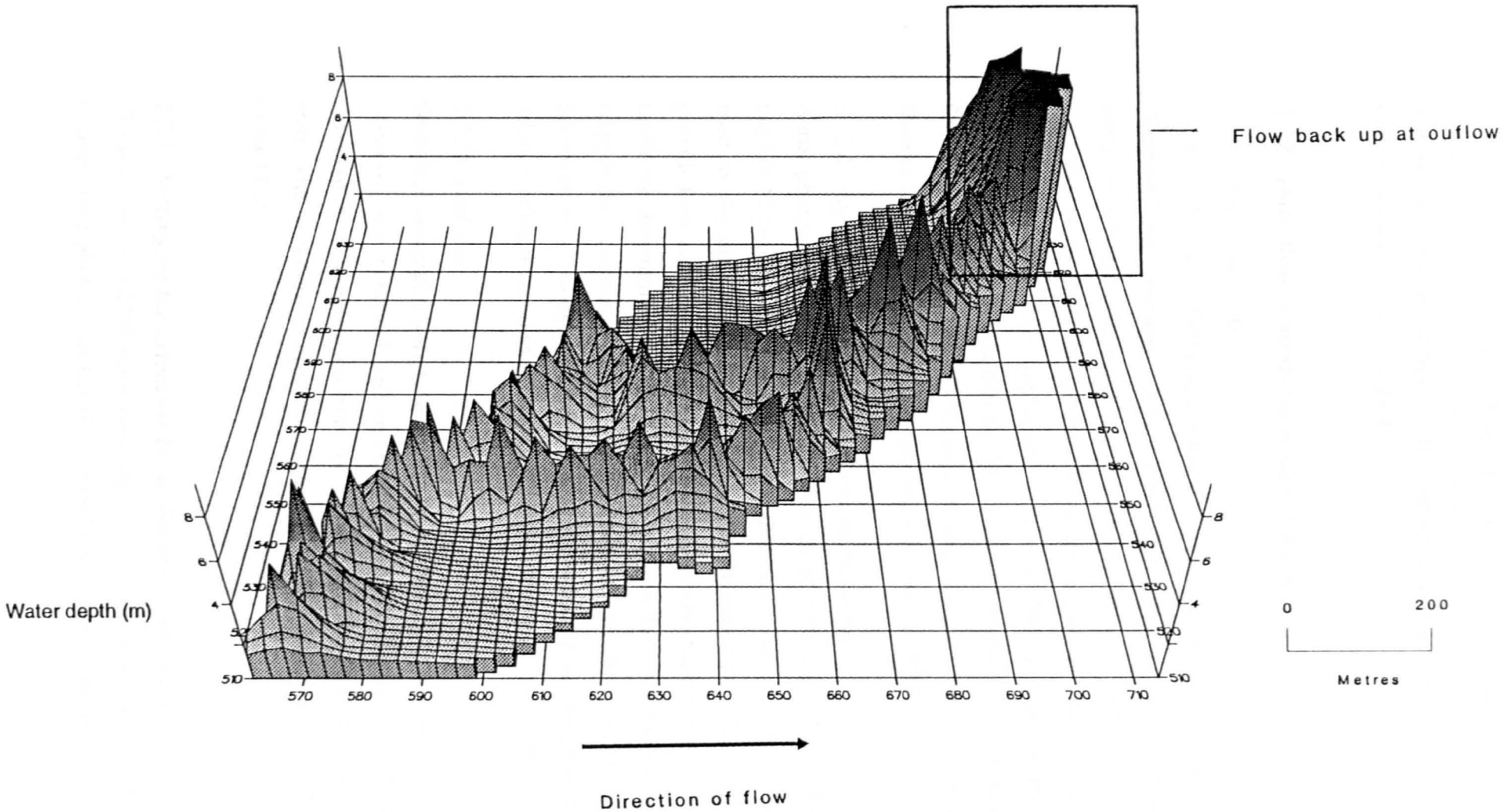

Figure 3.9: Uniras plot of observed depths at the downstream end of the reach to show the backing up effect which was seen at Rewe (after Bates, 1993)

was still carried out at Rewe. The set-up of RMA-2 for this new Rewe to Stoke Cannon section is now described.

3.7.2 *Data Requirements for mesh extension*

3.7.2.1 Topographic data

Ordnance Survey 1:2500 maps of the area were used to establish the location of river channels, large drainage channels, roads and railways, built up areas and wooded areas. Spot heights and bench marks were also extracted from these maps. Since the OS 1:2500 series maps do not show topographic contours, these were extracted from the OS 1:25,000 maps to supplement the spot heights and bench marks obtained from the 1:2500 maps. In addition a 1:2500 map of the Stoke Cannon Flood Alleviation Scheme was provided by the National Rivers Authority South Western Region. This showed the area flooded by an event which occurred in 1960.

3.7.2.2 Maps and aerial photographs of previous inundations

Aerial photographs of the reach, taken on 28/12/1979 were provided by the NRA of the 1 in 12 year event which occurred at that time. This event was one of the events used in the simulations carried out in this investigation. The aerial photographs provided information on the maximum inundation extent for this event which was useful for determining the location of the edge of the finite element mesh where the edge of the floodplain was not obvious from topographic data. In addition, further information on floodplain topography was obtained from the photographs, such as 'islands' of higher ground and areas of ponding in topographic hollows.

3.7.2.3 Field data

Several photographs were taken along the reach to give an indication of topographic variation, size of channels and vegetation types. A cross-section of the floodplain was surveyed 50 m downstream from the Stoke Cannon road Bridge using a leveller and staff. This was done in order to construct a rating curve at the new downstream end of the FEM.

3.7.3 *Setting up the extension to the finite element mesh*

The relevant OS 1:2500 maps covering the reach from Rewe to Stoke Cannon were enlarged on a photocopier five times, care being taken to ensure that sufficient overlap

was created each time. The magnification of each enlargement was 143% and the resultant scale after the fifth enlargement was 1:450.

The final enlarged map was laid out with tracing paper placed over it. The main features were traced from this map and the contours shown on the 1:25,000 map were drawn on by eye. The limit of inundation was also drawn on by eye from the aerial photographs and the 1:2500 map of the Stoke Cannon Flood Alleviation Scheme.

Following on from this, the locations of the nodes and elements of the finite element mesh were determined using the information on the traced map. The mesh was constructed in a downstream direction starting with nodes at the downstream end of the existing Woodmill to Rewe mesh. The location of the channel elements was defined first, by dividing the channel into several sections longitudinally, each section having a maximum length of approximately 150m. In doing this, it was necessary to significantly simplify the channel to prevent the solution from being too complex. This degree of simplification was felt to be appropriate, providing a realistic compromise between physical representation and the constraints of time and model capability. In order to avoid instability in the channel and surrounding area, an angle between two longitudinal sections was not allowed to be less than 110^{o} as shown in Figure 3.10. A trapezoidal channel cross section represented by six nodes was used.

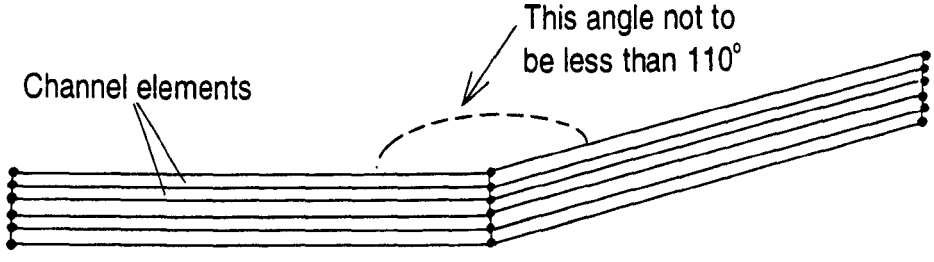

Figure 3.10: Illustration of the minimum angle permitted between adjacent segments

The rest of the mesh was developed outwards from the channel elements using the rules outlined below:

- All elements were defined by 3 or 4 nodes
- No element side was greater than 150m
- Situations where large volumes of water flow from a large element to a small element were avoided since this would have caused problems with mass continuity.

- Elements were aligned in the downstream direction as much as possible with longitudinal lines running parallel to the channel. This was to ensure the smooth advance and recession of floodwaters.

Included in the mesh structure for this reach were two roads which crossed the floodplain. From the aerial photographs it could be seen that significant ponding occurred on the upstream side of these roads during flooding. The roads were represented by a double line of nodes elevated above the surrounding floodplain to form a raised barrier.

Once the location of elements and nodes had been determined, each node was assigned a height. The altitude of the upstream base of channel nodes for the Rewe to Stoke Cannon section of the mesh was known from the gauging station at Rewe which had been previously surveyed. The altitude of the base of channel nodes at the downstream end were calculated from the measured distance from the benchmark on Stoke Cannon Bridge to the water surface and the depth of water in measured in the channel. The intermediate mid-channel node heights were interpolated between these two elevations. Over the floodplain surface, node heights were interpolated using the height data provided by the maps. Following this, the relative location of each node within the mesh was determined. Graph paper with one inch squares was laid under the traced map. The x and y co-ordinates of each node were fixed on a relative scale which had its origin on the original mesh at Woodmill. The squares on the graph paper were aligned with referenced control points on the tracing of the Woodmill to Rewe section.

Each element was assigned a roughness class from one of ten classes. These were based on the Manning's 'n' coefficient and were determined on the basis of the dominant land cover type of the area contained within each element. The roughness classes used were the same as those used for the original Woodmill to Rewe mesh and are shown in Table 3.3.

COVER	MANNING'S N COEFFICIENT	ROUGHNESS CLASS
Channel bed		
Clear	0.030	1
Vegetated	0.035	2
In bank sides		
Grass	0.040	3
Trees	0.042	4
Scrub	0.040	5
Out of bank		
Trees	0.050	6
Scrub	0.050	7
Grass	0.045	8
Floodplain		
Grass	0.045	9
Trees	0.055	10

Table 3.3: Roughness classes assigned to elements

This new section of the reach was tested separately before joining it to the existing reach which already had a stable geometry. In order to ensure that the flow of water into and out of the mesh was parallel to the mesh boundary, a control structure was added to the upstream and downstream ends of the new mesh section. The elements within this structure were assigned a roughness of class 1 (clear channel) and all the nodes were given the same elevation as the first pair of channel nodes at the upstream end (upstream structure) and the last pair of channel nodes at the downstream end (downstream structure).

3.7.3.1 Producing the geometry file

The mesh geometry was input to RMA-2 in the form of a geometry file generated by the pre-processing program, RMA-1. An example RMA-1 input file is shown in the Appendices. The geometry file was divided into three sections. The first of these contained data relating to the plot and information on scaling. The second section included the connection table. This was a list of element numbers, each element number being followed by the node numbers defining that element. The node numbers were entered consecutively in an anticlockwise direction, followed by the roughness class which was been assigned to the element. The final section of the geometry file showed the co-ordinate data for the nodes in the mesh. Each node

number was followed by the x and y co-ordinates derived from the plot and the z co-ordinate for the node height above sea level.

In running the RMA-1 program some initial problems were encountered. For example RMA-1 failed to produce a geometry file in the case of elements defined by nodes for which no co-ordinate or height data existed in the final part of the geometry file. These were identified from the RMA-1 output file. Once RMA-1 had run successfully, the output geometry file was plotted on the screen using a plotting routine provided by RMA. Using this screen plot, other errors could be identified. These included node numbers which had been mis-read during the construction of the connection table and nodes which were in the wrong place because of incorrect x and y co-ordinates.

Once the more obvious errors had been identified and corrected, a certain amount of mesh refinement was necessary. For example, problems of instability were likely to be caused where the channel narrowed. It was therefore necessary to widen the channel in places by changing the co-ordinates of some nodes. In addition, a certain amount of element refinement was carried out. From the screen plots, it could be seen that there was a need to reorganise elements in some areas of the mesh such as areas where there was a sudden change in element size or the mesh was unnecessarily complex. Adjustments included removing unnecessary elements, altering element sizes and distribution and changing some node co-ordinates.

3.7.3.2 Developing the initial conditions for RMA-2

There were two stages involved in developing the initial conditions for dynamic RMA-2 simulations. This procedure was necessary to develop an initial condition where all the elements within the FEM were inundated and therefore included within the solution at the initial dynamic time step. If the floodplain was initially dry, the addition of water at the upstream end at the start of the dynamic simulation would cause model instability since a large number of elements would become inundated and enter the solution at each time step.

The first stage in this initialisation procedure involved carrying out a steady state simulation. In order to do this, the entire reach was flooded by specifying a downstream stage boundary condition where the stage was equal to the height of the nodes at the top end of the reach. In this way the reach was flooded like a reservoir with the downstream boundary condition acting as a dam. A constant discharge was applied to the upstream end of the reach for six 0.5 hour time steps. A constant discharge was also produced at the downstream end. Figure 3.11a shows a

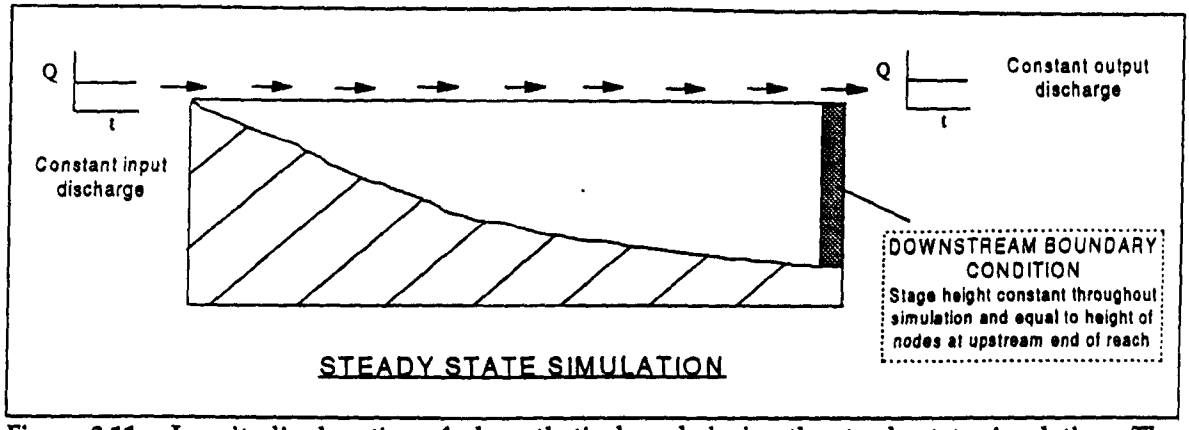

Figure 3.11a: Longitudinal section of a hypothetical reach during the steady state simulation. The downstream boundary condition is represented as a dam at the downstream end of a reservoir.

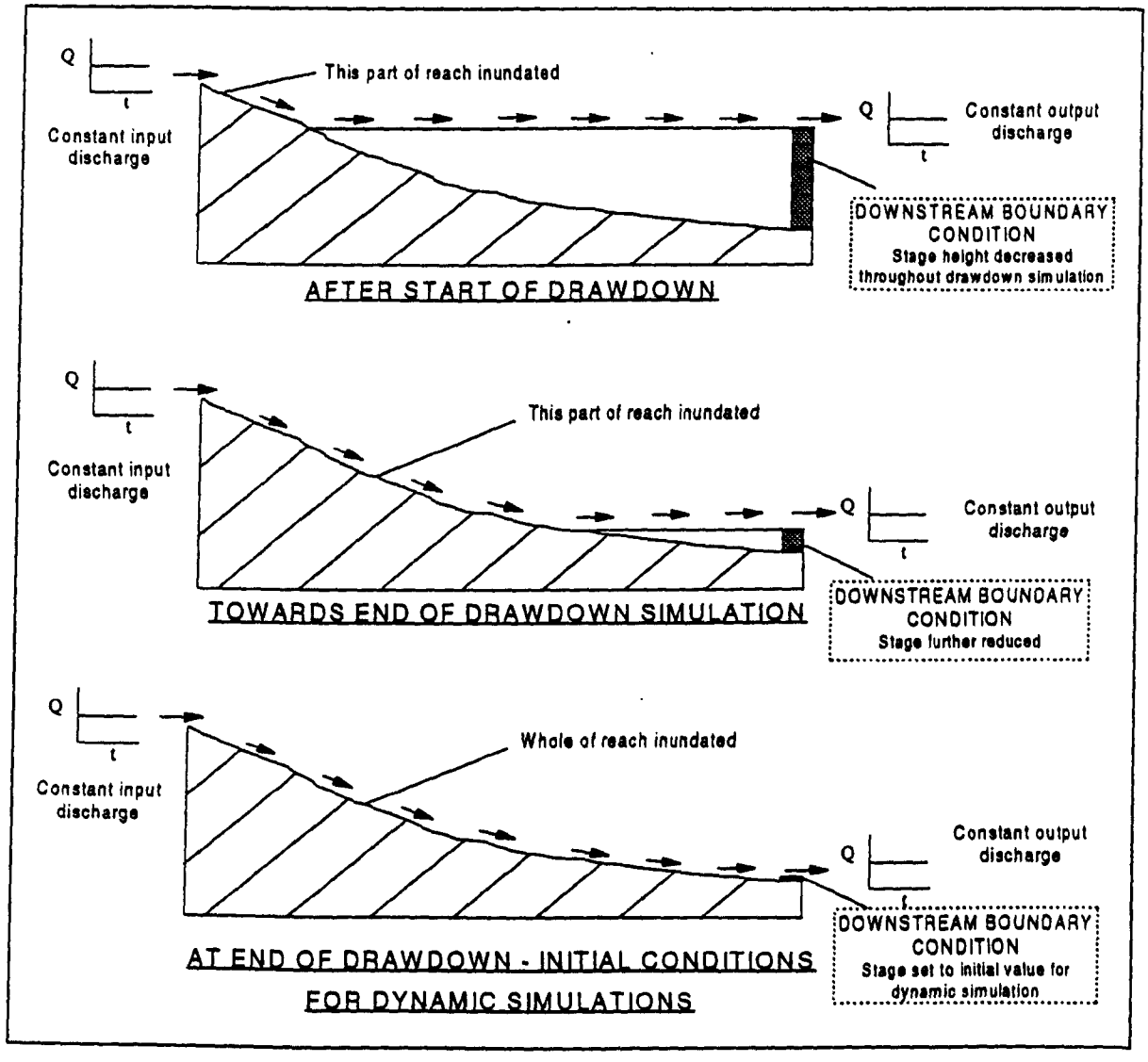

Figure 3.11b: Longitudinal section of the same hypothetical reach during the drawdown simulation. The stage height governing the downstream boundary condition is gradually reduced through the period of the simulation. At the end of this simulation the initial conditions for the dynamic simulations have been developed.

longitudinal section of a hypothetical reach during this steady state simulation where the downstream boundary condition is represented as a barrier or dam at the downstream end of the reach. This steady state simulation was found to run stably when carried out for the new section of FEM.

The next stage in the initialisation involved draining the reach while keeping all the elements within the solution by ensuring they were fully inundated. This drawdown was carried out by applying the same constant discharge at the upstream end but gradually decreasing the downstream stage boundary condition to allow the reach to gradually drain. This is illustrated in Figure 3.11b. Several problems of instability occurred at this stage which were solved by further mesh refinement. Longitudinal gradients in excess of 2m km^{-1} have often been found to result in model instability. The average gradient of the floodplain over the reach (1.86m km^{-1}) was quite close to this threshold. Because of this, instability occurred just upstream of the Huxham Road (above Stoke Cannon) where the gradients necessary to simulate a raised barrier exceeded the threshold. Since the gradient of the floodplain was so close to this threshold, it was not possible to accommodate the gradients necessary to represent the road as a raised barrier. Therefore, it was decided to increase the roughness of the road elements to provide resistance to flow. However, when the drawdown was repeated, the model still produced an unstable solution at this point in the mesh. This could have been caused by the relatively small size of the road elements. It was therefore decided to remove the Huxham road which crossed the floodplain upstream from Stoke Cannon. The A396 (below Stoke Cannon) was not removed from the mesh as the model provided a stable solution once the height of the road nodes had been lowered.

Once the instability problems had been eliminated, the new section of mesh was added to the existing Woodmill to Rewe section. In order to join these two sections, the downstream control structure from the Woodmill to Rewe mesh and the upstream structure from the Rewe to Stoke Cannon mesh were removed. New elements were created to join the existing nodes in the two meshes. The new FEM was then initialised by running steady state and drawdown simulations for the whole reach from Woodmill to Stoke Cannon. The initial dynamic simulation was then carried out prior to re-calibrating the model for the entire reach. A plot of the FEM including the new Rewe to Stoke Cannon extension is shown in Figure 3.12.

Figure 3.12: **The RMA-2 application to the Culm reach showing the Rewe to Stoke Cannon extension of the FEM**

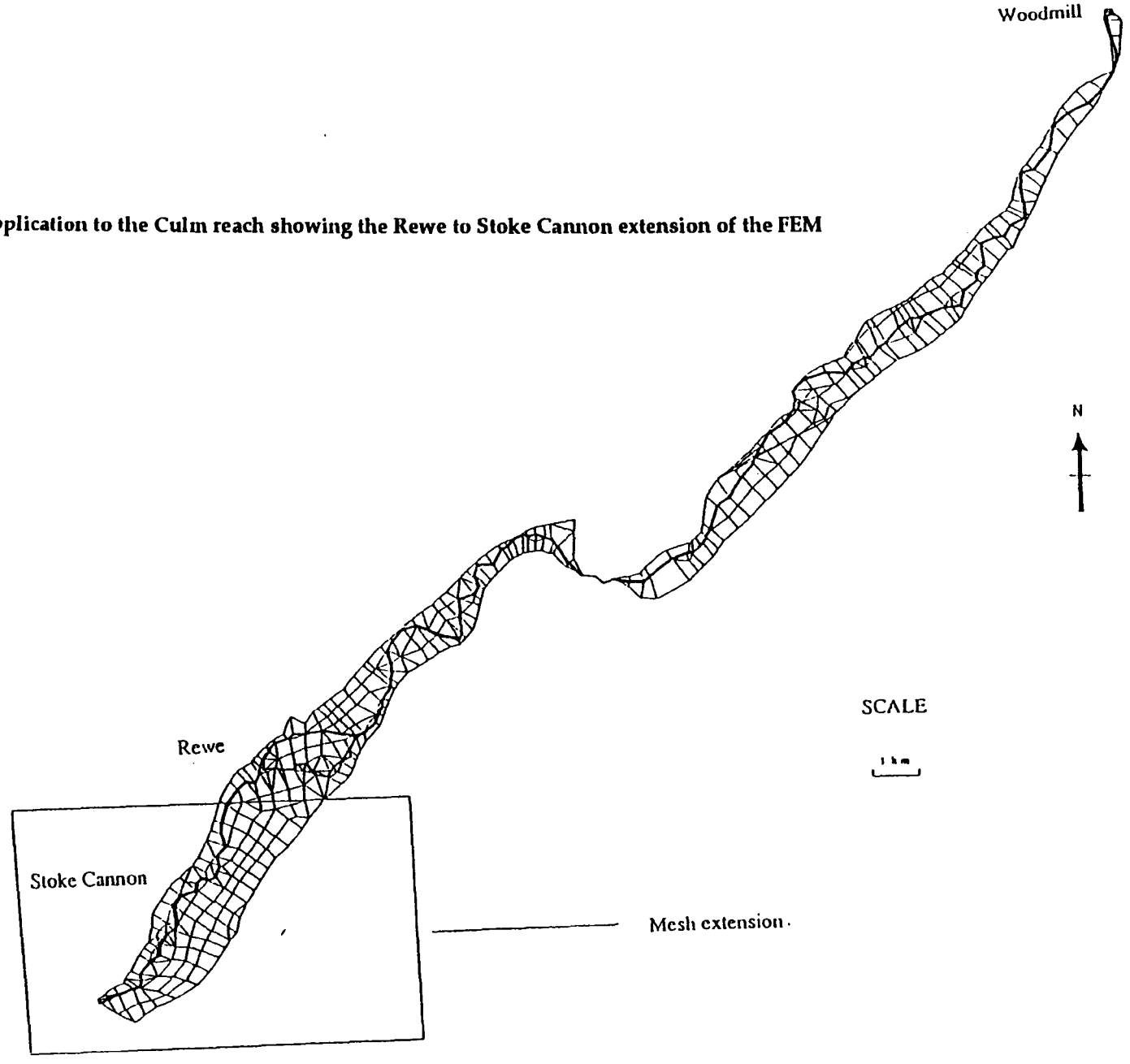

3.7.3.3 Derivation of the new downstream stage-discharge relationship at Stoke Cannon

The stage-discharge relationship at the downstream end of the reach was established using one of the hydrological procedures contained within the MILHY modelling package developed by Williams and Hann (1972, 1973) which is described in detail by Baird and Anderson (1990).

The procedure was used to derive a stage-discharge relationship through the application of the Manning equation.

$$q = \frac{1.486}{n}\left(aR^{2/3}Sl^{1/2}\right) \qquad 3.18$$

Where:

n = Manning's coefficient of roughness

a = cross section area (ft^2)

R = hydraulic radius (ft)

Sl = slope of energy gradient

A cross-section of the channel and floodplain was surveyed at Stoke Cannon 50 m downstream of the road bridge. From this, MILHY was used to establish twenty values on the rating curve incorporating the impact of the momentum exchange between the main channel and floodplain flow segments during the development of the rating curve. Once established, the rating curve was used to provide the new downstream boundary condition.

3.7.3.4 Issues associated with the rating curve at Rewe

The relationship established at Rewe was found to give reasonable predictions for in-bank flows. However when calculating discharges for out-of-bank conditions, a small change in the stage resulted in a large change in discharge. This was due to the very shallow gradient of the curve for out-of-bank conditions. Figure 3.13 illustrates this point. The observed input and output hydrographs for the for the 1 in 1 year event are shown together with the discharge hydrographs resulting from a ± 5% error in the stage measurement. From these it can be seen that there is a considerable variation in discharge over this range.

In order to compare observed and predicted stage hydrographs, the measured stage and the predicted depth for the channel nodes at the location of the Rewe gauge were compared. When comparing the discharge hydrographs, the observed discharge was calculated using the stage-discharge relationship at Rewe whereas the predicted discharge was calculated using a subroutine which calculated the discharge for the

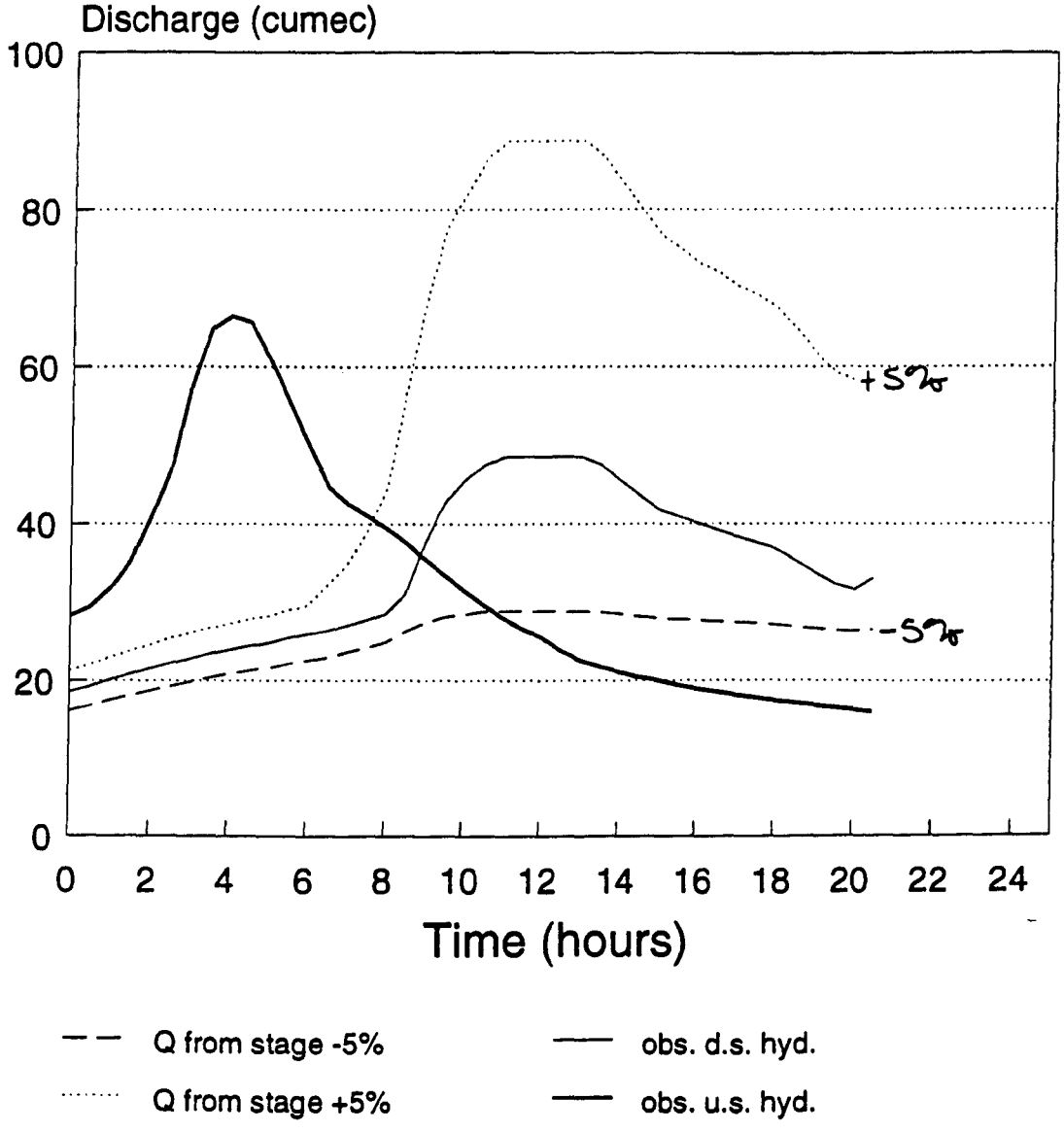

Figure 3.13: Observed upstream and downstream discharge hydrographs. The downstream discharge hydrographs calculated for a ± 5% error in the stage measurement using the rating curve shown in Figure 3.2 are also shown.

section from the depth and velocity predictions made by RMA-2. It was therefore felt to be inappropriate to compare discharge hydrographs during the calibration procedure described in the next section. Calibration was carried out using the observed and predicted stage hydrographs. However, it was decided to be acceptable to use the RMA-2 predicted discharge hydrographs in the comparison between the *predicted* hydrographs produced during the sensitivity analysis since these would all be derived from the RMA-2 predictions using the same method.

3.7.4 Re-calibrating the model

The calibration of the model was re-evaluated for the whole reach using the same 1 in 1 year event as that used by Bates and co-workers. Previous work has indicated that the parameter to which RMA-2 is most sensitive is floodplain roughness (Baird and Anderson, 1990). The calibration procedure for RMA-2 involves altering the Manning's n value for roughness classes 9 and 10 (floodplain elements) to alter the timing, peak stage and discharge of the floodwave in order to produce a predicted hydrograph which is as similar as possible to the observed downstream hydrograph. Increasing the value of n for these roughness classes increases the floodplain roughness, slowing the passage of the floodwave and attenuating the downstream hydrograph so that the hydrograph peak occurs later and the peak discharge is decreased. Similarly, if the Manning's n value is decreased, the lower floodplain roughness allows the downstream hydrograph to peak sooner with a corresponding increase in the peak discharge.

The RMA-2 model was calibrated on the basis of the timing of the observed and predicted hydrograph peaks as this had a very significant effect on the areas of the floodplain which were inundated at the time at which the downstream hydrograph peak occurred as well as for predictions of resultant velocity and depth at each of the prediction nodes. If the model was calibrated on the basis of peak stage or discharge there could have been major implications for the accuracy of these predictions. In addition, if the predicted peak timing was incorrect, the resultant volumetric errors on the rising and recession limbs of the hydrograph could be considerable. It was for these reasons RMA-2 was calibrated on the basis of peak timing.

When RMA-2 was originally applied to the River Culm reach, the model calibration was carried out using a 1 in 1 year event which occurred in 1982 (12/11/82 to 13/11/82). This is a different 1 in 1 year event to the one used in this investigation. A Manning's n value of 0.1 for roughness classes 9 and 10 was used in the final

calibration for the 1982 event. When this calibrated model was applied to the 1990 1 in 1 year event used here, the timing of the downstream hydrograph peak was found to be the same as that of the observed hydrograph as can be seen in Table 3.4.

	Peak time (hours)	Peak stage (m)
Observed	11.5	2.335
Predicted	11.5	2.122

Table 3.4: The observed and predicted peak stage and timing observed at Rewe. The predicted hydrograph was produced using the extended FEM

3.8. CONCLUSION

In this chapter, a number of aims have been achieved. A suitable study reach has been selected; an 11 km reach of the River Culm which has a substantial history of inundation together with suitable data from upstream and downstream gauging stations and a considerable amount of information on previous inundation extents. A 2-dimensional floodplain inundation model, RMA-2, has been selected for application to this reach. The model meets the requirements made by the proposed investigation and has previously been applied to the Culm reach in a previous study (Bates et al. 1992). Using this set-up a pilot study was carried out by applying outflows (observed along the base of a hillslope for another catchment) to the edge of the RMA-2 FEM. From the results of this investigation it was concluded that contributions from hillslopes bordering the floodplain reach are likely to be important under some circumstances.

A problem was identified associated with the application of RMA-2 to the Culm where water was observed to back up at the downstream end of the reach. Since this is the location of the downstream gauging station at which comparisons are to be made between observed and predicted hydrographs it was desirable that this effect should be removed. The problem was overcome by extending the finite element mesh 3 km downstream and developing a new stage-discharge relationship for the downstream end. Comparison between hydrographs will still be carried out at the downstream gauging station at Rewe.

Chapter Four now describes the selection and set up of a hillslope hydrology model to simulate inflows from a range of different hillslope types. The first stage of the sensitivity analysis described in Chapter Four will also be described.

Chapter 4

MODELLING HILLSLOPE INFLOWS

4.1 INTRODUCTION

The results of the pilot study described in the previous chapter have shown that the addition of inflows can influence floodplain model predictions. The next phase in the research programme is to identify the range of hillslope-floodplain environments where the addition of inflows has a measurable effect on model predictions. In this chapter the selection and set up of a hillslope hydrology model to simulate hillslope inflows is described. Chapter Two discussed the proposed method of using a hillslope hydrology model to simulate a range of hillslope environments, by changing selected input parameters to represent a range of different hillslope types and examining the sensitivity of the coupled scheme to changes in these parameter values. The first stage of this sensitivity analysis is described here and involves selecting five key hillslope and assessing the sensitivity of the hillslope model to changes made to these. The second stage of the sensitivity analysis is discussed in chapters Five and Six.

First in order to select and apply a hillslope model and to interpret the model outputs, an understanding of the physical processes of runoff mechanisms was required. The first part of this chapter describes the development of the variable source area concept and was discussed in Chapter One. Here the processes of water movement through the soil profile are considered. The selection of a hillslope hydrology model is discussed in light of the unique requirements made by this particular application. Chapter One provided an outline of the range of hillslope hydrology models currently available. This chapter describes the two models which were examined in more detail; a semi-distributed conceptual model and a physically based distributed hillslope hydrology model. A hillslope section, approximately 1km wide, was then selected from the slopes bordering the reach and the model was set up for that hillslope. The slope was used only as a geometric template because of the semi-theoretical approach which was adopted. This involved altering the values of five key parameters over a range of different values which might be expected to be observed for a number of different hillslope types in the field. The sensitivity of the hillslope model to changes in each of these parameter values was assessed after carrying out a number of model simulations. Examination of the results allowed selection of the hillslope simulations to use in the second stage of the sensitivity analysis as inflows to RMA-2. In order to

use output hydrographs from the hillslope model as an input to RMA-2, the discharge at each time-step was spatially averaged along the base of the hillslope. The final section describes the program written to do this. Once the spatially averaged hydrographs were prepared, the next stages in the process of coupling the models were carried out. These are presented in Chapter Five.

4.2 HILLSLOPE PROCESSES

4.2.1 Soil moisture characteristic curve

Establishment of the soil moisture characteristic curve is the first stage in any predictive scheme since by using this curve, the hydraulic conductivity at a range of suctions can be found. The main forces holding water in the soil are capillary forces, resulting from surface tension at the interface between soil air and soil water; adsorption onto soil particles, where water is held mainly by electrostatic forces and osmotic pressure due to solutes in the soil water.

If a body of soil is considered where the actual pressure at all points through that body is atmospheric and the hydrostatic pressure and suction applied to the soil body are zero, the soil water is at equilibrium and no movement occurs. When a slight suction is applied, the water pressure becomes slightly sub-atmostpheric although no outflow will occur until the *air entry suction* threshold value is reached. At this point the largest pore within the soil body begins to empty. This threshold suction value is small for coarse textured and well aggregated soils. Since coarse textured soils are often more nearly uniform in size the critical air entry phenomena may be more distinct and sharply defined than for fine textured soils such as clays. Further increases in the applied suction result in the release of more water as more of the relatively large pores empty and progressively smaller pores yield water. At very high suctions only the narrowest pores retain water. Increasing suction is associated with decreasing soil wetness which results in thinner hydration envelopes around the soil particles. At equilibrium the amount of water remaining in the soil is a function of the sizes and volumes of the water filled pores and is therefore a function of the matric suction. This function is usually measured experimentally and is represented by the "soil moisture retention curve" or "soil moisture characteristic curve" (Childs, 1940). The soil moisture characteristic curve is strongly affected by the texture and structure of the soil. If texture is considered, a soil with relatively large pores such as sand will produce a curve with a rapid initial decrease in soil water once the air entry suction is

exceeded since once these pores are emptied, there is relatively little moisture still held within the soil (Figure 4.1). An increase in the clay content produces a more gradual slope of curve due to a more uniform pore size distribution which results in a more moderate decrease in water content with increasing suction.

Soil structure also affects the shape of the soil-moisture characteristic curve. This is particularly so in the low suction range. Soil compaction decreases the total porosity and especially the total volume of large inter-aggregate pores. The consequent decrease in the saturation content results in a smaller initial decrease in the water content at low suctions. Another consequence of compaction is to increase the volume of pores of an intermediate size (large pores compacted to intermediate) while inter-aggregate micropores are unaffected meaning that the soil moisture characteristic curves for compacted and uncompacted soils are nearly identical at high suctions (Figure 4.1).

The relationship between matric potential and soil wetness is not generally unique and single valued. At equilibrium, soil wetness values at a given suction are generally higher when drying than when wetting since soil takes in water more easily than it releases it. This hysteresis effect was observed and reported by Philip (1964). It is caused by several factors. The geometric non-uniformity of pores sizes means that a large pore surrounded by smaller pores will empty at much higher suctions than it will fill since the drying of this pore can only occur after the surrounding smaller pores are dry; during the wetting phase the rate at which the large pore fills is determined by the size of that pore. The contact angle is greater resulting in a greater radius of curvature in an advancing meniscus than in a receding one, also entrapped air further reduces the water content of a newly wetted soil. Other phenomena which are a function of the soil history can also contribute to the hysteresis effect.

Dependence of the curve on particle size distribution and bulk density has been widely considered (Hall et al., 1977; Arya and Paris, 1981; Brakenseik and Rawls, 1983). Arya and Paris define the *pore size distribution* which reflects the effect of bulk density and particle size distribution. Hall and Brakenseik and Rawls describe multiple regression models which consider both parameters.

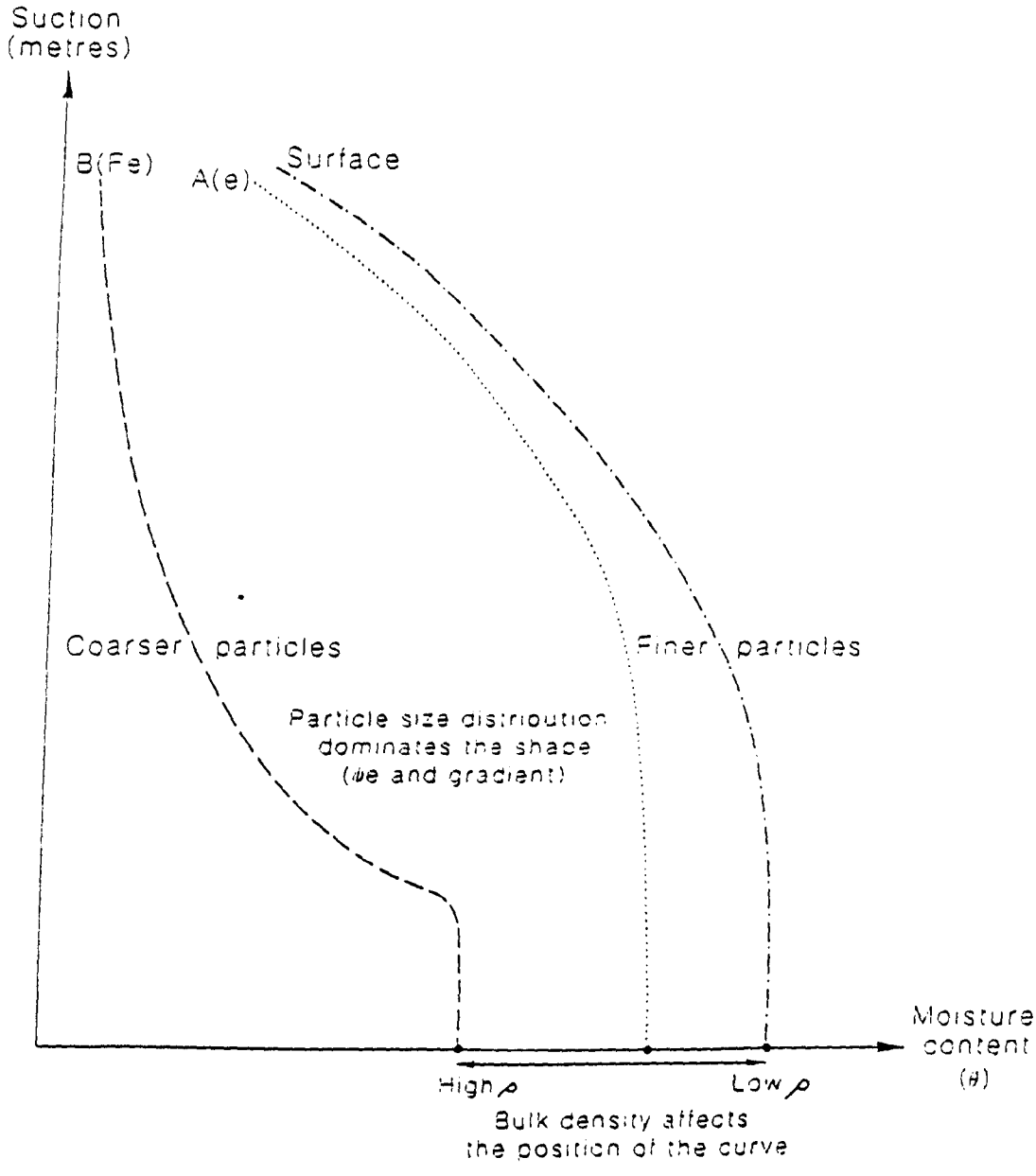

Figure 4.1: **Illustrating the dependence of the soil moisture characteristic curve on the particle size distribution and the bulk density (after Hillel, 1980)**

4.2.2 *Flow of water in saturated soil and the saturated hydraulic conductivity*

Water movement between two points in a saturated soil body is brought about by a difference in pressure between those two points. The pressure at each point is the sum of the hydrostatic and atmospheric pressure at that point. Atmospheric pressure is uniform throughout the soil body so may be ignored in this context. Hydrostatic pressure has two components; gravitational pressure potential and hydraulic head potential. The gravitational pressure at a point is expressed as the height of a point above an arbitrary reference plane, z_o, and is always positive. The pressure head potential is positive under a free water surface although it can be negative (i.e.: less than atmospheric pressure) under the circumstances described in Section 4.2.3. The hydraulic head at a point is expressed as the height of the head of water above that point. Flow between two ends of a horizontal column of soil is influenced only by the difference in the pressure-head at each end of the column. Since the whole column is at the same height above the gravitational reference plane the difference in the gravitational head is zero. In the case of a vertical column immersed in water, any flow is affected both by the gravitational and hydraulic head potentials. The gravitational potential at the base of the column, z_b is less than that at the top of the column, $z_b + h$ (where h is the length of the column). The gravitational potential increases with height at a ratio of 1:1. The pressure head potential is expressed as the height of the column of water resting on the point of consideration and increases with depth at a ratio of 1:1. Thus the sum of the pressure and gravitational components of the total hydraulic head is the same all the way up column meaning it is in equilibrium.

The distribution of soil pores results in highly irregular tortuous and interconnected flow paths which are limited by constrictions and dead ends. Flow through complex media is thus generally described in terms of the macroscopic flow velocity vector which is the overall average of the microscopic velocities over the total volume of the soil. In this way the body of the soil is treated as a uniform medium with flow spread over the whole cross section. Flux is the term used to describe the volume of water passing through a unit cross sectional area per unit time and has the same dimensions as flow velocity. In a field soil, the velocity is highly variable meaning that the average velocity is the best description of velocity. The average velocity of a flowing liquid is greater than the flux. This is because flow does not occur through the entire cross-sectional area because a proportion of this area is plugged by soil particles and only

the porous fraction is open to flow. Since the conducting area is smaller than the cross-sectional area, the actual average velocity of the liquid must be greater than the flux.

The *hydraulic conductivity* is the ratio of the flux to the hydraulic gradient. The flow of water between two cross-sections, X and Y in a macroscopically uniform soil body is directly proportional to the cross sectional area, A, of that body and the hydraulic head drop (or hydraulic gradient) between A and B and is inversely proportional to the length of the column. Darcy was the first to express this relationship quantitatively and the generally accepted form of Darcy's Law for 3-dimensional flow states that:

$$q = -K\nabla H \qquad 4.1$$

Where:

q = rate of flow

K = hydraulic conductivity

∇H = change in head with distance

Hydraulic conductivity (K) has two components; the first of these is the *permeability* (k) or *intrinsic permeability* and is a measure of the readiness with which a porous medium transmits water and other fluids. It is ideally an exclusive property of the medium. The second component is the *fluidity* of the fluid which is affected by factors such as viscosity and temperature. The hydraulic conductivity is a function of the soil structure and texture. For example, clay has a higher porosity than sand although sand has a higher hydraulic conductivity, typical values being between 10^{-4} - 10^{-5} m s^{-1} for sand and 10^{-6} - 10^{-9} m s^{-1} for clay

4.2.3 *Flow in unsaturated soil*

Most of the processes involving soil water in the field are associated with unsaturated soils. Unsaturated flow processes are complicated and difficult to describe quantitatively since complex relationships exist between water content, suction and conductivity. The formulation and solution of unsaturated flow problems is a major issue in soil physics and often requires the use of indirect methods of analysis based on approximations or numeric techniques.

Water in an unsaturated soil is subject to subatomic pressures or *suctions* caused by the physical affinity of water to soil particle surfaces and capillary pores. The *suction gradient*, if it exists, produces a moving force causing water to move from a low suction

zone to a high suction zone. Water flows in pores which remain water filled at the existing suction and creeps along hydration films over particle surfaces with a tendency to equilibrate potential. The wetting front moving force is the greatest and suctions can be many bars cm^{-1} and the gradient causing the moving force can be thousands of times greater than the gravitational force. Such forces are required to move water in very dry soils.

The hydraulic conductivity for a given soil is dependent upon the suction and moisture content of that soil. When a soil is saturated, all the pores are filled and the hydraulic conductivity is at its maximum value. In an unsaturated soil, some of the pores become air filled resulting in a decrease in the conductive portion of the soil cross-sectional area. When a suction is applied to a saturated soil, the first pores to empty are the largest. These empty pores increase the *tortuosity* of the flow path each 'parcel' of water has to take, since they must now be circumnavigated. Coarse textured soils have a large percentage of large pores which empty at relatively low suctions and the remaining water sometimes remains as capillary wedges in isolated pockets. Although at saturation high hydraulic conductivities are associated with these soils, finer textured soils have a greater hydraulic conductivity under unsaturated conditions particularly at higher suctions. Aggregated soils contain large inter-aggregate boundaries which when empty form barriers. For these and coarse textured soils there is a marked decrease in hydraulic conductivity as the moisture conditions become unsaturated. Much work has been carried out to derive methods to estimate the unsaturated hydraulic conductivity from moisture retention functions (Childs and Collis-George (1950), Millington and Quirk (1983), Campbell (1974)).

4.3 SELECTION OF A HILLSLOPE HYDROLOGY MODEL

4.3.1 *The range of models available and model attributes required by this application*

Chapter Two discussed the approach used in this investigation; a hillslope section bordering the Culm reach was modelled to provide an additional input to RMA-2. The hillslope outflows were spatially averaged by calculating the discharge per unit length at each time step and this spatially averaged discharge was to be applied to each element along the edge of the RMA-2 finite element mesh, weighted by the length of the element edge. The application therefore required a hillslope hydrology model capable of producing output along the base of the slope rather than at a single point

(the catchment outlet). This meant that the model should allow the catchment to be split into sub-units to enable an individual hillslope to be modelled rather than the whole catchment; the channel component for example was not required because an isolated hillslope was modelled. Ideally this model should be a semi or fully distributed model. The fact that no data were available for the slope made the additional prerequisite that the model should not rely on calibration procedures for parameterisation.

In the light of these requirements two models were considered for this application; the semi-distributed conceptual model TOPMODEL and the distributed Variable Source Area Simulator (VSAS3), a quasi-3 dimensional physically based hillslope model.

4.3.2 *TOPMODEL*

TOPMODEL (topography-based hydrological model) is a physically based semi-distributed rainfall-runoff model (Beven and Kirkby, 1979; Beven et al., 1984; Beven, 1987). It represents some of the heterogeneity occurring within a catchment but requires measurement of relatively few characteristics. The spatial variability of variable source areas is combined with the average response of the soil-water storage of the basin. This reduces the number of model parameters and the fieldwork required but still retains the variable source area concept.

The topography of the catchment is represented in TOPMODEL by means of a topographic index $\ln(a/\tan\beta)$ where a is the area drained per unit contour length and $\tan\beta$ is the local gradient at that point a is calculated for a grid square by summing the area of the squares upslope contributing water to that square. The proportion of water contributed by a given grid square to the adjacent downslope squares is weighted using the $\tan\beta$ component of the index. The index is calculated from a Digital Terrain Model (DTM) across a grid covering the catchment. Grid squares with a high $\ln(a/\tan\beta)$ value reflect relatively wet areas of the catchment, those which drain a large area (such as valley bottoms and zones of flow convergence) or are flat (interfluves). Areas with lower index values usually drain smaller areas or have steeper slopes. A 2-d map of $\ln(a/\tan\beta)$ for an upland catchment is shown in Figure 4.2. TOPMODEL assumes that areas with the same $\ln(a/\tan\beta)$ value behave in a hydrologically similar manner. Once local values of the index have been calculated for each point, the distributed hydrological effects are lumped by calculating the

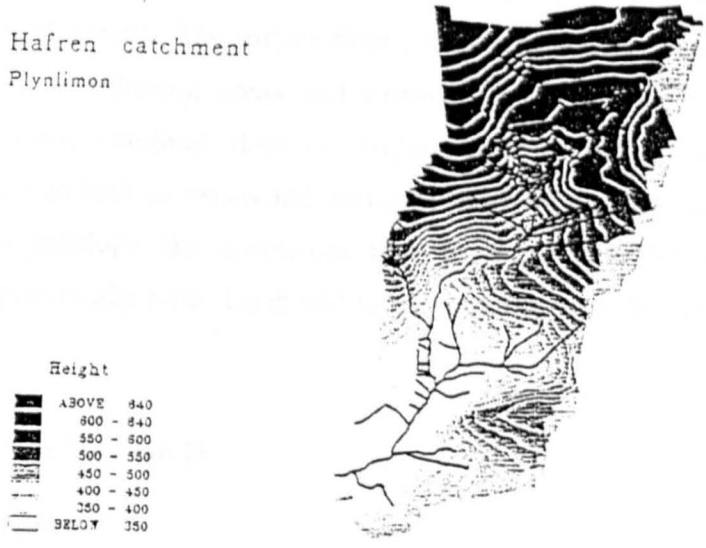

Figure 4. Contour map of the Hafren catchment

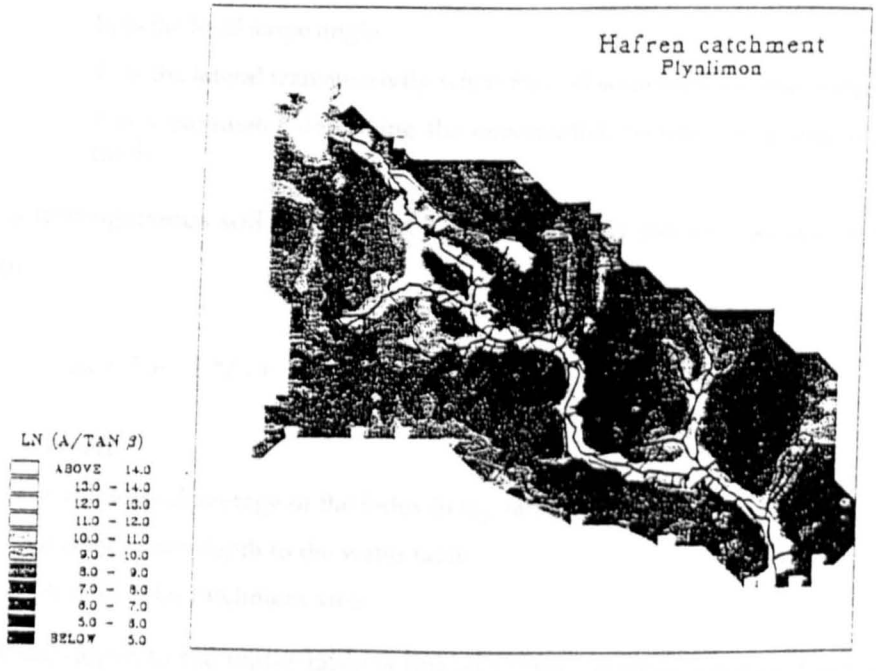

Figure 4.2: **Two-dimensional map of ln (a/tan β) index for the Hafren catchment (after Robson, 1992)**

proportion of the catchment with each index value. These hydrologically similar zones are then modelled separately.

In its basic form TOPMODEL identifies two sources of stream water; water draining from subsurface zones and surface water contributed by saturated and near saturated areas of the catchment. The surface flow component is generated by rainfall landing on saturated contributing areas and causing rapid movement to the stream via macropore flow, overland flow or displacement of old water. The saturated contributing area both increases and decreases in extent during a storm event. For any point on the hillslope, the downslope flow from the saturated area is assumed to decrease exponentially with depth and to be proportional to the local surface gradient tan β_i.

$$qsi = T_0 e^{-z^i} * f \tan \beta i \qquad 4.2$$

Where:

qs_i is the local lateral saturated flow per unit length of contour ($m^2 hr^{-1}$)

z_i is the local depth to the water table (m)

b_i is the local slope angle

T_0 is the lateral transmissivity when the soil is saturated to the surface ($m^2 hr^{-1}$)

f is a parameter describing the exponential decrease in transmissivity with depth (m^{-1})

For a homogeneous soil of constant T_0 the total flow per unit area is given by (Beven, 1986)

$$qs = T_0 e - z * f - l \qquad 4.3$$

Where:

λ is the areal average of the index $\ln (a_i / \tan b_i)$

z is the mean depth to the water table

A is the total catchment area

The local depth to the water table is linked to the catchment mean depth to water table by

$$z_i = z + (\lambda - \ln(a_i / \tan \beta_i))/f \qquad 4.4$$

From this, it is possible to determine areas where the water table is at the surface (i.e.: the variable source area). This information is used to calculate q_{SCA}, the average flow

per unit area of the catchment generated by rainfall on the saturated contributing areas. Thus at a given time t the total flow per unit area is

$$q_t = qs_t + qSCA \qquad 4.5$$

At each time step the value of z is updated ready for use in the next interval.

$$z_{t+1} = z_t + (qs_t - qv_t)/\Delta\Theta \qquad 4.6$$

Where:

$\Delta\Theta$ is the effective storage capacity of the soil

qv_t is the total vertical flow through the unsaturated zone down to the saturated zone.

Local vertical flow is given by

$$qv_{t_i} = K_0 e^{-zi} * f \qquad 4.7$$

Where:

K_0 is the vertical conductivity at the surface

This equation assumes that the hydraulic conductivity has an exponential profile with depth (with the same decay parameter, f, as for lateral flow) and that just at the water table there is a unit hydraulic gradient.

All the information required to set up the model can be obtained from topographic maps and from field measurement. Although calibration of the model does not depend on the availability of an observed discharge record the decay coefficient, f, is usually derived from the recession limb of the observed hydrograph. It is also possible to derive this parameter from field measurements of hydraulic conductivity although this involves a large amount of fieldwork and considerable uncertainties are associated with the techniques used.

4.3.3 *The Variable Source Area Simulator*

The original version of the Variable Source Area Simulator (VSAS) was developed by Troendle (1979). This was based on earlier work carried out by Hewlett and Nutter (1970) and Hewlett and Troendle (1975). The model was written as a mathematical representation of the variable source area concept proposed by Hewlett and Hibbert (1963, 1967). This first version of VSAS3 was written to concentrate computing power on the computation of soil water flow and the representation of topography. Bernier (1982, 1985) developed a new version, VSAS2, which allowed the area of the catchment

producing saturated overland flow to be spatially and temporally variable and act as a "rapid extension of the channel system" (Hewlett and Hibbert 1967). This was done by adding a new routine to recalculate the catchment area when the streamside regions became saturated, treating saturated areas as part of the channel system. A further version of the model, VSAS3, was developed by Whitelaw (1988). The main developments were; to treat the soil water flow in a three dimensional manner, altering the topographical input and improving the calculation of the unsaturated hydraulic conductivity.

VSAS3 divides the catchment into a number of user-defined polygons called segments which stretch from the watershed to the stream boundary. Each segment is an autonomous hydrological unit and flow does not occur between adjacent segments. Figure 4.3 shows the segmentation for the VSAS2 application to the Whitehall catchment carried out by Bernier (1982).

Segments are then subdivided slopewise into up to 10 increments using a partitioning rule which results in increments progressively increasing in size from the slope base to the watershed. This gives a finer spatial resolution at the slope base, which allows for a more accurate representation of the expansion and contraction of the variable source area. Increments are divided with depth into a number of elements. These are the basic unit of VSAS3 and the centre points assigned to individual elements are the solution points for the finite difference scheme used by VSAS3.

Soil water flow is the most significant part of the VSAS3 structure. It is assumed that all rain falling onto an element infiltrates the soil surface and is accounted for either by subsurface soil water or, if the input volume is too great for the element storage, by saturated overland flow. Whitelaw (1988) provides a description of the equations describing the soil water component of VSAS3 which is summarised here.

The rate of subsurface flow is calculated using the Richards generalisation of Darcy's Law. Richards (1931) adapted this law to account for soil water flow in unsaturated conditions by combining the Darcy equation with the continuity equation. Darcy's law states that

$$q = -K(\theta)\nabla H \qquad 4.8$$

Where:

q = apparent water velocity (cm hr^{-1})

K = unsaturated hydraulic conductivity (cm hr^{-1})

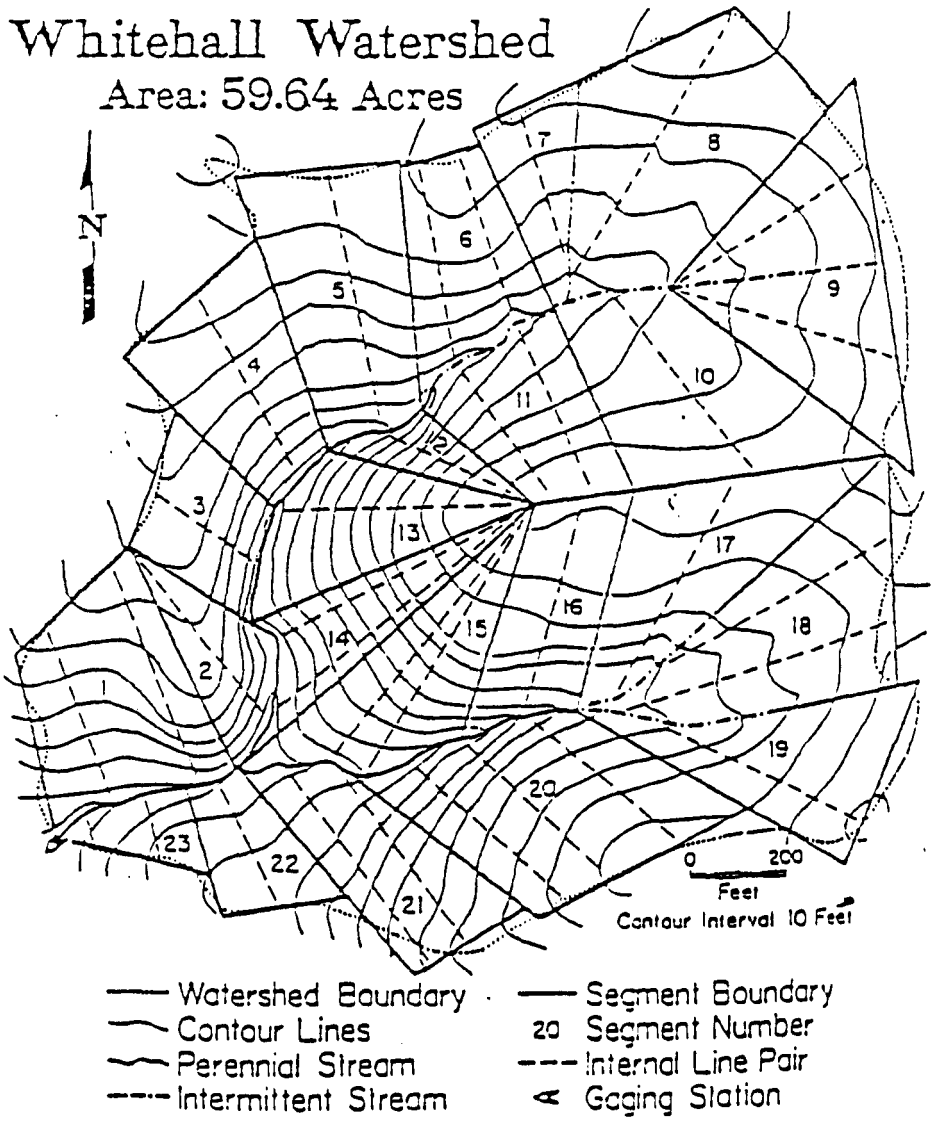

Figure 4.3: Segmentation of Whitehall Watershed for VSAS2 simulation (after Bernier, 1992)

θ = soil water content ($cm^3\ cm^{-3}$)

∇H = hydraulic gradient ($cm\ cm^{-1}$)

The second source of the main flow equation is the continuity equation for a single non boundary soil element. This can be stated as:

$$\frac{\partial \theta}{\partial t} = \nabla . q \qquad 4.9$$

Combining the above equations gives the main flow equation in its basic form:

$$\frac{\partial \theta}{\partial t} = \nabla (k(\theta) \nabla . H) \qquad 4.10$$

If

$$H = \Psi + Z \qquad 4.11$$

Where:

Ψ = suction

and

$$\Psi = \Psi(\theta) \quad \text{(which can represent a pressure as well as a suction)} \qquad 4.12$$

then expanding the expression in the x and y dimensions gives:

$$\frac{\partial \theta}{\partial t} = \frac{\partial}{\partial x}\left(k(\theta) \times \left(\frac{\partial \psi}{\partial x} + \frac{\partial Z}{\partial x} \right) \right) + \frac{\partial}{\partial Z}\left(k(\theta)\, Z \left(\frac{\partial \psi}{\partial Z} + 1 \right) \right) \qquad 4.13$$

$\partial Z/\partial x$ would be 0 in a horizontal direction but it has been left in the expression to allow X to represent a slope, i.e.: $x.\cos\alpha$

Bernier (1982) makes the substitution,

$$X^* = x.\cos\alpha \qquad 4.14$$

$$\frac{\partial \theta}{\partial t} = \cos\alpha \frac{\partial}{\partial X^*}\left[k(\theta)_{X^*} \left(\frac{\partial H}{\partial X^*} + \frac{\partial Z}{\partial X^*} \right) \right] + \frac{\partial}{\partial Z}\left[k(\theta)_{Z} \left(\frac{\partial H}{\partial Z} + 1 \right) \right] \qquad 4.15$$

This is the final flow equation which is solved numerically using the finite difference

method. Values within this expression can all be obtained from the model geometry and the set time step with the exception of k (θ) and Ψ. The values of k in the expression are obtained from k(θ) values obtained using the Millington-Quirk soil moisture algorithm. This method was developed by Millington and Quirk (1959) to transform a known soil suction-moisture curve into an equivalent unsaturated hydraulic conductivity curve.

4.3.4 *Model selection*

The two models were evaluated in light of the approach to be used in this investigation. First, if the ease with which data may be extracted along the base of the slope is considered it can be seen that whilst the VSAS3 segmentation makes it relatively easy to extract outflows from the base of each segment, it is not so easy to extract this data from TOPMODEL. Due to the nature of the spatial lumping into hydrologically similar zones the TOPMODEL structure does not currently facilitate the extraction of runoff from points within the catchment, i.e.: along the edge of the slope base. It would be necessary to adopt one of two approaches. The first would be to model the catchment areas contributing to each of the base of slope grid squares separately to give a distributed output along the slope base which would be time-consuming. Alternatively, since a spatially averaged output is to be used, minor alterations could be made to the code to extract the total outflow at each time step. Normally outflows are contributed to channel flow. In the case of this proposed application, only the hillslopes would be modelled so outflows could be extracted at the slope base and divided by the slope width to give a spatially averaged output. The method of catchment subdivision used by VSAS3 makes the model ideally suited in this respect. Outputs from each of the segments are cumulated and lagged by a time interval estimated to take account of the channel transport time and it is relatively easy to extract segment outflows by modelling each segment separately to obtain an output file for that segment. These outflows would only require a small amount of pre-processing prior to input to RMA-2.

Another factor which must be taken into account is the fact that no hydrographs or other hydrological data are available for the hillslopes of the Culm. For TOPMODEL the parameter, f, the decay coefficient of soil hydraulic conductivity with depth, has to be derived either from the recession limb of the observed hydrograph or from field measurements of hydraulic conductivity. However, the semi-theoretical approach made to this application would allow typical values of hydraulic conductivity for the

various soil types to be used. All the parameters required by VSAS3 can be derived from field measurements and empirical relationships thus typical values can also be used for the hillslope environments to be considered. The ease with which the parameter values can be changed for the sensitivity analysis is another important issue. The five parameters selected in Chapter Two were; rainfall event, hydraulic conductivity, soil depth, antecedent conditions and slope angle. Obviously the rainfall event and antecedent conditions are the easiest parameters to change for both models. For each hydraulic conductivity value used, the whole slope area will be assumed to be homogenous. Therefore applying the same soil properties to every hillslope sub unit will be relatively simple to implement which would also apply when changing the soil depth. However, changing the slope angle for TOPMODEL could present problems. This is because TOPMODEL is set up from a DTM of the hillslope. The average angle for the whole slope can be calculated from individual grid squares. Changing this average would be a complicated process, particularly if the aspect and relative slope of grid squares was not to be altered at the same time. The VSAS3 structure makes this process considerably simpler. The angle of each segment increment is easy to obtain and changing the average angle would not require many calculations.

Considering the points above, VSAS3 was selected to simulate hillslope inflows due to the lack of data available to set up the model, the ease with which runoff may be extracted along the base of the slope and the fact that changing the values of the parameters selected for the sensitivity analysis will not require complex calculations. VSAS3 has an additional advantage over TOPMODEL for simulating hillslope inflows in that future applications following on from this first pass study may require spatially distributed predictions along the slope base to investigate the effects of catchment heterogeneity on local inundation extents. TOPMODEL does incorporate spatial heterogeneity but does not produce a spatially distributed output at the slope base.

4.4 VSAS3 STRUCTURE

The structure of the Variable Source Area Simulator is now discussed starting with the discretisation used to represent the geometry of the catchment or slope. The required model inputs are described (template input files and lists of input parameters may be found in the appendices). Once the input parameters have been set up, the simulation commences after a period of model initialisation. The final sections describe the

process representation of rainfall input, overland and channel flow and subsurface flow as well as the mathematical solution scheme. Finally the model outputs are described.

4.4.1 *Catchment subdivision*

Segments

The catchment is divided into a number of segments, the location of which is determined by hand using large scale (e.g.: 1:5000) topographic maps of the catchment and any knowledge of flow paths within it. Segments have various geometric properties including length, depth, slope width and shape. These geometric properties are, to a large extent, determined by conditions imposed by the model structure. Each segment is modelled as a separate hydrological unit and stretches from the slope base to the watershed. Water is assumed to exit a segment only at the base by flowing into a stream channel, this requires the segment boundaries (normally a ridge), watershed boundary and soil base to be impermeable. The central flow line which runs down the centre of each segment should be orthogonal to the contours as this is the flow line along which all subsurface flow moves to the stream. Segments can be rectangular, square, convergent or divergent in shape and segment boundaries may overlap in order to accommodate these conditions. The number of segments used is dependent upon the size and topographic characteristics of the basin; previous applications to catchments of 0.68 and 1.85 km^2 have used 9 and 29 segments respectively.

Once the locations of segment boundaries have been determined various properties are assigned to the segments which are then sub-divided as shown in Figure 4.4. Any impermeable areas and channels occurring within the bounds of a segment are expressed as a percentage. Up to five soil layers may be assigned to each segment. The depth assigned to each layer is assumed to be uniform over the whole area of the segment. A percentage of each soil depth represented as stones can also be input. This is converted to a volume which is then discounted from the element volume area. This assumes that the stones are impervious and therefore the volume of the soil available for soil moisture flow is diminished.

Increments

Each segment is divided slopewise into up to 10 increments. This division is carried out in a logistic manner using the partitioning rule shown below:

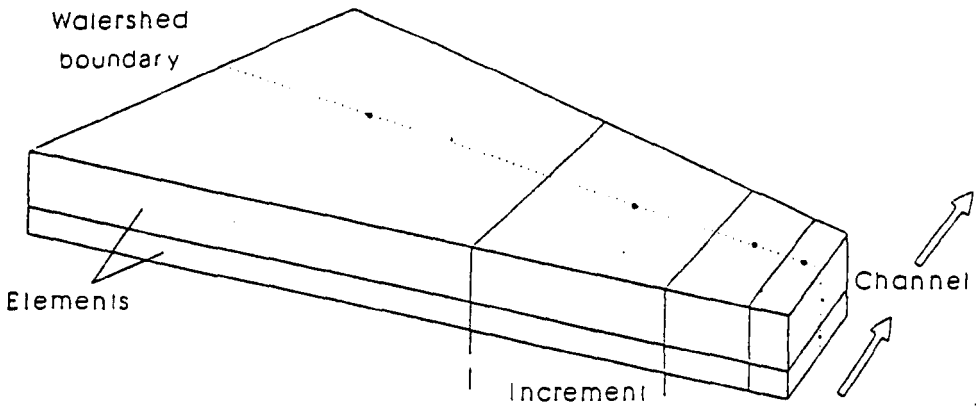

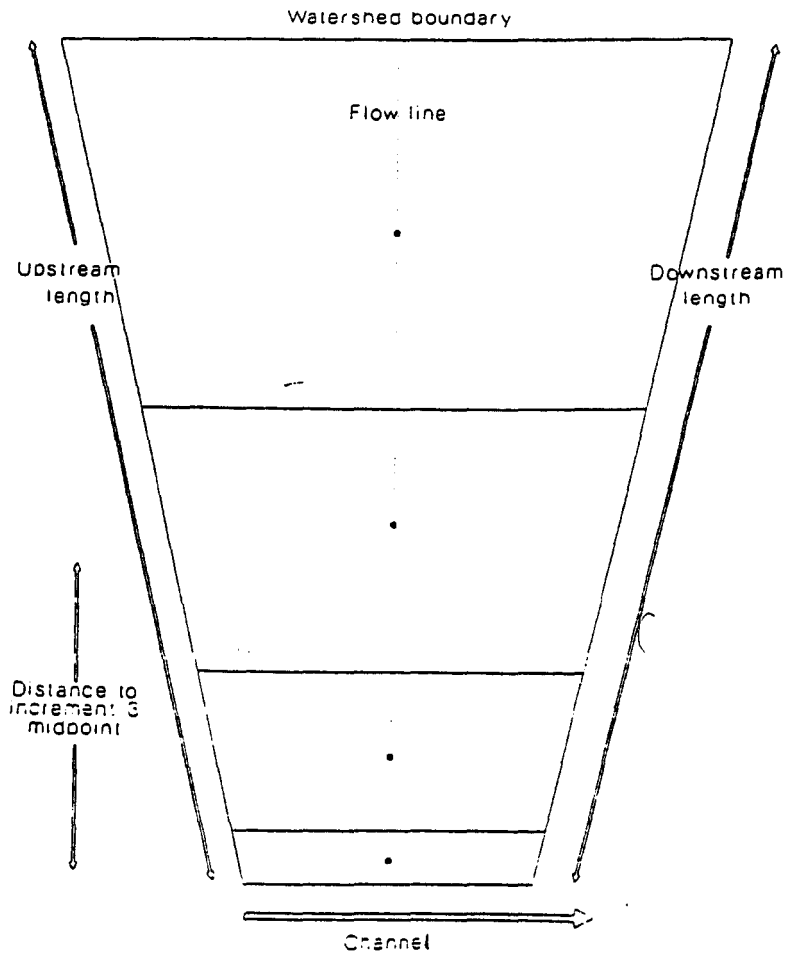

Figure 4.4: **Segment subdivisions (after Davie, 1992)**

$$d_n = D\frac{n-1^2}{N} \qquad 4.16$$

Where:

d_n = distance from the base of the segment to the lower edge of the increment (n) in question

D = total distance from the stream to the ridge

N = total number of increments chosen to represent the slope

The percentage of the total slope included in each increment by this rule, for the example of n=10 is; 1%, 3%, 5%, 7%, 9%, 11%, 13%, 15%, 17% and 19% moving upslope from the slope base which allows for a finer spatial representation at the slope base.

Elements

Increments are sub-divided with depth into up to five elements, this number being determined by the number of soil layers assigned to the parent segment. Elements are the basic unit of VSAS3 and the element centre points are the solution points for the block centred finite difference scheme used by VSAS3. Linkage between the element centres is the flow line along which it is assumed all the subsurface flow moves to the stream. For each centre point, the following parameters are derived from topographic map and field investigations:

- The surface elevation
- Distance to the stream
- The soil depth to impermeable bedrock
- Soil and hydrologic parameters (discussed in the next section)

Pre-processing of geometric data

VSAS3 calculates the relevant volumes, distances and areas (e.g.: element volume, distance between element centres, surface area between elements) required for the soil water flow equations in a subroutine before the start of the actual simulation. The geometric input parameters are listed in the appendices together with a template geometry input file in the Appendix.

4.4.2 *Precipitation and interception*

Rainfall is read in as hourly values prior to the start of the simulation and the model calculates the flows into and out of each segment in turn for the whole storm. The

hourly rainfall is divided into even increments, the size of these increments being an input value (the internal time step). All of the process representation is calculated at this internal time step except for channel flow which is lagged for every hour. The precipitation input is pre-processed by an interception component before reaching the ground. This operates as a tank storage which must be filled before water can reach the ground. Once full, the interception component plays no further part in the simulation unless it is emptied; this can only occur after a 24 hour rain-free period after which water is assumed to have evaporated and storage emptying occurs instantaneously. Rainfall and interception are assumed to cover the entire catchment evenly with an even depth of water being applied to each segment.

4.4.3 *Overland and channel flow components*

Overland flow

There are two sources of overland flow; these represent direct runoff from impermeable areas and saturated overland flow. The first of these is derived from the impermeable surface area, if defined, and channel area for each segment. These areas are treated as a separate unit and combined as a directly contributing area. The ratio of this area to the segment area is determined during the model initialisation phase. At each internal timestep the rainfall contribution to the segment is multiplied by this fraction. The resultant volume is delivered directly to the channel for routing with the rest of the flow for that hour. The remaining rainfall input is added to the segment as rainfall. Saturated overland flow is produced when the surface becomes saturated from beneath. If this occurs from the subsurface simulation, the excess is moved downslope filling in any unsaturated elements until the stream is reached. The final quantity contributes to direct runoff and subsurface contributions to stormflow.

Channel flow

Flows are accounted for each hour then lagged according to the estimated time of travel from each segment to the basin outlet. This involves passing a certain proportion of a given hour's flow to the following hour. Flows from each segment simulation are thus accumulated to form the final outflow hydrograph. In this application, no channel flow component is included and the hourly output from each segment is extracted separately.

4.4.4 *Soil hydrological characteristics*

Segments are divided into hydrologic zones, zones being regions with distinct soil hydrologic properties that stretch across the segment width. These zones are delimited along the line running through the element centres using the position upslope to the top of that soil zone's properties, expressed as a percentage of the total slope length. Elements are then assigned hydrologic properties according to the zone in which the element centre falls. Soil elements are thus assumed to be isotropic. Each element is also assigned an initial moisture content expressed as a percentage.

As outlined in Section 4.3.3 the rate of subsurface flow is calculated using the Richards generalisation of Darcy's law. This is combined with the continuity equation to give an equation for soil water flow in 3-D. Most of the soil hydrologic characteristics required to solve the governing equations can be derived from empirical relationships backed up by fieldwork. Brackenseik and Rawls (1983) describe a number of relationships between soil particle size distribution and soil hydrologic properties which can be used to do this. The values of soil moisture content (porosity), saturated hydraulic conductivity and a suction-moisture curve are input for each soil zone together with the standard deviations of each value. The actual values of these parameters for each element are then stochastically derived by VSAS3 before the simulation, taking the values randomly from a normal distribution of the defined mean and standard deviation. This attempts to account for the heterogeneity in soil physical properties that is known to occur in field.

The Millington-Quirk algorithm (Millington and Quirk, 1961) is used to mathematically transform a known soil suction - soil moisture curve to an unsaturated conductivity - soil moisture curve. The new curve is based on the stochastically derived values of saturated moisture content and saturated hydraulic conductivity together with probability of flow continuity between pores of a certain size (the maximum size is governed by the moisture content). An example of a suction - moisture curve and the corresponding unsaturated hydraulic conductivities derived using this method is shown in Figure 4.5. The algorithm was included in the VSAS3 structure by Whitelaw (1988) to give a greater degree of theoretical foundation than the purely empirical Campbell method which was previously used. The Millington-Quirk algorithm is shown below:

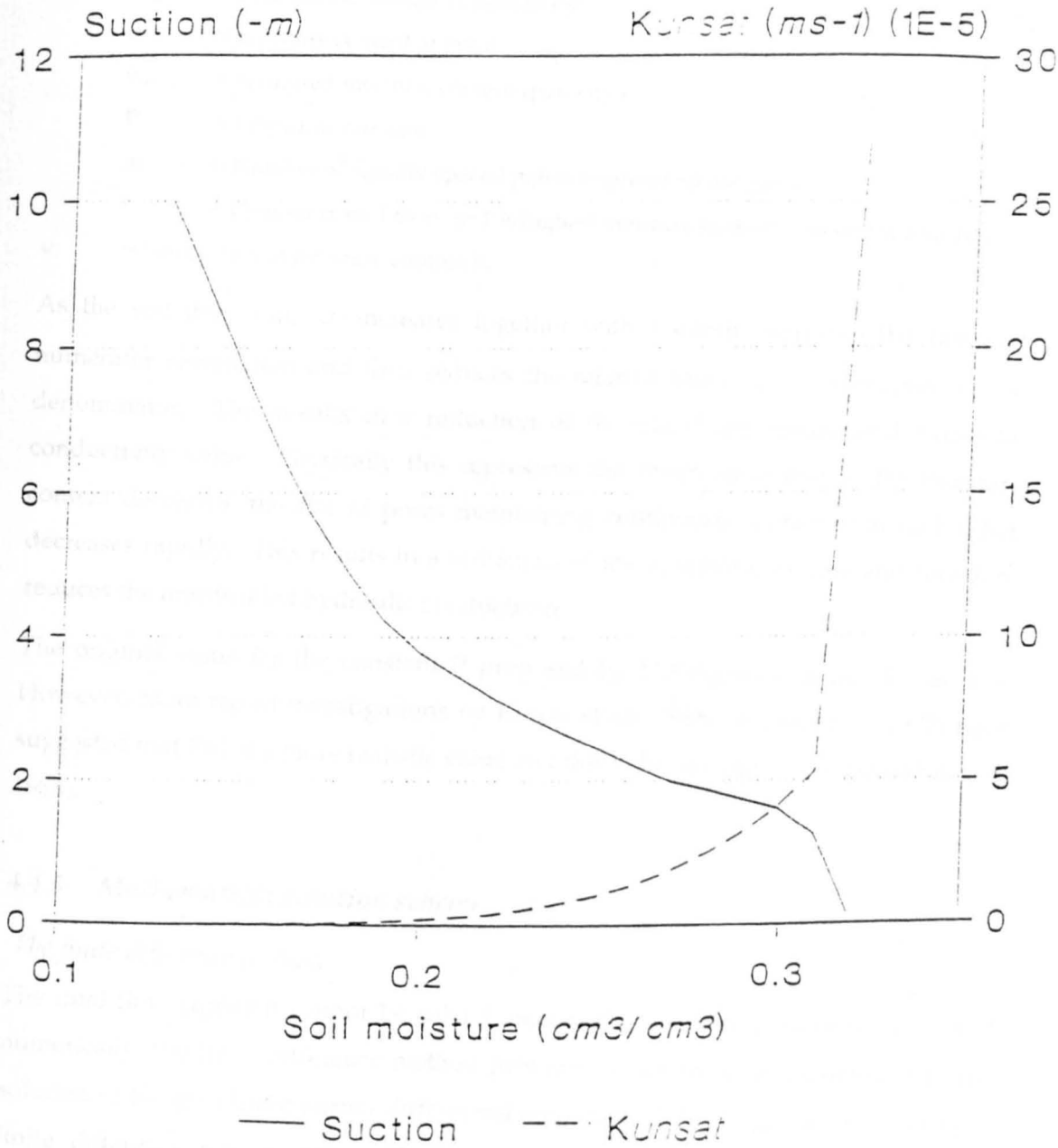

Figure 4.5: **Example of a suction-moisture curve and unsaturated hydraulic characteristics derived using the Millington-Quirk method (after Davie, 1992)**

$$k(\theta)_i = k_{sat}\left(\frac{\theta_i}{\theta_{sat}}\right)^p \frac{\sum_{j=i}^{m}\left((2j+1-2i)\psi_j^{-2}\right)}{\sum_{j=1}^{m}\left((2j-1)\psi_j^{-2}\right)} \qquad 4.17$$

Where: $K(\theta)_i$ = unsaturated hydraulic conductivity at point i on the suction moisture curve

K_{sat} = saturated hydraulic conductivity

θ_i = moisture content at point i

θ_{sat} = Saturated moisture content (porosity)

P = Empirical constant

m = Number of equally spaced points required on the θ axis

i = Counter from 1 to m (i=1 is highest moisture content ∴ lowest soil suction)

ψ_j = Soil suction at moisture content θ_i

As the soil dries out, ψ increases together with i which decreases the range of numerator summation and thus reduces the relative value of the numerator to the denominator. This results in a reduction of the calculated unsaturated hydraulic conductivity value. Physically this represents the observation that as the moisture content decreases, the size of pores maintaining continuous contact with each other decreases rapidly. This results in a reduction of the possible flow rate and therefore reduces the unsaturated hydraulic conductivity.

The original value for the constant P proposed by Millington and Quirk was 4/3. However, more recent investigations by Kunze et al. (1968) and Jackson (1972) have suggested that P=1 is a more realistic value and this value is used in VSAS3 (Whitelaw, 1988).

4.4.5 *Mathematical solution scheme*

The finite difference method

The final flow equation cannot be solved analytically and therefore must be solved numerically, the finite difference method provides a numerical approximation to the solution of the governing partial differential equations. VSAS3 uses a "block-centred finite difference scheme where the smooth function representing the change in moisture content over time and space is approximated by linear sections over time and space is approximated by linear sections over finite time and space increments" (Bernier 1982). The continuum of the system being modelled by a finite difference model is represented by a series of small discrete areas or elements. Finite difference

models may be either node based or grid based, depending on the location of the solutional locations. Grid based (or mesh centred) models have solutional nodes at the corners of elements whereas node based (block centred) models such as VSAS3 have solutional nodes located at the centre of each element. Whereas grid based schemes are easier to deal with in terms of boundaries, block centred schemes are intuitively better since the solutional node is at the centre of the region it represents. The set of equations describing the behaviour of the system at each solutional location is derived from the original partial differential equation. After the inclusion of boundary conditions, this set of equations is solved by a numerical method to provide spatially distributed values of the variable in question. In the case of VSAS3, this discretisation is extended to include the time dimension so the spatial results are derived at a series of different times. Flows are calculated in the following order:

1. Slopewise flows
2. Vertical flows

4.4.6 *Model Outputs*

Two output files are produced by VSAS3. The first of these contains the predicted hourly discharge from each segment which is lagged and cumulated to produce an hourly catchment outflow prediction. Alternatively, if the segments are modelled separately, this file displays the predicted hourly discharge from that segment. The second file contains the soil moisture conditions (percentage saturation, moisture content and suction) for each soil element and at each timestep.

4.5 SETTING UP VSAS3

VSAS3 was set up for an initial simulation prior to carrying out the sensitivity analysis. This section describes setting up the model for the Culm hillslope section.

4.5.1 *Selection of a template slope and slope segmentation*

The hillslope section used as the geometric template for the application of VSAS3 is shown in Figure 4.6 together with the segmentation derived for it. The area within the selected slope contains relatively few roads and built up areas and has a fairly uniform slope profile. It was selected from four possible hillslope sections bordering the Culm, each of approximately 1km width. Slopes at the upstream end of the reach were considered since those at the downstream end were found to be very shallow and

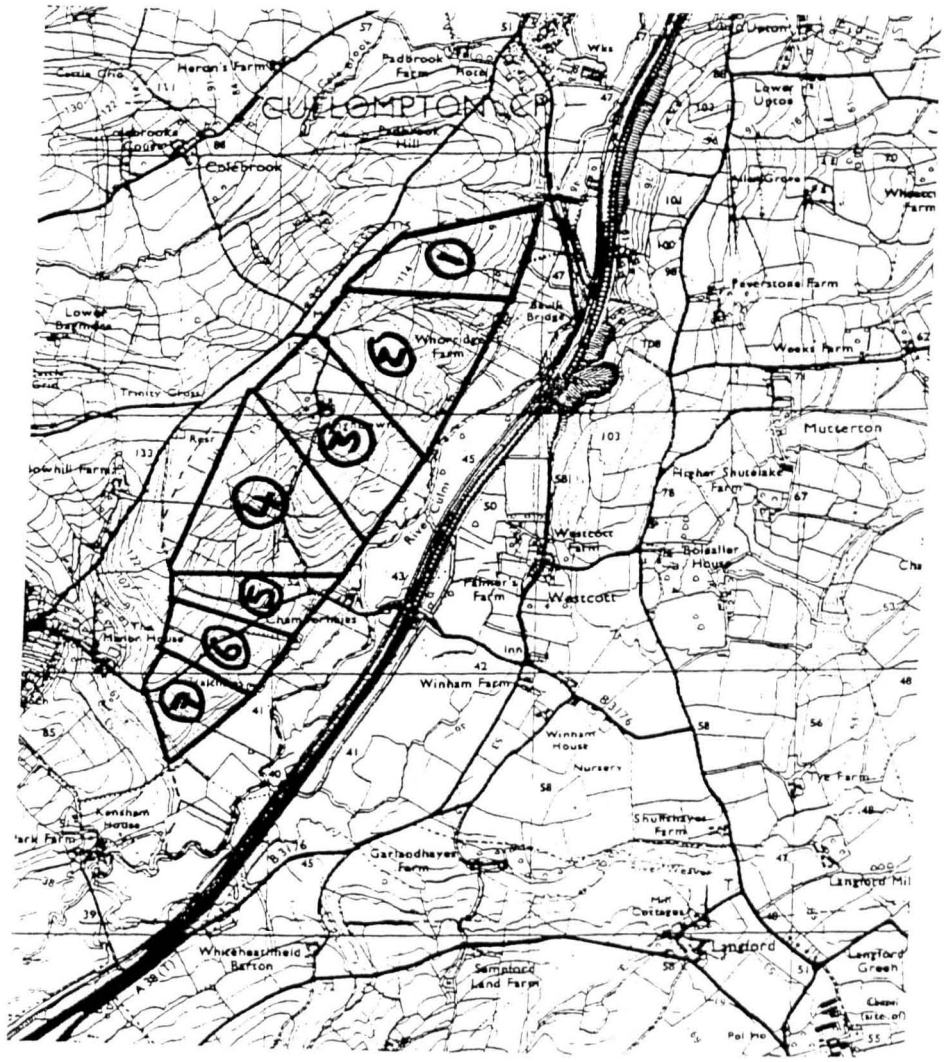

Figure 4.6: Segmentation of the Culm hillslope

therefore unsuitable for using as a geometric template to represent a full range of hillslope environments. It was felt to be appropriate to select a slope with as straight a profile as possible. Since the slope convergence / divergence was not being investigated in the sensitivity analysis a straight profile provided the best 'mean' for this unaltered parameter. Obviously some variation occurred within the profile although the overall profile was straight.

The segmentation was set up for this slope from an enlarged copy of the 1:25 000 maps available for the catchment. From this enlarged map, the contours, channels and spot heights were traced. The tracing was used as the basis for locating the segment boundaries.

Seven segments were allocated to the slope; segment boundaries were determined by examining the contours to estimate likely areas of flow convergence and divergence. Where small channels were marked, it was assumed that flow convergence occurred so these were assigned to the centre of a segment. The sides of segments were located, where possible, down the line of likely no-flow boundaries such as areas of flow divergence.

Once the location of the segments had been determined, the length of each segment was measured from the plot. Individual segments were divided slopewise into 10 increments by running a program which used the partitioning rule described in Section 4.4.1. This program also calculated the location of increment centre points. The height of each centre point was interpolated from the contour heights by hand. The width of each segment at the channel and watershed was measured together with the lengths of the upstream and downstream sides of the segment. A depth of 0.5 m was assigned to the soil for the initial simulation and each segment was divided vertically into three soil layers of equal depth (0.17 m). No impermeable areas or channels were included.

4.5.2 *Rainfall event*

Rainfall data were supplied by the National Rivers Authority South Western region. Several rain gauges are located within the watershed of the River Culm although no gauge is located on the slope of interest. It was therefore necessary to adjust data from the nearest gauges which are located at Hemyock and Kentisbeare (Figure 4.7). Although the Hemyock gauge is closest, a daily rainfall total only was available. Due to this, the hourly rainfalls recorded at Kentisbeare were adjusted so that the daily

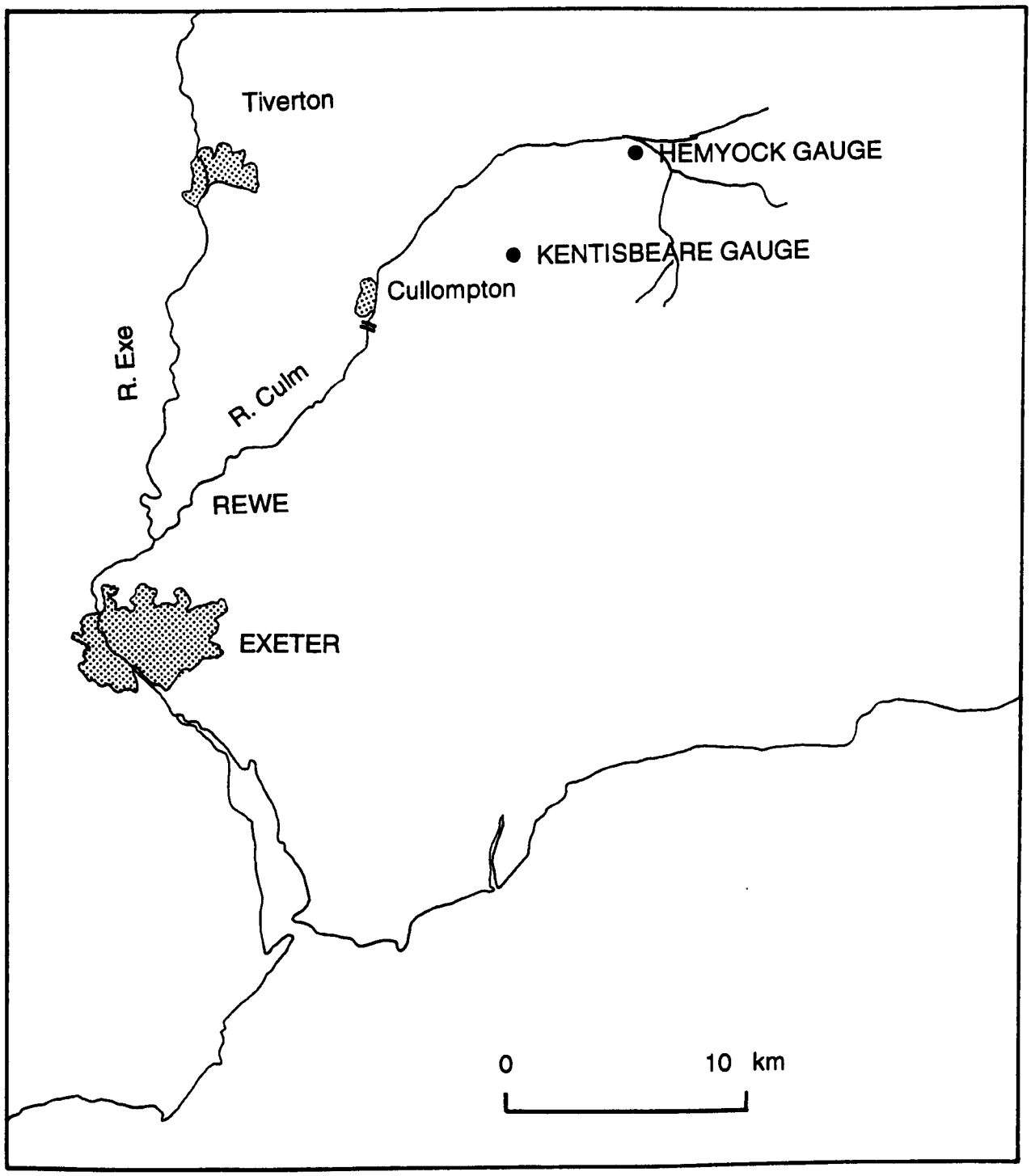

Figure 4.7: The locations of the gauges at Hemyock and Kentisbeare

total was equal to that recorded at Hemyock. Data was available from two gauges are located at Kentisbeare, an hourly gauge and a daily check gauge. The first stage in the data conversion was to digitise the charts from the hourly gauge. The total rainfall from the hourly gauge was then calculated for each of the days of interest and was compared with the volume for the check gauge. If these differed, the hourly values were adjusted to give a daily total which was the same as that recorded by the check gauge. After this, the hourly figures were adjusted so that the total daily volume was the same as that recorded at Hemyock. This process is illustrated in Figure 4.8. The event used for the initial simulation was the 1 in 1 year event of 27-01-90 to 28-01-90. This is the event which produced the input hydrograph used in the RMA-2 1 in 1 year simulation.

The rainfall graph for this event is shown in Figure 4.9 together with the observed upstream hydrograph at Rewe which was the input hydrograph applied to RMA-2. From this it can be seen that most of the recorded rainfall occurs during the 24 hours preceding the start of the RMA-2 simulation; because of this, rainfall data were also digitised for this period and included in the VSAS3 input file. This ensured that the VSAS3 simulation included the whole rainfall event which was felt to be important since it was very likely to affect the characteristics of the part of the predicted hillslope hydrograph to be used in the coupled simulation. The hourly rainfall data, in cm, was entered into an input file and was applied separately to each of the seven segments for a given simulation.

4.5.3 *Soil hydrologic characteristics*

All the soil elements were assumed to have similar soil hydrologic properties. The saturated moisture content (porosity) for these were obtained using empirical relationships derived from extensive fieldwork carried out by Brakenseik and Rawls (1983) who studied 1,322 soils. They describe a number of relationships between the soil particle size distribution and soil hydrologic properties, including the saturated hydraulic conductivity of a given soil. The initial value used in this investigation, 5.56 x 10^{-6} for a loamy soil, was estimated from the soil property chart shown in Figure 4.10. A value of 0.485 was assigned for the saturated moisture content which reflects the volumetric water content of the soil at saturation.

A suction-moisture curve was also required since VSAS3 calculates equivalent unsaturated hydraulic conductivities using this curve (Section 4.4.3).

FOR EACH DATE OF INTEREST (Day(n)):

1) Calcluate daily rainfall total at Hemyock

$$\Sigma H_h = H_{h1} + H_{h2} + H_{h3} \ldots . H_{h23}$$

Where: ΣH_h = Daily total for Hemyock hourly gauge

H_{h1}, H_{h2}, H_{h3} = Hourly values from Hemyock hourly gauge

2) Convert hourly rainfall values so that the total from the Hemyock hourly gauge is the same as the Hemyock daily check guage (H_d) value for Day(n)

If the sum of hourly rainfall totals is less than the depth recorded by the daily check gauge for Day(n) ($\Sigma H_h < H_d$) then increase each H_h value by the difference between these values, expressed as a percentage of H_d:

$$H_{h(n)^*} = H_{h(n)} + \left[\frac{(H_d - \Sigma H_h)H_{h(n)}}{100}\right]$$

$$\therefore \Sigma H_{h^*} = H_d$$

Where: $H_{h(n)^*}$ = The corrected nth hourly value

$H_{h(n)}$ = The original nth hourly value

H_d = RF depth recorded by Hemyock daily check gauge

Alternatively if $\Sigma H_h > H_d$, decrease each H_h value by the difference between these values expressed as a percentage of H_d

$$H_{h(n)^*} = H_{h(n)} - \left[\frac{(\Sigma H_h - H_d)H_{h(n)}}{100}\right]$$

$$\therefore \Sigma H_{h^*} = H_d$$

3) Convert corrected Hemyock hourly rainfall values to give a new daily total ($\Sigma H_{h^{**}}$) which is equal to the daily value recorded at Kentisbeare (K_d)

If the rainfall total for that Day(n) at Hemyock is less than that recorded at Kentisbeare ($H_d < Kd$) then increase each corrected hourly value at Hemyock by the difference between these two daily totals expressed as a percentage of the daily value recorded at Hemyock.

$$H_{h(n)^{**}} = H_{h(n)^*} + \left[\frac{(K_d - H_d)H_{h(n)^*}}{100}\right]$$

$$\therefore \Sigma H_{h(n)^{**}} = K_d$$

Where $H_{h(n)^{**}}$ = The final nth hourly rainfall value ($\Sigma H_{h^{**}} = K_d$)

Alternatively, if the rainfall total for that day at Hemyock is less than that recorded at Kentisbeare ($H_d > Kd$) then decrease each corrected hourly value at Hemyock by the difference between these two daily totals expressed as a percentage of the daily value recorded at Hemyock.

$$H_{h(n)^{**}} = H_{h(n)^*} - \left[\frac{(H_d - K_d)H_{h(n)^*}}{100}\right]$$

$$\therefore \Sigma H_{h(n)^{**}} = K_d$$

Figure 4.8: Illustration of the method used to convert the rainfall input

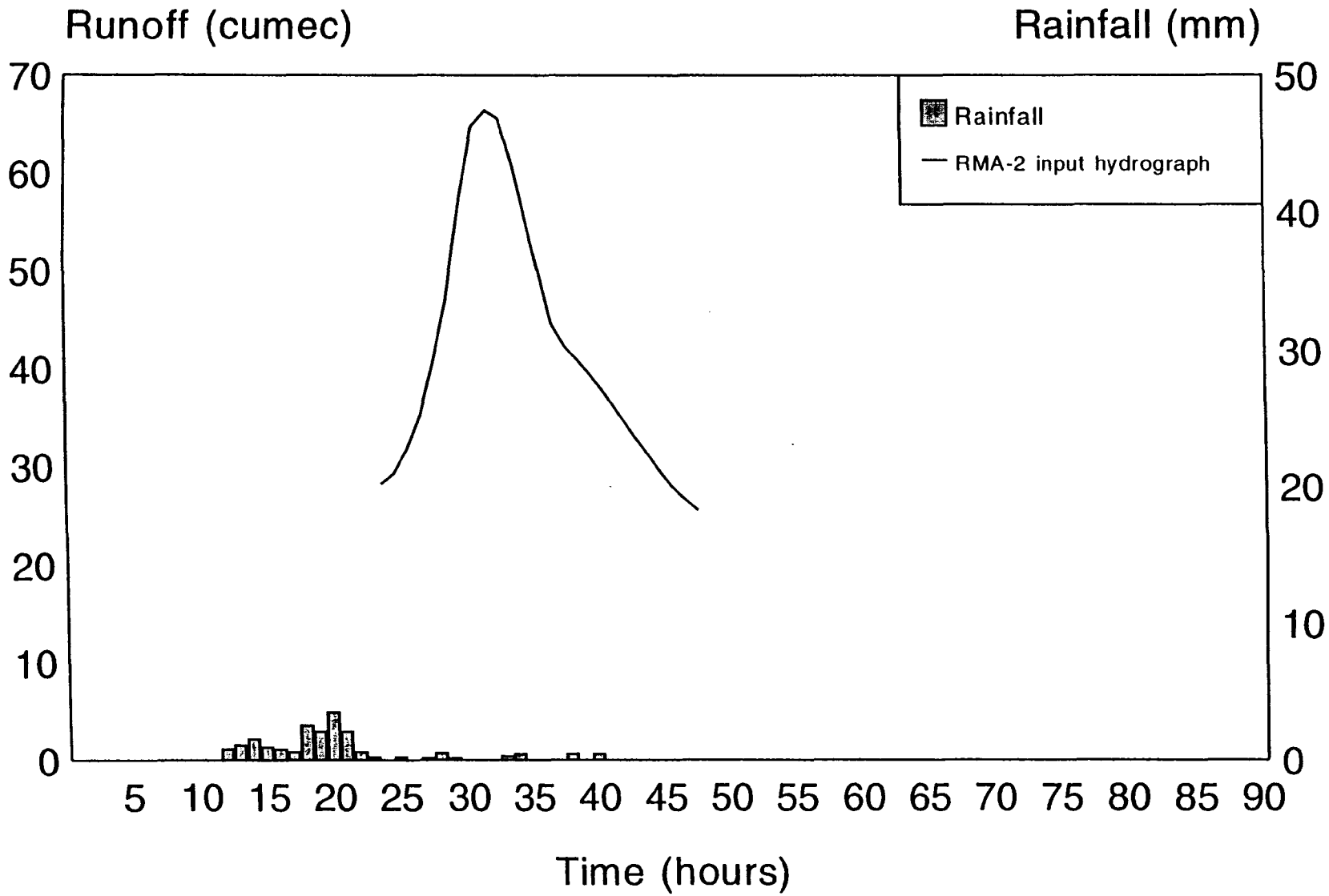

Figure 4.9: **1 in 1 year hydrograph produced by VSAS3 for the Culm hillslope**

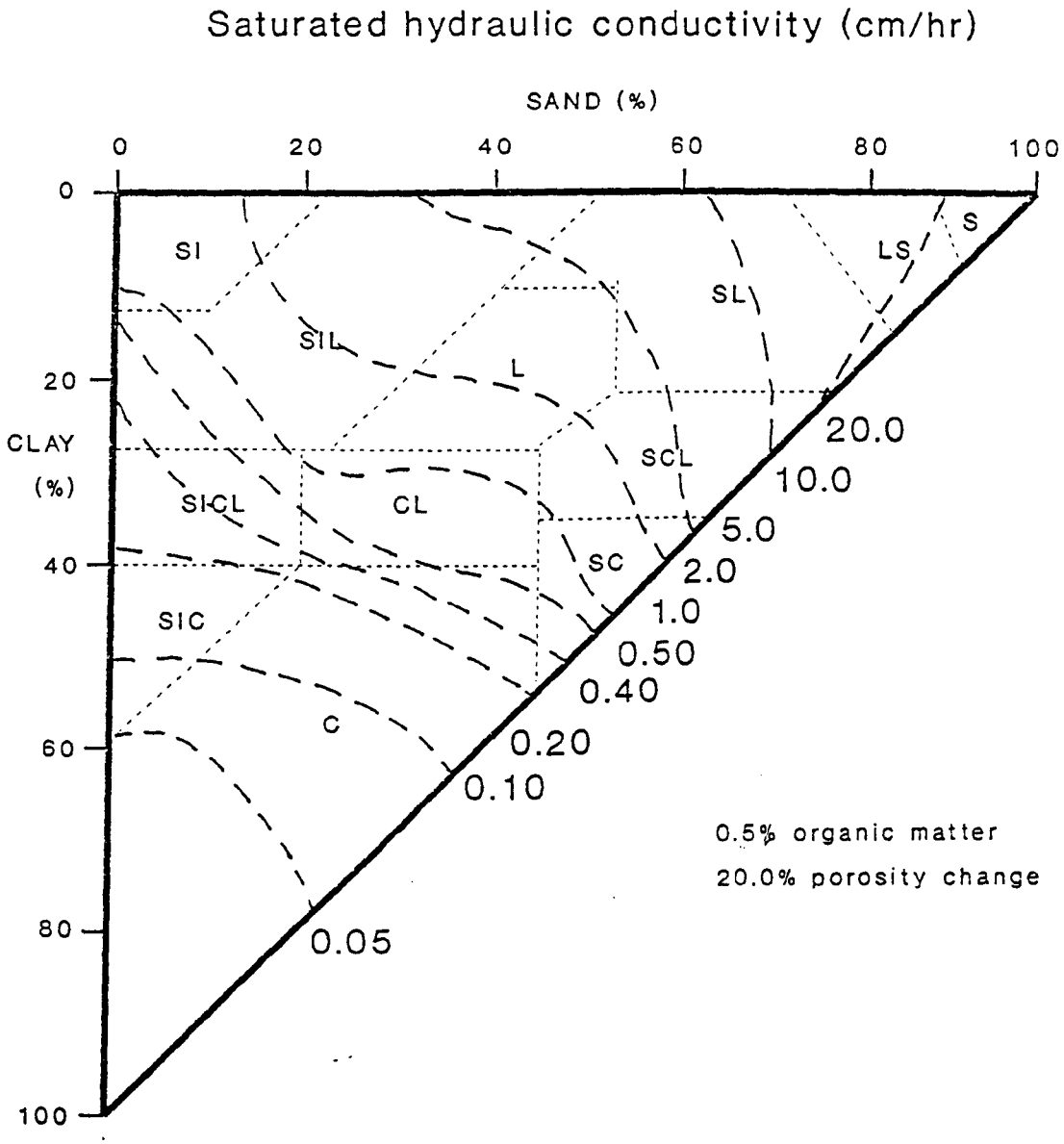

Figure 4.10: **Example of soil property chart based on physical characteristics (after Brakenseik and Rawls, 1983)**

Suction	-10.00	-5.08	-3.35	-1.98	-1.05	-0.001
Moisture content	0.265	0.290	0.310	0.340	0.355	0.484

Table 4.1: Suction - moisture relationship for loam soil

A suction-moisture curve for loamy soil was obtained from Hall et al. (1977) who present figures showing typical suction-moisture curves for 10 of the 11 soil classes on the British Soil Survey textural triangle. These curves were derived by sampling 22 soil groups in England. The suction-moisture curve for a loam soil is shown in Table 4.1.

4.5.4 Initial moisture conditions

The initial moisture conditions used for the original VSAS3 simulation were set up for a slope with a saturated base. The volumetric moisture content at the watershed corresponded to a suction of - 0.02 m and intermediate values were interpolated. The initial moisture conditions applied to the soil elements for each segment simulation is shown below expressed as a unit moisture content (the percentage of the porous volume which is saturated):

	1.000	1.000	1.000	1.000	0.980	0.980	0.950	0.950	0.950	0.950
	1.000	1.000	1.000	1.000	1.000	0.980	0.980	0.980	0.980	0.980
CHANNEL	1.000	1.000	1.000	1.000	1.000	1.000	0.980	0.980	0.980	0.980

4.6 VSAS3 SENSITIVITY ANALYSIS

The purpose of the sensitivity analysis was to find out the effect of changes to selected input parameters on VSAS3 predictions as a preliminary to applying these as inflows to RMA-2; the second stage of the sensitivity analysis. As discussed in Chapter Two, five parameters were selected. For each parameter, three VSAS3 simulations were carried out, altering the parameter over a range of values while all the other parameters were held constant. This attempted to represent the variation in each parameter that might be expected to occur over a range of hillslope environments which might be found in the field. The method of changing the parameters is flexible enough to allow further model runs to be implemented in the future.

4.6.1 Model parameters selected and the range of values assigned to them

Rainfall event

Three storm events were used in this investigation. These had different return periods and were selected for the following reasons:

i) Availability of rainfall data

ii) Availability of observed hydrographs at Woodmill and Rewe to run RMA-2

iii) The range of return periods covered by these events

Each VSAS3 simulation was started 24 hours before the start of the corresponding RMA-2 simulation for the reason explained in Section 4.5.2. The relative timing of the VSAS3 and RMA-2 simulations is shown in Table 4.2:

Event return period	VSAS3 start date	VSAS3 start time	RMA-2 start date	RMA-2 start time	VSAS3 and RMA-2 end date	VSAS3 and RMA-2 end time
1 in 1 yr.	27-01-90	0045	28-01-90	0045	28-01-90	2145
1 in 5 yr.	25-01-84	0300	26-01-84	0300	28-01-84	1630
1 in 12 yr.	26-12-79	1630	27-12-79	1630	28-12-79	2100

Table 4.2: The timing of VSAS3 and RMA-2 simulations carried out. The coupled simulation was carried out over the same period of time as the RMA-2 simulation.

Hourly rainfall data was again only available at Hemyock, together with a daily total from the check gauge although at Kentisbeare a daily total was also available for all the dates within the range covered by the two events. After digitising the hourly rainfall amounts from the charts, the data was adjusted in the manner described in Figure 4.8. The rainfall graphs are shown together with the predicted hillslope hydrographs in Figures 4.15 and 4.16.

Saturated hydraulic conductivity

In changing the soil hydraulic properties, all the soil layers were assumed to have similar soil hydrologic properties. Three model simulations were carried out covering a range of soil textures from sand to clay loam. The saturated moisture contents (porosity) for these were obtained using the empirical relationships derived by Brakenseik and Rawls in the same way as for the loamy soil. The hydraulic conductivities are displayed in Table 4.3.

Run number	Soil type	Saturated hydraulic conductivity value
V01	loam	5.56×10^{-6} m s^{-1}
V04	clay loam	1.39×10^{-6} m s^{-1}
V05	sand	1.00×10^{-4} m s^{-1}

Table 4.3: Saturated hydraulic conductivity values used in the VSAS3 sensitivity analysis.

In addition, new suction-moisture curves were applied for each soil texture since the new soil textures would also have different unsaturated hydraulic conductivities at a range of suctions. The suction - moisture curves from Hall et al. (1977) were used for these soils in the same way as the original suction-moisture curve.

Soil depth

A range of depths was considered, varying from 0.1m to 1.0m. The initial VSAS3 run used a soil depth of 0.5m. In order to alter the depth, seven new geometry input files were created for each new soil depth value. In addition, the depths of the layers was adjusted so that they were still equal, layers with depths of 0.03 m and 0.3 m were used respectively for the 0.1 m and 1.0 m soil depths.

Initial moisture conditions

The initial moisture conditions input file used in the initial VSAS3 simulation were set up for a slope with a saturated base. An input file representing dryer initial moisture conditions was created by running VSAS3 for segment 1 with no rainfall input, using the original initial moisture input file as a starting point and effectively draining the slope. The model was run for 168 time steps (equivalent to one week). The resultant elemental soil moisture contents at the end of this simulation are shown below and were used as a new input file to simulate dryer conditions:

	0.958	0.958	0.958	0.937	0.936	0.954	0.928	0.928	0.928	0.928
	0.966	0.967	0.996	0.964	0.958	1.000	0.955	0.957	0.955	0.961
CHANNEL	0.988	0.984	1.000	0.987	0.979	1.000	0.981	0.995	0.980	1.000

The difference between the two initial moisture input files used was not very great so another input file was set up to represent much dryer initial moisture conditions. The antecedent moisture conditions were estimated using volumetric moisture contents of 0.425 at the slope base and 0.320 at the watershed and interpolating between them. These values were selected because of the increase in suction for these moisture

contents on the loam suction-moisture curve used in these investigations. The suction at the slope base was 0.045 m and at the watershed 4.7 m. A suction of 4 m is typical of drought conditions in the UK. If the suction - moisture curve shown in Table 4.1 is examined, it can be seen that for a loam soil there is a sharp increase in moisture conditions as the suction increases to values above - 1 m. The unit percentage moisture contents for each soil element are shown below:

	0.425	0.420	0.410	0.395	0.380	0.365	0.350	0.335	0.320	0.320
	0.425	0.425	0.420	0.410	0.395	0.380	0.365	0.350	0.335	0.320
CHANNEL	0.425	0.425	0.425	0.420	0.420	0.410	0.395	0.380	0.250	0.335

However, since this did not produce any runoff during the period of the simulation, another file was created with moisture contents corresponding to suctions less than - 1 m which was used as the third input file for the sensitivity analysis:

	0.800	0.800	0.800	0.800	0.780	0.780	0.750	0.750	0.750	0.750
	0.800	0.800	0.800	0.800	0.780	0.780	0.780	0.780	0.780	0.780
CHANNEL	0.800	0.800	0.800	0.800	0.800	0.800	0.780	0.780	0.780	0.780

Slope angle

The average angle of the Culm test slope is 8°; this mean was calculated from the angles of the 70 increments from the 7 segments defining the Culm hillslope. Input files using average slope angles of 12° and 45° were also set up. The method employed to do this is described below:

1) For each segment, the increment angles were obtained. This was done by interpolating between adjacent increment centre points upslope to obtain the height at the base and top of each increment. The distances of the increment base and top from the segment base were obtained from the output file of the segment partitioning program (Section 4.4.1). The angle of the increment was calculated using this information.

2) The mean angle of each segment ($\bar{\theta}$) was calculated as the mean of the increment angles within that segment (Figure 4.11i).

3) The mean angle for the slope (θ_{slope}) was calculated as the mean of the segment means.

i) Calculating the mean angle for a segment:

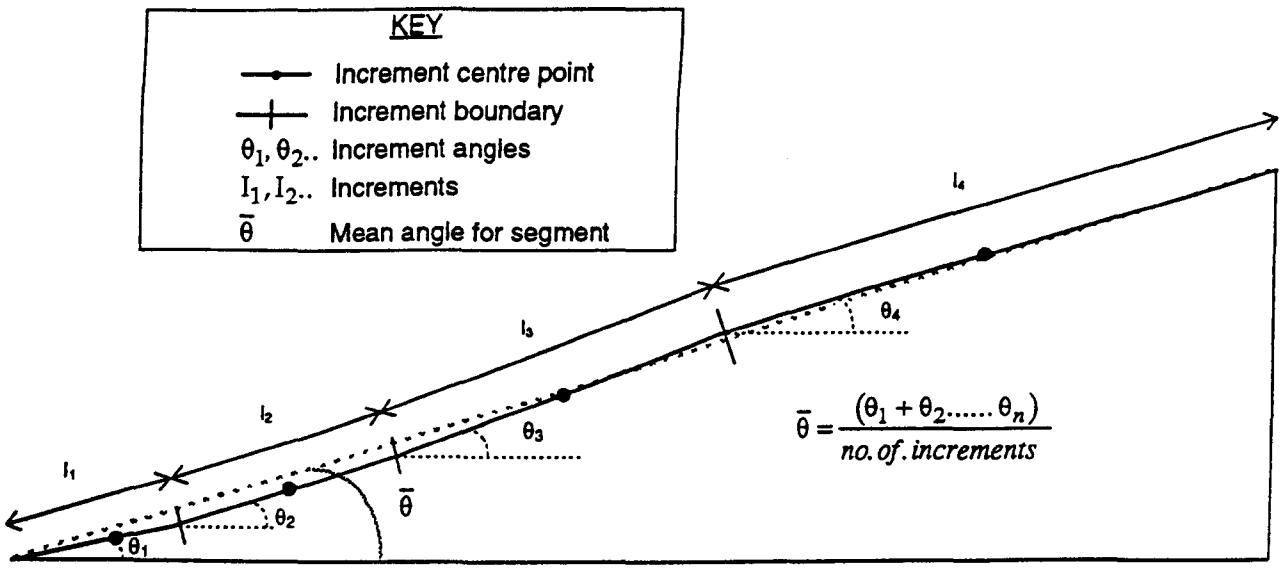

ii) For a segment, S_x, with a mean increment angle, $\bar{\theta}_x$ the deviation, D_x from the mean angle for the slope ($\bar{\theta}_{slope}$),is given by:

$$D_x = \left[\frac{\bar{\theta}_{slope} - \bar{\theta}_x}{\bar{\theta}_{slope}}\right] \times 100$$

iii) For a new mean slope angle $\bar{\theta}'_{slope}$, the new angle θ'_x for the segment S_x is given by:

$$\theta_x' = \bar{\theta}'_{slope} + \left[\frac{\left(D_x \cdot \bar{\theta}'_{slope}\right)}{100}\right]$$

From this new angle, the new heights of increment centre points and boundaries can be obtained (The distance of these from the slope base remains the same). All the increments within a particular segment will now have the same angle

Figure 4.11: Illustration of the method used to re-calculate slope and segment angles

4) The percentage deviation of each segment mean from the slope mean (D_x) was then calculated (Figure 4.11ii).

5) Assigning a new mean angle ($\bar{\theta}'$) to the slope involved calculating new segment angles by weighting $\bar{\theta}'$ by each segment's percentage deviation from the mean (Figure 4.11iii). The new segment angles are shown in Table 4.4.

6) For each segment, the horizontal distance from the segment base to the base, top and centre point of each increment was the same for all slope angles. New increment heights were calculated from the new segment angle ($\bar{\theta}'_x$).

Segment number	Segment angle (mean angle of slope = 7.75°)	Deviation from mean	Segment angle when $\bar{\theta}'$ = 12°	Segment angle when $\bar{\theta}'$ = 45°
1	8.12	+ 4.8%	12.58°	47.16°
2	7.22	- 6.8%	11.18°	41.94°
3	6.88	- 11.2%	10.66°	39.96°
4	8.31	+ 7.2 %	12.86°	48.24°
5	7.84	+ 1.2 %	12.14°	45.54°
6	7.51	- 3.1 %	11.62°	43.61°
7	8.35	+ 7.7 %	12.92°	48.47°

Table 4.4: Segment angles, deviations and new angles for slopes of 12° and 45°

The slope profiles produced for Segment 1 using this method are shown in Figure 4.12. From these it can be seen that the longitudinal profile of each segment has been changed. Originally it was proposed to extend the method outlined above to calculate increment deviations within each segment from the segment mean thus maintaining the shape of the slope profile. However, this would have involved considerably more calculations. Therefore, it was proposed to examine the sensitivity of VSAS3 to changes in angle of the simplified segment profiles. If this was found to be significant, the profiles would be adjusted since the altered profile could affect the degree of this sensitivity.

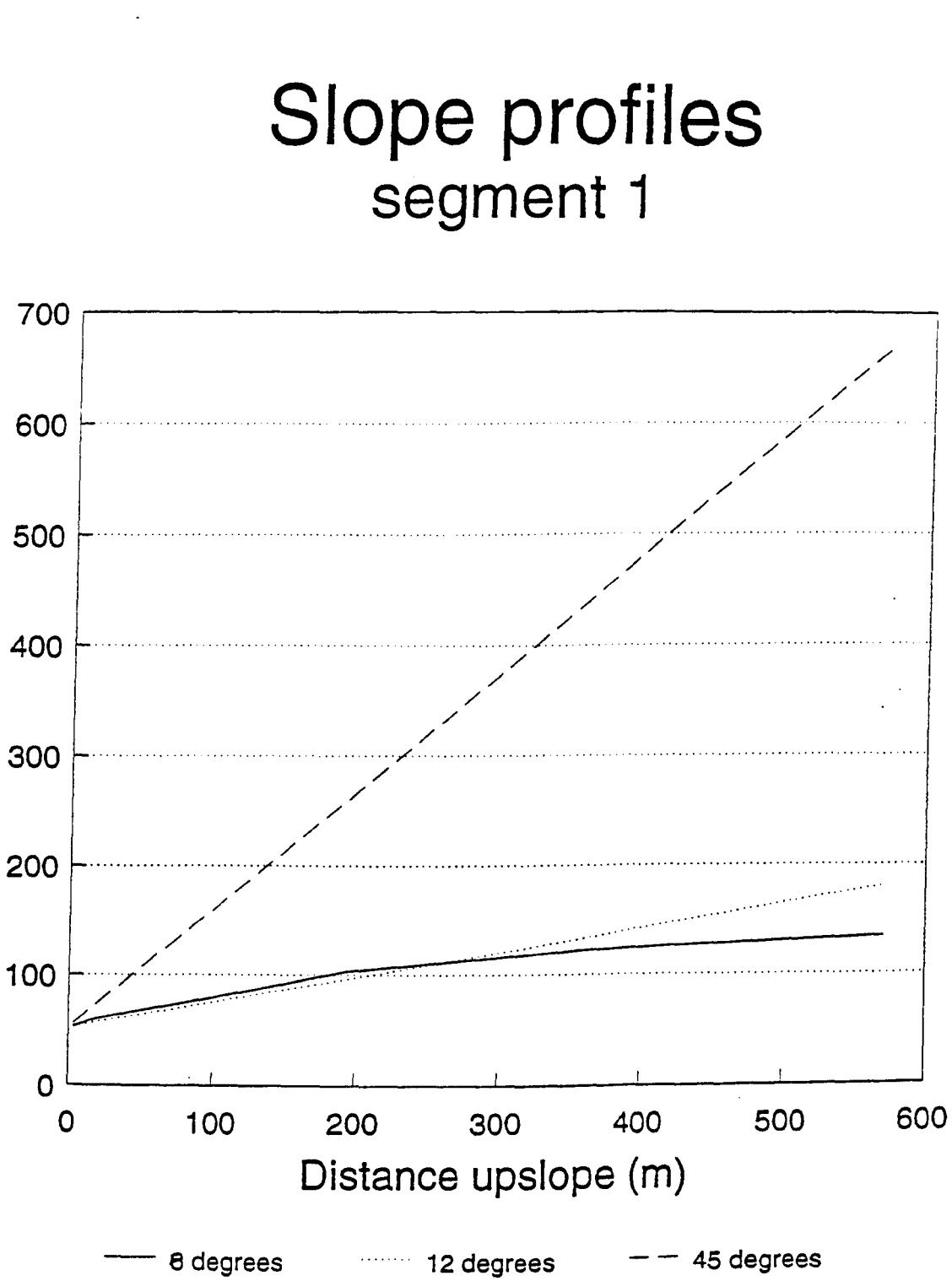

Figure 4.12: The slope profiles generated using the method illustrated in Figure 4.12

4.6.2 *Running VSAS3*

A UNIX macro was written to carry out the simulations. This macro first obtained the appropriate input files from the storage directory. During each simulation, the model was run seven times; once for each segment. At the end of each segment run, the output files produced were uniquely identified and the geometry file for the next segment run obtained. At the end of each set of segment runs, the output files were concatenated to create a big file containing the seven predicted hydrographs for that simulation.

This was stored in an output directory together with the soil moisture data file for segment 1. The next simulation was then carried out in the same way. A summary of the model simulations carried out is shown in Table 4.5.

Simulation number	Rainfall event return period	Hydraulic conductivity ($m\ s^{-1}$)	Soil depth (m)	Unit moisture % at slope base	Slope angle
V01	1 in 1 y	5.56×10^{-6}	0.5	1.000	8°
V02	1 in 5 y	5.56×10^{-6}	0.5	1.000	8°
V03	1 in 12 y	5.56×10^{-6}	0.5	1.000	8°
V04	1 in 1 y	1.39×10^{-6}	0.5	1.000	8°
V05	1 in 1 y	1.00×10^{-4}	0.5	1.000	8°
V06	1 in 1 y	5.56×10^{-6}	0.1	1.000	8°
V07	1 in 1 y	5.56×10^{-6}	1.0	1.000	8°
V08	1 in 1 y	5.56×10^{-6}	0.5	0.980	8°
V09	1 in 1 y	5.56×10^{-6}	0.5	0.800	8°
V10	1 in 1 y	5.56×10^{-6}	0.5	1.000	12°
V11	1 in 1 y	5.56×10^{-6}	0.5	1.000	45°

Table 4.5: VSAS3 simulations carried out for the first stage of sensitivity analysis.

4.7 RESULTS OF THE SENSITIVITY ANALYSIS

4.7.1 *Comparing output from the simulations*

The hydrographs produced by the simulations were compared in terms of the total volume of runoff produced, the volume of runoff produced after the 24 hour 'run in' period ,the timing and discharge of the hydrograph peak, hydrograph shape and soil moisture conditions at selected time steps. A program, *hydsum.f* (shown in the Appendix) was written to calculate the discharge from the slope in $m^3 s^{-1}$ at each time step as well as the total volume of runoff produced by the slope for each simulation. The program summed the volumes of runoff produced by each of the seven segments (in $m^3 h^{-1}$) for all time steps to obtain a total volume in m^3. In addition the discharge from the whole slope at each hour by dividing the hourly total by 3600 to obtain a rate of discharge from the slope for that hour in $m^3 s^{-1}$. The hydrographs produced are shown in the following sections.

4.7.2 *Sensitivity to rainfall events with different return periods*

Hydrographs for the 1 in 1, 1 in 5 and 1 in 12 year return period events are shown in Figures 4.13 - 4.15. Table 4.6 shows the effect of these events with different return periods of the characteristics of the runoff produced by the hillslope. This is also shown in terms of the total depth, intensity, peak and timing of the rainfall input in each case. The return period for each, defined at the downstream end of the reach, would be dependant on a number of factors in addition to the total depth of rainfall such as antecedent conditions, rainfall distribution over the catchment, and rainfall intensity and duration. For these simulations the same initial moisture conditions were used for the hillslope and for this reason, the sensitivity of VSAS3 to the total depth of rainfall for each event was examined. It can be seen that the greatest total depth of rainfall was produced by the 1 in 12 year event and the total volume of runoff produced for each event showed an increase with increasing rainfall depth. The volume of runoff produced after 24 hours was also found to increase with the total rainfall depth.

The timing of the rainfall peak was dependant on the characteristics of each individual storm. The peak rainfall of the 1 in 1 and 1 in 5 year events produced a simultaneous hydrograph peak whereas the hydrograph peak for the 1 in 12 year event was delayed. The reason for this observation can be seen if the depth of rainfall prior to the peak rainfall is considered. This was 13.8 mm for the 1 in 1 year event, 31.6 mm for the 1 in

Rainfall - Runoff hydrograph for 1 in 1 year event (27/1/90 - 30/1/90)

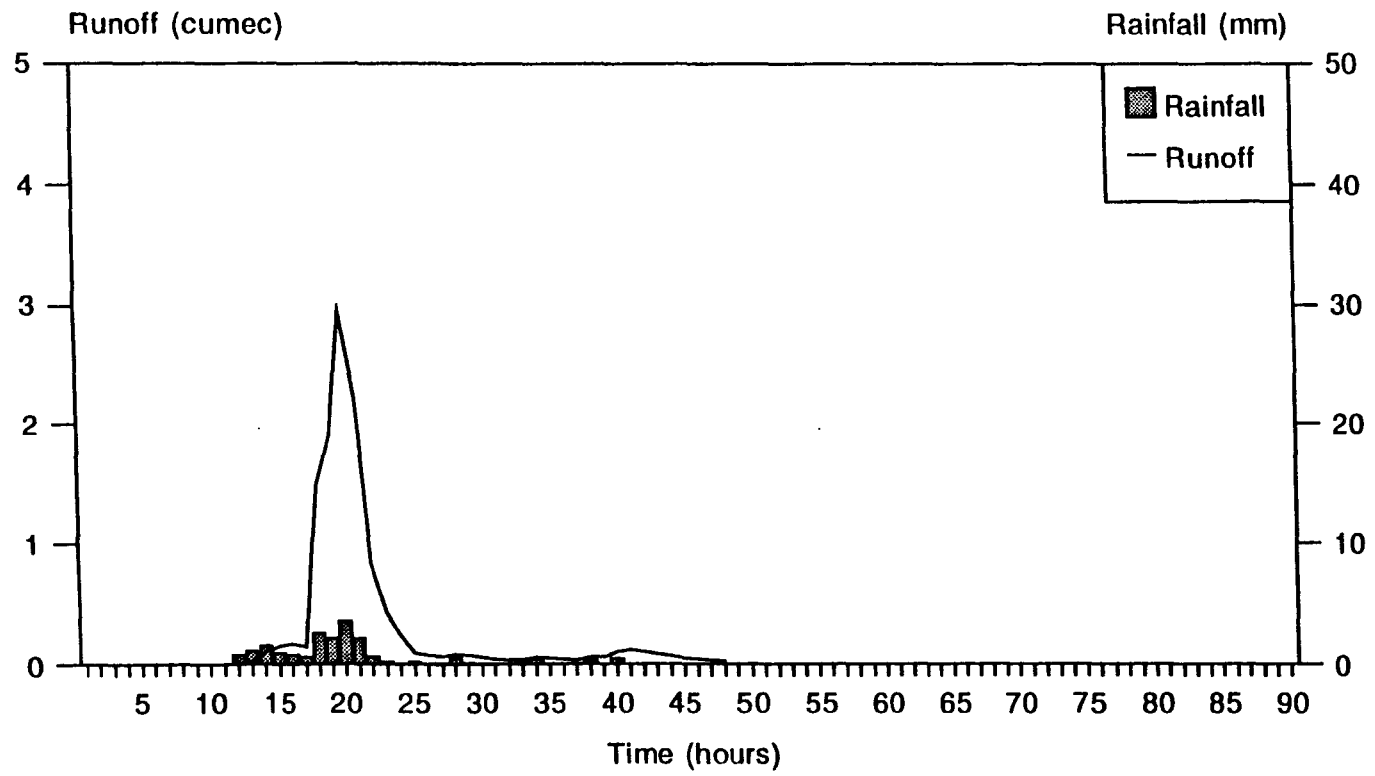

Figure 4.13: Rainfall-runoff hydrograph produced by VSAS3 for the 1 in 1 year event

Rainfall - Runoff hydrograph for 1 in 5 year event (24/1/84 - 28/1/84)

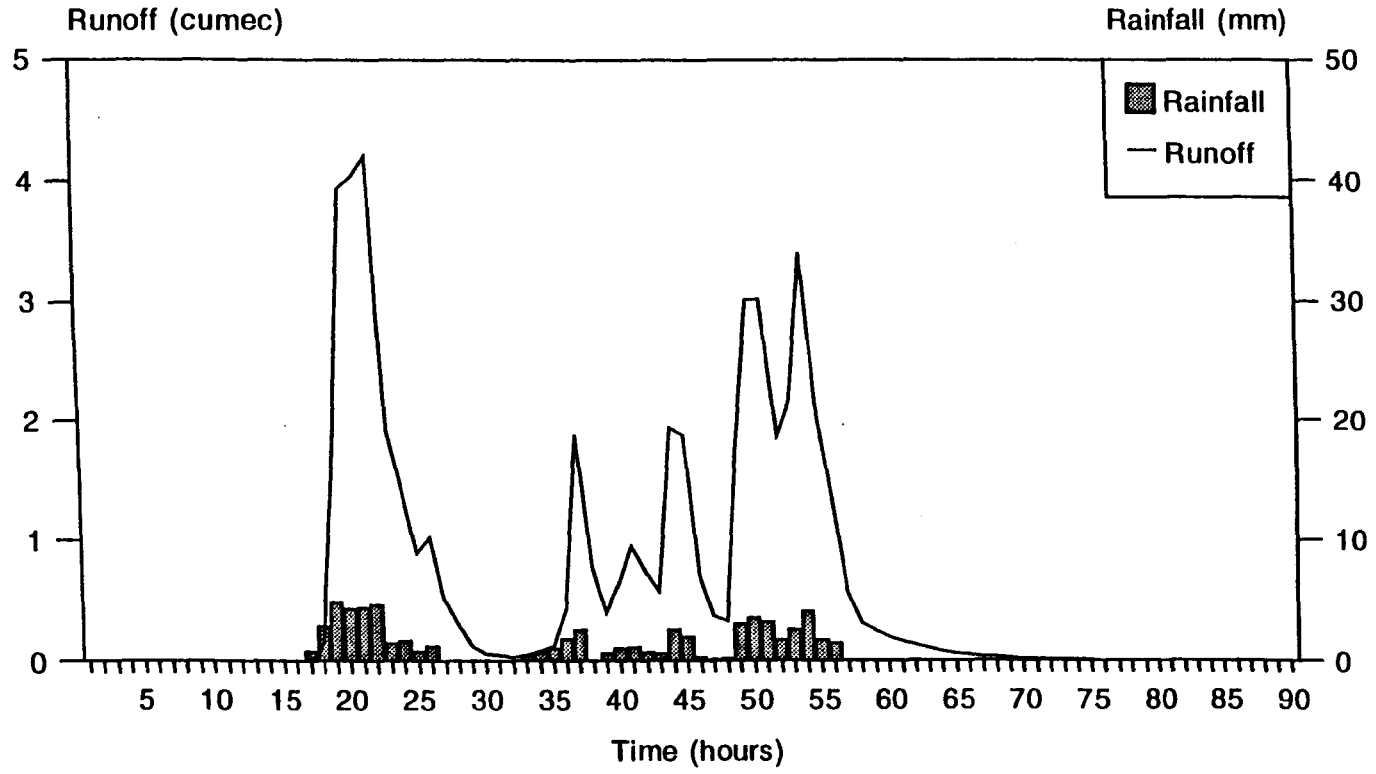

Figure 4.14: Rainfall-runoff hydrograph produced by VSAS3 for the 1 in 5 year event

Rainfall - Runoff hydrograph for 1 in 12 year event (26/12/79 - 29/12/79)

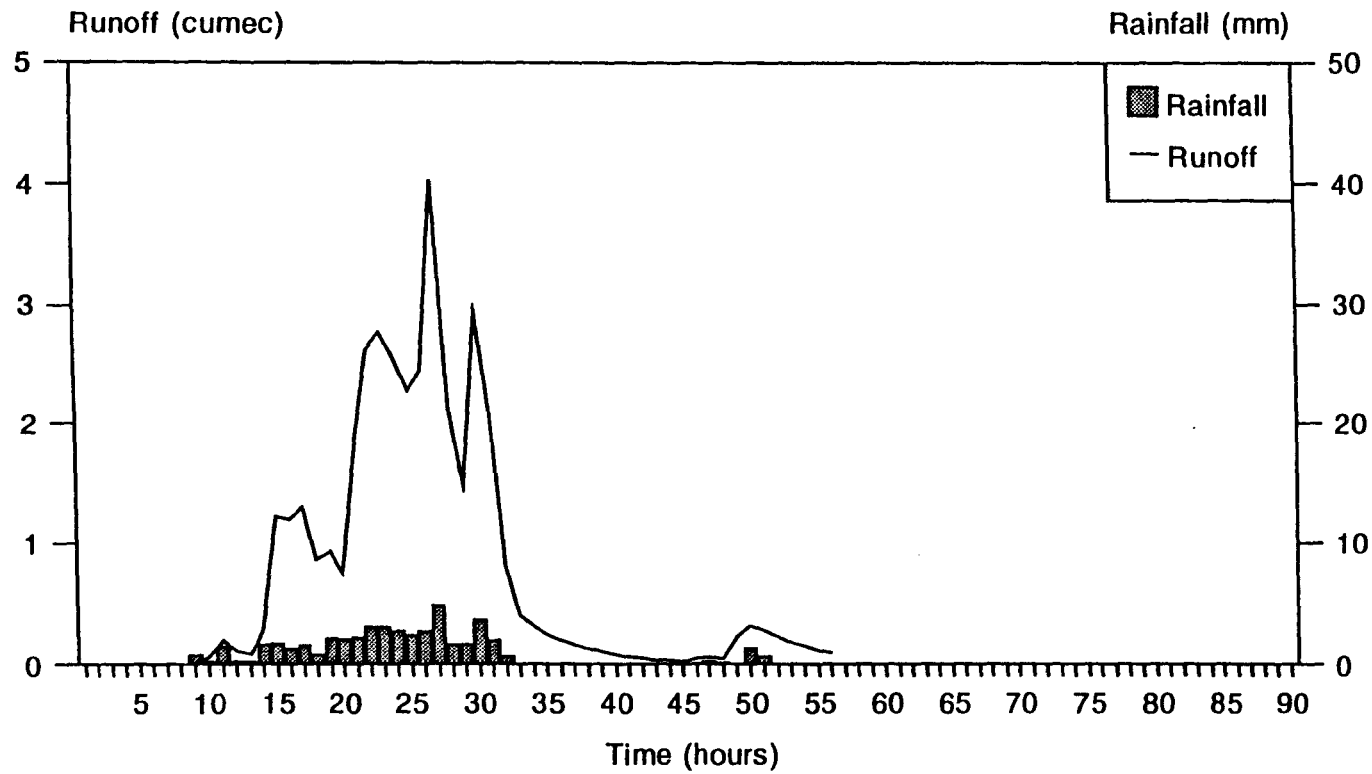

Figure 4.15: Rainfall-runoff hydrographs produced by VSAS3 for the 1 in 12 year event

5 year event and 3.7 mm for the 1 in 12 year event. The only event with a hydrograph peak within the period of the coupled simulation was the 1 in 12 year event.

Simulation (& return period)	Rainfall. depth (mm)	Rainfall peak (mm) & peak t	Rainfall intensity (mm h^{-1})	Total volume produced by slope (m^3)	Volume produced after t = 24h (m^3)	Time of hydrograph peak (hours)	Peak discharge ($m^3 s^{-1}$)
V01 (1 in 1 y).	19.1	3.5 (20 h)	0.42	43989.50	5644.40	20 h	2.96
V02 (1 in 5 y).	47.9	4.8 (27 h)	0.90	139064.10	78231.60	27 h	4.03
V03 (1 in 12 y).	63.2	4.8 (19 h)	0.74	191389.20	122150.90	22 h	4.21

4.6: Sensitivity to rainfall events with different return periods.

4.7.3 Sensitivity to changes in saturated hydraulic conductivity

From Table 4.7 and Figure 4.16 it can be seen that in general terms the total volume of runoff decreases with increasing saturated hydraulic conductivity. However this is not true for the peak discharge, which appears to be inversely related to the saturated hydraulic conductivity, or for the total volume of runoff produced after t = 24 hours.

Simulation no. & saturated hydraulic conductivity	Total volume produced by slope (m^3)	Time of hydrograph peak (hours)	Peak discharge ($m^3 s^{-1}$)	Total volume produced after t = 24 h
V04 (clay loam) 1.39×10^{-6} m s^{-1}	44505.80	20	2.97	5523.60
V01 (loam) 5.56×10^{6} m s^{-1}	43980.10	20	2.96	5644.40
V05 (sand) 1.0×10^{4} m s^{-1}	38429.40	20	2.45	10307.30

Table 4.7: Sensitivity to changes in saturated hydraulic conductivity

The reason for these observations can be explained by examining the soil moisture status at selected time steps for segment 1 shown in Figure 4.17 (it should be noted that the increment subdivision is represented with equal spacing whereas the partitioning rule meant that increments increased in size from the slope base to the watershed). In order to produce runoff as overland flow at the base of a segment, one or all of the soil elements of the base increment must be saturated. Once no more water can infiltrate a

Rainfall - Runoff hydrographs for different hydraulic conductivities (27/1/90 - 30/1/90)

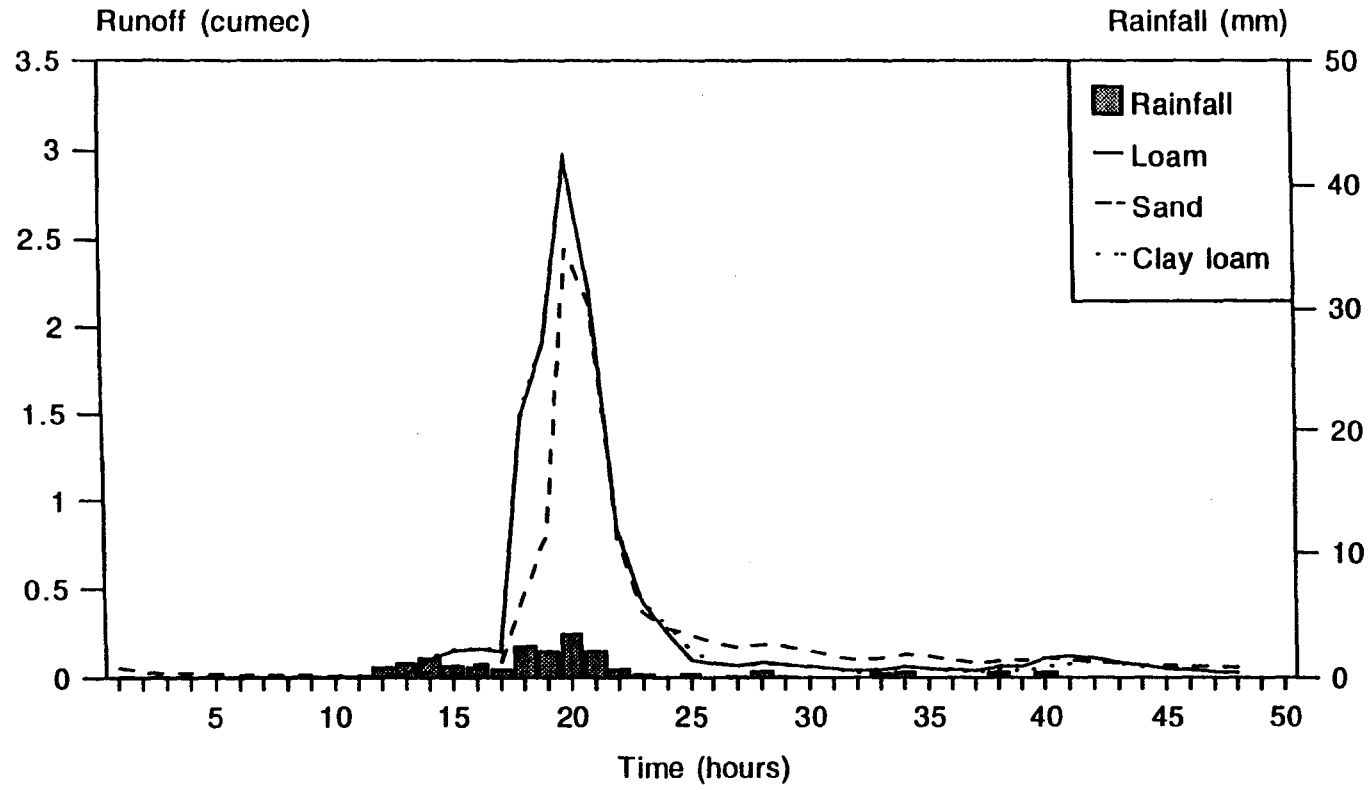

Figure 4.16: Rainfall-runoff hydrographs produced by VSAS3 using different hydraulic conductivities

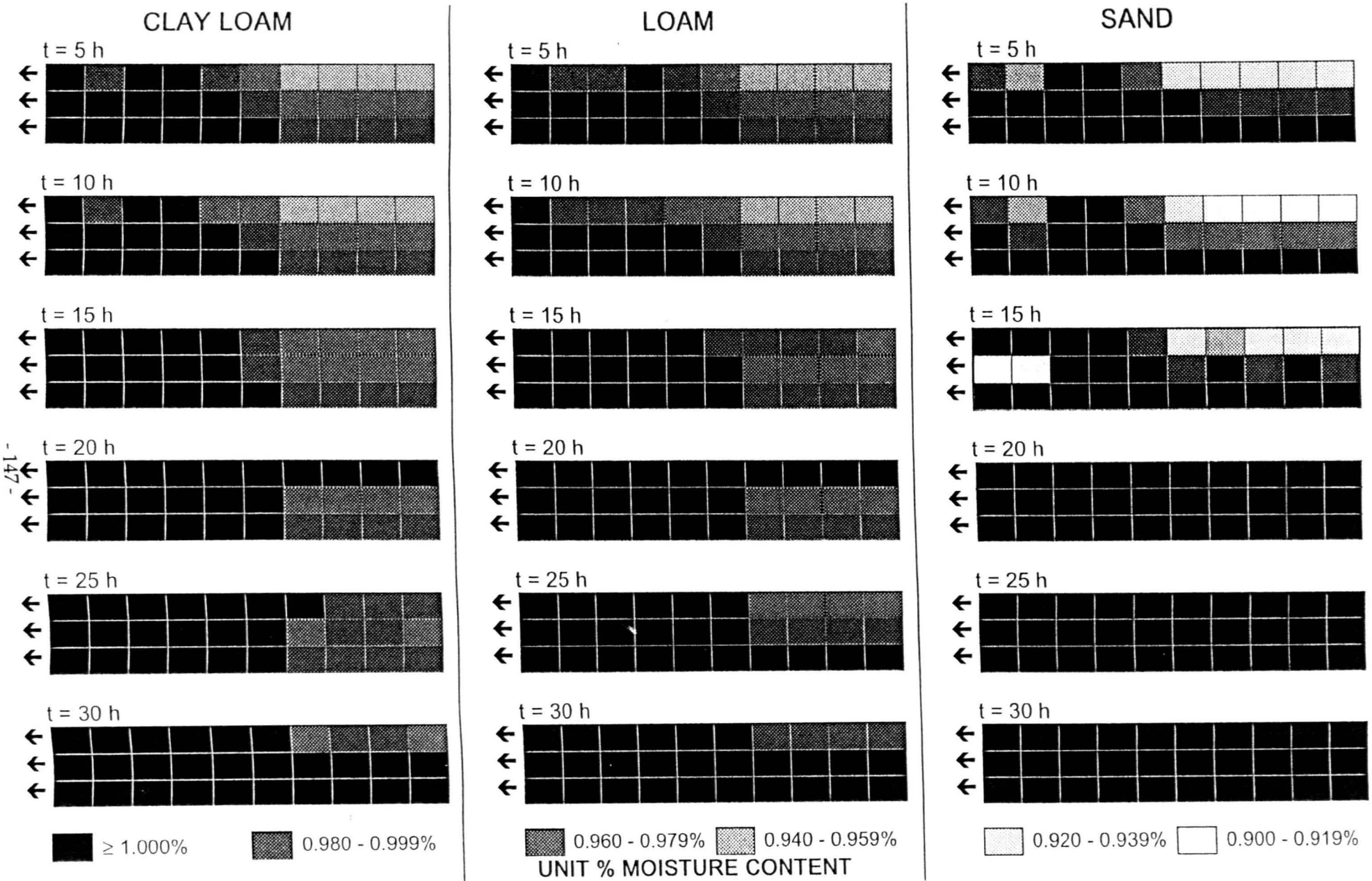

Figure 4.17: Soil profiles showing moisture contents at selected time steps for the different saturated hydraulic conductivities

surface element due to that element being saturated or the infiltration rate being exceeded, overland flow is produced.

Since a sandy soil has a higher permeability and saturated hydraulic conductivity, the rate at which water drains from the soil and at which rainfall infiltrates is greater than for loam and clay loam soils. From the hydrographs it can be seen that before the onset of rainfall, the highest discharge is produced by the sandy soil. For example, at VSAS3 time step 10 the slope discharge is 0.015 $m^3 s^{-1}$ compared with 0.00069 $m^3 s^{-1}$ for the clay loam. This meant that the sandy soil was relatively dry at the onset of the rainfall input (at t =12 hours). This, coupled with the fact that the clay loam and loam soils have lower infiltration rates meant that the sandy soil produced the least runoff during the rising limb and at the hydrograph peak. However the greater saturated hydraulic conductivity meant that this soil produced more runoff during the recession limb. The fact that only the sandy soil became fully saturated enhanced this effect. At time step 25, the sandy soil was producing 0.24 $m^3 s^{-1}$ compared with 0.16 $m^3 s^{-1}$ for the clay loam and 0.097 $m^3 s^{-1}$ for the loam.

The loam soil contributed less than the clay loam during the recession period (the time period of the coupled simulation). This could be caused by the relative importance of the overland flow and throughflow contributions for the two hydraulic conductivities; the relatively larger overland flow component from the clay loam soil having more significance than the larger throughflow component produced by the loam soil over this period. After 30 hours however, the difference was considerably less marked (clay loam produced 0.061 $m^3 s^{-1}$ and loam 0.060 $m^3 s^{-1}$) since there was no rainfall input at that or the preceding time step meaning that any saturated overland flow was reduced.

4.7.4 *Sensitivity to changes in soil depth*

Table 4.8 and Figures 4.18 and 4.19 show that the total volume of runoff and peak discharge decreased with increasing soil depth. Although the 0.1 m soil also produced the greatest volume of runoff after the first 24 hours, the deepest (1.0 m) soil produced a larger total volume of runoff during the recession period than the shallower 0.5 m soil.

Rainfall - Runoff hydrographs for different soil depths (27/1/90 - 30/1/90)

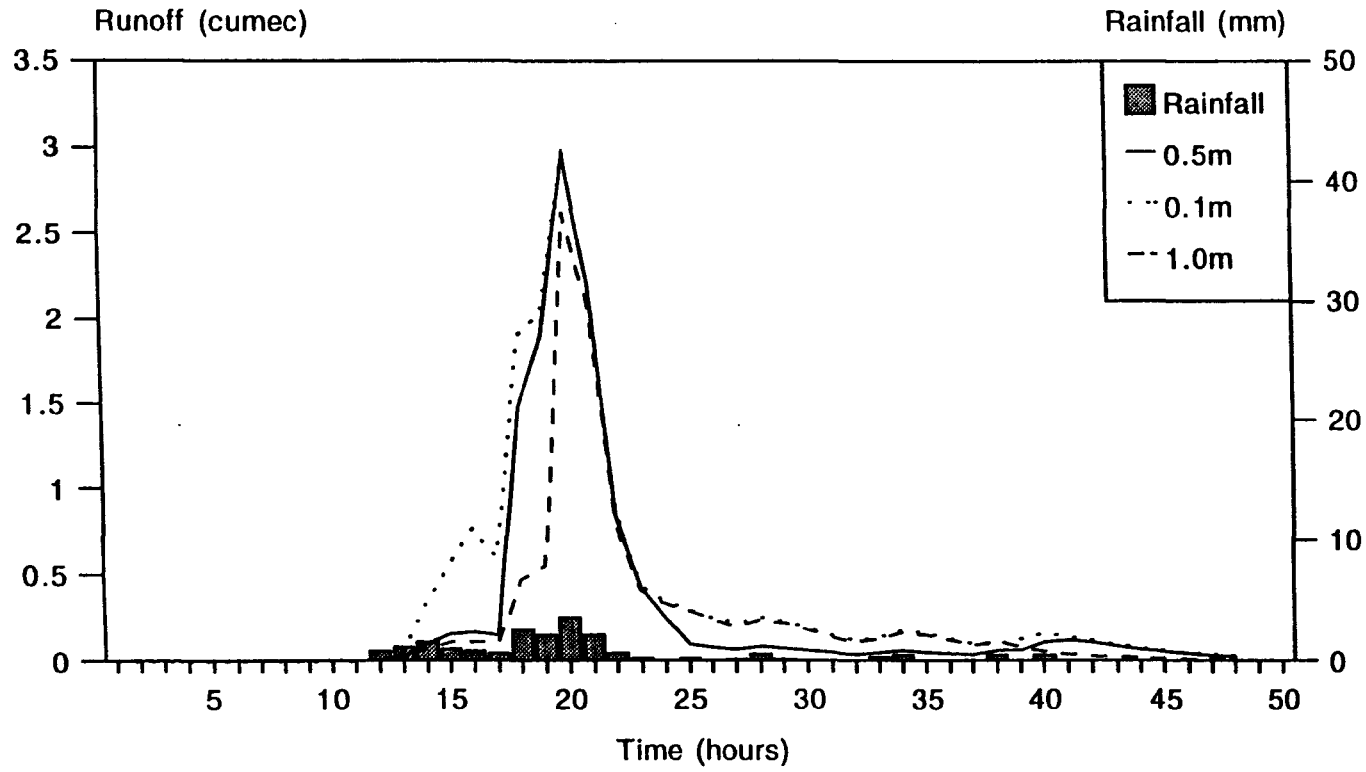

Figure 4.18: Rainfall-runoff hydrographs produced by VSAS3 using different soil depths

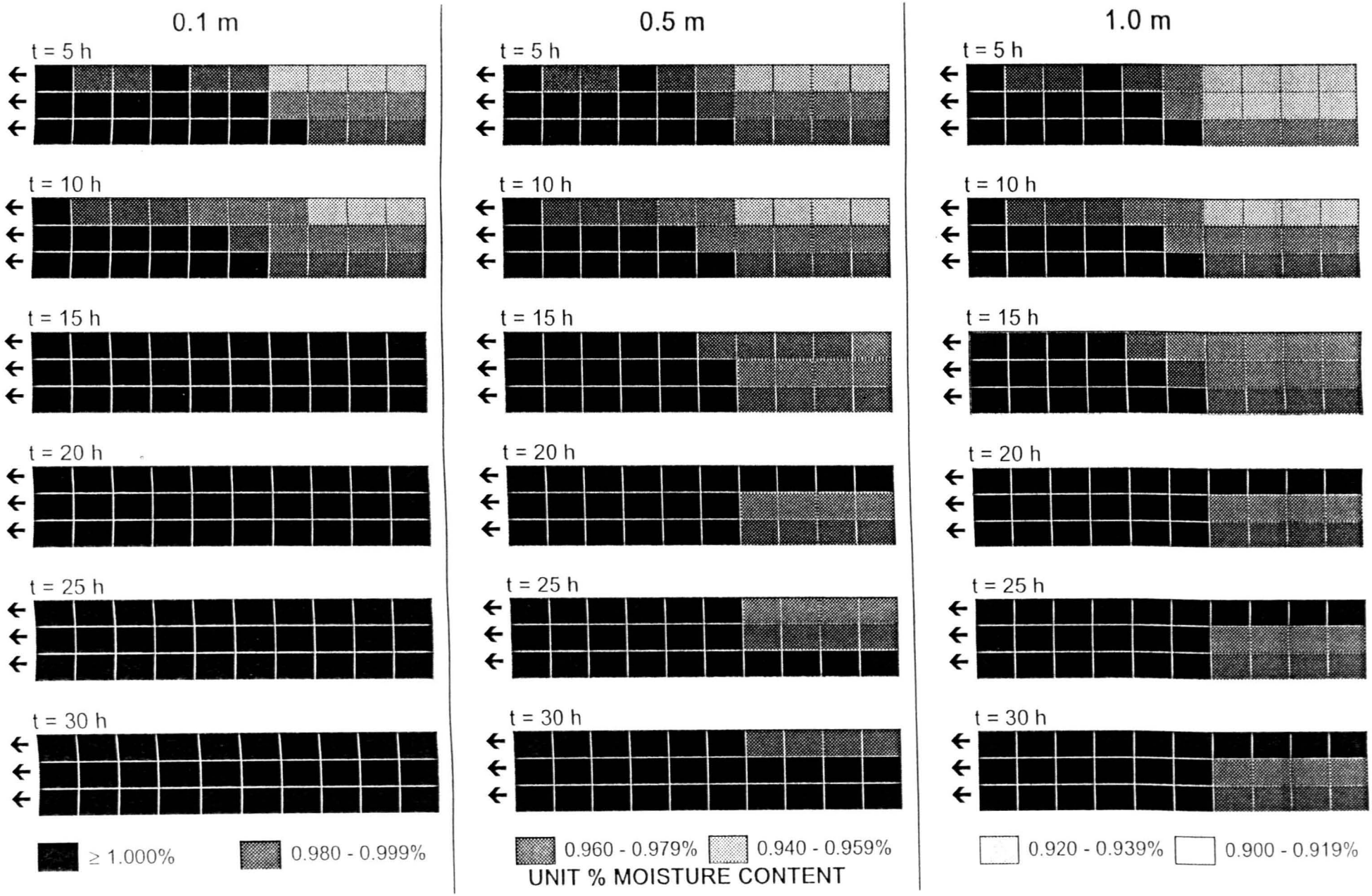

Figure 4.19: Soil profiles showing moisture contents at selected time steps for the different soil depths

Simulation no. & soil depth	Total volume produced by slope (m^3)	Time of hydrograph peak (hours)	Peak discharge ($m^3 s^{-1}$)	Total volume of runoff produced after t = 24
V06 (0.1m)	59756.00	20.0	2.97	12670.00
V01 (0.5m)	43980.10	20.0	2.96	5644.40
V07 (1.0m)	37455.80	20.0	2.62	9854.20

Table 4.8: Sensitivity to changes in soil depth

The moisture status for all these soil profiles was identical prior to rainfall input; the soils appeared to drain at the same rate per unit volume and showed similar moisture characteristics during the first 12 time steps (Figure 4.19). For example, the 1.0m depth profile produced a discharge of 0.0045 $m^3 s^{-1}$ at time step 10 which was an order of magnitude greater than the discharge of 0.00047 $m^3 s^{-1}$ produced by the 0.1m soil depth. In contrast to this, following the start of the rainfall input, it was the 0.1m soil which produced the greatest volume of runoff and showed the flashiest response. This is because the shallow soil profile allowed that profile to quickly become saturated (Figure 4.19) allowing large saturated overland flow contributions. By comparison, the deeper 0.5 and 0.1m soils never became fully saturated due to their relatively greater soil volumes although the 0.5m soil did produce a similar peak discharge to the 0.1m soil. The rising limb and peak discharge of the 1.0m soil was considerably reduced although the peak discharge for all three soil profiles occurred at the same time. During the recession limb, the 0.1m profile produced the greatest volume of runoff although the runoff volume produced did not show a simple linear relationship with soil depth since the 1.0m profile produced a greater volume of runoff than the 0.5m soil during this period. This was because the large volume of the deepest soil meant that a correspondingly large volume of water was stored within the soil whereas the saturated shallow 0.1m profile could quickly respond to further rainfall inputs. At time step 30 the 0.5m depth profile was producing 0.09 $m^3 s^{-1}$ compared to 0.30 $m^3 s^{-1}$ for the 0.1m depth and 0.29 $m^3 s^{-1}$ for the 1.0m depth.

4.7.5 *Sensitivity to changes in initial moisture conditions*

Table 4.9 and Figures 4.20 and 4.21 show that the total volume of runoff was reduced when dryer initial moisture conditions were applied to the slope.

Examining the moisture status (Figure 4.21) reveals that under almost saturated initial conditions runoff was produced from start of simulation whereas runoff was not

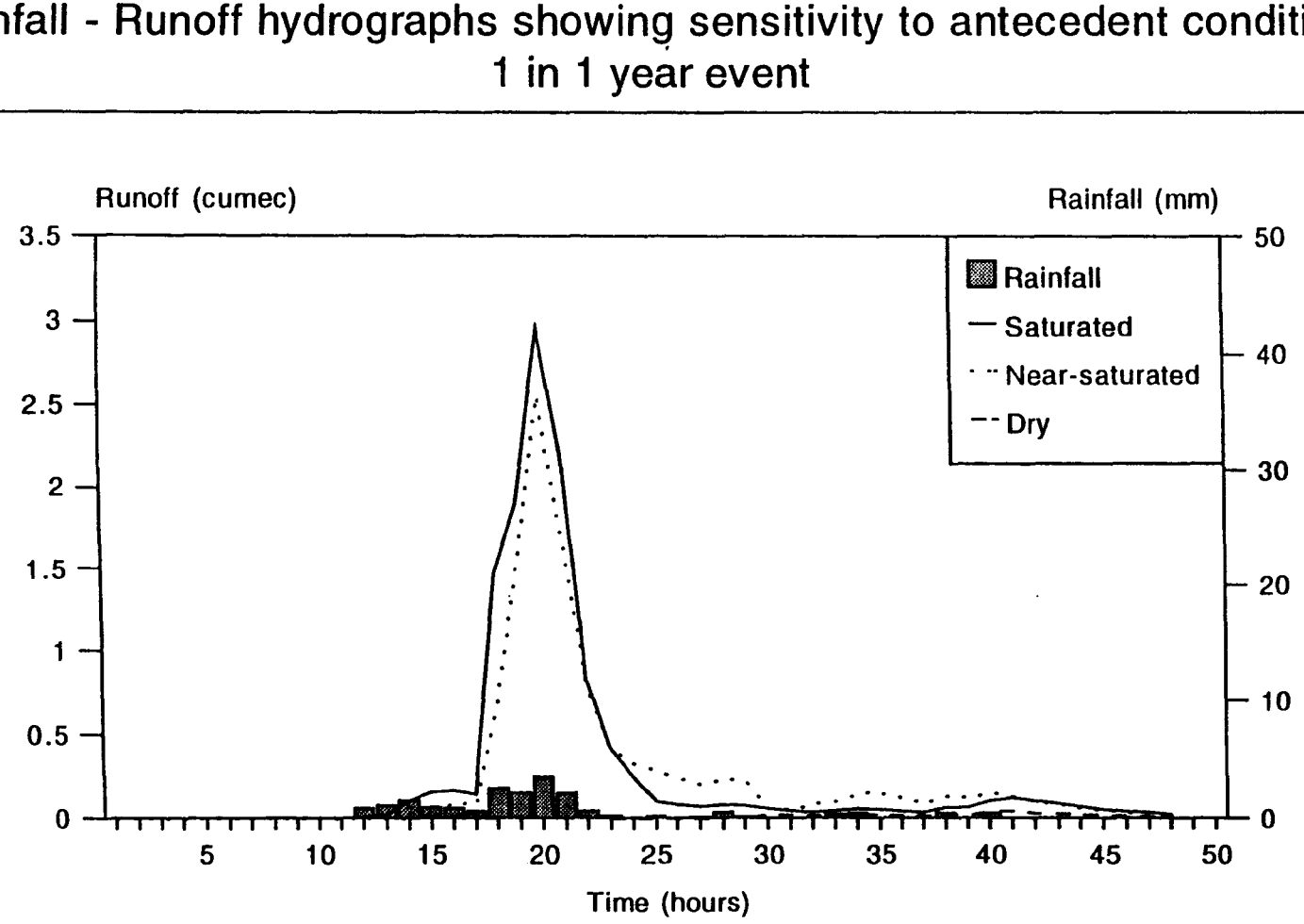

Figure 4.20: Rainfall-runoff hydrographs produced by VSAS3 using different initial moistures

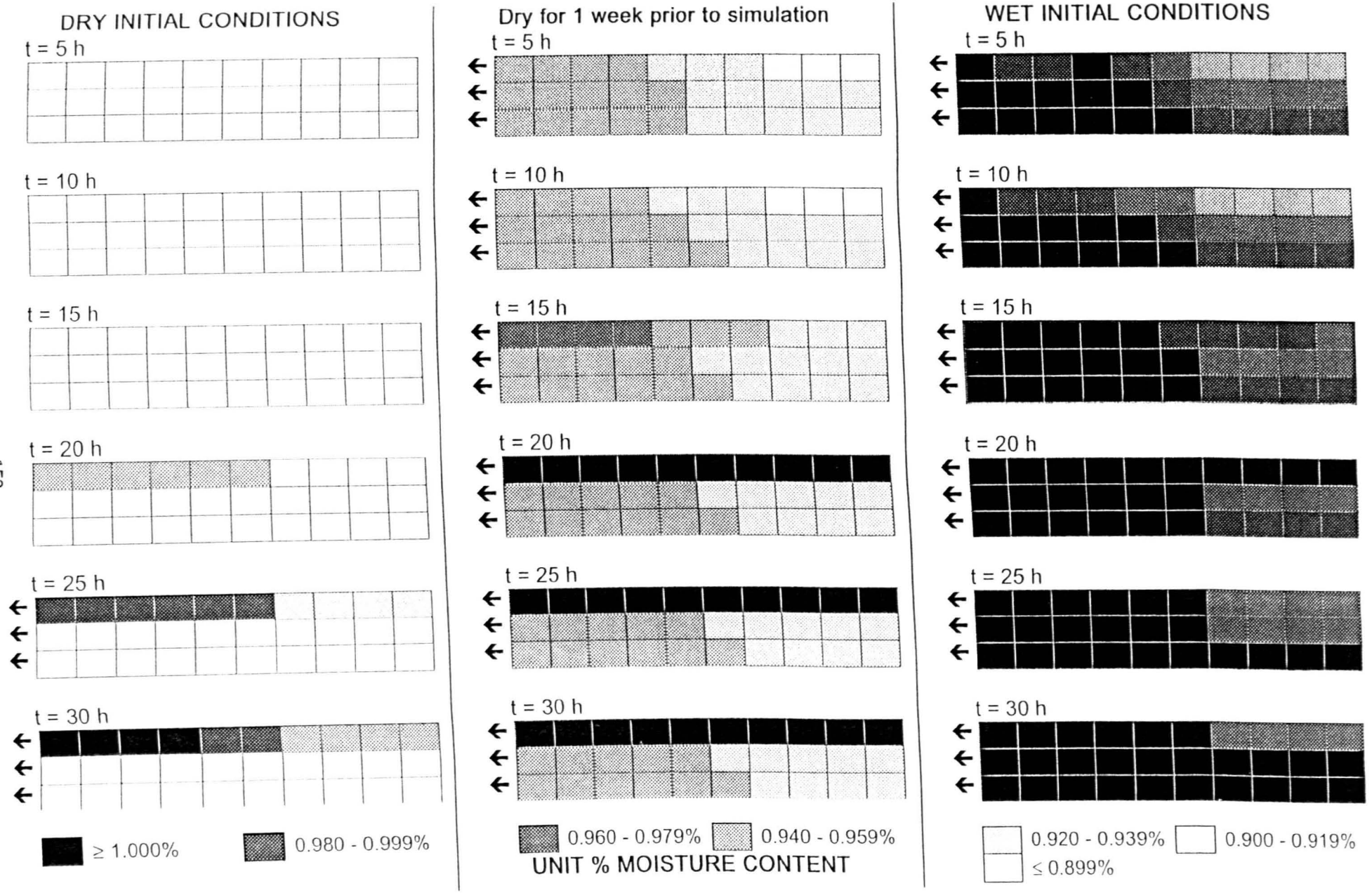

Figure 4.21: Soil profiles showing moisture contents at selected time steps for different initial moisture conditions

produced until 16 hours after the start of the simulation under intermediate initial moisture conditions and 23 hours by the driest soil. The peak runoff produced was also greatest for the almost saturated profile although attenuation of the hydrograph peak timing was only observed for the driest slope (time to peak = 21 hours). However during the recession phase, the soil with an intermediate initial moisture status produced the most runoff. From Figure 4.21 it can be seen that during the simulation whilst the surface layer became completely saturated the moisture status of the lower layers remained almost constant throughout the simulation. A similar response can be seen for the driest profile. The reason for this is probably due to the effect noted by Hewlett and Troendle (1975) where water flows more or less parallel to the slope surface, depending on local moisture contents, soil conductivities and the steepness of gradients. The saturated hydraulic conductivity through the saturated surface elements would be considerably greater than that vertically downwards to the dryer subsurface elements resulting in a preferential flow path down slope through the surface elements. Figure 4.21 shows that there is evidence of vertical movement through the almost saturated soil profile where the difference in the hydraulic gradient through the surface layers and vertically through the profile was considerably less marked. This meant that the volume of water draining to the subsurface layers was considerably greater than for the dryer profiles and resulted in a reduced volume of runoff being produced at the slope base.

Simulation no. & volumetric moisture content	Total volume produced by slope (m^3)	Time of hydrograph peak (hours)	Peak discharge ($m^3 s^{-1}$)	Total volume produced by slope after t = 24
V01 (1.000%)	43980.10	20	2.96	5644.40
V08 (0.988%)	40589.89	20	2.56	8834.40
V09 (0.800%)	1539.10	41	0.05	677.60

Table 4.9: Sensitivity of VSAS3 to changes in antecedent conditions

4.7.6 *Sensitivity to changes in slope angle*

There appeared to be very little difference between the simulations in terms of either runoff totals (Table 4.10) or hydrograph characteristics (Figure 4.22). The difference between the profiles might have be more marked if dryer antecedent moisture conditions had been used. Examination of the soil moisture profiles (Figure 4.23) shows that the only noticeable difference between them occurs prior to the onset of

Rainfall - Runoff hydrographs for different slope angles 1 in 1 year event

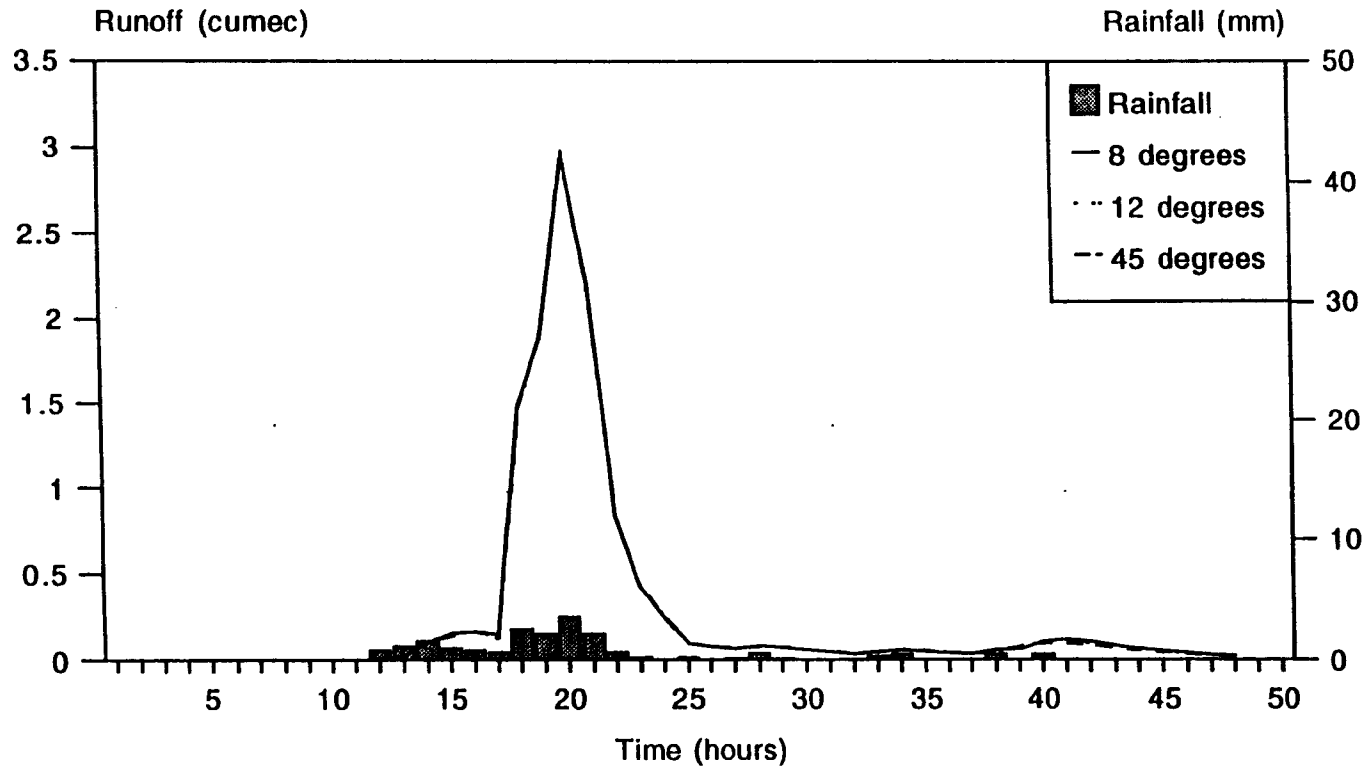

Figure 4.22: Rainfall-runoff hydrographs produced by VSAS3 using different slope angles

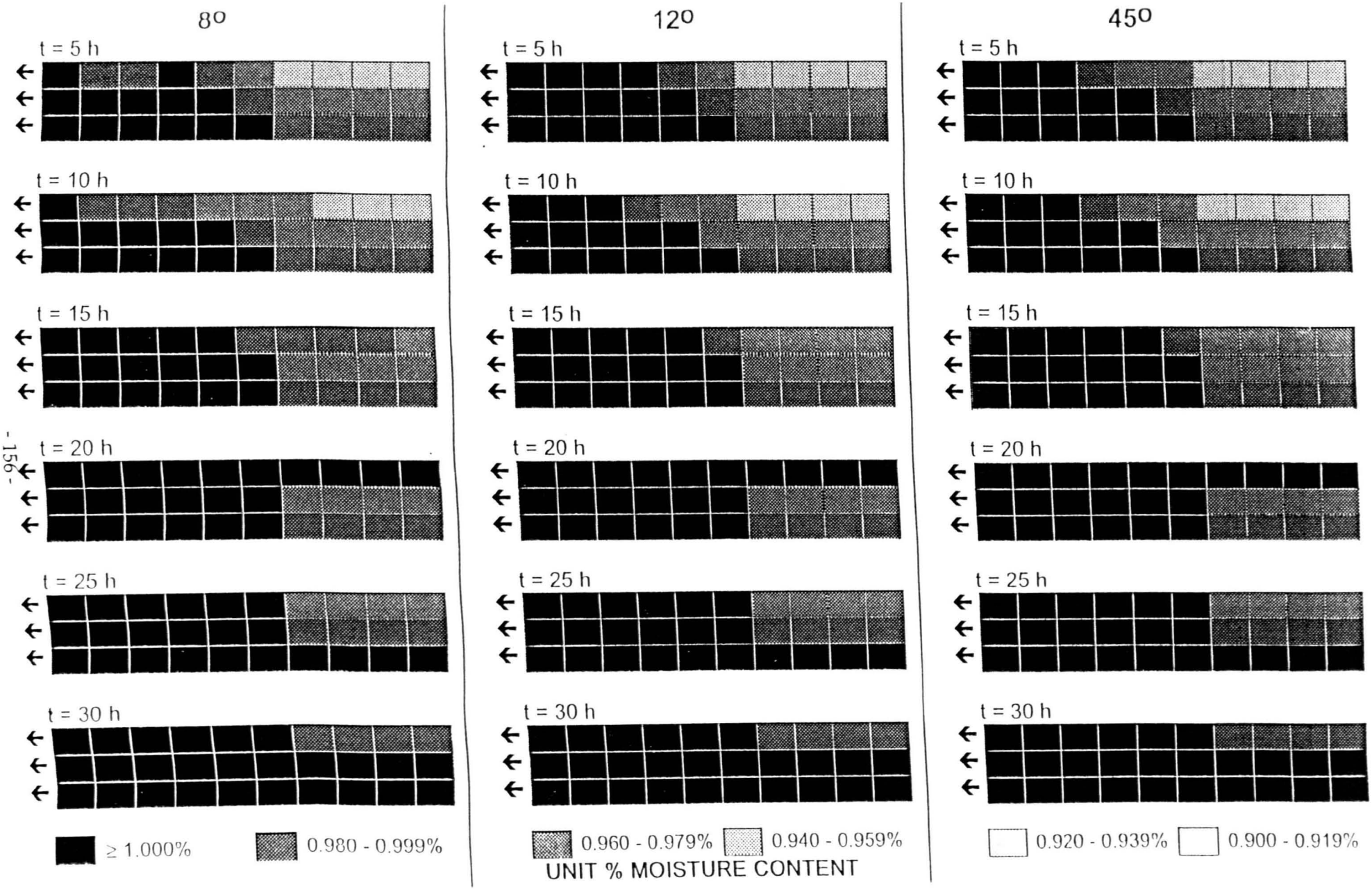

Figure 4.23: Soil profiles showing moisture contents at selected time steps for different slope angles

rainfall where all three profiles had identical moisture contents towards the watershed although at the slope base the surface layer of the 8° slope was slightly dryer than the other profiles. This profile also appeared to become saturated at a slightly faster rate although the hydrograph peak discharge was the same in each case.

Simulation no. & slope angle	Total volume produced by slope (m^3)	Time of hydrograph peak (hours)	Peak discharge ($m^3 s^{-1}$)	Total volume produced after t = 24
V01 (8°)	43989.60	20	2.96	5644.40
V10 (12°)	44146.00	20	2.96	5644.40
V11 (45°)	43927.20	20	2.96	5655.30

Table 4.10: Sensitivity to changes in slope angle

4.7.7 Relative sensitivity of VSAS3 to the model parameters

Table 4.11 shows the comparison made between the different parameters selected for the sensitivity analysis in terms of the relative sensitivity of the coupled scheme to changes in each parameter. Two sets of calculations were made for each parameter; because three values were used for each parameter, the percentage increase in the parameter value and change in the total runoff produced were calculated between the first and second and second and third value used. The percentage change in the total runoff volume for a 1% increase in the parameter value was calculated by dividing the percentage change by the percentage in the parameter over the range which had caused that change in outflow volume. These final values were used to compare the relative sensitivity of VSAs3 to the five parameters, which was found to be (in order of decreasing sensitivity):

1. Initial moisture conditions
2. Rainfall event
3. Soil depth
4. Saturated hydraulic conductivity

Slope angle

Parameter	Range of values over which change occurs	% increase in parameter value over this range	% increase in total runoff over this range	% change in total runoff volume for 1% change in parameter value
Rainfall	1 in 1 to 1 in 5 19.1 mm to 47.9 mm	+ 147.12%	+ 216.13%	+ 1.47%
	1 in 5 to 1 in 12 47.9 mm to 63.2 mm	+ 31.94%	+ 37.63%	+ 1.18%
Hydraulic conductivity	clay loam to loam 1.39×10^{-6} m s^{-1} to 5.56×10^{-6} m s^{-1}	+ 300.00%	- 1.18%	- 0.0039%
	loam to sand 5.56×10^{-6} m s^{-1} to 1.00×10^{-6} m s^{-1}	+ 1698.56%	- 12.6%	- 0.0074%
Soil depth	0.1 m to 0.5 m	+ 400.00%	- 26.4%	- 0.066%
	0.5 m to 1.0 m	+ 100.00%	- 14.83%	- 0.15%
Antecedent conditions	0.8 to 0.988	+ 23.50%	+ 2537.25%	+ 107.97%
	0.988 to 1.00	+ 1.21%	+ 7.71%	+ 6.37%
Slope angle	8° to 12°	+ 50.00%	- 0.36%	- 0.0072%
	12° to 45°	+ 275.00%	+ 0.50%	+ 0.0018%

Table 4.11: Percentage change in hydrograph volume and peak discharge caused by a 1% change in each of the parameter values

change in the parameter value appears, perhaps not surprisingly, to be far from a simple linear relationship for any of the parameters examined. In addition, the range of values considered might not have been fully representative of the full range of environments which occurs world-wide. Since this range had a considerable impact on the result of the percentage change in total runoff volume for a 1% change in the parameter value it would have been desirable to carry out further simulations for each parameter to extend this range had time allowed. However, it was possible to obtain a reasonable idea of the relative sensitivity of the model to these parameters for the purposes of this first pass investigation.

4.8 USING VSAS3 OUTPUT AS AN INPUT TO RMA-2

4.8.1 Spatial averaging of VSAS3 predictions

The VSAS3 output hydrographs had to be post-processed prior to application to RMA-2. Since a hillslope section was modelled rather than the whole length of hillslopes bordering the reach, the VSAS3 output hydrographs had to be spatially averaged. Each of the seven segments produced a different volume of water for each of the hourly time steps during each VSAS3 simulation, this being dependent upon the area of each segment as well as the segment characteristics. At each time step, the discharge from each of the seven segments was cumulated to give a discharge for the whole slope. This was then divided by the width of the slope to give a discharge per unit length of the slope.

The FORTRAN program *hydsum.f*, described in Section 4.7.1, carried out this process. The hourly discharge calculated for the slope section by *hydsum.f* was spatially averaged by dividing this value by the width of the base of the slope to give a discharge per unit width. At this stage, this value was in $m^3 h^{-1}$ per metre of slope. Since RMA-2 ultimately requires that the inflow value be expressed in $ft\ s^{-1}$, the inflows values were converted to $ft^3 s^{-1}$ per foot of slope. This value was written to an output file, the *'inflows'* file containing a discharge in cusecs per foot hillslope width, for each VSAS3 time step and was a spatially averaged hydrograph for the event.

Hydsum.f also summed the hourly discharge from each segment at each time step to obtain the total volume of water produced by the hillslope. This value was then multiplied by the length of the floodplain/hillslope boundary on both sides of the reach (Chapter 5 describes how this was derived) to get the total volume applied as side flows to the reach for each coupled model run. This value was used for

comparing the volume of water contributed by the hillslopes with the volume entering at the upstream end of the reach for each of the coupled simulations.

4.9 CONCLUSIONS

This chapter started with a consideration of the main hillslope processes which operate including runoff pathways and the mechanisms by which water travels through the soil. A description was then made of the selection of a hillslope hydrology model and the 1km wide hillslope section bordering the Culm reach to which it was applied. This was then used as the basis for the first stage of the sensitivity analysis; assessing the sensitivity of VSAS3 to five key hillslope parameters (rainfall event, slope angle, antecedent conditions, saturated hydraulic conductivity and soil depth). A number of VSAS3 simulations were carried out using different values for these parameters to examine the sensitivity of the model to each parameter. From this, hillslope output hydrographs resulting from these simulations were selected to use as an additional input to RMA-2 in coupling the models. The first stage in this coupling process, spatially averaging the hillslope hydrographs, has been carried out.

Chapter Five now goes on to explain the coupling mechanism adopted together with a description of the simulations carried out in the second stage of the sensitivity analysis. The results of the sensitivity analysis are presented in Chapter Six.

Chapter Five

COUPLING AND RUNNING THE MODELS

5.1 INTRODUCTION

This chapter describes the method by which the models were coupled and the sensitivity analysis which was carried out to examine the significance of applying hillslope inflows as an additional input to the floodplain inundation model.

The side inflow capability which is a feature of RMA-2 was described in Chapter Three. The results of the pilot study described in that chapter indicated that inflows can have a significant impact on floodplain inundation predictions. Chapter Four described how a hillslope hydrology model, VSAS3, was selected and set up for a hillslope section bordering the reach. A sensitivity analysis was carried out in two stages; the first stage involved examining the sensitivity of VSAS3 to five hillslope input parameters. The second stage is described in this chapter and involved investigating the sensitivity of the floodplain inundation model to changes in hillslope parameters. This was carried out by coupling the models; applying the inflows generated by the VSAS3 simulations as an additional input to RMA-2. This chapter outlines the design and implementation of the coupling mechanism and the coupled simulations carried out during the sensitivity analysis. The results of the sensitivity analysis are presented in Chapter Six.

The first stage in coupling the models involved selecting a suitable coupling mechanism. In doing this, the processes of water delivery to the floodplain were considered and a compromise sought between representing physical reality and the number of cumulative errors which would be incorporated by making the coupling process too complex. The selected coupling mechanism was then implemented and the simulations carried out for the sensitivity analysis. A further set of coupled simulations was carried out to study the importance of the timing of the hillslope response relative to the floodplain input hydrograph.

5.2 SELECTING A COUPLING MECHANISM

The coupling mechanism was the tool which enabled water to be transferred from VSAS3 to RMA-2 as an additional input. Several different methods could have been employed to effect this transfer. These varied considerably in complexity and physical

representation and in order to consider them it was necessary to consider the mechanisms of water delivery to the floodplain

5.2.1 *Methods of water delivery to the floodplain*

Streamflow at any instant contains groundwater contributed at previous times and different locations within the drainage area. When the stream channel is in direct contact with an unconfined aquifer, streamflow may re-charge groundwater or receive discharge from the groundwater depending on the relative levels. A stream receiving discharge from groundwater is termed a *gaining stream* (Figure 5.1a) whereas one contributing discharge to groundwater is a *losing stream* (Figure 5.1b). This is not a simple classification since a gaining stream may often becomes a losing stream and a losing stream may start receiving discharge from the groundwater to become a gaining stream (Keppel and Renard, 1962; Norris and Eagon, 1971). Cooper and Rorabaugh (1963) derived solutions for changes in groundwater near the stream, groundwater flow to the stream and bank storage. Their analysis also included a family of asymmetric flood-wave storage hydrographs which facilitate the study of the effects of a wide variety of hydrograph shapes on groundwater. Stream fluctuation can therefore produce large variations in the magnitude and direction of local groundwater flow.

During and after a storm period in a small drainage basin, the water table rises and, as a result of this, the baseflow also increases. In the upper reaches of a watershed, subsurface controls to streamflow aid in the build-up of the floodwave. In the lower reaches, during the flood period, stream groundwater levels temporarily increase near the channel due to inflow from the stream. The volume of water stored in this way and later released after the flood is termed bank storage and was first defined by Todd (1955).

Field data are rarely adequate to evaluate bank storage and its rate of inflow and outflow and analytic and modelling approaches are necessary to obtain quantitative estimates for specified boundary conditions. The effects of bank storage is shown schematically in Figure 5.2.

Floodplain inundation therefore occurs as the result of several processes although the exact processes operating are very hard to observe and is influenced by several factors such as the dominant hillslope transport mechanisms, the floodplain width, the floodplain surface permeability, and the relative volumes of water coming from

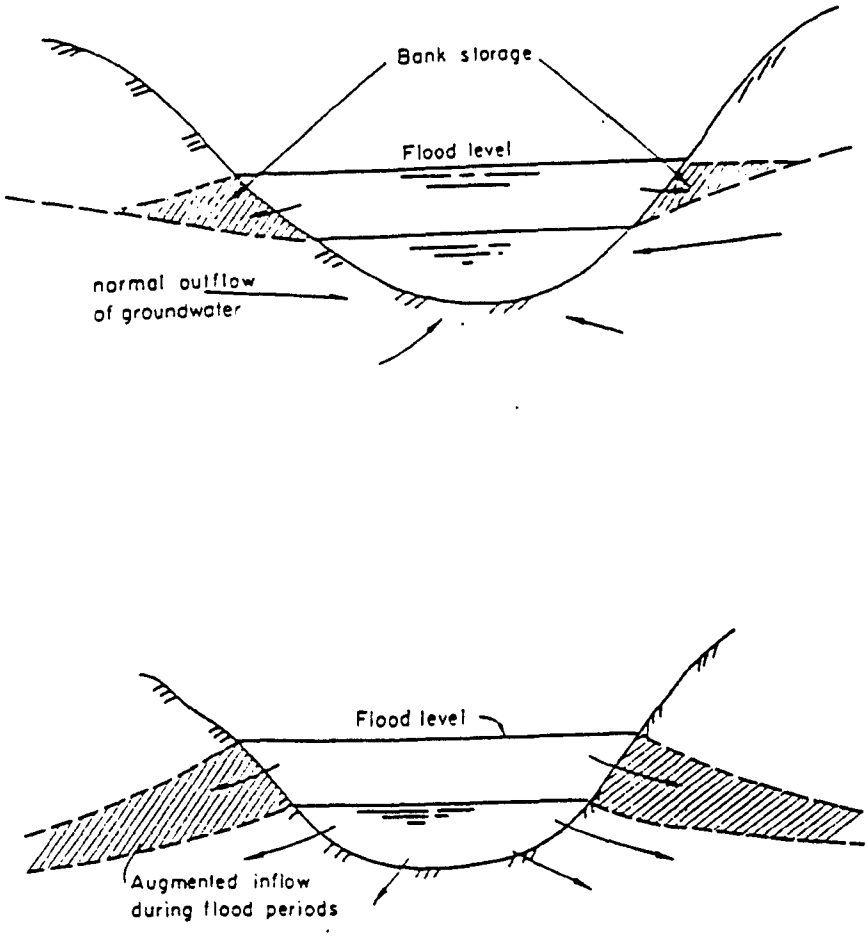

Figure 5.1: Schematic diagram of a) gaining stream and b) losing stream (after Wilson 1990).

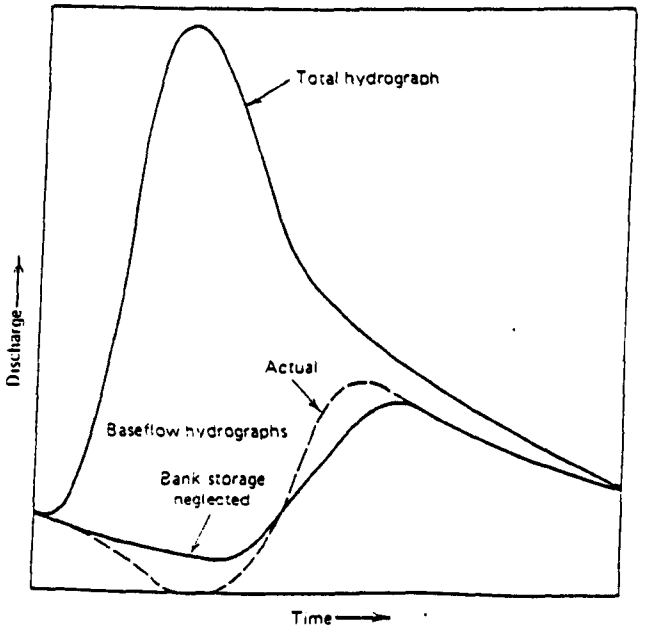

Figure 5.2: Schematic diagram of the variation of base flow during a flood hydrograph with and without effects of bank storage (after Singh 1968).

upstream and from the adjacent hillslopes. As a result, no simple model exists to describe the complex processes operating in the delivery of water to the floodplain.

5.2.2 *Proposed methods of simulating the water delivery from hillslopes to floodplain*

For the purposes of this investigation, three possible methods of coupling the models were considered. These are now discussed in turn and were:

i) Adding water to the elements at the edge of the floodplain

ii) Lagging contributions to elements across the floodplain

iii) Using a groundwater model to effect the transfer

The first of these methods was the most simplistic to be considered and involves simply applying VSAS3 output to elements at the edge of the floodplain. This method treats the process of water delivery to the floodplain as a black box. VSAS3 output is expressed as a discharge per unit length of the boundary between the hillslope and floodplain and is applied over the area of all the elements along the edge of the reach. The actual volume applied to an element is weighted according to the length of that element in juxtaposition with the hillslope. This method could potentially provide quite a realistic representation of the processes occurring in an upland reach where a narrow floodplain is bounded by steep hillslopes. In this case, it is likely that the base of the hillslope is saturated, acting as a variable source area which will result in the rapid transport of water to the floodplain. Since the floodplain is narrow, it is likely that during a storm event, the whole width of the floodplain will be inundated, this area of inundation merging with the variable source area. In modelling terms, simply 'dumping' water at the edge of the floodplain would provide quite a reasonable interpretation of the processes occurring. However, the physical representation of this scheme is not so strong for a lowland reach such as the Culm study reach where shallow hillslopes border a floodplain which is relatively wide, particularly towards Rewe. In this case it is possible that all the contributions to the floodplain from the hillslopes are made as throughflow and contributions to groundwater. The wider parts of the floodplain do not always become completely inundated, with dry areas occurring at the edge of the floodplain throughout many events. Adding water to the edge of the Culm FEM might cause localised areas of ponding, although the volume of water involved over the surface of the element may not cause any change in inundation particularly before and after the hillslope hydrograph has peaked when

this volume may be very small. Using this first method, this water would probably travel as overland flow across the floodplain to contribute to the depth inundated area. In the real world, if water was added to the edge of a floodplain which was dry it would probably infiltrate. RMA-2 currently has no infiltration component so using this coupling method, all the runoff produced by VSAS3 would enter RMA-2 with no losses to groundwater. It is therefore possible that the volume of water on the surface of the floodplain could be over-estimated.

The second method proposed also used the side element capability. There is no reason why this capability should be exclusively used to supply water to elements at the edge of the FEM and it is possible to apply water to elements in the 'centre' of the mesh as well. In order to attempt to emulate the delivery of water to the floodplain from groundwater, this second method of coupling the models attempts to provide a slightly more physically realistic representation within the constraints of the present model structure. This second method assumes that water travels from the hillslopes to the floodplain as throughflow and baseflow, contributing to an increase in groundwater level near the channel. It is assumed that the groundwater will eventually rise above the floodplain surface to augment the inundation caused by the arrival of the floodwave from upstream. Adding water to elements across the floodplain attempts to emulate this process, lagging the contributions temporally to represent the time taken for this contribution to travel from the hillslopes to the near-channel floodplain. However, this method involves making the assumption that the transfer of water between groundwater and floodplain is a one way process which, from the discussion in the previous section, is obviously not the case. In addition, in the absence of knowledge about the groundwater behaviour, the appropriate time lag and distribution of water between the floodplain elements will not be known and assumptions would have to be made about the groundwater behaviour.

The final method considered was the most complex. It was proposed to use a groundwater model as the vehicle for moving water from VSAS3 to RMA-2. Water produced by VSAS3 would be used as an input to a 2 or 3-dimensional groundwater model set up to model flow beneath the floodplain. Water would be added to the elements of this groundwater model underlying the edge of the floodplain. The groundwater model would then govern the discharge contributed to the floodplain. An alternative approach would be to model the hillslope and groundwater components using a three-dimensional groundwater model such as that used by Freeze (1972a). It would be necessary to make several modifications to RMA-2 if using

either of these approaches. The actual coupling to RMA-2 would be problematical as there is no groundwater component or allowance made for exfiltration from the channel, infiltration through the floodplain surface or the water table rising above the surface of the floodplain. Since infiltration from the floodplain surface and exfiltration from the channel are important sources of groundwater, in addition to the throughflow contributions, they cannot be ignored. This method would require the use of parallel processing, running the groundwater model and RMA-2 in parallel in order to incorporate the transfer of water into and out of the groundwater store through the floodplain surface. Implementing this method would also involve straying too far from the main aims of the research which are to establish what effect, if any, the application of side inflows has on floodplain inundation and the range of environments where this is significant. It would not be appropriate to attempt to provide as physically realistic as possible a coupling mechanism when the significance of hillslope contributions had not yet been established.

5.2.3 *Selecting a coupling mechanism*

If the first two methods in the previous section are considered, the complexities of floodplain-groundwater interaction mean that the method of lagging contributions makes a greater number of assumptions about the processes operating than simply applying water at the edge of the floodplain. It is argued that because of this it is less justifiable to use it. Figure 5.3 shows the predicted inundation extent for the 1 in 1 year event at various time steps. From this it can be seen that most of the floodplain is inundated during the event. It was felt that because of this simply adding water to elements at the edge of the floodplain would not cause too many problems, at least in terms of model stability. It was also important to remember that this investigation used a semi-theoretical approach and that the inflows provided by VSAS3 represented a wide range of environments. These would include upland hillslope environments with narrow valley bottoms for which this method of simulating water delivery to the floodplain would probably be highly appropriate.

For lowland floodplain environments, it is possible that water generated by the bordering hillslopes makes a more significant contribution to the base flow component rather than to peak flow, although it is also possible that water may be transported across the floodplain to inundated areas more rapidly as throughflow. Most importantly, since this was a first pass investigation, if inflows were found to be

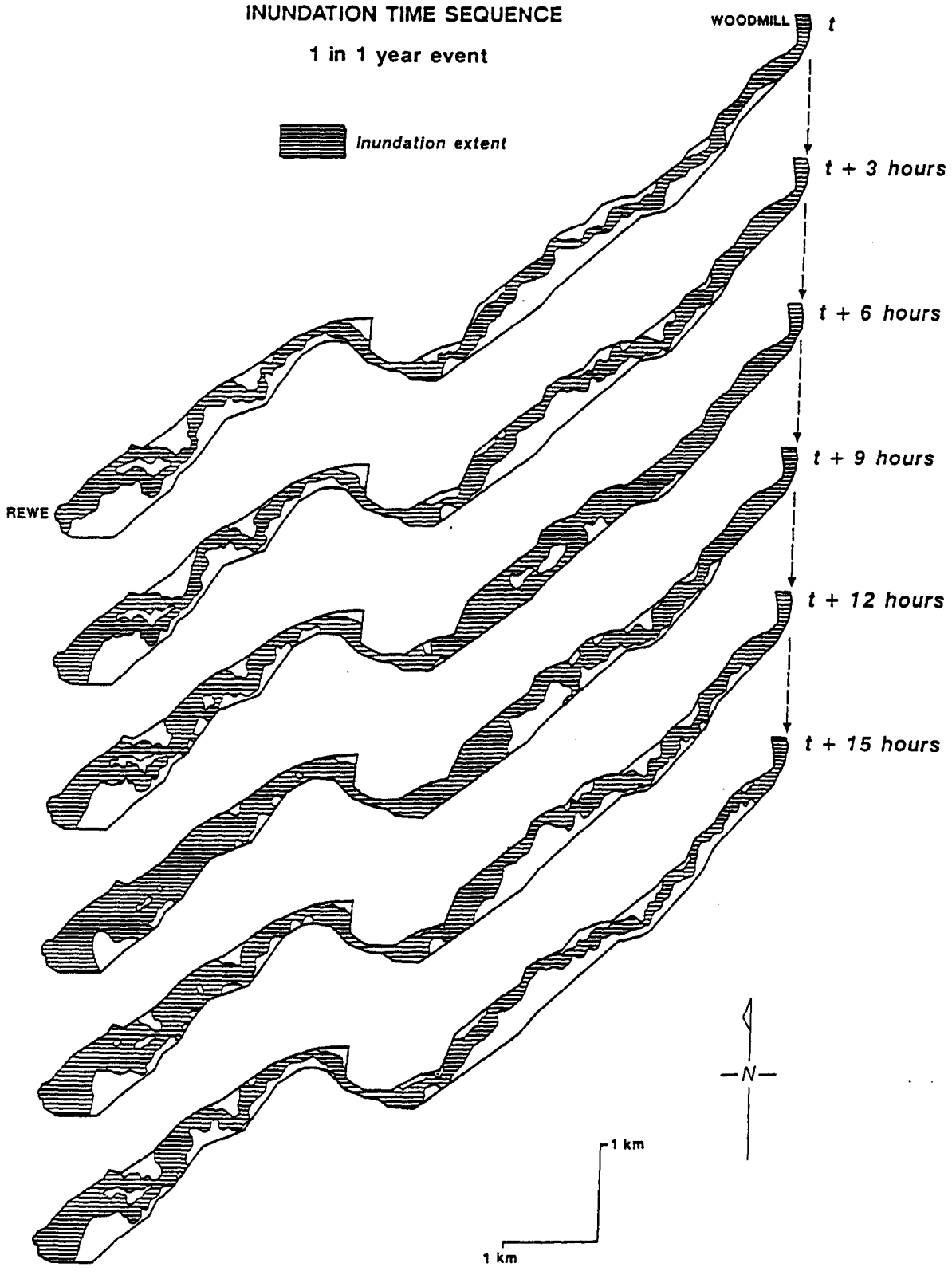

Figure 5.3: **Inundation time sequence for a 1 in 1 year event (after Bates, 1993)**

unimportant the additional time spent developing a more physically representative coupling mechanism could not have been justified.

The method of applying inflows to elements at the edge of the FEM was therefore selected. If inflows were found from this investigation to be important it would then be appropriate to consider making the coupling mechanism more sophisticated. Using this method, all the water produced by VSAS3 was delivered to the floodplain, and the volume contributed was probably over-estimated. The sensitivity analysis carried out may not therefore have been fully representative of the range of environments represented. However, the sensitivity of RMA-2, or any two-dimensional floodplain inundation model, to a range of different inflow volumes is not known. If it is subsequently discovered that the volume actually contributed from a particular hillslope environment for a given storm event is considerably less than that predicted in this study, the significance of that contribution can be re-evaluated by seeing if that volume still falls within the range of input volumes (expressed as a percentage of the reach input hydrograph) classified as 'significant'.

5.3 COUPLING VSAS3 TO RMA-2

5.3.1 Overview of the method used

Figure 5.4 gives a diagrammatic representation of the method used. There were several stages involved in converting the VSAS3 outflow hydrograph to a form suitable for input to RMA-2. The first stage involved in this process was described in Chapter Four where the VSAS3 output hydrograph was spatially averaged at each time step and converted to a discharge per unit length. Once the identification numbers of the elements and nodes defining the edge of the FEM had been found and the element side lengths calculated, inflows could be divided between the elements. The volume contributed to a particular element at a given time step was weighted according to the length of the element side by multiplying the discharge per unit length for that time step with the length of the element side.

Before the inflow value for each element was written to the modified RMA-2 input file, it was divided by the element area to yield an input in ft s^{-1}. Several FORTRAN programs were written to convert the data during the conversion process. These are described in the following sections and program listings may be found in the appendices.

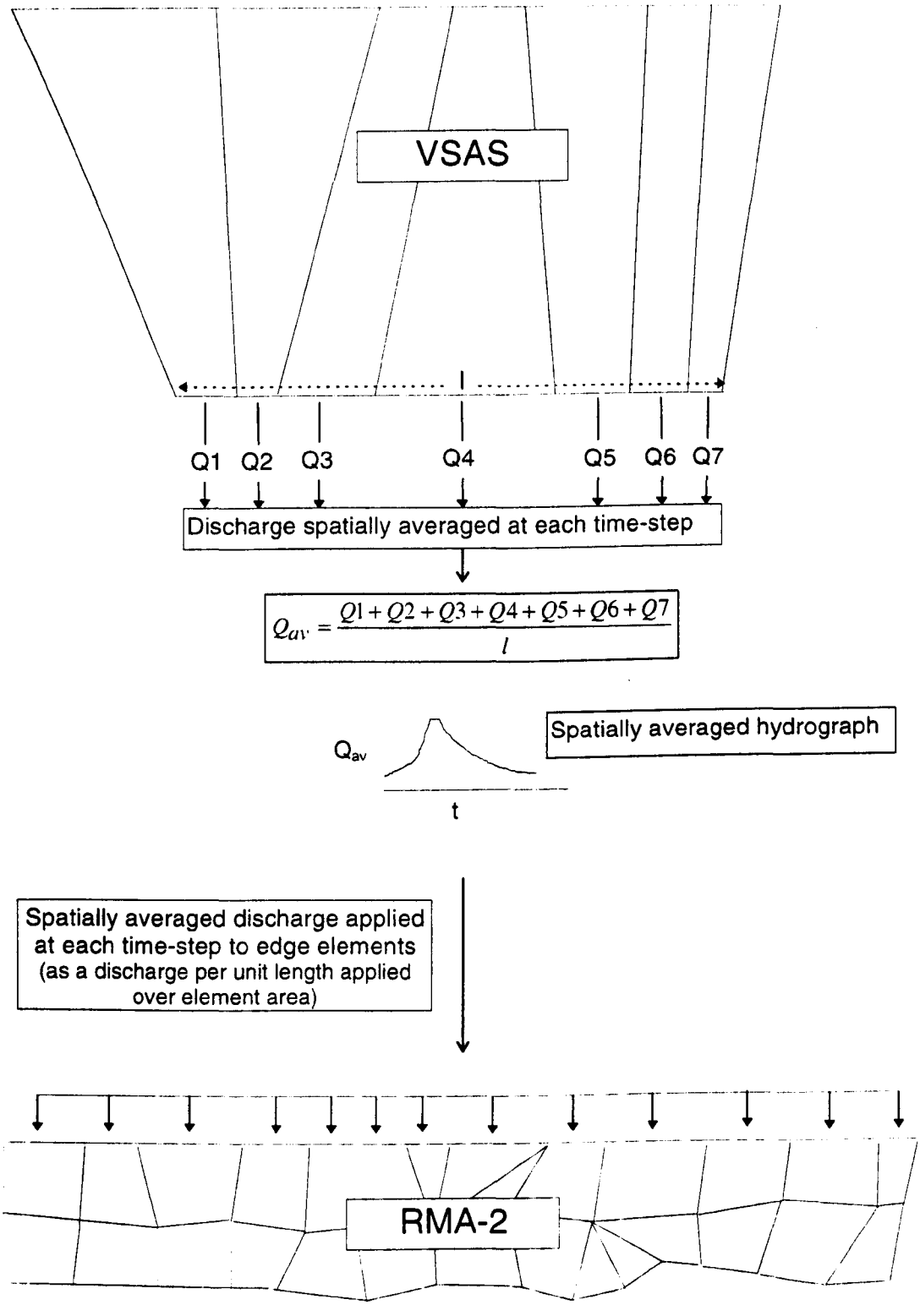

Figure 5.4: Illustration of the mechanism used to couple VSAS3 and RMA-2

5.3.2 *Identifying elements along the edge of the reach*

5.3.2.1 Why there is a problem

In order to apply inflows to RMA-2 the identification numbers of the elements at the edge of the FEM were required. In addition, the identification numbers for the nodes bounding each element at the edge of the FEM were needed in order to calculate the length of each element side forming the mesh boundary. The identification of these numbers caused a problem since there was no easy way of finding them. Examination of the original plots would enable the identification of some elements and nodes. However, the problem with this method was that the process of mesh refinement was carried out after the mesh was drawn on paper meaning that the final version of the FEM used in the RMA-2 simulation differed somewhat from the original plot. The process of mesh refinement involved re-ordering and moving certain elements and nodes, while other elements were added or removed from the FEM. It would have been possible to identify all the required element and node numbers by hand in conjunction with the Connection Table (which forms part of the RMA-1 input file described in Chapter One) although this would have been very time consuming. Instead, a program was written to identify the elements and nodes along the edge of the FEM.

5.3.2.2 The program written to identify elements and nodes along the edges of the FEM

A program *edgefinder.f* was created to carry out this task. Figure 5.5 shows a section of the reach and will be used to discuss the fundamental concepts behind the program. From this figure it can be seen that most of the nodes at the edge of the mesh only define the corners of two elements.

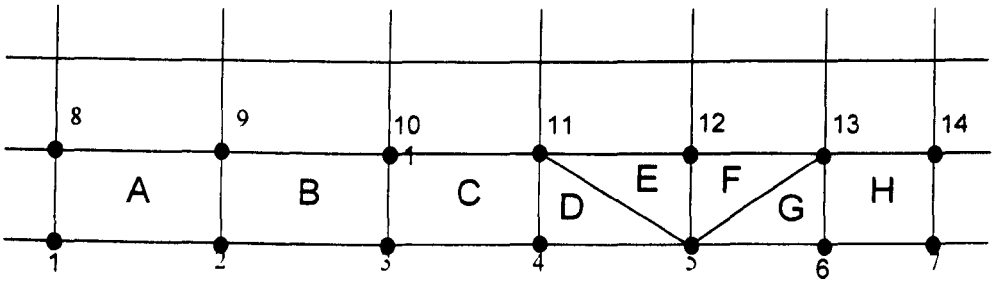

Figure 5.5: An example section of an RMA-2 FEM. In this example, elements are identified by letters and nodes by numbers.

From Figure 5.5 it can be seen that elements A, B and C are all at the edge of the FEM and the edge nodes bounding them are contained within only two elements. From the

connection table for this mesh section (Table 5.1) it can be seen that nodes 1,2,3 and 4 are each only found in two elements.

Element	Node 1	Node 2	Node 3	Node 4
A	1	2	9	8
B	2	3	10	9
C	3	4	11	10
D	4	5	11	
E	5	12	11	
F	5	13	12	
G	5	6	13	
H	6	7	14	13

Table 5.1: The connection table for the FEM section shown in Figure 5.5

The first step in the program involved identifying all the nodes such as these. The connection table was read into an array from the RMA-1 geometry input file by *edgefinder.f* and a list was made of all the node numbers together with the number of times each node number occurred. All those which only occurred twice were assumed to be edge nodes and were stored in an array.

Since the RMA-2 mesh consisted of both three and four sided elements more complex cases occurred. It was possible that edge nodes might be at the corner of 3 or more elements as in the case of node 5 in the example which is at the corner of four elements; D, E, F and G. From step one in the example shown, the following nodes would have been identified nodes 1, 2, 3, 4, 6 and 7. The program would have stored each node number together with the two other nodes it is adjacent to in an array. After step one in the program, the storage array would look like this where 'missing' nodes were given the identifier 9999:

Node	Adjacent node 1	Adjacent node 2
2	1	3
3	2	4
4	3	9999
6	9999	7

From this it can be seen that there is an unidentified node next to node 4. Node 4 is known, from the connection table array, to be at the corner of elements C and D. From the connection table the nodes bounding elements C and D are found:

C	3	4	11	10
D	4	5	11	

Since the two edge nodes in element C have been identified, it is necessary to identify the second edge node in element D. This element is a triangle and therefore node 4 is adjacent to both the other nodes, 5 and 11. Node 4 and one of these other nodes is shared with element C. The third node is the missing edge node. Referring to the connection table for element C, nodes 11 and 3 are adjacent to node 4. Since node 11 occurs in both elements C and D, the missing edge node must be node 5. This process was repeated for each 'missing' node by *edgefinder.f* and was the second stage in the program.

Once stage two had been completed the storage array was written to an output file. At this stage, a small number of very complex cases had not been identified. These were located by hand with the aid of the *edgefinder* output file and the connection table. A count was made of the number of edge elements from a plot of the FEM to check that this number was consistent with the total number of edge nodes identified. These were added to the edgefinder results file. This file was used as the input to a further program; *sorter.f* which produced an output file containing the node pairs at the edge of the FEM for each edge element.

5.3.2.3 *The program written to calculate element edge lengths*

The output file produced by *sorter.f* containing the edge node pairs was then used as one of the input files to the program *finedge.f*. The RMA-1 input geometry file was also used as an input together with a further file containing the areas of the elements within the FEM. *Finedge.f* obtained the element numbers corresponding to each node pair and then found the x and y co-ordinates for each node in the RMA-1 input file.

From this, the distance between each pair of nodes was calculated using Pythagoras to give the length of the outer edge of each element.

The output file from *finedge.f* contained the element number, the distance between the two nodes on the outer edge of the element and the area of the element. The total length of all the elements at the edge of the reach was found to be 28.06 km which was consistent with the reach length of 14 km (edge elements occur along both sides of the reach). The process of identifying all the elements at the edge of the reach only had to be carried out once. The final output file, produced by *finedge.f* contained the element data required for all further calculations.

5.3.3 *Distribution of water between the elements*

The distribution of water between the elements was carried out by the program *filemake.f*. This program required 3 input files; *elenarea.dat* (containing the element numbers and lengths of the element sides and generated by *finedge.f*), *inflows.dat* (containing the inflow per unit length and generated by *hydsum.f*) and the RMA-2 input file for that event. For each time step, *filemake.f* read in the inflow per unit length from the inflows file and for each of the 172 elements, the volume of water delivered to each element was determined by multiplying this discharge by the length of the element side. This volume was then divided by the corresponding element area (read in from *elenarea.dat*) to give a final inflow value for that element. The element number and this final inflow value were then written to the new 'inflows' version of the RMA-2 input file which was the same as the original version except that at each time step, inflows were specified along with the number of elements for which the addition of an inflow volume was required. Also, following the dynamic input data block for each time step, the 172 edge element identification numbers were listed together with the appropriate element inflow volumes for that time step. This process was repeated for each time step in the original input file. The new version of the RMA-2 file was then ready for input to RMA-2.

5.4 CARRYING OUT THE SENSITIVITY ANALYSIS

The control (no inflows) and coupled simulations carried out during the sensitivity analysis are shown in Table 5.2.

Coupled simulation	Event used for coupled simulation	VSAS3 simulation	VSAS3 simulation description	VSAS3 time steps used
CTRL01	1 in 1 year control (no inflows)	NO INFLOWS		
CTRL02	1 in 5 year control (no inflows)	NO INFLOWS		
CTRL03	1 in 12 year control (no inflows)	NO INFLOWS		
VSAS01	1 in 1 year	01	Initial simulation for 1 in 1 year storm	24 - 45
VSAS02	1 in 5 year	02	Hillslope simulation for 1 in 5 year storm	24 - 85.5
VSAS03	1 in 12 year	03	Hillslope simulation for 1 in 12 year storm	24 - 47.5
VSAS04	1 in 1 year	04	Soil with saturated hydraulic conductivity of clay loam	24 -45
VSAS05	1 in 1 year	05	Soil with saturated hydraulic conductivity of sand	24 -45
VSAS06	1 in 1 year	06	Soil with depth of 0.1 m	24 -45
VSAS07	1 in 1 year	07	Soil with depth of 1.0 m	24 -45
VSAS08	1 in 1 year	08	Dry initial moisture conditions	24 -45
VSAS09	1 in 1 year	09	Dry for 1 week	24 -45
VSAS10	1 in 1 year	10	Slope angle of 12°	24 -45
VSAS11	1 in 1 year	11	Slope angle of 45°	24 -45

Table 5.2: Simulations carried out during the sensitivity analysis

Three control simulations were carried out, for the 1 in 1, 1 in 5 and 1 in 12 year events respectively. In addition, a coupled simulation was carried out for these events using the inflow hydrographs generated by the VSAS3 simulations for each event. In this way, the results of the coupled simulations VSAS01, VSAS02 and VSAS03 could be compared to examine the sensitivity of RMA-2 to changes in the total rainfall depth applied to the hillslope.

The rest of the coupled simulations used the same 1 in 1 year event to provide the RMA-2 input hydrograph. The VSAS3 simulations used the observed rainfall for this

event as the hillslope input. In this way, the event was the same for all the remaining simulations and only the remaining parameters to which the sensitivity of RMA-2 was being assessed were altered. The 1 in 1 year event was selected because it was a single peaked event and during it, the floodplain did not become completely inundated. This allowed any changes in the inundation extent caused by the addition of hillslope inflows to be examined.

A UNIX macro was written to provide the correct input files for each simulation, run the model and uniquely identify the results files produced. The results are described in the next chapter.

5.5 AN EXAMINATION OF THE IMPORTANCE OF THE RELATIVE TIMING OF THE HILLSLOPE AND FLOODPLAIN HYDROGRAPH PEAKS

5.5.1 *The significance of relative timing*

Figures 5.6, 5.7 and 5.8 display the input hydrographs used in the coupled simulations for each of the three events. These show the total volume of inflows applied along the edge of the reach at each time step together with the RMA-2 input hydrographs for each of the three events considered. The shaded area on these graphs indicates the period of time over which the coupled simulations were carried out. Examination of Figure 5.6 shows that very little water was contributed from the hillslopes during the coupled simulation for the 1 in 1 year event and that most of the discharge produced by the hillslopes had occurred prior to this. The timing of the 1 in 5 year coupled simulation shown in Figure 5.7 meant that the second hillslope hydrograph peak occurred during this coupled simulation while the main hillslope hydrograph peak actually occurred during the 1 in 12 year coupled simulation. Table 5.3 shows the hillslope input volumes expressed as a percentage of the reach input hydrograph for these events.

Simulation	Event	Reach inflow hydrograph (m3)	Inflows applied (m3)	Inflows as a % of reach inflow hydrograph
01	1 in 1	3.95×10^6	6.82×10^4	1.73%
02	1 in 5	1.80×10^7	2.50×10^6	13.89%
03	1 in 12	1.15×10^7	1.44×10^6	12.52%

Table 5.3: Inflow volumes expressed as a percentage of the reach inflow hydrograph

Input hydrographs
Inflows and RMA-2 (1 in 1)

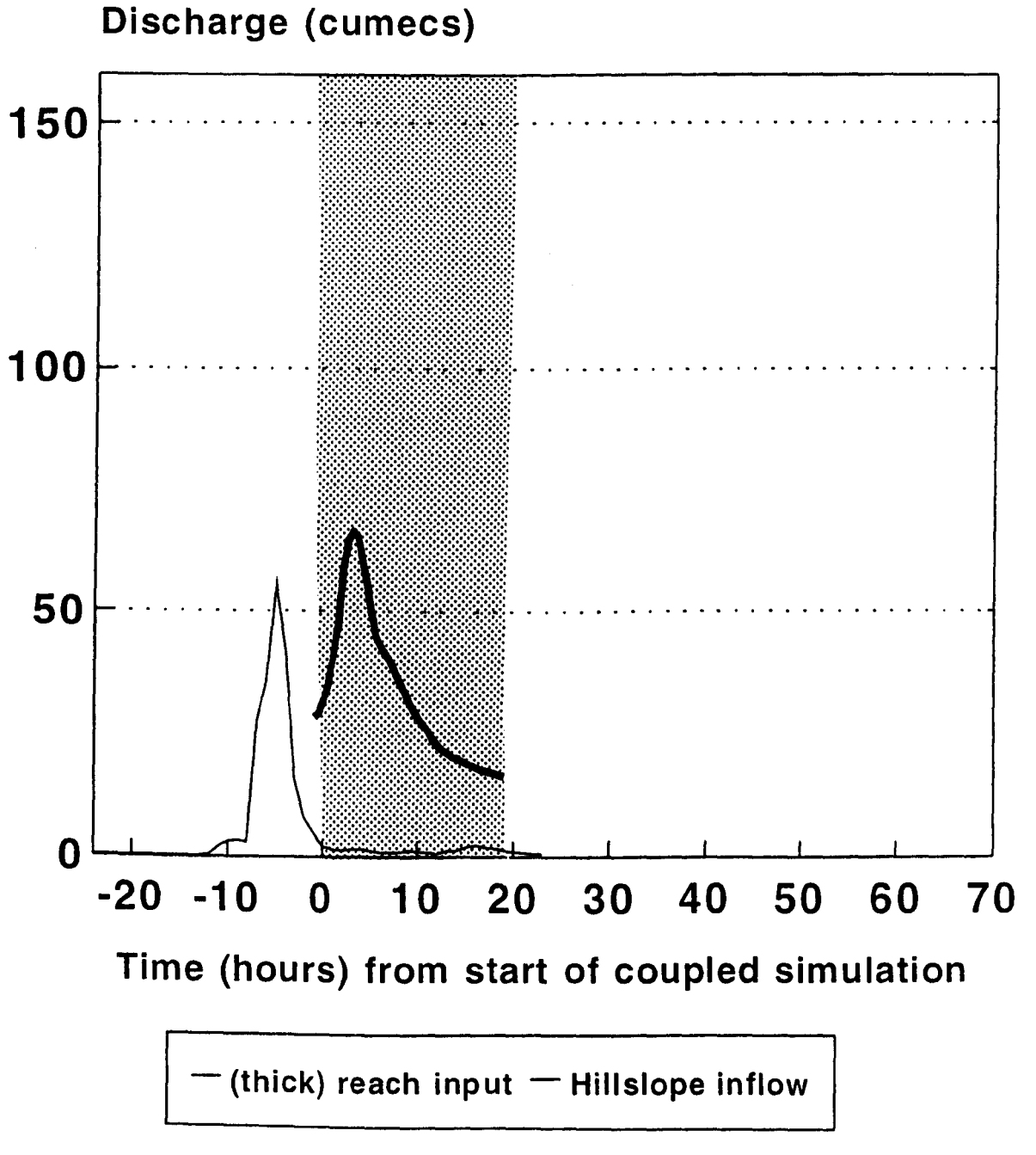

Figure 5.6: Input hydrographs for the 1 in 1 year coupled simulation showing the reach input and hillslope inflows hydrographs

Input hydrographs
Inflows & RMA-2 (1 in 5)

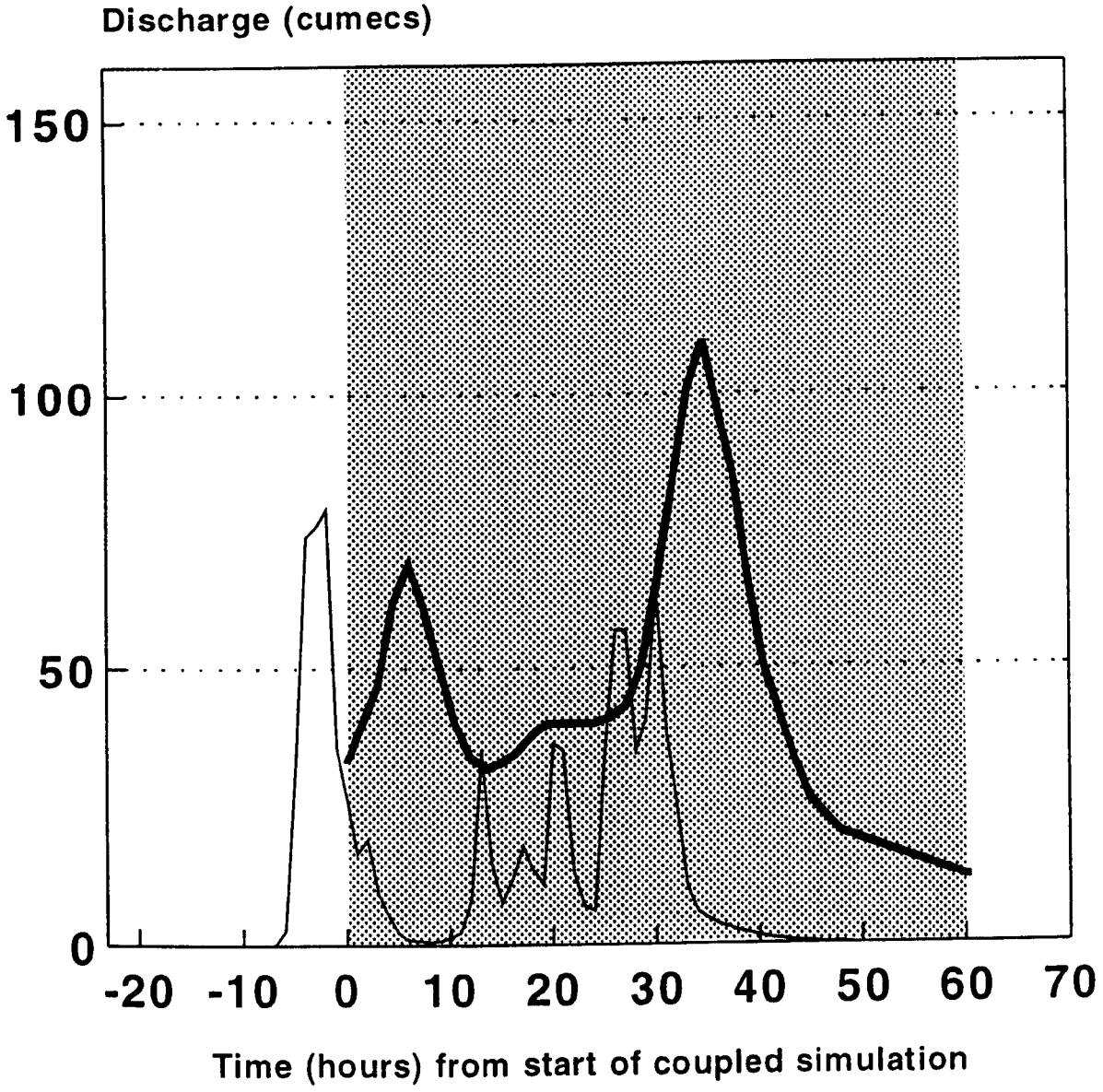

Figure 5.7: Input hydrographs for the 1 in 5 year coupled simulation showing the reach input and hillslope inflows hydrographs

Input hydrographsInflows

Inflows and RMA-2 (1 in 12)

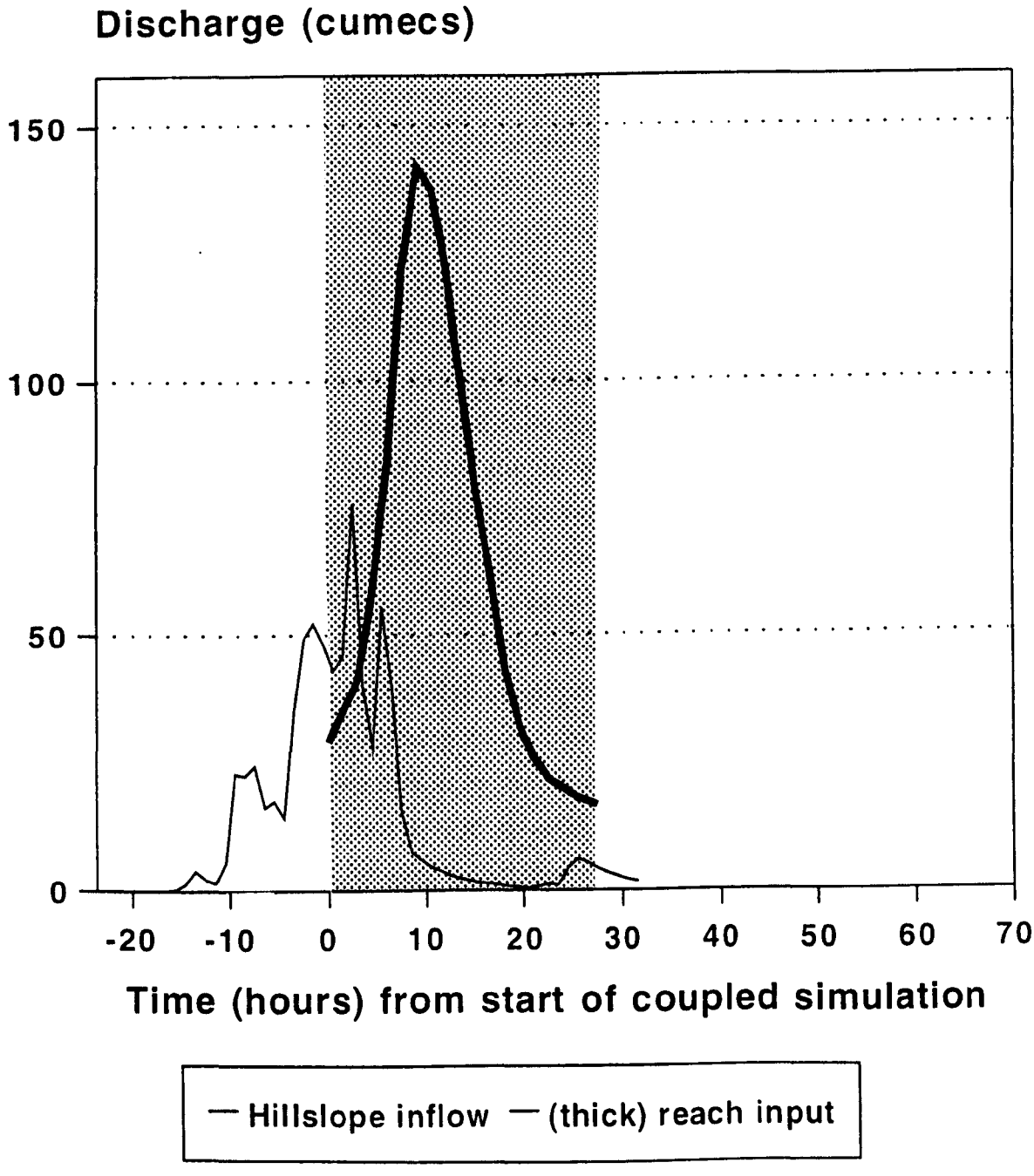

Figure 5.8: Input hydrographs for the 1 in 12 year coupled simulation showing the reach input and hillslope inflows hydrographs

When the sensitivity analysis was carried out for all parameters, except rainfall depth, the 1 in 1 year event was used, therefore the sensitivity of the coupled scheme to the recession phase of the inflows hydrograph was examined.

Chapter Two discussed the range of different hillslope - floodplain environments which might occur and proposed that the relative timing of the hillslope inflows hydrograph peak and the floodplain peak was unlikely to be the same for different environments. It was suggested that this relative timing would be influenced by several factors. These included the response of the hillslope to the rainfall input (which would in addition be affected by factors such as the antecedent conditions) and the speed with which the hillslope contribution was transported to the floodplain. The location of the reach of interest within its catchment would also affect timing. If this was near the headwaters, the time lag between the rainfall input and the arrival of the floodwave at the upstream end of the reach would be considerably less than that for a lowland reach where the floodwave had a relatively longer distance to travel.

Examining the sensitivity of the coupled scheme to inflows from the recession limb made the assumption that the hillslopes contributed water directly to the edge of the floodplain. For the Culm reach, the main flood wave is typically observed to take approximately 24 hours to reach the gauge at Woodmill (at the upstream end of the reach). If the hillslopes adjacent to the floodplain responded within this period then it is possible that the inflows from the hillslopes might contribute a significant volume before the main floodwave, as in the sensitivity analysis. Alternatively there might be a delay due to a slower hillslope response or to the hillslope contribution taking a more complex pathway during the process of delivery to the floodplain. In this case the peak hillslope contribution to the floodplain might occur during the time of the simulation or indeed even after it. It was therefore proposed to examine this case and, in turn, the effect of changing the relative timing of the hillslope and floodplain peaks so that they occurred simultaneously. Whilst this would not reflect the probable attenuation which would be observed in the hillslope input hydrograph if a slower pathway was taken by the water, it would give a good indication of the importance of relative timing. In addition, since the inflow volume from this part of the hillslope hydrograph would be greater, the effect of adding larger inflows could be examined in volumetric terms.

5.5.2 *Further model simulations carried out to examine the importance of relative timing*

The sensitivity analysis was extended to examine this issue by carrying out further coupled simulations, shifting the time base of the inflows hydrographs so that the inflow peak was simultaneous with the reach upstream hydrograph peak. New RMA-2 input files were created for each additional simulation by re-running the program *filemake.f* and specifying the new part of the VSAS3 output hydrographs from which inflows were to be calculated.

Coupled simulation	Event used for coupled simulation	VSAS3 simulation	VSAS3 simulation description	VSAS3 time steps used
VSASSP01	1 in 1 year	01	Initial simulation for 1 in 1 year storm	16.5-37.5
VSASSP04	1 in 1 year	04	Soil with saturated hydraulic conductivity of clay loam	16.5-37.5
VSASSP05	1 in 1 year	05	Soil with saturated hydraulic conductivity of sand	16.5-37.5
VSASSP06	1 in 1 year	06	Soil with depth of 0.1 m	16.5-37.5
VSASSP07	1 in 1 year	07	Soil with depth of 1.0 m	16.5-37.5
VSASSP08	1 in 1 year	08	Dry initial moisture conditions	16.5-37.5
VSASSP09	1 in 1 year	09	Dry for 1 week	16.5-37.5
VSASSP10	1 in 1 year	10	Slope angle of 12°	16.5-37.5
VSASSP11	1 in 1 year	11	Slope angle of 45°	16.5-37.5

Table 5.4: Simulations carried out during the sensitivity analysis to changes in hillslope parameters when the hillslope hydrograph was applied so its peak occurred at the same time as the reach input hydrograph

Since the reach input peak occurred 4.5 hours into the RMA-2 simulation, inflows were applied from VSAS3 starting at 16.5 hours (the mean of the discharge produced at 16.0 hours and 17.0 hours). Therefore the peak inflow volume applied 4.5 hours into the coupled simulation was the mean discharge between the discharge produced by VSAS3 between 20.0 hours (peak) and 21.0 hours.

A new RMA-2 input file was created for each of the additional simulations shown in Table 5.4. The new simulations were again carried out using a UNIX macro. The results of these simulations are discussed in Chapter Six.

5.6 CONCLUSIONS

This chapter has described the design and implementation of a mechanism to couple the hillslope hydrology model VSAS3 to the floodplain inundation model RMA-2 in order to carry out the second part of the sensitivity analysis; the sensitivity of RMA-2 to changes in the selected hillslope parameters.

A method of coupling VSAS3 to RMA-2 was selected by considering the processes of water delivery to the floodplain in the context of this first pass investigation into the significance of this additional input. Since the importance of hillslope inflows was not known, it was felt to be inappropriate to develop a sophisticated and physically-realistic coupling mechanism. A simple mechanism was therefore adopted and using this the spatially averaged VSAS3 hydrographs produced during the first part of the sensitivity analysis (described in Chapter Four) were incorporated into new RMA-2 input files. The second part of the sensitivity analysis examined the sensitivity of RMA-2 to changes in the hillslope input parameters through applying the hillslope inflows produced during the first part of the sensitivity analysis.

Following this, a further investigation was made into the importance of the relative timing of the floodplain and hillslope hydrograph peaks. This was carried out by creating further RMA-2 input files incorporating the same VSAS3 inflows but with an altered time base so that the inflow peak occurred simultaneously with the reach input peak. These further simulations were carried out to find out if any difference was observed in the sensitivity of RMA-2 to changes in the hillslope parameters.

The results of these investigations are presented and examined in Chapter Six.

Chapter Six

ANALYSING THE RESULTS

6.1. INTRODUCTION

This chapter discusses the results produced by coupling VSAS3 to RMA-2 and consists of four main parts. Following a description of the methods used to analyse the results, the first part of the sensitivity analysis, described in Chapter Four, involved examining the sensitivity of VSAS3 to changes in five hillslope parameters. The outflows from these VSAS3 simulations were then applied to elements along the edge of the RMA-2 FEM as an additional model input. The method used to couple the models was described in Chapter Five together with a summary of the coupled model simulations carried out. The sensitivity of RMA-2 to the different applied inflows produced by changing the values of the hillslope parameters, is discussed in Section 6.3 in terms of the relative degree of change which was found to occur in the output hydrograph characteristics. Following this, Section 6.4 discusses the importance of the relative timing of the hillslope and floodplain response to a storm event. As observed in Chapter Five the hillslope hydrograph peak for the 1 in 1 year event occurred before the start of the coupled simulation. Therefore the sensitivity analysis examined the sensitivity of RMA-2 predictions to hillslope inflows from the recession limb of the hillslope hydrograph. In order to examine the importance of relative timing, the time base of the hillslope input was shifted so that the hillslope hydrograph peak occurred at the same time as the floodplain input peak. The sensitivity of RMA-2 to this altered input was examined.

The sensitivity of RMA-2 was also investigated in terms of more localised effects resulting from the addition of inflows, such as changes in depth at selected locations and the overall change to the maximum inundation extent. Finally the effect of adding different inflow volumes was analysed in terms of the volumetric change to the output hydrograph and hydrograph peak.

6.2. ANALYSING THE RESULTS

During the analysis of the results a considerable amount of comparison was made between inflow and outflow volumes. In order to conduct this part of the investigation accurately it was important to consider several factors affecting the exact

value of the volume of water actually applied to and output by the coupled scheme. First as discussed in Chapters 4 and 5, the VSAS3 simulation was carried out for a 24 hour 'run-in' period prior to the start of the coupled simulation. Therefore, any water produced by VSAS3 during this period was not contributed to the floodplain as an input to RMA-2. Only the predicted volume of water yielded by the hillslope *after* this 24 hour period was applied to RMA-2. The second factor to be considered was that the coupled modelling scheme did not necessarily run stably for all the time steps for which input data was provided. This was because towards the end of a simulation, on the recession limb of the upstream input hydrograph, less and less water was input to the system, reducing the inundated area substantially. The large number of elements simultaneously leaving the finite element solution at this stage caused model instability. Inflows predicted by VSAS3 were included in the RMA-2 input file for all time steps for which upstream input was provided. When calculating the total volume of water contributed from the hillslopes, only water contributed from the start of the coupled simulation to the time at which the model became unstable was included. Similarly, when the volume of water contributed to the floodplain from upstream was calculated, only the volume applied before the time step at which the model became unstable was considered. This point is illustrated in Figure 6.1 which shows the relative timing of the VSAS3 and RMA-2 simulations for the 1 in 1 year event.

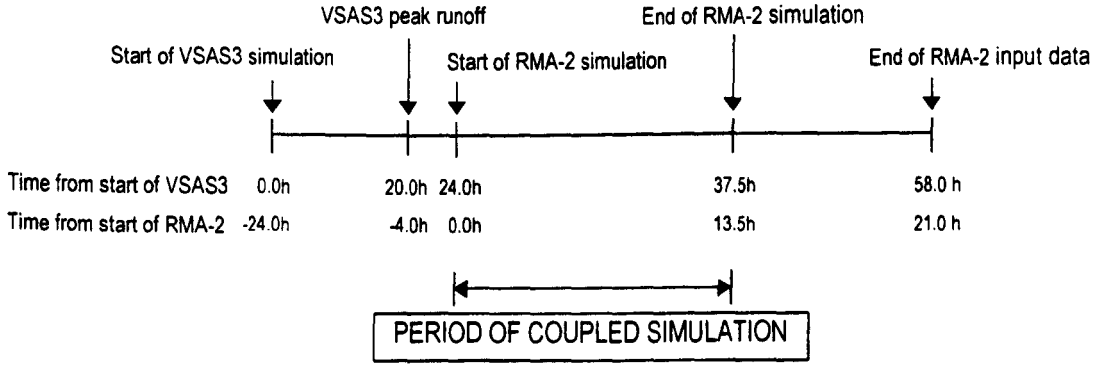

Figure 6.1: Illustration of the relative timing of the 1 in 1 VSAS3 and RMA-2 input.

For this event the coupled simulation ran stably for 27 time steps (13.5 hours). The 1 in 5 and 1 in 12 year control simulations ran for 89 and 40 time steps respectively corresponding to 44.5 hours and 20.0 hours. In some cases the addition of inflows was found to increase model stability at the end of a simulation due to the increased volume of water which allowed more elements to remain within the mathematical solution, thus enabling the coupled simulation to run for additional time steps. Where

this was the case, the input and output volumes for additional time steps were included in volumetric calculations.

6.3. RESULTS OF THE SENSITIVITY ANALYSIS

The results were analysed in several ways. The sensitivity analysis was the main part of this investigation, although the results were also examined to determine the effect of inflows in a more general context. The sensitivity analysis considered the effect of changing each of the selected VSAS3 input parameters in terms of resulting changes to the hillslope and subsequently the floodplain hydrograph characteristics. The second stage of the sensitivity analysis discussed in this chapter compared the effects that changes to each of the parameters had on the total volume and peak discharge produced by the coupled scheme. In order to do this, various calculations were made for each of the five parameters in the sensitivity analysis:

1. The percentage difference between the three values used for the input parameter.
2. The resulting percentage change in the hydrograph predicted by VSAS3 for the template slope for these values (Chapter Four). The whole hillslope hydrograph produced by VSAS3 was considered in this calculation.
3. The total volume of the three RMA-2 output hydrographs produced by the three coupled simulations and from this, the percentage change in total volume between them.
4. The percentage change in the peak runoff produced for each coupled simulation.

From these calculations, the percentage change in total volume and peak discharge resulting from a 1% change in each parameter value could be examined. Using this the parameters to which the coupled scheme was most sensitive could be identified.

6.3.1 Sensitivity of the coupled scheme to changes in rainfall event

The results of the first part of the sensitivity analysis discussed in Chapter Four showed that the parameter VSAS3 was most sensitive to was the rainfall event. There was found to be a considerable difference between the events in terms of the hillslope hydrograph shape and total volume. In examining the sensitivity of the coupled scheme to inflows resulting from different rainfall events three different RMA-2 input hydrographs were used as the upstream input to the reach. These were observed hydrographs corresponding to the rainfall events used in the VSAS3 simulations. Although variation between the output hydrographs for the coupled events was partly

due to the effect of the changed inflow volumes applied, it was also affected by the different RMA-2 input hydrographs used. The characteristics of each RMA-2 input hydrograph were a function of several factors influencing the catchment response upstream of the study reach such as the antecedent conditions and spatial distribution of rainfall. The VSAS3 simulations carried out for the three rainfall events all used the same initial moisture conditions meaning that differences in the predicted runoff characteristics were only a function of the volume, intensity and temporal distribution of the rainfall applied to the slope. In addition to this the fact that the three events were of different durations also meant that it was not possible to carry out a direct comparison between the total volumes produced by the coupled simulations. Instead, for each coupled simulation the percentage increase in total output volume (with inflows) from the control output volume was calculated for each event. The relative sensitivity of the coupled scheme to different rainfall events was then taken to be the difference in this percentage increase in output which occurred *between* the events. From this, the percentage change in the relative volumetric increase in output between events for a 1% change in the rainfall input to the hillslope was calculated (by dividing the percentage change in the runoff by the original percentage change to the rainfall depth). In the same way the percentage change between the control and inflows peak runoff was calculated so that this percentage increase could be compared between events. These calculations are shown in Table 6.1 below.

The greatest percentage increase in total volume for an event was observed for the 1 in 12 year event even though the total volume of rainfall and the resultant volume of the inflows hydrograph was less than that for the 1 in 5 year event. If attention is turned to Figures 6.2, 6.3 and 6.4 it can be seen that the inflows hydrograph for the 1 in 12 event peaked within the period of the coupled simulation. This was not the case for the 1 in 5 year or 1 in 1 year events. Although the 1 in 12 inflows peak occurred 15 hours before the main input hydrograph peak, a considerable volume was contributed during the rising limb of the RMA-2 input hydrograph. Figure 6.5 shows the percentage difference between the output hydrographs from the control and coupled simulations for this event. The greatest difference between these output hydrographs occurred on the rising limb of the hydrographs at 8.0 hours. From Figure 6.2 it can be seen that the inflows applied during the 1 in 1 year coupled simulation were produced during the recession limb of the hillslope input hydrograph when the discharge was relatively low.

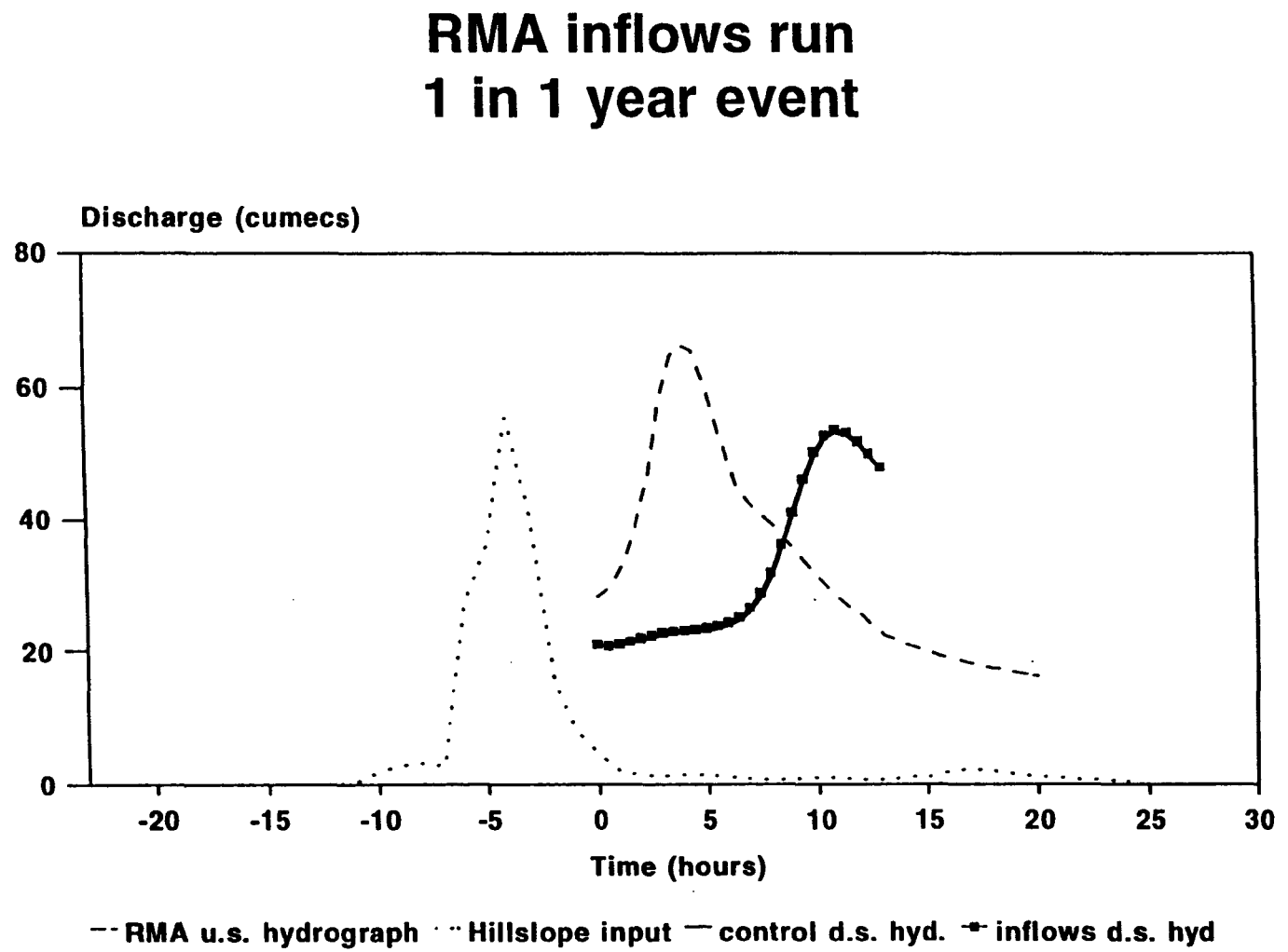

Figure 6.2: Predicted hydrographs produced by the control and coupled simulations for the 1 in 1 year event. The RMA-2 and hillslope input hydrographs are also shown

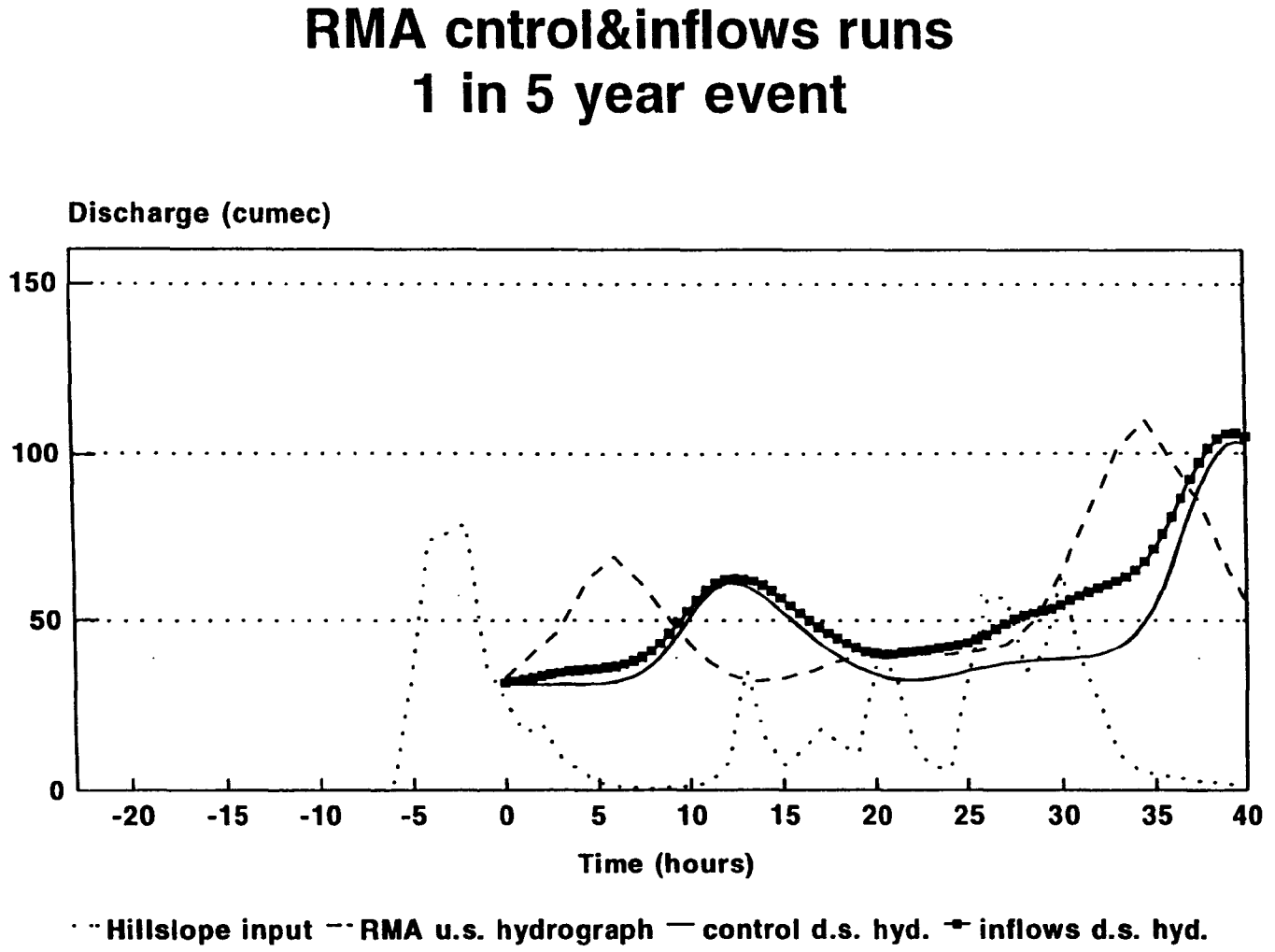

Figure 6.3:Predicted hydrographs produced by the control and coupled simulations for the 1 in 5 year event. The RMA-2 and hillslope input hydrographs are also shown

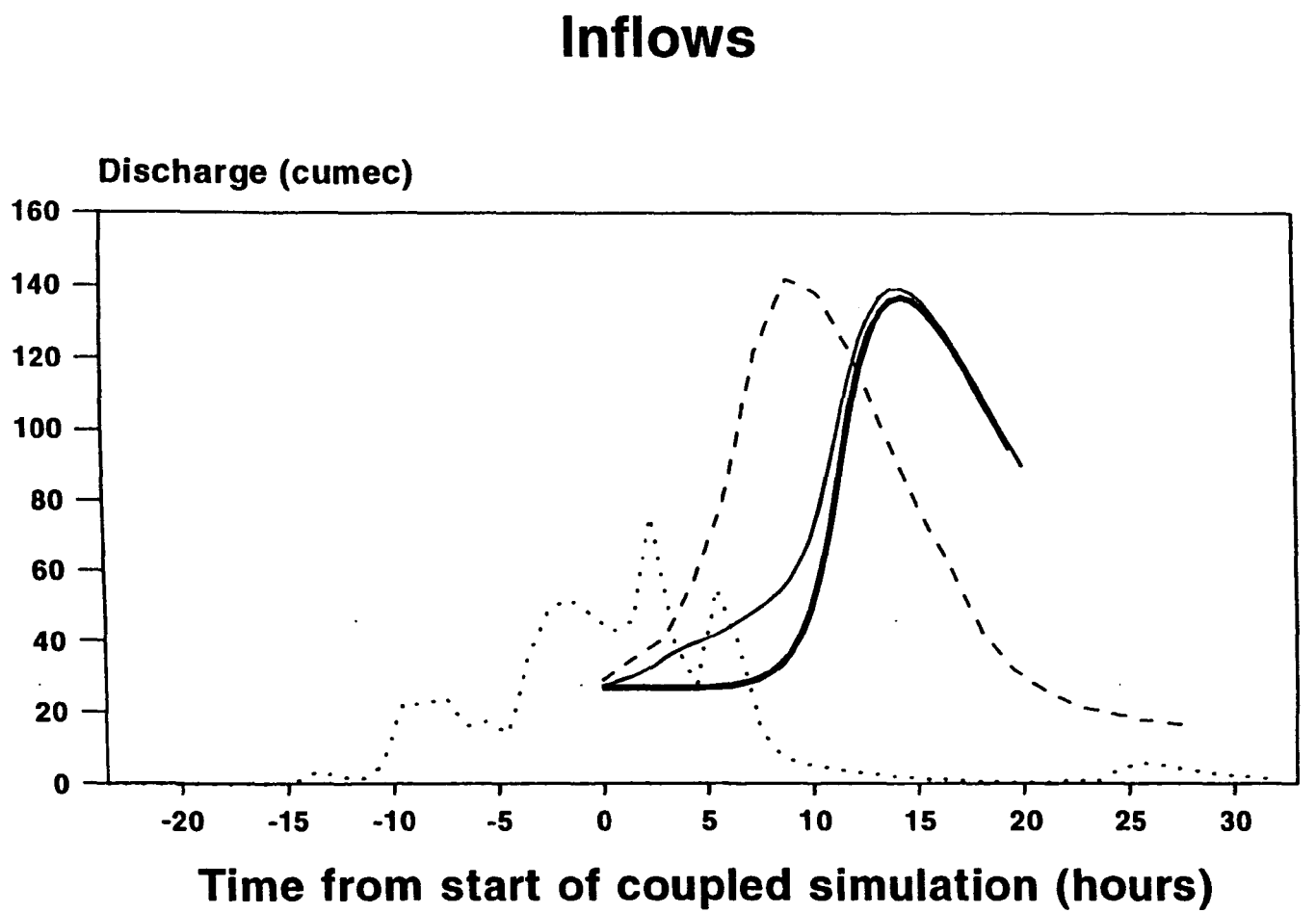

Figure 6.4: Hydrographs for the 1 in 12 year event for control and with inflows. The RMA-2 and hillslope input hydrographs are also shown. The shaded area shows duration of the coupled simulation

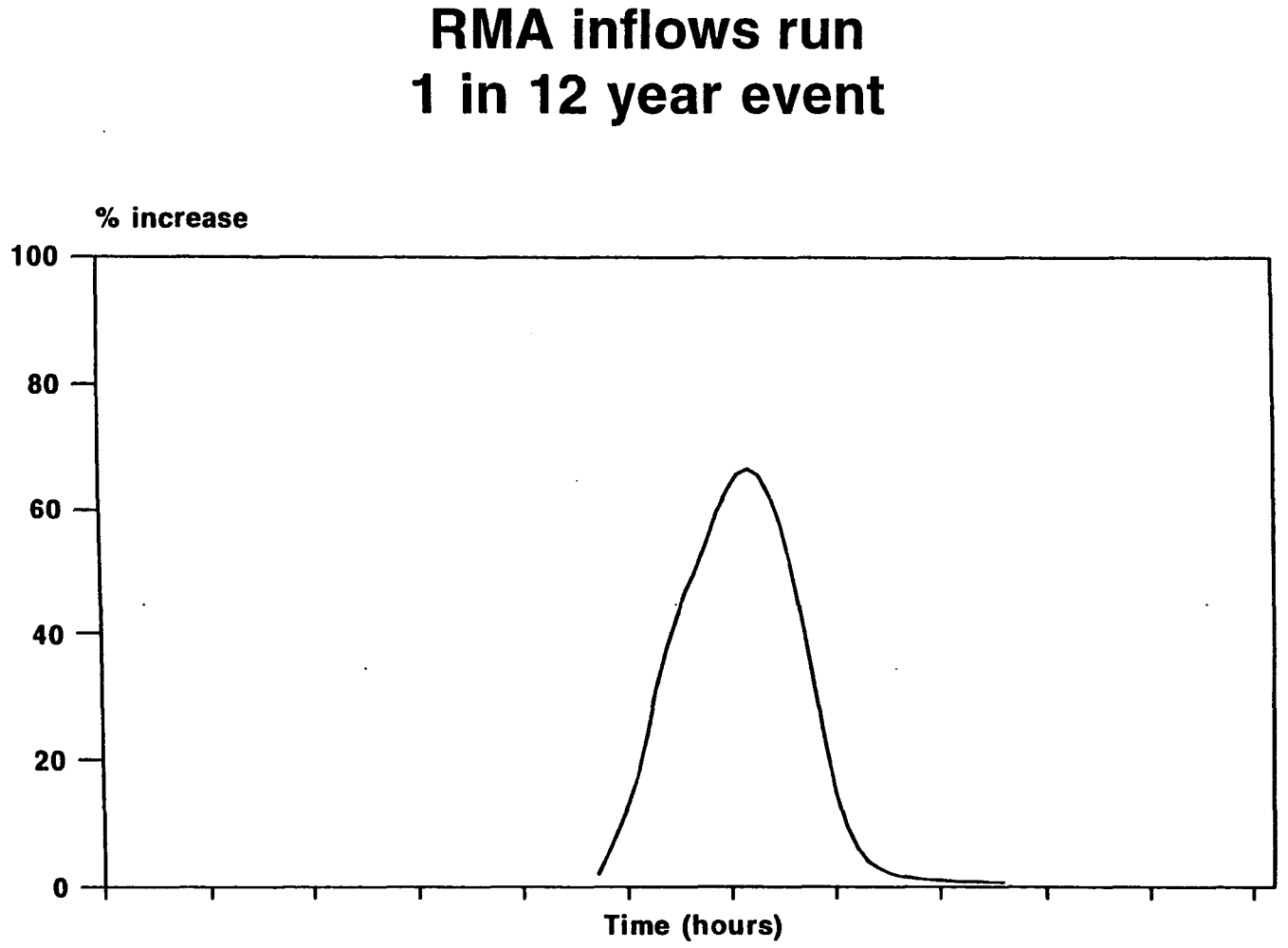

Figure 6.5: Graph showing the change in discharges from the control and inflows hydrograph produced for the 1 in 12 year event and expressed as a percentage of the control discharge at each time step

For this reason the difference between the coupled output hydrograph and the control was comparatively minor and was also fairly constant with respect to time. Figure 6.3 shows that for the 1 in 5 year event a secondary peak occurred during the coupled simulation. It can be seen that this contributed a significant volume of water to the coupled output hydrograph between hours 15.00 and 40.00. Indeed the greatest absolute increase in total volume between the control and coupled simulation was seen for the 1 in 5 year event although the greatest percentage increase was brought about by the inflows produced by the 1 in 12 year event. The 1 in 5 year event also showed the greatest increase in hydrograph peak discharge.

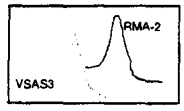 WITH INFLOWS NO TIME SHIFT	RAINFALL DEPTH		
	19.1 mm (1 in 1 year)	63.2 mm (1 in 5 year)	47.9 mm (1 in 12 year)
% increase in parameter value	N/A	+ 230.89%	- 24.21%
% change in VSAS3 total volume for 1% change in parameter value	N/A	+1.18%	+ 1.47%
Total volume of runoff produced by RMA-2 control simulation	$3.16 \times 10^6 m^3$	$1.6 \times 10^7 m^3$	$1.0 \times 10^7 m^3$
Total volume of runoff produced by coupled simulation	$3.20 \times 10^6 m^3$	$1.82 \times 10^7 m^3$	$1.16 \times 10^7 m^3$
% increase in total volume from control	1.27%	13.75%	16.00%
% change in percentage increase BETWEEN events	N/A	982.68%	16.37%
% change in total volume for 1% change in parameter value	N/A	4.26%	- 0.68%
Peak discharge for control	$53.235 m^3 s^{-1}$	$103.439 m^3 s^{-1}$	$136.825 m^3 s^{-1}$
Peak discharge for coupled simulation	$53.801 m^3 s^{-1}$	$106.049 m^3 s^{-1}$	$139.278 m^3 s^{-1}$
% change in peak discharge for event	1.07%	2.52%	1.79%
% difference BETWEEN events	N/A	136.62%	- 28.97%
% change in peak discharge for a 1% change in parameter value	N/A	0.59%	1.20%

Table 6.1: The results of the sensitivity analysis carried out for different rainfall events.

6.3.2 *Sensitivity of the coupled scheme to changes in saturated hydraulic conductivity*

For this and the remaining parameters the same (1 in 1 year) hydrograph was applied at the upstream end and the 1 in 1 year rainfall event was used as the hillslope input in all cases. Therefore the inflows applied were from the recession limb of the hillslope hydrograph. In Chapter Four it was observed that the total volume of runoff produced by VSAS3 was found to decrease with increasing hydraulic conductivity. This pattern was not found to occur during the recession limb where the sand soil (1.00×10^{-4} m s^{-1}) produced the greatest volume of runoff. The smallest volume was produced by the loam soil (5.56×10^{-6} m s^{-1}) with the clay loam (1.39×10^{-6} m s^{-1}) producing a greater volume of runoff than the loam. This was reflected by the output hydrographs from the coupled simulations shown in Figure 6.6. Comparing these hydrographs at the start of the coupled simulations only a slight difference in discharge was observed although this difference increased until approximately five hours into the simulation after which it remained almost constant. At the time of the peak, the discharge for the sand soil increased at a slightly faster rate than that for the other soil hydraulic conductivities giving a larger hydrograph peak discharge. The hillslope hydrograph for this soil also showed a slight increase at this time in response to an additional rainfall input after the main event. Table 6.2 shows the calculations carried out for this parameter. Since the only input which was being altered in the coupled simulations was the hillslope input hydrograph it was possible to make a direct comparison between the total volume of runoff produced by each coupled event and in the same way for comparing hydrograph peak discharge.

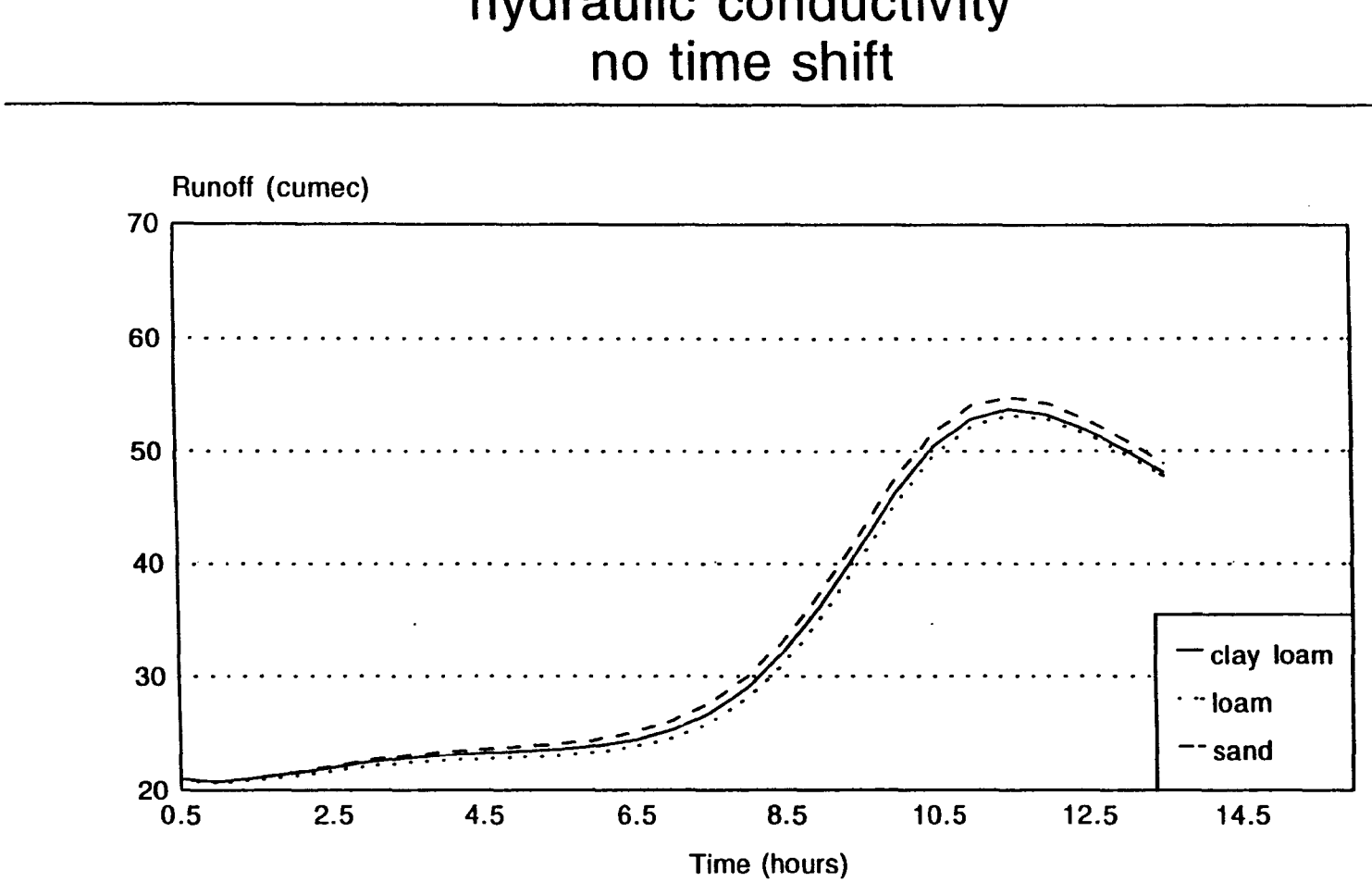

Figure 6.6: Hydrographs produced by the coupled simulations using the three different saturated hydraulic conductivities

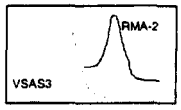 WITH INFLOWS NO TIME SHIFT	SATURATED HYDRAULIC CONDUCTIVITY		
	1.39×10^{-6} m s^{-1} (clay loam)	5.56×10^{-6} m s^{-1} (loam)	1.00×10^{-4} m s^{-1} (sand)
% increase in parameter value	N/A	+ 300.00%	+ 1698.56%
% change in VSAS3 total volume for 1% change in parameter value	N/A	- 1.18%	- 12.60%
Total volume of runoff produced by coupled simulation	3.21×10^{6} m^{3}	3.20×10^{6} m^{3}	3.27×10^{6} m^{3}
% change in total volume produced by coupled simulation	N/A	- 0.31%	+ 2.19%
% change in total volume for 1% change in parameter value	N/A	- 0.0010%	+ 0.0013%
Peak discharge	53.818 m^{3}s^{-1}	53.254 m^{3}s^{-1}	54.837 m^{3}s^{-1}
% change in peak discharge	N/A	- 1.05 %	+ 2.97 %
% change in peak discharge for a 1% change in parameter value	N/A	- 0.0035%	+ 0.0017%

Table 6.2: Sensitivity of RMA-2 to changes in saturated hydraulic conductivity with no time shift applied to VSAS3 inflows

6.3.3 *Sensitivity of the coupled scheme to changes in soil depth*

An increase in the soil depth was found to result in a decrease in the total volume of discharge produced by VSAS3. Again this relationship was not found to be the same during the recession limb where the intermediate depth soil (0.5 m) produced a considerably smaller volume of runoff than the shallowest (0.1 m) and deepest (1.0 m) soils. Reasons for these differences were proposed in Chapter Four.

The results of the coupled simulation (Figure 6.7 and Table 6.3) again show that the 0.1m soil produced the greatest increase in discharge from the control although the difference between this hydrograph and that for the coupled simulation using inflows from the 1.0 m soil was very slight. The greatest difference occurred between the coupled hydrographs for the 1.0 m and the 0.5 m soils. In terms of hydrograph peaks the greatest difference was again seen to occur between the 0.5 and 1.0 m soils with very little difference observed between the 1.0 m and 0.1 m soils. Although there was very little difference between the three hydrographs at the start of the coupled simulation, the difference became most marked at the time of the hydrograph peak. These observations correspond with changes to the hillslope hydrographs shown in Chapter Four.

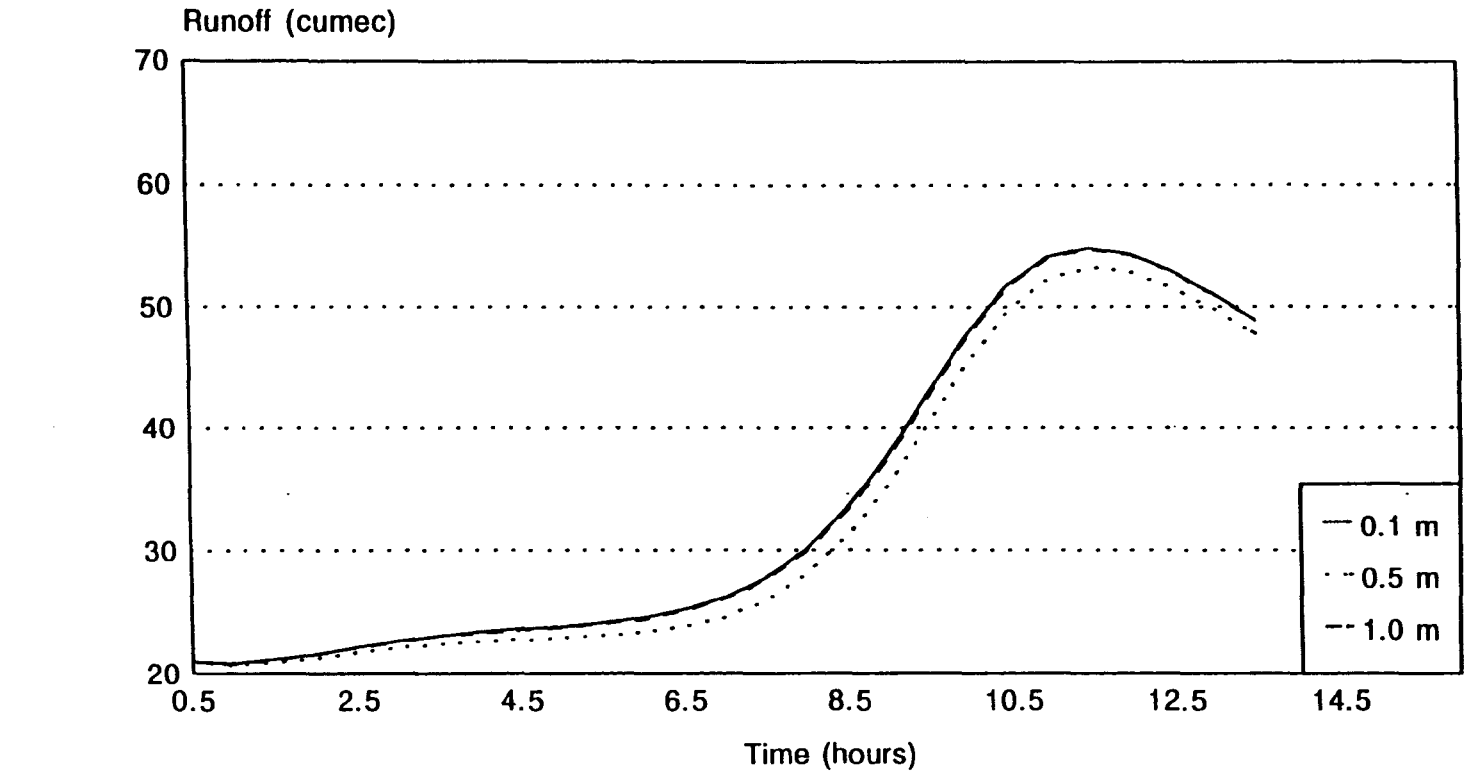

Figure 6.7: Hydrographs produced by the coupled simulations using three different soil depths

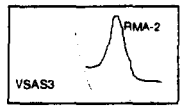 NO TIME SHIFT	SOIL DEPTH		
	0.1 m	0.5 m	1.0 m
% increase in parameter value	N/A	+ 400.00%	+ 50.00%
% change in VSAS3 total volume for 1% change in parameter value	N/A	- 26.40%	- 14.83%
Total volume of runoff produced during coupled simulation	3.28×10^6 m^3	3.20×10^6 m^3	3.27×10^6 m^3
% change in total volume produced by coupled simulation	N/A	- 2.44%	+ 2.19%
% change in total volume for 1% change in parameter value	N/A	- 0.0061%	- 0.044%
Peak discharge	54.900 m^{3}s^{-1}	53.801 m^{3}s^{-1}	54.837 m^{3}s^{-1}
% change in peak discharge	N/A	- 2.00%	- 1.93%
% change in peak discharge for a 1% change in parameter value	N/A	- 0.005%	- 0.039%

Table 6.3: Sensitivity of RMA-2 to changes in soil depth with no time shift applied to VSAS3 inflows

6.3.4 *Sensitivity of the coupled scheme to changes in initial moisture conditions*

The results of the VSAS3 simulations indicated that that for increasingly wet antecedent conditions, the total volume of water produced by the hillslope increased correspondingly. However, this was not the case during the recession limb where the soil which had been dried for one week prior to the simulation (and had an initial unit moisture content of 0.988 at the slope base) actually contributed more runoff than the initially saturated soil. Chapter Four explained these observed differences which were reflected in the output hydrographs from the coupled simulations shown in Figure 6.8.

Hydrographs for initial moisture conditions no time shift

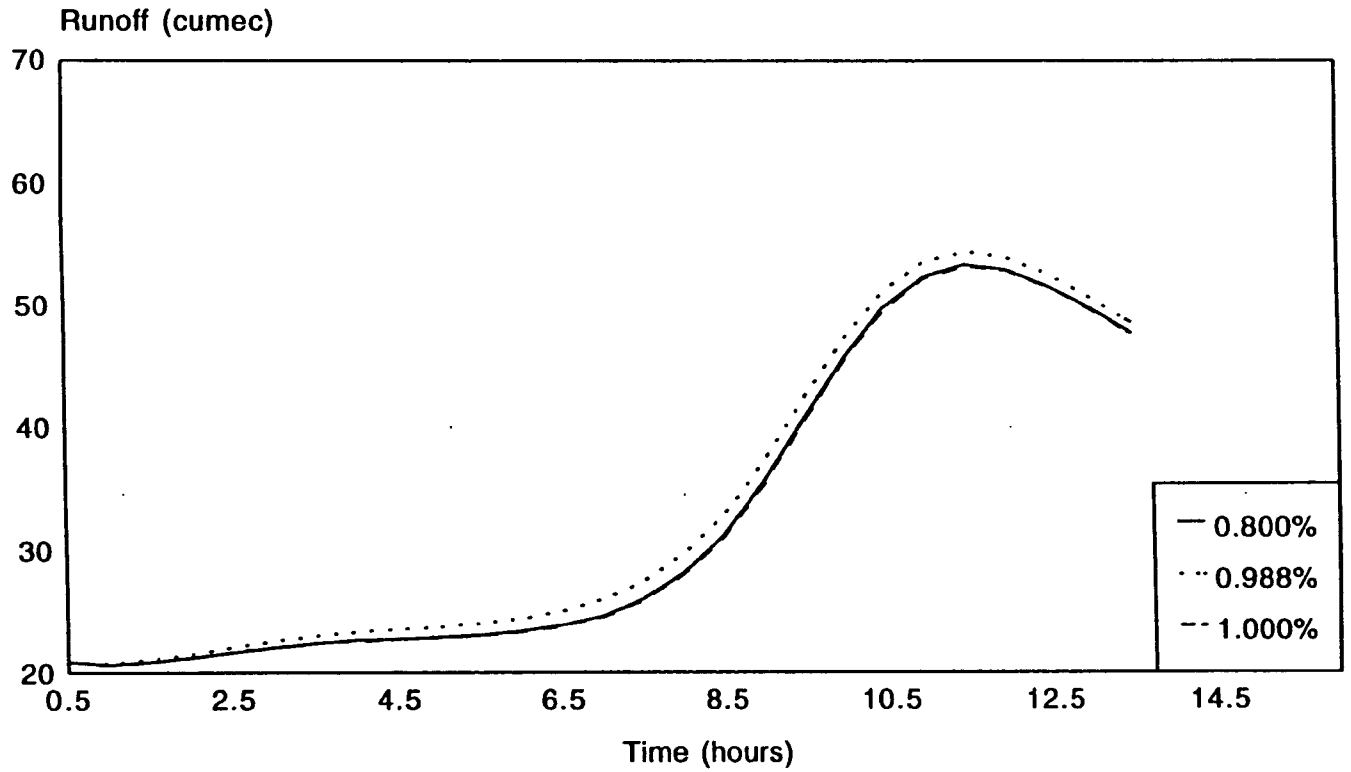

Figure 6.8: Hydrographs produced by the coupled simulations using the three different initial moisture conditions

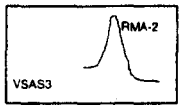	INITIAL MOISTURE CONDITIONS (UNIT PERCENTAGE)		
NO TIME SHIFT	0.800%	0.988%	1.000%
% increase in parameter value	N/A	+ 23.5%	+ 1.21%
% change in VSAS3 total volume 1% change in parameter value	N/A	+ 107.96%	+ 6.37%
Total volume of runoff produced by coupled simulation	3.16×10^6 m^3	3.26×10^6 m^3	3.20×10^6 m^3
% change in total volume produced by coupled simulations	N/A	+ 3.16%	- 1.84%
% change in RMA-2 total volume for 1% change in parameter value	N/A	+ 0.13%	- 1.52%
Peak discharge	53.390 m^{3}s^{-1}	54.459 m^{3}s^{-1}	53.254 m^{3}s^{-1}
% change in peak discharge	N/A	+ 2.00%	- 2.21%
% change in peak discharge for a 1% change in parameter value	N/A	+ 0.085%	- 1.83%

Table 6.4: Sensitivity of RMA-2 to changes in initial moisture conditions with no time shift applied to VSAS3 inflows

6.3.5 *Sensitivity of the coupled scheme to changes in slope angle*

Very little difference was observed between the VSAS3 hydrographs produced for slopes with different angles, either during the whole event or through the recession phase. Hydrographs from the coupled simulations were plotted although are not shown here as there was no visible difference between them. There was a slight difference between the output hydrographs from the coupled simulations, calculations are shown in Table 6.5. Changes in the output hydrographs reflect the differences between the recession phase of the three hillslope hydrographs input to the coupled scheme. The total volume of runoff produced appeared to increase slightly with increasing slope angle. This was also true for increases in peak discharge

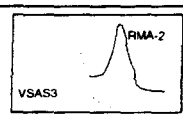 NO TIME SHIFT	SLOPE ANGLE		
	8°	12°	45°
% increase in parameter value	N/A	+ 50.00%	+ 275.00%
% change in VSAS3 total volume for 1% change in parameter value	N/A	- 0.0072%	0.0018%
Total volume of runoff produced by coupled simulation	3.20×10^6 m^3	3.20×10^6 m^3	3.21×10^6 m^3
% change in total volume produced by coupled simulation	N/A	0.24%	0.32%
% change in total volume for 1% change in parameter value	N/A	0.0048%	0.0012%
RMA-2 peak discharge	53.801 m^{3}s^{-1}	53.820 m^{3}s^{-1}	53.824 m^{3}s^{-1}
% change in peak discharge	N/A	- 0.035%	0.0074%
% change in peak discharge for a 1% change in parameter value	N/A	0.00070%	0.000027

Table 6.5: Sensitivity of RMA-2 to changes in slope angle with no time shift applied to hillslope inflows

6.3.6 *Overview of the results of the sensitivity analysis*

A summary of the results of the sensitivity analysis is shown graphically in Figure 6.9 where the total volume produced by the output hydrograph by each coupled simulation is plotted against the value of the parameter. The five parameters are plotted on the same axis for purposes of comparison. The relative sensitivity of the parameters is shown in Table 6.6. In this table, for each parameter the percentage change in the output hydrograph volume and peak is expressed as two values. This is because there were originally three values for each parameter and three resultant hydrographs. The relationship between the change to the parameter value and the resultant percentage change in the output hydrograph did not appear to be linear for any parameter and was dependent on the actual values over which the parameter was changed as well as the percentage change. Therefore each pair of values was not averaged although they were ranked in terms of the percentage change resulting from a 1% change in the parameter value for the purpose of comparison.

From the table it can be seen that in terms of changes to the total volume of runoff produced, the coupled scheme appears to be most sensitive to:

1) Rainfall event

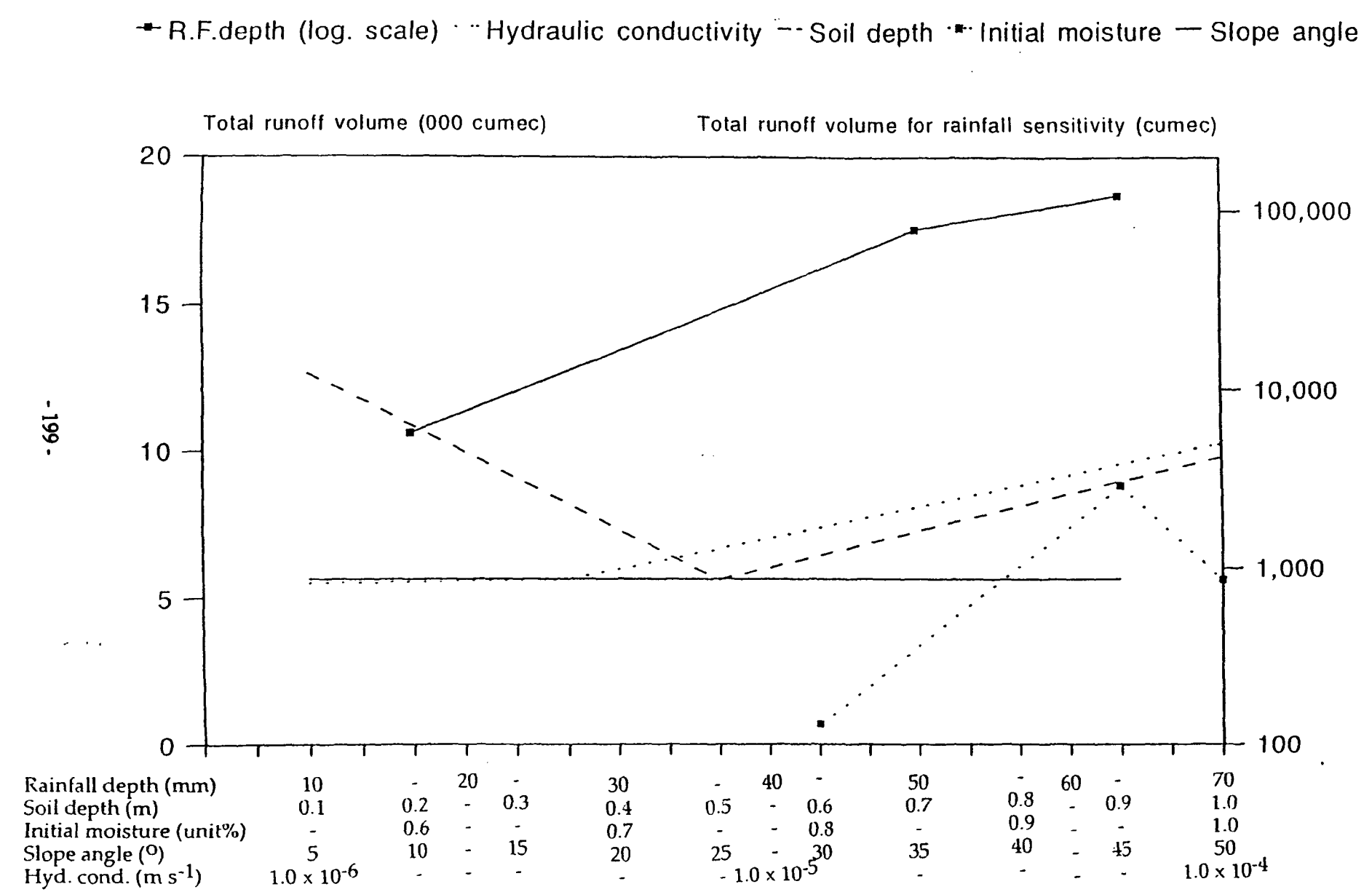

Figure 6.9: Graphs showing the relative sensitivity of the coupled scheme to the five selected parameters in terms of the total volume of runoff produced

2) Initial moisture conditions

3) Soil depth

4) Slope angle

5) Soil hydraulic conductivity

Parameter	% change in parameter value	% change in total volume for a 1% change in parameter value	Rank	% change to peak volume for a 1% change in parameter value	Rank
RAINFALL	+ 230.89%	+ 4.26%	1	+ 0.59%	3
DEPTH	- 24.21%	- 0.68%	3	+ 1.20%	2
HYDRAULIC	+ 300.00%	- 0.0010%	10	- 0.0035%	7
CONDUCTIVITY	+1698.56%	+ 0.0013%	8	+ 0.0017%	8
SOIL	+ 400.00%	- 0.0061%	6	- 0.0050%	6
DEPTH	+ 50.00%	- 0.044%	5	- 0.039%	5
INITIAL MOISTURE	+ 23.50%	+ 0.13%	4	+ 0.085%	4
CONDITIONS	+ 1.21%	- 1.52%	2	- 1.83%	1
SLOPE	+ 50.00%	+ 0.0048%	7	+ 0.00070%	9
ANGLE	+ 275.00%	+ 0.0012%	9	+ 0.000027%	10

Table 6.6: Composite table summarising the results of the sensitivity analysis of the coupled scheme to different hillslope inflows produced by altering five key parameters.

In terms of changes to the peak discharge resulting from a 1% change in each parameter value, the scheme appeared to be most sensitive to the initial moisture conditions. Also, a relatively greater sensitivity to saturated hydraulic conductivity compared to slope angle was demonstrated.

1) Initial moisture conditions

2) Rainfall event

3) Soil depth

4) Soil hydraulic conductivity

5) Slope angle

It should be noted that these observations only apply to the range of events examined. In the field world-wide a much greater range of values might be expected to occur. Due to the constraints of time it was only possible to carry out three coupled simulations for each parameter. However now that the coupled scheme is implemented it would be relatively simple to carry out further coupled simulations to explore the issue further. It was felt that the simulations carried out were sufficient to

demonstrate that there was an observable difference both between the changes made to each parameter value and between parameter values. In addition, the parameters may be inter-related which could account for some of the observed non-linearity of the relationship between the change made to a parameter and the resultant change to the output hydrograph. In this investigation, the value of each parameter was altered separately with all the other parameters being held at a constant value.

This sensitivity analysis examined the sensitivity of the coupled scheme to the recession limb of the inflows hydrographs produced by the selected parameters with the exception of event return period. The next part of the investigation involved carrying out further coupled model simulations with hillslope inflows applied from the rising limb and peak of the hillslope hydrographs. This was carried out to see if there was any difference in the observed sensitivity of the coupled scheme to the selected parameters when inflows from this part of the hydrograph were used. Because of the difficulty in making comparisons between the three rainfall events and the fact that the 1 in 12 year hillslope peaked within the original coupled simulation the rainfall event was not included in this part of the investigation.

6.4. THE EFFECT OF CHANGING THE RELATIVE TIMING OF THE HILLSLOPE AND FLOODPLAIN HYDROGRAPH PEAKS ON THE RESULTS OF THE SENSITIVITY ANALYSIS

The eleven VSAS3 simulations were carried out just once but a different part of the resulting output hydrograph was used as the input to a further twelve coupled simulations where the timing of the hillslope hydrograph was altered so that the hillslope input peak occurred at the same time as the RMA-2 input peak. Nine of the VSAS3 hydrographs were selected, the rainfall events with 1 in 5 and 1 in 12 year return periods were excluded. The method used for altering the relative timing of the input hydrographs was described in Chapter Five.

6.4.1 *The sensitivity of the coupled scheme to changes made to the saturated hydraulic conductivity (simultaneous input hydrograph peaks)*

As previously observed, the total hillslope discharge from the slope was observed to decrease with increasing saturated hydraulic conductivity. The results of the coupled simulations using inflows from the recession limb showed that the greatest increase to the total volume and peak discharge was produced by inflows yielded by the sand soil, followed by the clay loam and those from the loam soil which showed the

peak, this pattern was changed as can be seen in Figure 6.10. For the first 2.5 hours of the coupled simulations there was very little difference between the three output hydrographs. Throughout the event the difference between coupled hydrographs using inflows from clay loam and loam soils was slight. The difference between the loam and sand soils was more marked and increased to a maximum at 6.5 hours into the coupled simulation. At this time the discharge from the coupled simulation using loam soil inflows was 11.43% greater than that for the sand soil. The greatest difference observed between these two soils in terms of the inflows applied occurred 2.0 hours into the coupled simulation giving a lag between maximum difference in and maximum difference out of 4.5 hours. Although the timing of the passage of the main flood wave was 6.5 hours, the lag time for the inflows was probably less as inflows were applied along the whole length of the reach. The increase to the maximum difference of 11.43% was much more gradual than the increase to the maximum difference for the corresponding VSAS3 hydrographs. This attenuation was probably also caused by the fact that inflows were applied along the whole length of the reach. After this time the difference became less marked until the end of the simulation where again there was very little difference between the three hydrographs. These observations are reflected by the data shown in Table 6.7.

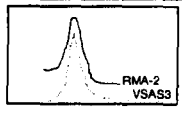 SIMULTANEOUS PEAK	SATURATED HYDRAULIC CONDUCTIVITY		
	1.39×10^{-6} m s^{-1} (clay loam)	5.56×10^{-6} m s^{-1} (loam)	1.00×10^{-4} m s^{-1} (sand)
% increase in parameter value	N/A	+ 300.00%	+ 1698.56%
% change in VSAS3 total volume for 1% change in parameter value	N/A	- 1.18%	- 12.60%
Total volume of runoff produced by coupled simulation	3.76×10^{6} m^{3}	3.75×10^{6} m^{3}	3.58×10^{6} m^{3}
% change in total volume produced by coupled simulation	N/A	- 0.27%	- 4.5%
% change in total volume for 1% change in parameter value	N/A	- 0.00090%	- 0.0026%
Peak discharge	61.744 m^{3}s^{-1}	61.493 m^{3}s^{-1}	60.023 m^{3}s^{-1}
% change in peak discharge	N/A	- 0.41%	- 2.79%
% change in peak discharge for a 1% change in parameter value	N/A	- 0.0014%	- 0.0016%

Table 6.7: Sensitivity of RMA-2 to changes in saturated hydraulic conductivity with 11 hour time shift applied to VSAS3 inflows

hydraulic conductivity simultaneous peak

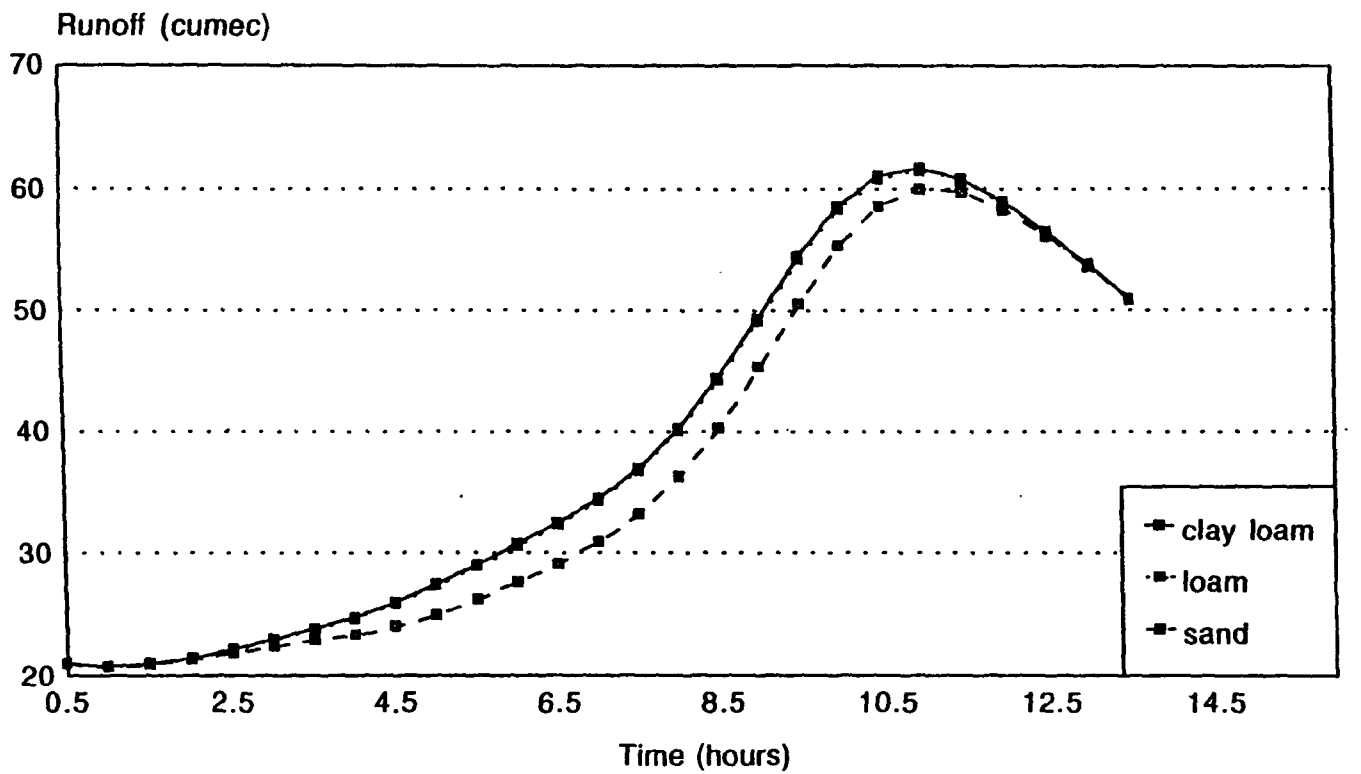

6.10: Hydrographs produced by the coupled simulations with simultaneous input peaks using the three saturated hydraulic conductivities

6.4.2 *The sensitivity of the coupled scheme to changes made to the soil depth (simultaneous input hydrograph peaks)*

Using inflows with no time shift, the greatest increase in the output hydrograph was seen for the 0.1 m and 1.0 m soils with the intermediate 0.5 m soil resulting in a comparatively smaller increase (Figure 6.11, Table 6.8). When inflows were applied with a shifted time base generated by hillslopes with increasing soil depths there was a decrease in the total output volume from the coupled scheme. This was again consistent with the characteristics of the VSAS3 hydrographs over the time period in question. The absolute difference in discharge caused over the range of soil depths was greater than that observed for the original sensitivity analysis. The greatest difference in discharge between the coupled simulations for the 0.1 m and 1.0 m soils occurred at 6.0 hours. The corresponding maximum difference in inflows was 0.5 hours after the start of the coupled simulation. This was equivalent to a lag of 5.5 hours between the maximum difference in hillslope input and the maximum difference between the coupled output hydrographs.

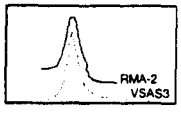	SOIL DEPTH		
SIMULTANEOUS PEAK	0.1 m	0.5 m	1.0 m
% increase in parameter value	N/A	+ 400.00%	+ 50.00%
% change in VSAS3 total volume for 1% change in parameter value	N/A	- 26.40%	- 14.83%
Total volume of runoff produced by coupled simulation	3.87×10^6	3.75×10^6	3.59×10^6
% change in total volume produced by coupled simulation	N/A	- 3.10%	- 4.27%
% change in total volume for 1% change in parameter value	N/A	- 0.0078%	- 0.085%
Peak discharge	62.466 m^3s^{-1}	61.493 m^3s^{-1}	60.170 m^3s^{-1}
% change in peak discharge	N/A	- 1.56%	- 2.15%
% change in peak discharge for a 1% change in parameter value	N/A	- 0.0039%	- 0.043%

Table 6.8: Sensitivity of RMA-2 to changes in soil depth with 11 hour time shift applied to VSAS3 inflows

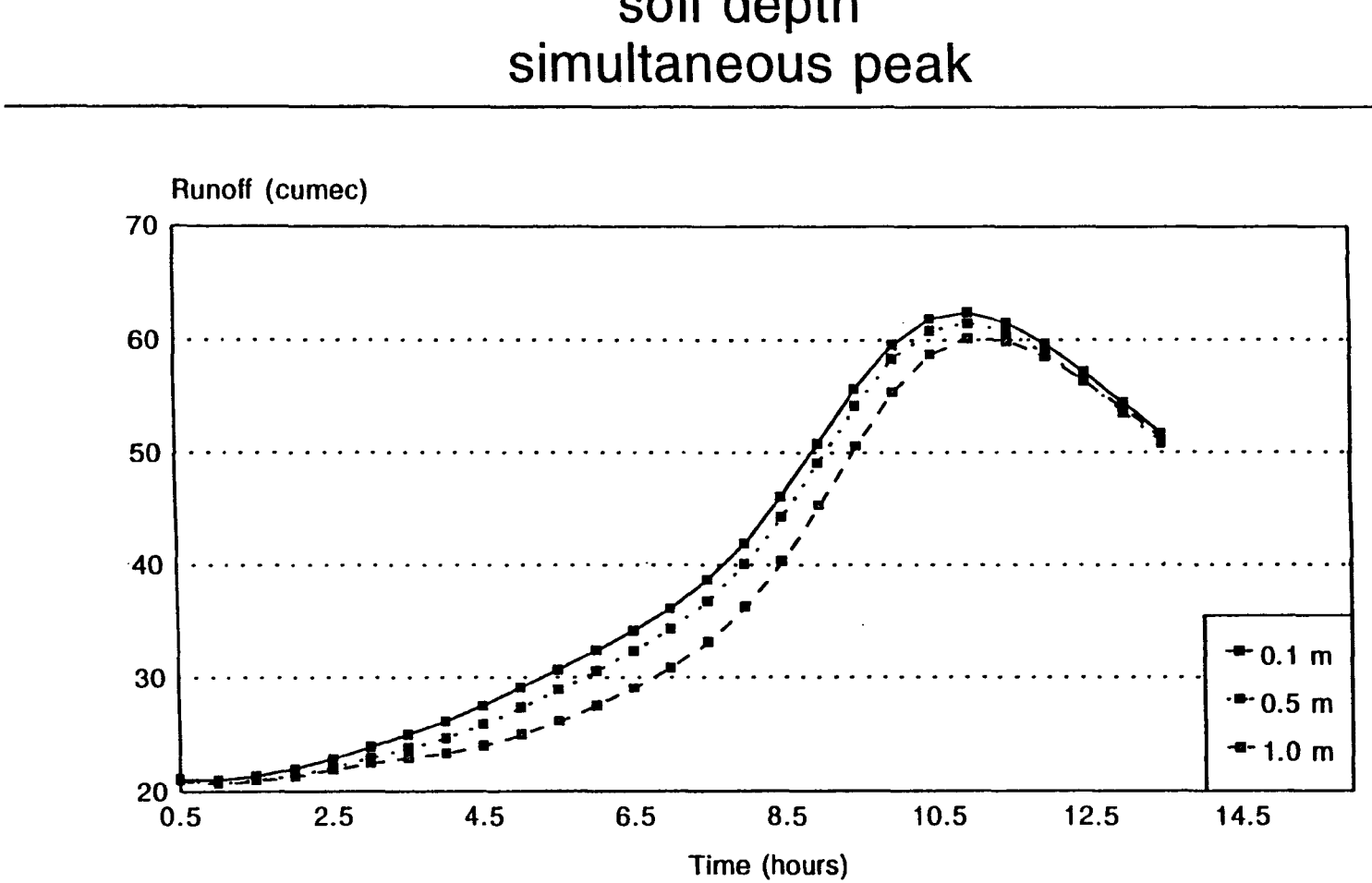

Figure 6.11: Hydrographs produced by the coupled simulations with simultaneous input peaks using three different soil depths

6.4.3 *The sensitivity of the coupled scheme to changes made to the initial moisture conditions (simultaneous input hydrograph peaks)*

With increasingly saturated initial moisture conditions, the reach downstream discharge hydrograph was also found to increase. This was in contrast to the results from the original sensitivity analysis where the difference in total runoff was produced by inflows from the hillslope with a unit percentage moisture content of 0.988%. In addition, the time shift meant that no inflows were produced by the soil with dry antecedent conditions during the new period over which the hillslopes were contributing to the floodplain. The output hydrographs from these coupled simulations are shown in Figure 6.12 and the relative sensitivity of the coupled model to the new inflows is shown in Table 6.9.

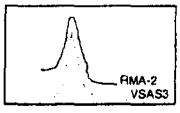 SIMULTANEOUS PEAK	INITIAL MOISTURE CONDITIONS (UNIT PERCENTAGE)		
	0.800%	0.988%	1.000%
% increase in parameter value	N/A	23.5%	1.21%
% change in VSAS3 total volume 1% change in parameter value	N/A	107.97%	6.37%
Total volume of runoff produced by coupled simulation	3.16×10^6	3.64×10^6	3.75×10^6
% change in total volume produced by coupled simulation	N/A	+ 15.9%	+ 3.02%
% change in total volume produced for 1% change in parameter value	N/A	+ 0.68%	2.50%
Peak discharge	53.254 m^3s^{-1}	60.604 m^3s^{-1}	61.493 m^3s^{-1}
% change in peak discharge	N/A	13.80%	1.47%
% change in peak discharge for a 1% change in parameter value	N/A	0.59%	1.21%

Table 6.9: Sensitivity of RMA-2 to changes in initial moisture conditions with an 11 hour time shift applied to hillslope inflows

6.4.4 *The sensitivity of the coupled scheme to changes made to the slope angle (simultaneous input hydrograph peaks)*

Again there was very little difference between the hydrographs although a greater difference was seen between the hydrographs in terms of the total volume and peak

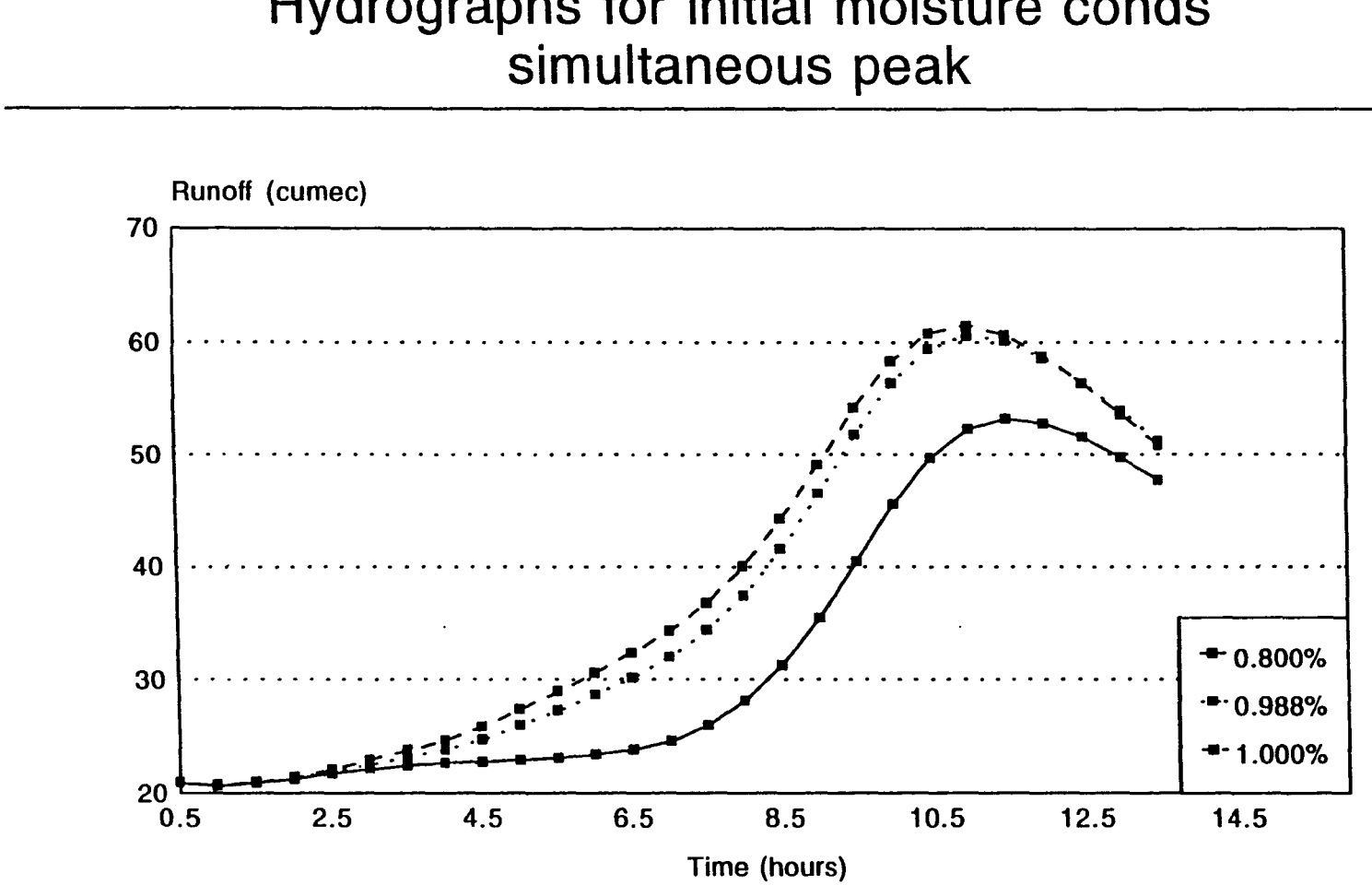

Figure 6.12: Hydrographs for coupled simulations with simultaneous input peaks using three different initial moisture conditions

volume of runoff. There was no visible difference between the output hydrographs for these three simulations which are not shown.

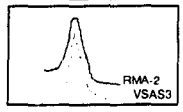 SIMULTANEOUS PEAK	SLOPE ANGLE		
	8°	12°	45°
% increase in parameter value	N/A	+ 50.00%	+ 275.00%
% change in VSAS3 total volume for 1% change in parameter value	N/A	- 0.0072%%	0.0018%
Total volume of runoff produced by RMA-2	3.75×10^6	3.76×10^6	3.74×10^6
% change in total volume produced by RMA-2	N/A	0.27%	- 0.53%
% change in total volume for 1% change in parameter value	N/A	0.0054%	- 0.0019%
Peak discharge	61.493 m^3s^{-1}	61.601 m^3s^{-1}	61.512 m^3s^{-1}
% change in peak discharge	N/A	0.18%	- 0.14%
% change in peak discharge for a 1% change in parameter value	N/A	0.0036%	- 0.00051%

Table 6.10: Sensitivity of RMA-2 to changes in slope angle with 11 hour time shift applied to hillslope inflows

6.4.5 Overview

Figure 6.13 shows sensitivity graphs for the coupled simulations incorporating the hillslope hydrograph peak, these were plotted in the same way as before. Table 6.11 shows the percentage change in the reach hydrograph outflow total volume and peak discharge observed for the coupled simulations using inflows with a shifted time base. When this table is compared with Table 6.6 it can be seen that there was very little difference in the relative sensitivity of the model to the four parameters for inflows from the peak and the recession limb. In terms of the total volume of runoff, an increased sensitivity was observed to certain parameters for the inflows with a peak simultaneous to that of the upstream input. The sensitivity to initial moisture conditions and soil depth for a 1% change in each parameter value resulted in a greater change. The difference in sensitivity observed for saturated hydraulic conductivity and slope angle was very slight. In terms of peak discharge, the coupled scheme was found to be slightly less sensitive to saturated hydraulic conductivity and soil depth

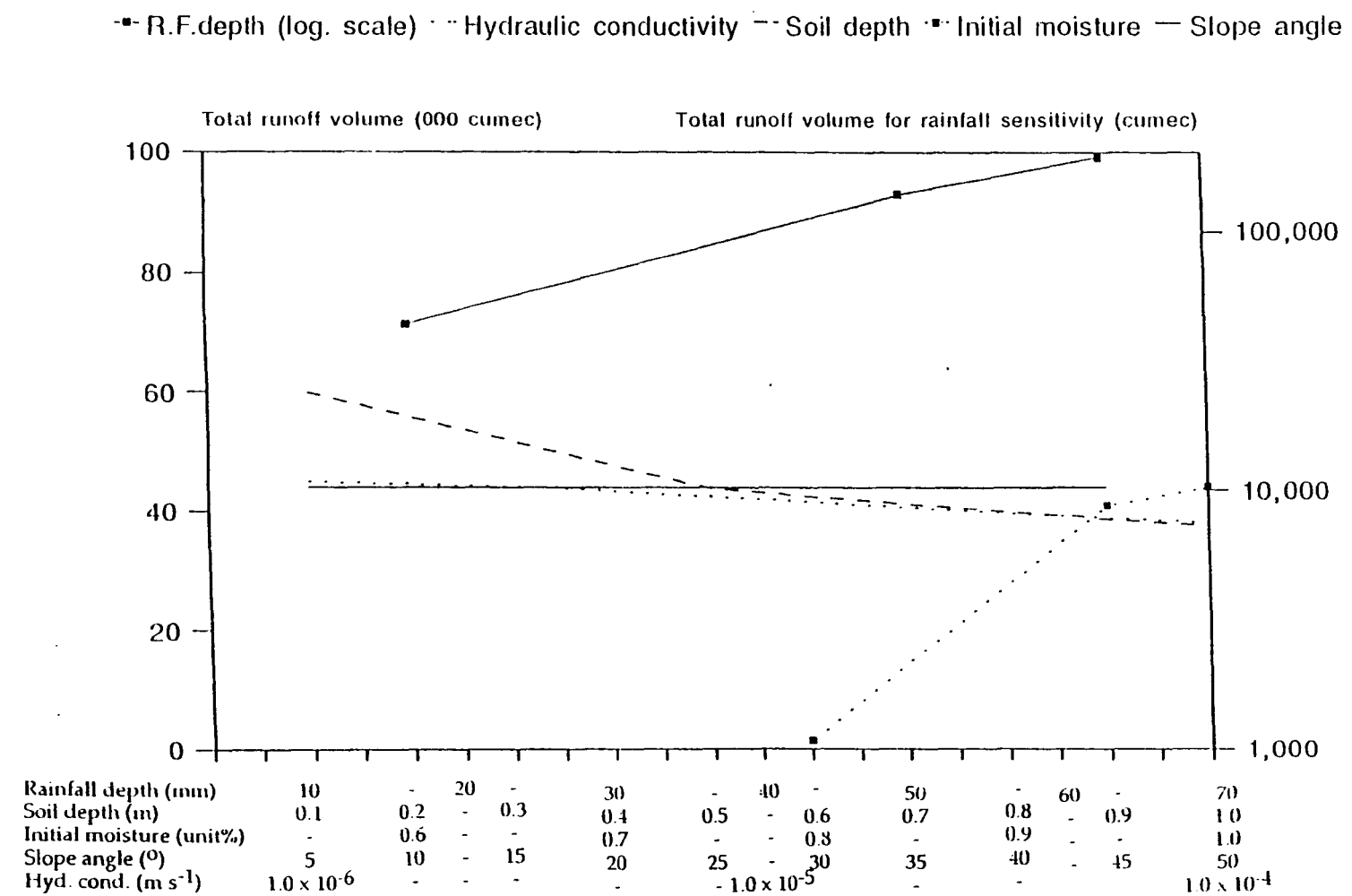

Figure 6.13: Graphs showing the relative sensitivity of the coupled scheme to the five selected parameters in terms of the total volume of runoff produced when the inflows and RMA-2 input hydrograph peaks were applied with a simultaneous peak

using a simultaneous inflows peak. Little difference was observed for initial moisture conditions although the peak discharge showed a greater difference for slope angle.

This conformed to the characteristics of the hillslope hydrograph for these simulations. A greater difference in the volume produced occurred over the time period of the second coupled simulation (simultaneous peaks).

Parameter	% change in parameter value	% change in total volume for a 1% change in parameter value	Rank	% change to peak volume for a 1% change in parameter value	Rank
HYDRAULIC	+ 300.00%	- 0.00090%	7	- 0.0014%	7
CONDUCTIVITY	+1698.56%	- 0.0026%	6	- 0.0016%	6
SOIL	+ 400.00%	- 0.0078%	4	- 0.0039%	5
DEPTH	+ 50.00%	- 0.085%	3	- 0.0043%	4
INITIAL MOISTURE	+ 23.50%	0.68%	2	0.59%	2
CONDITIONS	+ 1.21%	2.50%	1	1.21%	1
SLOPE	+ 50.00%	0.0054%	5	0.0036%	3
ANGLE	+ 275.00%	- 0.0019%	8	- 0.00051%	8

Table 6.11: Summary of the results of the sensitivity analysis of the coupled scheme to different hillslope inflows produced by altering five key parameters. The timing of the hillslope input was altered so that the hillslope hydrograph peak occurred at the same time as the upstream input hydrograph.

6.5. AN ANALYSIS OF THE LOCALISED EFFECTS CAUSED BY THE ADDITION OF INFLOWS

6.5.1 Changes in depth at selected cross sections

In order to examine changes in depth caused by the addition of inflows, two cross sections were selected. The first of these was near the upstream end of the reach with the other at the location of the downstream gauging station. The sites of these sections is indicated in Figure 6.14. The node identification numbers for nodes defining each section were identified from the original plots and checked with the connection table in the geometry input file (described in Chapter Three). The x, y and z co-ordinates of the nodes were also found from the geometry input file. From this information the cross sections were plotted. A program, *xsects.f* was written to extract water surface elevations for each of the nodes at a selected cross-section and at specified time steps from the RMA-2 results files. These water surface elevations were written to an output file from which the depth of the water at each section for the chosen time steps was plotted. The structure of the program allowed data for further cross-sections to be

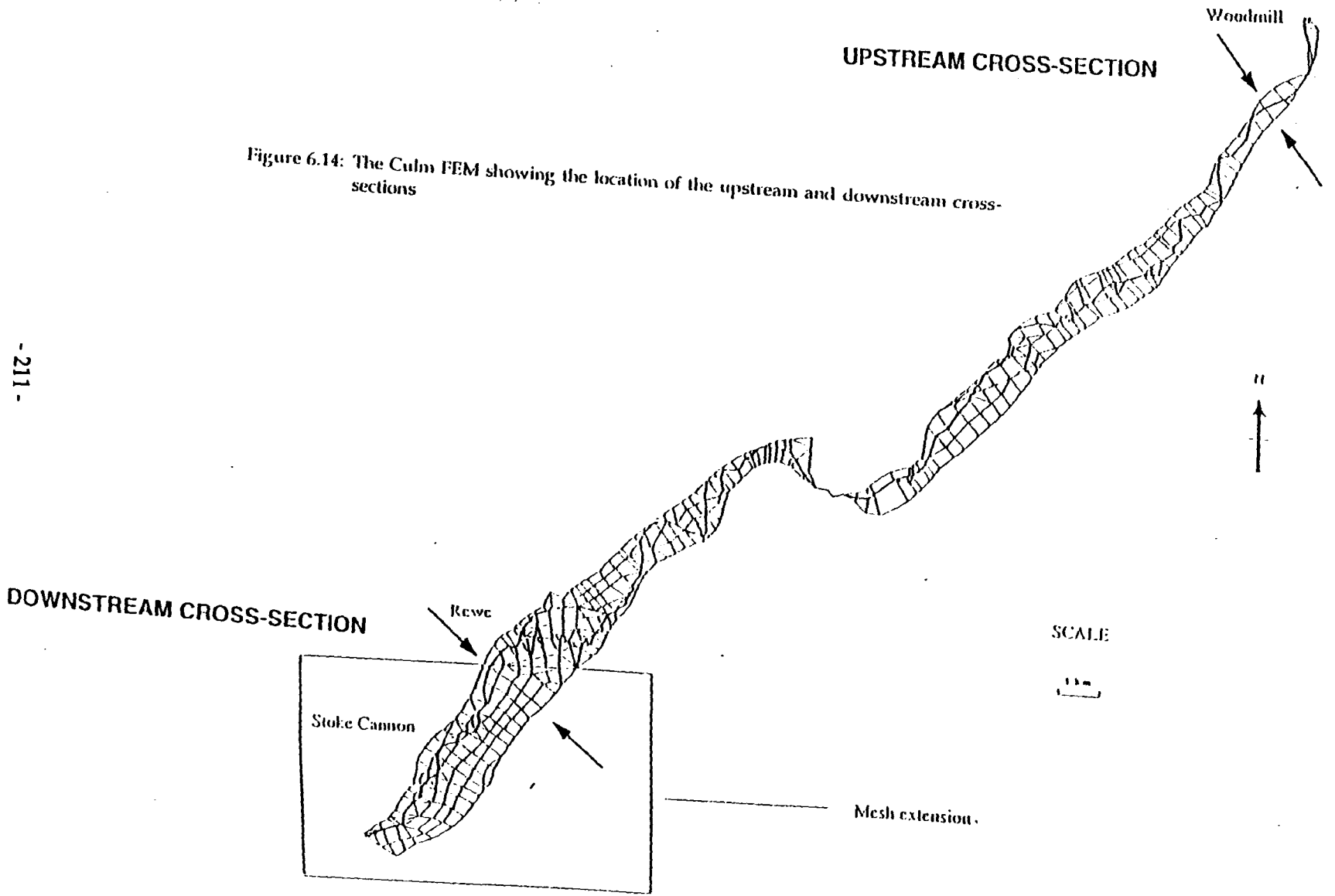

Figure 6.14: The Culm FEM showing the location of the upstream and downstream cross-sections

added should the need arise, although the most time-consuming aspect of including further sections was the identification of node numbers.

It was not possible to examine the relative effect of every simulation on the water depth at the chosen sections due to the amount of data involved and time limitations. Instead, as an alternative to carrying out a detailed sensitivity analysis of the effect of parameter changes on the water depth at each section, it was decided that it would be more appropriate to adopt a more generalised approach and examine the effect over a range of applied inflows. Therefore, as a starting point the 1 in 1 and 1 in 12 year events were selected and for each event the depth for the control and initial coupled simulation were compared to examine i) The effect of adding inflows for each event and ii) the relative difference between the events. Since the two events had very different temporal aspects, the comparison was not made at specific time steps. Instead, the effect was examined at the upstream section at the time of the peak input discharge from the upstream hydrograph (4.5 hours for the 1 in 1 year event and 9.5 hours for the 1 in 12 year event) and that at the downstream section at the time of the predicted peak output (11.5 hours and 15.0 hours respectively).

Figure 6.15 shows the upstream section at peak input discharge for the 1 in 1 year event. The depths predicted by the control (no inflows) and VSAS01 (inflows from initial VSAS3 1 in 1 year simulation) are shown. From this it can be seen that there is a visible increase in depth at this time step. The mean increase in depth across the section was 0.17 m

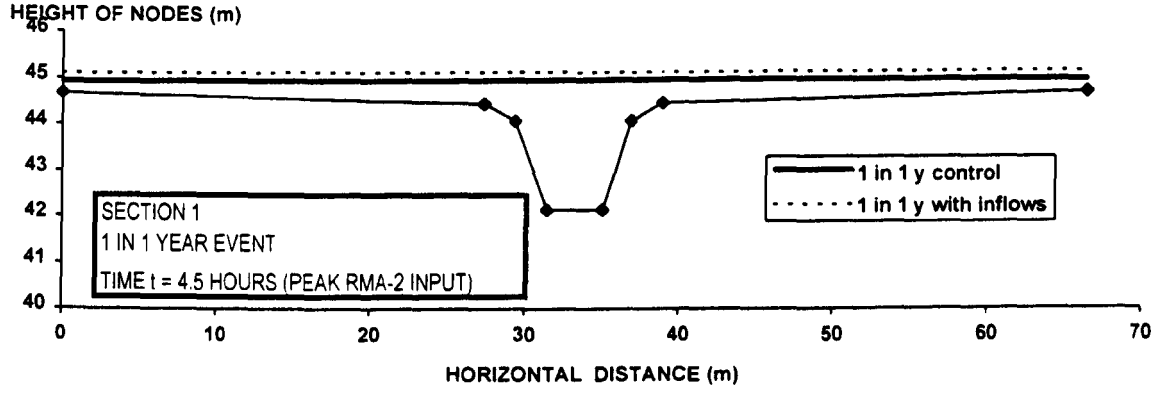

Figure 6.15: The depth of water at the upstream cross-section at 4.5 hours for the 1 in 1 year control and VSAS01 coupled simulations.

The upstream section for the 1 in 12 year event at peak input discharge is shown in Figure 6.16. The mean increase in depth across the section was almost twice that observed for the 1 in 1 year event at 0.3 m.

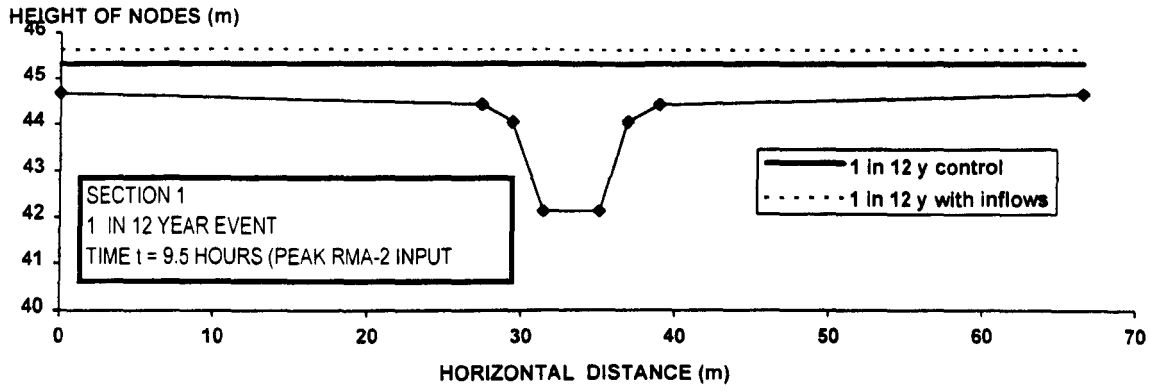

Figure 6.16: The depth of water at the upstream cross-section at 9.5 hours for the 1 in 12 year control and VSAS03 coupled simulations.

Figures 6.17 and 6.18 show the increase in depth at the downstream section for these simulations. There was no visible difference in depth for the 1 in 1 year event although a mean depth increase of 0.02 m was observed. Also, the floodplain was not fully inundated at this section during the 1 in 1 year event. The floodplain was considerably wider at this section than the upstream section. This was probably the reason why the increase in depth could only be seen for the 1 in 12 year event, which gave a 16% increase in the total volume of runoff and where the floodplain at the downstream section was fully inundated. The average increase in depth at this section was found to be 0.25 m.

An attempt was made to examine the change in depth caused by altering other parameters in the sensitivity analysis (initial moisture conditions and soil depth). No visible change occurred, although a slight change in depth was observed. It was felt however that the additional information obtained from carrying out an analysis of depth changes between these simulations would not be sufficient to justify doing this. Instead, the change in depth between the control and coupled simulation at three different time steps was examined for the 1 in 12 year event. This enabled the relative effect of inflows on depth with time to be examined at the upstream and downstream ends of the reach. The time steps selected were the initial time step (0.5 hours), the time at which the maximum difference was observed between the output hydrographs for the coupled simulation (8.0 hours) and the time of the hydrograph peak (15.0 hours). These are shown in Figure 6.19 for the upstream section and Figure 6.20 for the downstream section. Table 6.12 shows the mean depth increase between the control and coupled simulations at these time steps. Comparing these time steps, the maximum depth increase occurred at the upstream end at 8.0 hours although at the downstream end the maximum was at 15.0 hours.

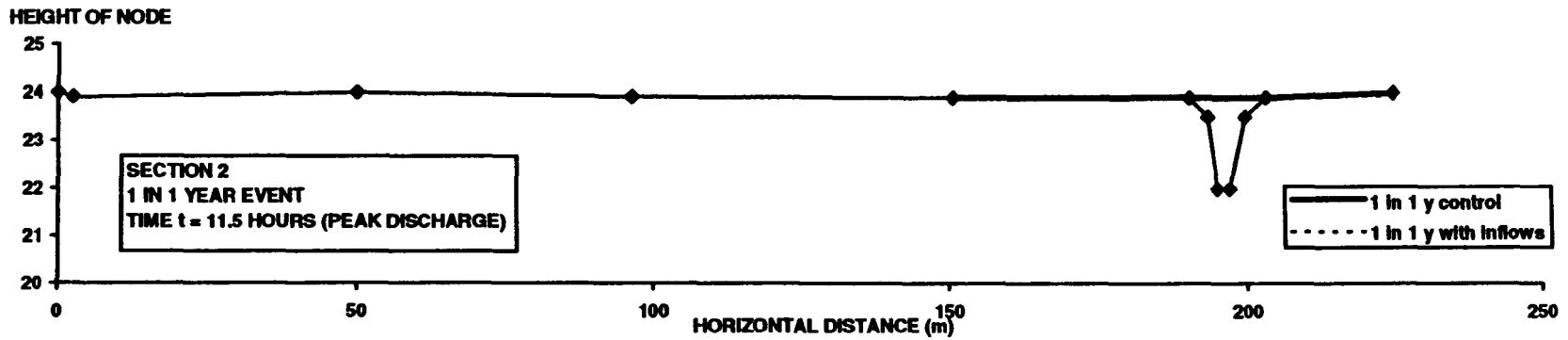

Figure 6.17: The depth of water at the downstream cross-section at 11.5 hours for the 1 in 1 year control and VSAS01 coupled simulations.

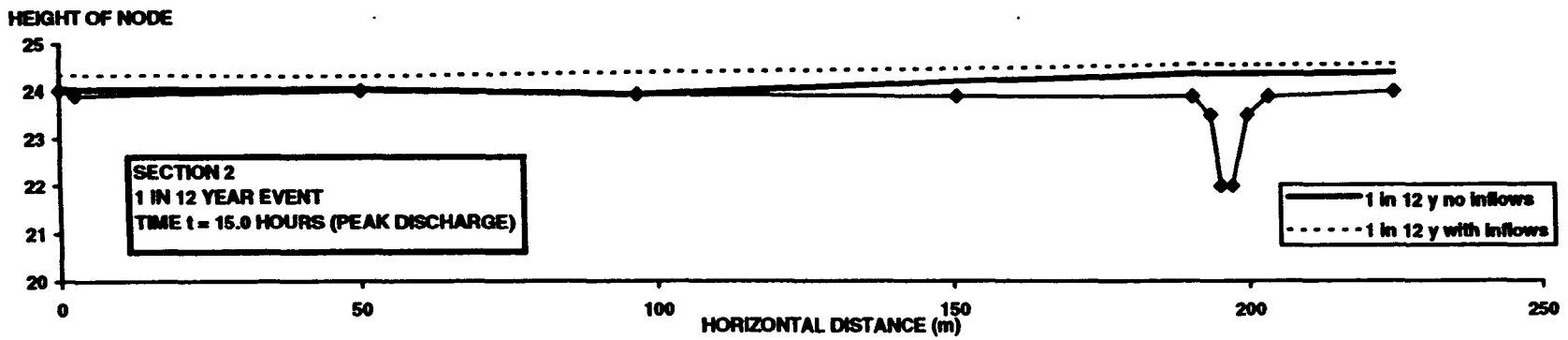

Figure 6.18: The depth of water at the downstream cross-section at 15.0 hours for the 1 in 12 year control and VSAS03 coupled simulations.

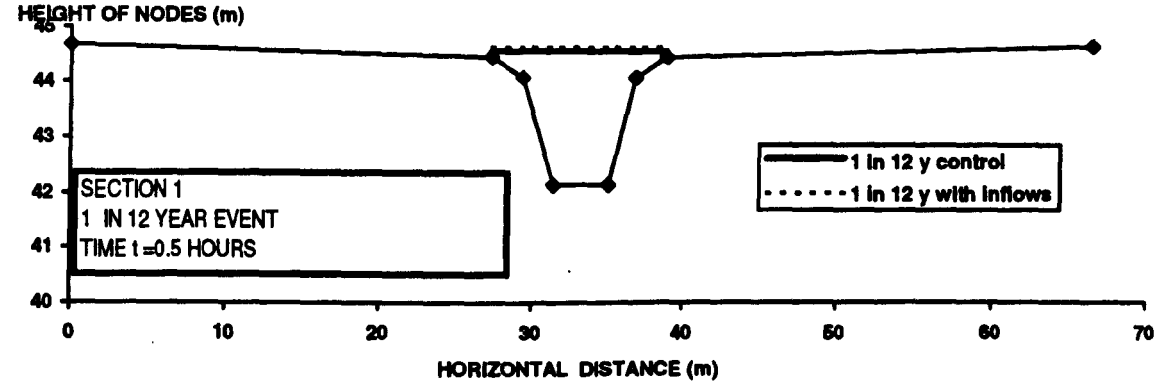

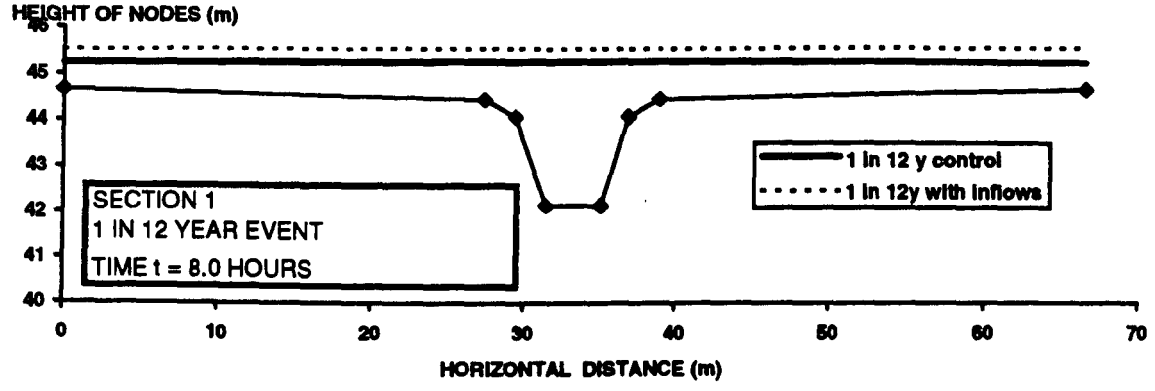

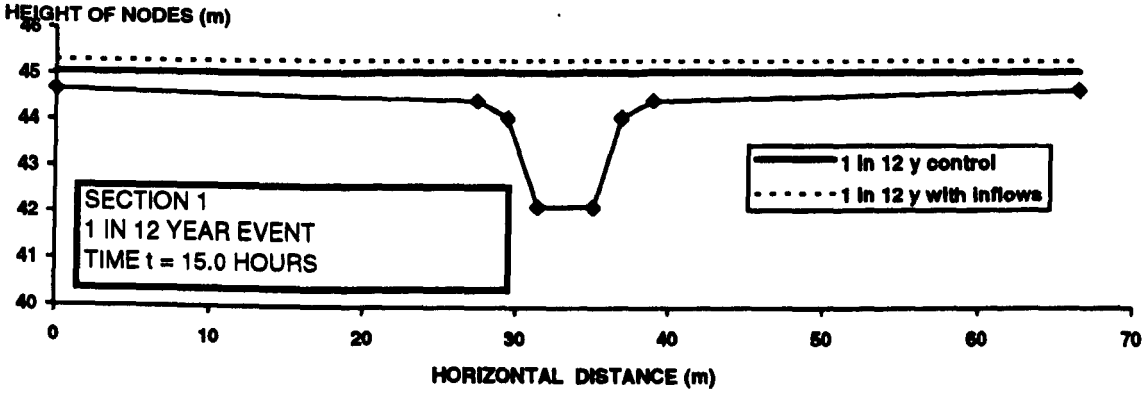

Figure 6.19: The upstream cross section for the 1 in 12 year event at time steps 0.5 hours, 8.0 hours and 15.0 hours.

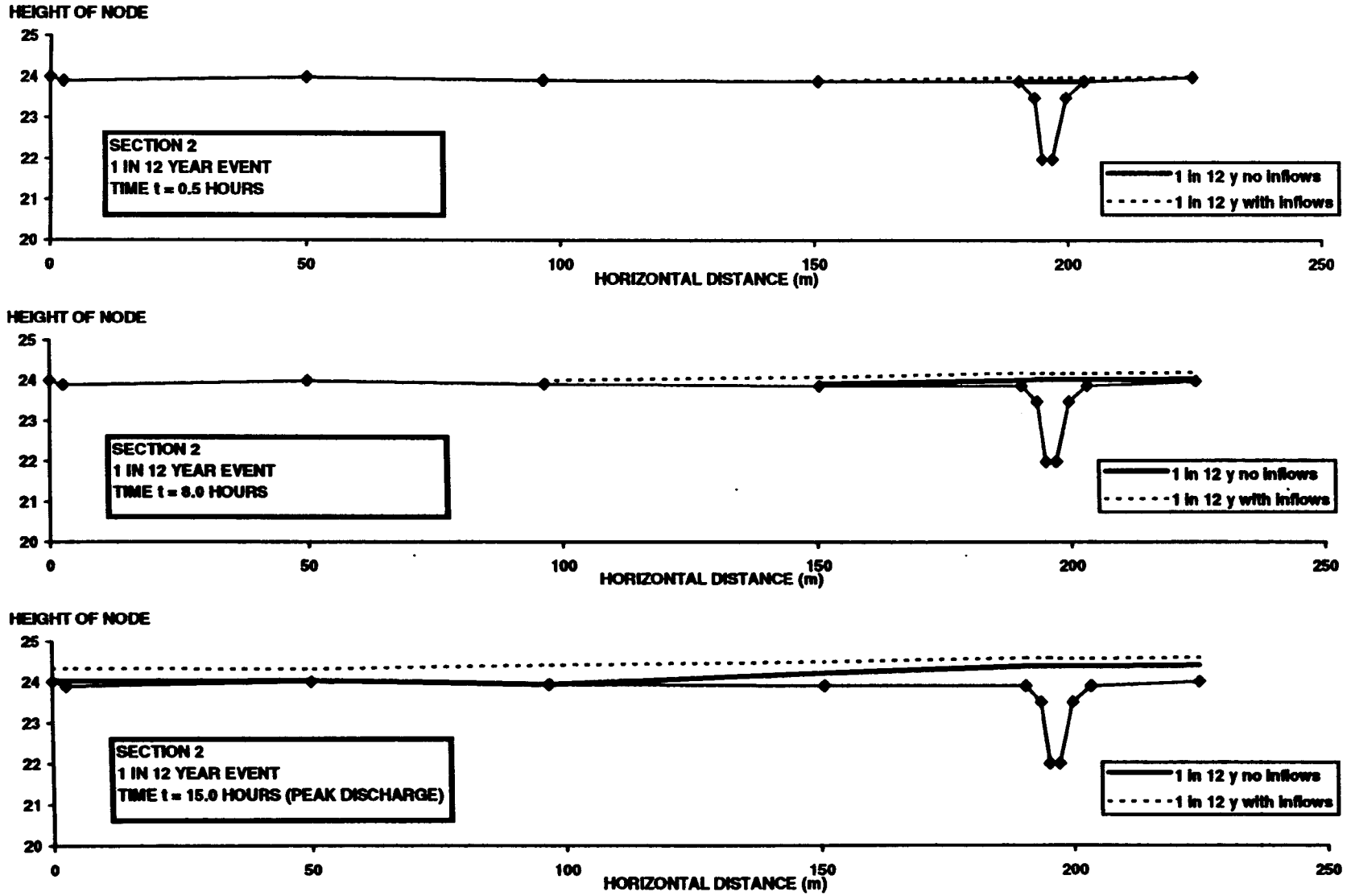

Figure 6.20: The downstream cross section for the 1 in 12 year event at time steps 0.5 hours, 8.0 hours and 15.0 hours.

This was the time at which the maximum output discharge was observed for both simulations although the maximum *difference* in discharge between the two hydrographs was at 8.0 hours. This highlights the fact that in comparing depths at selected cross sections it is important to remember that the stage-discharge relationship at a section is non-linear and that the water depth does not necessarily increase at the same rate as the discharge when inflows are applied to the reach. This is particularly important where overbank flows are considered and is one of the issues discussed in Chapter Seven where the effect inflows have on the calibration of the coupled scheme is examined.

Time (hours)	Depth increase at section 1 (upstream)	Depth increase at section 2 (downstream)
0.5	0.08 m	0.08 m
8.0	0.28 m	0.15 m
15.0	0.24 m	0.25 m

Table 6.12: Mean depth increases observed at the two cross sections for the 1 in 12 year event at selected time steps.

6.5.2 *Inundation plots*

The second part of the investigation into the localised effects brought about by the addition of hillslope inflows examined changes to the inundation extent over the whole reach. Following this, an examination was made of the effect of inflows on the inundation extent over the whole reach. In addition, the sensitivity of the coupled scheme to inflows in terms of the total inundation extent could be examined.

The inundation extent was plotted using the UNIRAS graphics package. To plot inundation extents for a given event, the results file was input to a program which read in the file and split into seven files, each representing a different section of the reach. These were converted into UNIRAS format, interpolating the depth at nodes over a regular grid. For each time step selected the seven files were plotted using UNIRAS sub-routines. Following this, the UNIRAS plots were traced by hand onto an outline of the reach. Inundation plots were prepared, showing the area of the floodplain inundated at different stages during the simulation to compare simulations with hillslope inflows with the control simulation (no inflows). As a starting point, the difference in inundation extent was considered between the control 1 in 1 year simulation and the coupled simulation using inflows produced by the 0.1 m deep soil

and applied with a simultaneous input peak. These simulations were selected because the maximum percentage increase from the control volume occurred for this coupled simulation. The difference in inundation extent was initially examined at the time of the peak of the coupled simulation at 11.0 hours which was the time at which the greatest difference was seen between the inflows simulation and the control simulation (which did not peak until 11.5 hours). The composite inundation plot is shown in Figure 6.21 and shows that although there was a visible difference between the two inundation extents, the range was not great enough to be able to examine the smaller changes which would occur between each set of simulations for a given parameter. In addition to this, the method used would introduce a high margin of error into calculations of the inundation extent. It appeared therefore that the cumulative effect of adding inflows in terms of volumetric changes in runoff produced by the reach, was more apparent than localised effects. However, in this investigation, inflows were spatially averaged and applied to all elements along the length of the reach. The fact that localised effects have been observed would be important for further investigations where inflows were not spatially averaged. This is discussed further in the final chapter.

6.6. AN INVESTIGATION INTO THE EFFECT OF CHANGES IN THE INFLOW VOLUME ON THE TOTAL VOLUME OF OUTFLOW PRODUCED BY THE COUPLED SCHEME

The effect of adding inflows to RMA-2 was then examined more generally in terms of changes to the total output volume, the peak discharge and timing and changes in the volume of water which went to storage. During the sensitivity analysis, inflows were expressed as a percentage of the RMA-2 upstream hydrograph. In the following discussion, the inflows percentage will be described as a percentage of the *total* input. Figure 6.22 shows the volume of water entering and leaving the reach for the 1 in 1 year control simulation. The volume of water going into storage over the surface of the floodplain was assumed to be:

storage volume = total input volume - total output volume

The fact that none of the simulations ran stably for all the time steps for which data were provided meant that the predicted volume of water on the floodplain at the end of the simulation might not all have necessarily gone into storage.

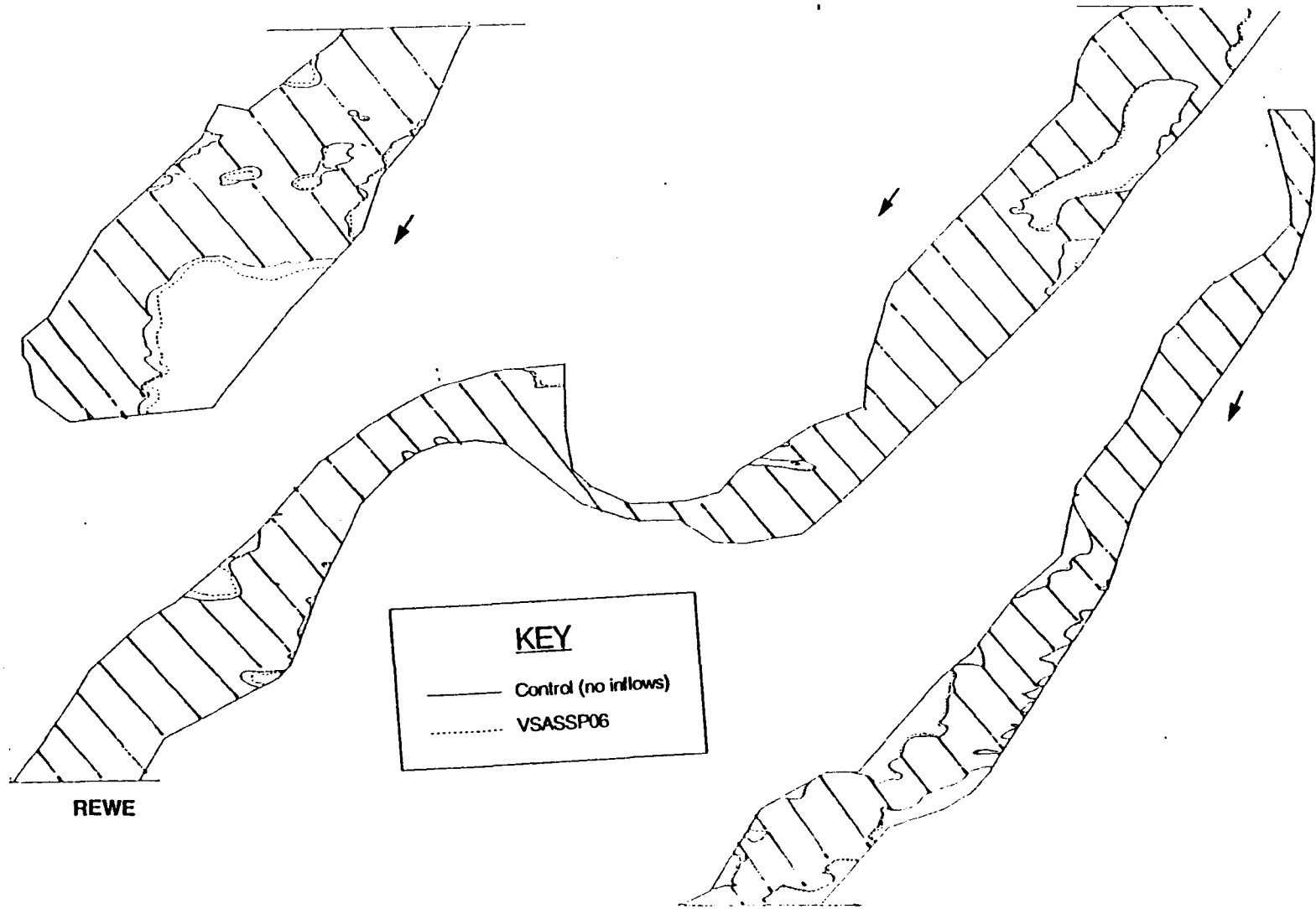

Figure 6.21: Composite inundation plot showing the extent of inundation for the 1 in 1 year event at 8.0 hours for the control simulation and coupled simulation VSASSP06

However, since the storage volume was calculated in the same way for each simulation it provided a means of comparing the percentage of the total input volume to go to storage when inflows with different total volumes were applied (Figure 6.23).

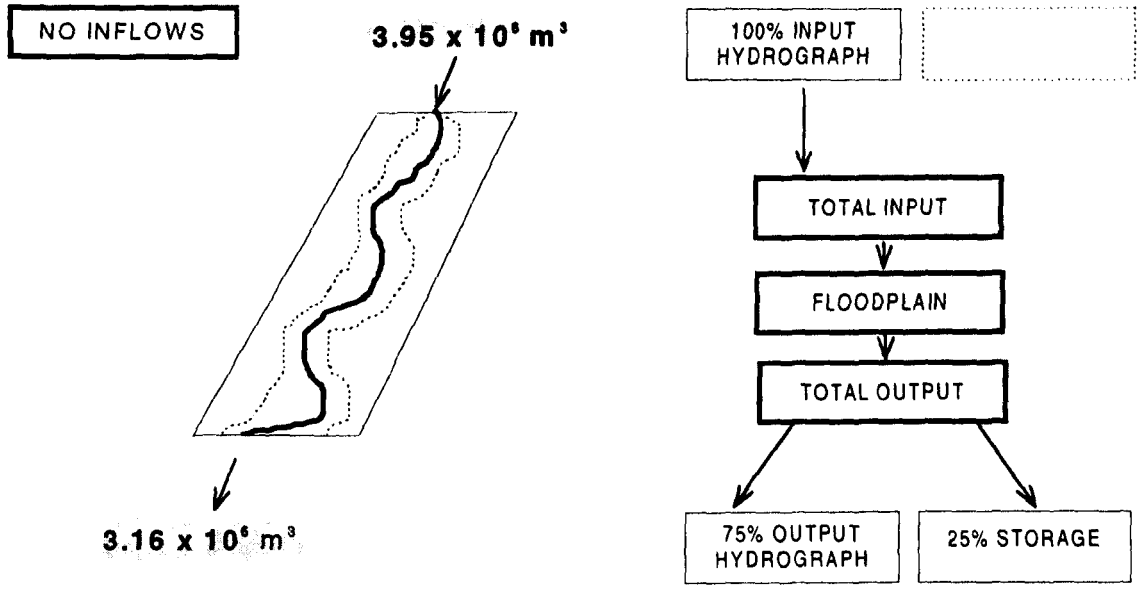

Figure 6.22: Inputs to and outputs from the floodplain system for the 1 in 1 year event when no hillslope inflows were applied.

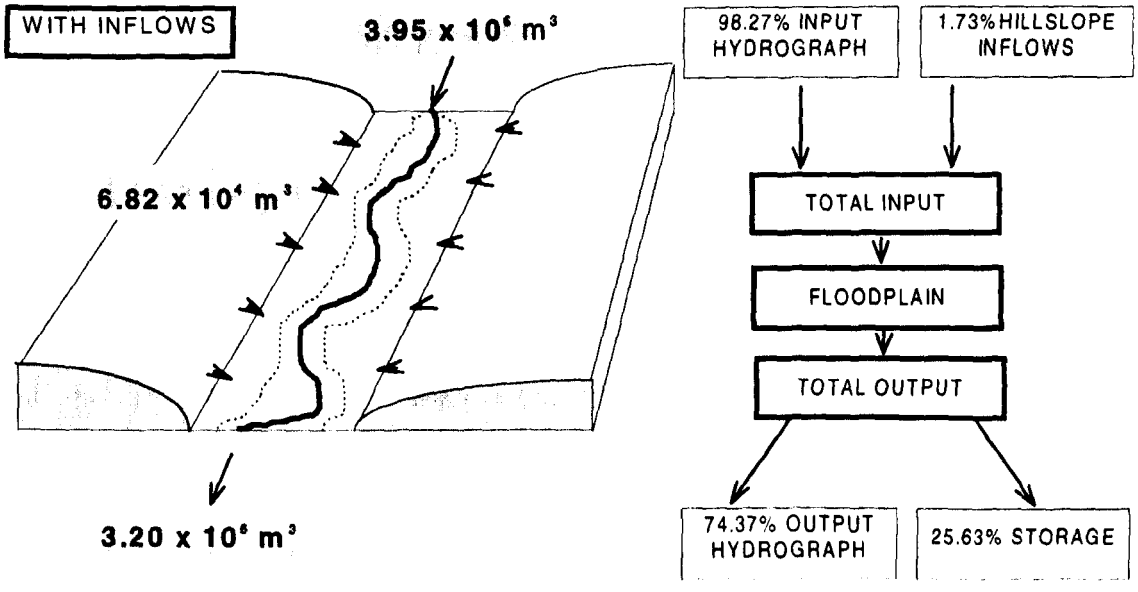

Figure 6.23: Inputs to and outputs from the floodplain system for the 1 in 1 year event with hillslope inflows from the initial VSAS3 simulation were applied with no time shift.

6.6.1 *Changes in total RMA-2 output or reach output hydrograph resulting from addition of inflows*

The total volume of water contributed to the floodplain during each coupled simulation was calculated as the sum of the reach input hydrograph and the inflows hydrograph. The total volume of hillslope inflows applied was calculated as a percentage of this total. The total volume of the output hydrographs had already been calculated during the sensitivity analysis. The difference between this volume and the total volume for the control simulation for the appropriate event was expressed as the percentage increase in volume from the control. The results of these calculations are shown in Table 6.13. A graph was plotted to show the relationship between the inflows as a percentage input and the resultant percentage increase to the reach outflow hydrograph. This is shown in Figure 6.24 and it can be seen that there appears to be a linear relationship between the two parameters. However, this may well be event - specific since the points for the 1 in 5 year and 1 in 12 year events do not appear to follow this trend. This could be for several reasons including the duration of the event, the volume of the input hydrograph and characteristics of the event such as the intensity and spatial distribution of rainfall.

6.6.2 *Changes to hydrograph peak discharge and timing*

The effect of the volumetric inflow percentage on the timing and discharge of the hydrograph peak was also examined. The increase to the hydrograph peak was expressed as the percentage increase from the control for the appropriate event. The results of this analysis are also shown in Table 6.13. From this it can be seen that while the timing of the peak was unaffected for any of the simulations using inflows with no time shift, inflows applied with a simultaneous peak (with the exception of inflows from the dry soil) caused the reach output hydrograph to peak 0.5 hours earlier. Although the inflow hydrograph peak was applied at the same time as the reach input hydrograph peak, the travel time for inflows applied to elements along the edge of the reach varied according to how far downstream a particular element was. This would explain the earlier peak for these coupled simulations. Where no time shift was used, inflows were applied from the recession limb of the hydrograph and no distinct peak occurred during this time. In addition, the volume of inflows applied was considerably reduced for these simulations.

A graph was plotted showing the relationship between the percentage input volume of the inflows applied and the resultant percentage increase to the reach and is shown in

NAME	SIMULATION DESCRIPTION		INFLOWS VOLUME (DURING COUPLED SIMULATION)		RMA-2 TOTALOUTPUT VOLUME.		RMA-2 PEAK DISCHARGE		
	Relative timing of input hyds.	Description	Total (m^3)	As % of RMA-2 input hyd.	Total (m^3)	% increase from control	Time (h)	Peak in $m^3 s^{-1}$	% increase from control
CTRL1	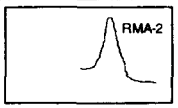 NO INFLOWS	CONTROL 1 IN 1 YEAR	0.00	0.00%	3.16×10^6	0.00%	11.5	53.234	0.00%
CTRL5		CONTROL 1 IN 5 YEAR	0.00	0.00%	1.60×10^7	0.00%	40.0	103.439	0.00%
CTRL12		CONTROL 1 IN 12 YEAR	0.00	0.00%	1.0×10^7	0.00%	15.0	136.825	0.00%
VSAS01	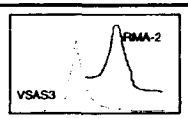 WITH INFLOWS NO TIME SHIFT ☐ Duration of coupled run	1 IN 1 YEAR + 1 IN 1 INFLOWS Sat.hyd.cond=5.56×10^{-6} Soil depth = 0.5 m Initial moisture=1.000% Slope angle = 8°	6.82×10^4	1.73%	3.20×10^6	1.42%	11.5	53.801	1.07%
VSAS02		1 IN 5 YR + 1 IN 5 INFLOWS	2.50×10^6	13.89%	1.82×10^7	13.75%	40.0	106.049	2.52%
VSAS03		1 IN 12 YR + 1IN 12 INFLOWS	1.44×10^6	12.52%	1.16×10^7	16.0%	15.0	139.278	1.79%
VSAS04		1 IN 1 + Sat.hyd.cond.=1.39×10^{-6}	7.67×10^4	1.94%	3.21×10^6	1.64%	11.5	53.818	1.10%
VSAS05		1 IN 1 + Sat.hyd.cond.=1.00×10^{-4}	1.45×10^5	3.68%	3.27×10^6	3.74%	11.5	54.837	3.01%
VSAS06		1 IN 1 + Soil depth = 0.1 m	1.85×10^5	4.68%	3.28×10^6	3.83%	11.5	54.900	3.13%
VSAS07		1 IN 1 + Soil depth = 1.0 m	1.72×10^5	4.37%	3.27×10^6	3.59%	11.5	54.779	2.90%
VSAS08		1 IN 1 + Initial moisture=0.800%	1.08×10^4	0.27%	3.16×10^6	0.16%	11.5	53.390	0.29%
VSAS09		1 IN 1 + Initial moisture=0.988%	1.53×10^5	3.88%	3.26×10^6	3.17%	11.5	54.459	2.30%
VSAS10		1 IN 1 + Slope angle = 12°	7.04×10^4	1.78%	3.20×10^6	1.46%	11.5	53.820	1.10%
VSAS11		1 IN 1 + Slope angle = 45°	7.09×10^4	1.80%	3.21×10^6	1.48%	11.5	53.824	1.11%
VSASSP01	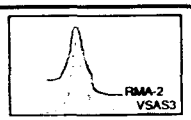 WITH INFLOWS RMA-2 + VSAS3 SAME PEAK t	1 IN 1 YR + 1IN1 INFLOWS	7.25×10^5	18.38%	3.75×10^6	18.85%	11.0	61.493	15.51%
VSASSP04		Sat.hyd.cond.=1.39×10^{-6}	7.41×10^5	18.78%	3.76×10^6	19.25%	11.0	61.744	15.99%
VSASSP05		Sat.hyd.cond.=1.00×10^{-4}	5.63×10^5	14.26%	3.58×10^6	13.56%	11.0	60.023	12.75%
VSASSP06		Soil depth = 0.1 m	8.99×10^5	22.77%	3.87×10^6	22.55%	11.0	62.466	17.34%
VSASSP07		Soil depth = 1.0m	5.77×10^5	14.61%	3.59×10^6	13.69%	11.0	60.170	13.03%
VSASSP08		Initial moisture=0.800%	3.22×10^2	0.0084%	3.16×10^6	0.00%	11.5	53.254	0.00%
VSASSP09		Initial moisture=0.988%	6.40×10^5	16.21%	3.64×10^6	15.46%	11.0	60.604	13.84%
VSASSP10		Slope angle = 12°	7.27×10^5	18.41%	3.76×10^6	18.88%	11.0	61.601	15.57%
VSASSP11		Slope angle = 45°	7.26×10^5	18.38%	3.74×10^6	18.85%	11.0	61.512	15.54%

Table 6.13: Calculations to show the overall effect of adding inflows to RMA-2. All simulations use 1 in 1 year rainfall unless stated

Figure 6.24: Graph of the volumetric increase predicted by the coupled simulation against the total volume of the inflows applied

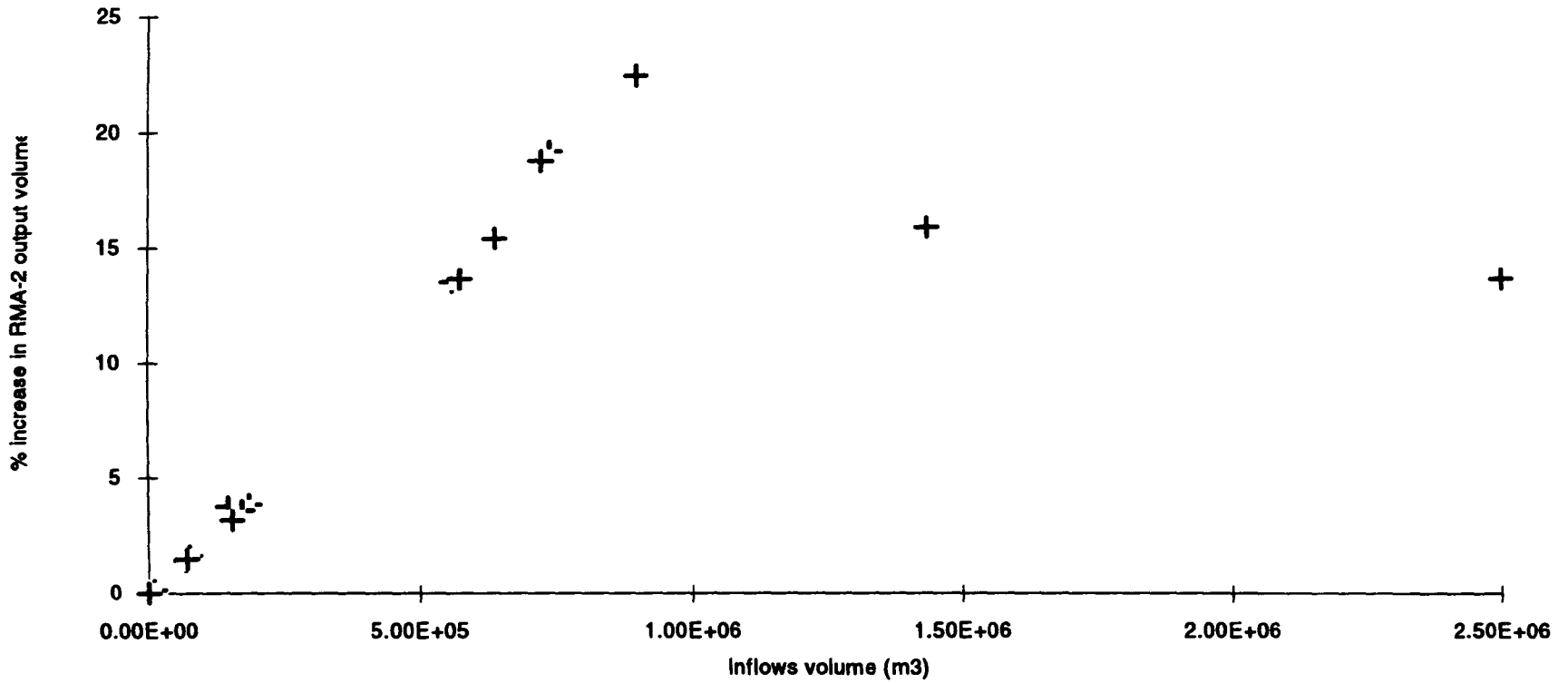

Figure 6.25. From this it can again be seen that there appears to be a linear relationship for the 1 in 1 year event.

6.6.3 *Changes to the percentage of the total input volume to enter storage*

The volume of water assumed to go to storage was calculated using the method described at the start of this Section. Table 6.14 shows the percentage of the total input volume to go to storage for each simulation. For simulations carried out using the 1 in 1 year event, there appeared to be little difference. The slight variation between the simulations can probably be attributed to variation between the inflow hydrograph characteristics. A considerably smaller percentage of the total input volume went to storage for the 1 in 5 year and 1 in 12 year events and a decrease in the percentage of the input going to storage was observed for the 1 in 12 year event. This could reflect the fact that these events were not of the same duration and had different hydrograph characteristics. Alternatively this difference could indicate that the method used for calculating the storage volume was more dependent upon the time at which the model became unstable than the actual volume which entered storage and could make this method of analysis questionable.

6.7. CONCLUSION

The results of the sensitivity analysis, for the five parameters examined, have shown that the coupled scheme was sensitive to changes (in order of decreasing model sensitivity) to:

1) Rainfall event

2) Initial moisture conditions

3) Soil depth

4) Slope angle

5) Hydraulic conductivity

These inflows were applied from the recession limb of the hillslope hydrograph. A further sensitivity analysis was carried out using inflows with a shifted time base which included the hillslope hydrograph peak.

Although the characteristics of the predicted downstream hydrographs were altered, together with the absolute percentage change in the output for a 1% change in each

Figure 6.25: Graph of the increase in peak discharge predicted by the coupled simulation against the total volume of the inflows applied

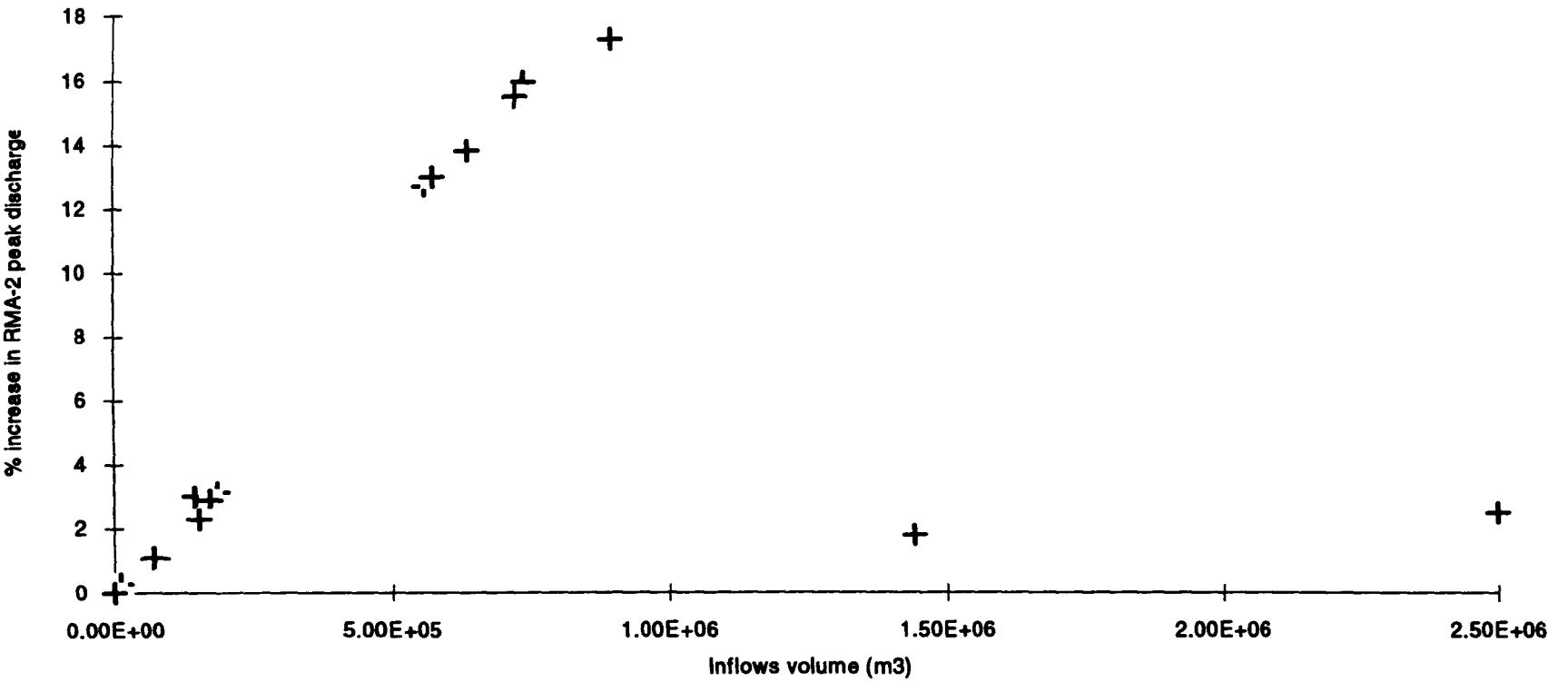

NAME	RELATIVE TIMING OF HYDROGRAPHS	SIMULATION DESCRIPTION	INFLOWS VOLUME AS % OF *TOTAL* INPUT	VOLUME TO STORAGE m^3	% OF TOTAL INPUT TO GO TO STORAGE
CTRL1	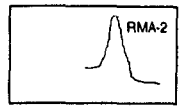 NO INFLOWS	CONTROL 1 IN 1 YEAR	0.00%	0.79×10^6	25.00%
CTRL5		CONTROL 1 IN 5 YEAR	0.00%	2.00×10^6	9.76%
CTRL12		CONTROL 1 IN 12 YEAR	0.00%	1.50×10^6	13.04%
VSAS01	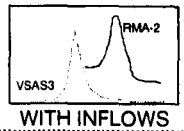 WITH INFLOWS	1 IN 1 YEAR + 1 IN 1 INFLOWS Sat.hyd.cond=5.56×10^{-6} Soil depth = 0.5 m Initial moisture=1.000% Slope angle = 8°	1.70%	0.82×10^6	25.63%
VSAS02	NO TIME SHIFT	1 IN 5 YR + 1 IN 5 INFLOWS	12.02%	2.30×10^6	11.22%
VSAS03	☐ Duration of	1 IN 12 YR + 1IN 12 INFLOWS		1.34×10^6	10.36%
VSAS04	coupled run	1 IN 1 + Sat.hyd.cond.=1.39×10^{-6}	1.90%	0.82×10^6	25.55%
VSAS05		1 IN 1 + Sat.hyd.cond.=1.00×10^{-4}	3.54%	0.83×10^6	25.38%
VSAS06		1 IN 1 + Soil depth = 0.1 m	4.47%	0.86×10^6	26.22%
VSAS07		1 IN 1 + Soil depth = 1.0 m	4.17%	0.85×10^6	25.99%
VSAS08		1 IN 1 + Initial moisture=0.800%	0.27%	0.80×10^6	25.32%
VSAS09		1 IN 1 + Initial moisture=0.988%	3.73%	0.84×10^6	25.77%
VSAS10		1 IN 1 + Slope angle = 12°	1.75%	0.82×10^6	25.63%
VSAS11		1 IN 1 + Slope angle = 45°	1.76%	0.81×10^6	25.23%
VSASSP01	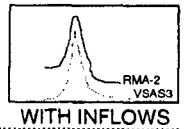 WITH INFLOWS	1 IN 1 YR + 1 IN 1 INFLOWS Sat.hyd.cond=5.56×10^{-6} Soil depth = 0.5 m Initial moisture=1.000% Slope angle = 8°	15.49%	0.93×10^6	24.8%
VSASSP04	RMA-2 + VSAS3	Sat.hyd.cond.=1.39×10^{-6}	15.80%	0.93×10^6	24.73%
VSASSP05	SAME PEAK t	Sat.hyd.cond.=1.00×10^{-4}	12.48%	0.93×10^6	25.98%
VSASSP06		Soil depth = 0.1 m	18.54%	0.98×10^6	25.32%
VSASSP07		Soil depth = 1.0m	12.74%	0.94×10^6	26.18%
VSASSP08		Initial moisture=0.800%	0.0082%	0.79×10^6	25.00%
VSASSP09		Initial moisture=0.988%	13.94%	0.95×10^6	26.10%
VSASSP10		Slope angle = 12°	15.53%	0.92×10^6	24.47%
VSASSP11		Slope angle = 45°	15.51%	0.94×10^6	25.13%

Table 6.14: The percentage of the total input which went to floodplain storage for each simulation

parameter value, the *relative* sensitivity of the model to these parameters remained unchanged.

An examination was made of the localised changes brought about when applying inflows produced by different rainfall events. This was carried out by comparing changes in depth at two cross-sections, at the upstream and downstream ends of the reach. This investigation showed that changes in depth were greater at the narrow upstream end of the floodplain that the considerably wider downstream section. An insight was also gained into the lag between the time at which the maximum inflows discharge was applied and that at which the maximum difference was seen between the predicted hydrographs for the downstream coupled and control simulations. This lag time was found to be less than the time it took for the main floodwave to travel the length of the reach. This was due to the fact that inflows were applied along the whole length of the reach.

Finally the effect of lateral hillslope inflows was considered in a more generalised context. It was found that the volume of water produced at the downstream end of the reach increased almost linearly with increasing inflow total volume. A similar relationship was seen between the downstream peak discharge and total volume of inflows applied. These relationships appeared to be different for the 1 in 12 and 1 in 5 year events. This indicated that the volume of water produced at the downstream end was not only dependent on the relative volume applied as inflows but possibly also on other characteristics of the inflows hydrograph. In each case, the percentage of the water input to the floodplain which went to storage was calculated. This was assumed to be the volume of water left on the floodplain at the end of each simulation, expressed as a percentage of the *total* input volume. This method was somewhat arbitrary due to the fact that the simulation ended when the model became unstable, rather than at the end of the period for which input data were provided. However, using this method it was found that when an increasing volume of inflows were applied to the floodplain, the ratio between the proportion of the total input which went to storage and were output from the reach remained fairly constant although this was not the case when comparing events with different return periods.

Inflows produced by hillslopes bordering a floodplain reach have been shown to be an important input to the floodplain system. Chapter Seven now goes on to describe the investigation which was carried out to assess the effect that this additional input has on the calibration of the floodplain model.

Chapter Seven

THE CALIBRATION ISSUE

7.1. INTRODUCTION

The results discussed in Chapter Six indicate that applying inflows as an extra input to a floodplain inundation model can, under certain circumstances, have a significant effect on the predictions of the model. This can be seen both at the reach scale, in terms of changes to the total reach outflow hydrograph volume and hydrograph characteristics, as well as at a more localised scale where changes in inundation patterns can be observed. Since the additional input from the hillslopes can have an appreciable influence on model predictions, it is important to consider the implications this may have in terms of the calibration of the floodplain model. This chapter considers this issue in terms of the degree of re-calibration necessary to produce a predicted downstream hydrograph which has the same peak time as the observed hydrograph for that event. As has been shown in the previous chapter, the effect that adding hillslope inflows had was dependent upon the magnitude and timing of the applied hillslope hydrograph. Bearing this in mind, the re-calibration procedure was carried out for selected coupled simulations considered to be representative of the variation in hydrograph characteristics for the range of hillslope types examined in the investigation as a whole.

This chapter starts by outlining the research design developed to examine this issue. Following this is a description of the additional model simulations set up. Finally the results of the investigation are presented and examined and conclusions made.

7.2. RESEARCH DESIGN

The aim of this investigation was to re-calibrate each coupled simulation so that; i) the timing of the hydrograph peak and ii) the peak stage were as close as possible to the observed hydrograph. The degree of re-calibration necessary for each coupled simulation was compared.

Due to the constraints of time, this process could not be carried out for every coupled model simulation. It was therefore necessary to choose a representative selection of the coupled simulations described in Chapters Five and Six. These were chosen to reflect the range of hydrograph and volumetric characteristics shown by all the

coupled simulations based on the 1990 1 in 1 year event. In doing this, the results of the simulations presented in Chapter Six were examined. The coupled simulations which produced the greatest and smallest volumetric change in the total reach outflow volume were selected together with a number of simulations which produced intermediate changes between these two extremes.

For each of these selected coupled simulations, the re-calibration procedure was carried out. This involved several stages. The procedure was first carried out for the coupled simulation which gave the greatest volumetric increase. This was chosen first to give an idea of the maximum amount of re-calibration necessary to act as a guide line when re-calibrating the remaining simulations. For each re-calibration the same RMA-2 input hydrograph was used and the same VSAS3 input hydrograph only the floodplain roughness was altered. The stages involved in the procedure carried out for each coupled simulation are listed below:

I. Using increasing values of Manning's 'n' at a selected interval, the model was re-run until the timing of the peak was the same as that of the observed hydrograph. Following this, further simulations were carried out, increasing the 'n' value further until the timing of the peak exceeded the observed peak.

II. The next stage involved examining the intermediate values of 'n' between the two values identified in Stage I. In the same way as before, the model was re-run until the 'n' value at which the timing of the peak exceeded that of the observed hydrograph.

III. The highest 'n' value which produced the same peak timing and the closest stage value as the observed hydrograph was identified as the re-calibration value of 'n' for that event.

Once this final value was identified, the process was carried out for the next selected coupled simulation. In examining the results, the amount of re-calibration necessary for each coupled simulation was quantified by 'n' value. Differences in the optimum 'n' value for each coupled simulation were used for purposes of comparison.

7.3. SETTING UP AND RUNNING THE RE-CALIBRATION SIMULATIONS

The coupled simulations which produced the smallest and greatest changes in the hydrograph output volume were VSAS08 (inflows produced by dry soil applied with no time shift) and VSASSP06 (soil depth of 0.1 m applied with simultaneous input

peaks) respectively. The events which had an intermediate effect on the output hydrograph volume are shown in table 7.1 below. The control simulation is shown for purposes of comparison.

Simulation	Peak stage (m)	% change	Peak timing
OBSERVED	2.335	N/A	11.5
CONTROL 1	2.122	N/A	11.5
VSAS08	2.124	0.09%	11.5
VSAS01	2.131	0.42%	11.5
VSAS06	2.149	1.27%	11.5
VSASSP01	2.250	6.03%	11.0
VSASSP06	2.265	6.74%	11.0

Table 7.1: Coupled simulations selected for re-calibration (the 1 in 1 year observed and control are shown for purposes of comparison)

7.3.1 The calibration procedure used for RMA-2

This procedure was discussed in Chapter Three and is summarised here. The parameter to which RMA-2 is most sensitive is floodplain roughness. The calibration procedure for RMA-2 uses different floodplain roughnesses to alter the timing, peak stage and discharge of the flood wave. The roughness classes which apply to the floodplain elements are classes 9 and 10. It is the Manning's 'n' value for these two roughness classes which is altered during the calibration procedure. Increasing the value of 'n' for these classes increases the floodplain roughness, slowing the passage of the flood wave and attenuating the downstream hydrograph so that the hydrograph peak occurs later and the peak discharge is reduced. Similarly, if the Manning's 'n' value is decreased, the lower floodplain roughness allows the downstream hydrograph to peak sooner with an increase in the peak discharge. For the reasons explained in Chapter Three, the model is calibrated on the basis of the hydrograph peak timing so that the observed and predicted hydrograph peaks occur at the same time. This ensures that the timing of the passage of the flood wave is well represented.

7.3.2 *Selection of Manning's 'n' values used to apply to the floodplain elements*

The same input hydrograph and hillslope hydrograph for each of the selected coupled simulations was applied to the reach while the floodplain roughness was altered. This process of re-calibration resulted in a further 37 model simulations. Since all the original coupled simulations either advanced the timing of the hydrograph peak or had no effect on the timing, it was necessary to slow the passage of the flood wave. Therefore only Manning's 'n' values greater than 0.1 were used. The process of re-calibration is illustrated through the example of the re-calibration of the coupled simulation VSASSP06. The results of the other simulations are shown in the next section.

The most appropriate interval to use between values of 'n' during the first stage of re-calibration was established when carrying out this initial set of re-calibration simulations for VSASSP06. The interval selected was 0.05 and five simulations were carried out using the 'n' values shown in Table 7.2. Also shown is the new peak timing and peak stage for each re-calibration.

Manning's 'n' value	0.105	0.110	0.115	0.120	0.125
Timing of peak (hours)	11.0	11.5	11.5	11.5	12.0
Peak stage (m)	2.286	2.290	2.295	2.300	2.304

Table 7.2: Initial set of re-calibration simulations carried out for coupled simulation VSASSP06.

The observed peak was 2.335 m and occurred 11.5 hours after the start time selected for the model simulations. Figure 7.1 shows the predicted stage hydrographs using Manning's 'n' values of 0.105, 0.115 and 0.125 for the floodplain elements. From this it can be seen that as the roughness was increased the peak stage increased and the timing of the peak was delayed. Therefore the optimum value of 'n' would be somewhere between 0.120 and 0.125. The next stage in the re-calibration process involved examining the effect on the hydrograph predictions for intermediate values between these two values of n. The interval selected was 0.001. The peak stage and timing are shown in Table 7.3 for each intermediate value of 'n' between 0.120 and 0.125.

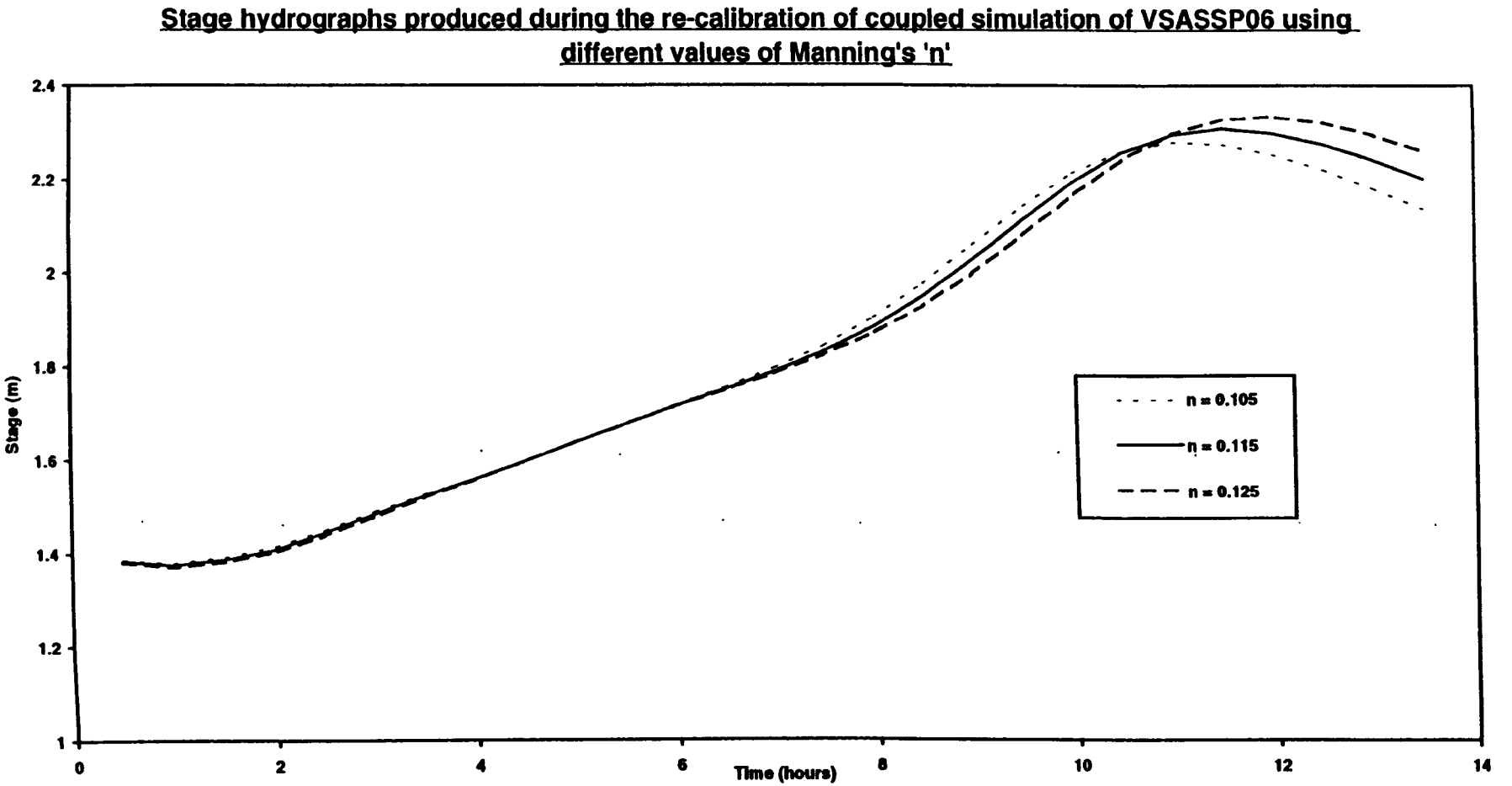

Figure 7.1: Stage hydrographs produced during the re-calibration of the coupled simulation SP06

Manning's 'n' value	0.121	0.122	0.123	0.124
Timing of peak (hours)	11.5	11.5	11.5	12.0
Peak stage (m)	2.300	2.301	2.302	2.303

Table 7.3: Initial set of re-calibration simulations carried out for coupled simulation VSASSP06.

From Table 7.3 it can be seen that the optimum value of 'n' for this coupled simulation was 0.124. It was decided that the coarse and fine intervals of 0.05 and 0.01 used in the re-calibration process for VSASSP06 were appropriate. The process described above was therefore repeated for the remaining coupled simulations.

7.3.3 *Carrying out the re-calibration simulations*

For each re-calibration simulation a new RMA-2 input file was created. This was identical to the parent input file used for the coupled simulation apart from the fact that the roughness classes for the floodplain elements had been assigned a new 'n' value. For each set of re-calibration simulations, a UNIX macro was written to obtain the appropriate input files, run each simulations and uniquely identify the output files. The program, *rating.f* described in Chapter Three was adapted to extract the predicted stage at Woodmill from the output files. The predicted stage at Woodmill (the water surface element for the channel nodes at that location) was extracted at each time step and written to a file. The program also identified the peak stage and timing for each output hydrograph. These were recorded and used to identify the optimum value of Manning's n.

7.4. RESULTS

Table 7.4 shows the peak timing and stage for all the re-calibration simulations carried out. The shaded cells in the table indicate the re-calibration for each coupled simulation considered which was considered to use the optimum value of Manning's n. In addition, a graph was plotted to show the relationship between the percentage increase in outflow volume (compared to the 1 in 1 year control simulation, CTRL01) and the optimum value of Manning's 'n' and is shown in Figure 7.2. From this it can be seen when increasing volumes of water were applied to the floodplain as hillslope inflows, a greater degree of re-calibration was required.

n value	0.101	0.102	0.013	0.104	0.105	0.106	0.107	0.108	0.109	0.110	0.111	0.112	0.113	0.114	0.115	0.116	0.117	0.118	0.119	0.120	0.121	0.122	0.123	0.124	0.125
Cntrl 1	11.5h 2.227	11.5h 2.228	11.5h 2.229	11.5h 2.229	12.0h 2.230																				
VSAS 12	11.5h 2.228	11.5h 2.229	11.5h 2.229	11.5h 2.230	12.0h 2.231																				
VSAS 01	11.5 2.230	11.5h 2.231	11.5h 2.232	11.5h 2.233	11.5h 2.234	12.0h 2.235				12.0h 2.239															
VSAS 06	11.5h 2.237	11.5h 2.238	11.5h 2.239	11.5h 2.240	11.5h 2.241	11.5h 2.242	12.0h 2.243	12.0h 2.244	12.0h 2.245	12.0h 2.247															
VSAS SP01					11.0h 2.280					11.5h 2.284					11.5h 2.290					11.5h 2.293	11.5h 2.293	12.0h 2.294	12.0h 2.295		12.0h 2.297
VSAS SP06					11.0h 2.286					11.5h 2.290					11.5h 2.295					11.5h 2.300	11.5h 2.300	11.5h 2.301	12.0h 2.302	12.0h 2.303	12.0h 2.304

Optimum n value for re-calibration

Table 7.4: Showing the optimum value of Manning's 'n' found by carrying out re-calibrations for each of the selected coupled simulations. For each re-calibration simulation carried out two values are shown. The first of these is the time in hours at which the hydrograph peak occurred, the second is the peak stage in metres

In addition it would appear that the peak stage prediction is improved, although the fact that RMA-2 has been observed to consistently under-predict the peak stage both in this and previous applications should not be ignored.

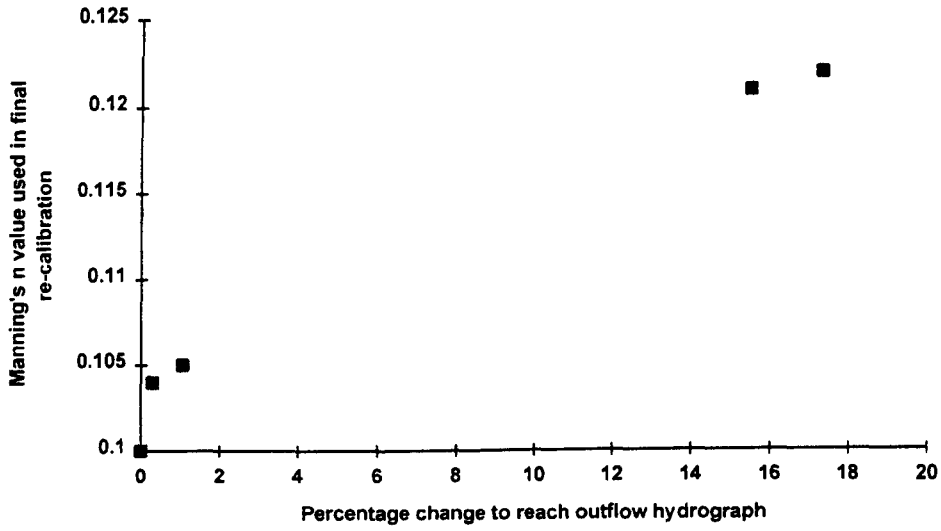

Figure 7.2: Graph of Manning's 'n' value used in the final re-calibration against the percentage

7.5. CONCLUSIONS

In this chapter the re-calibration procedure carried out for each of five selected coupled simulations has been described. It was found that in every case some degree of re-calibration was necessary. This indicates that if hillslope inflows are used as an additional input to a floodplain inundation model by coupling a hillslope hydrology model to that model to simulate lateral hillslope inflows that it would be necessary to re-calibrate that model. In addition, it appeared that, once the model had been re-calibrated, there was an improvement in the peak stage prediction. This could have been due either partly or wholly to the fact that RMA-2 has previously been observed to consistently under-predict peak stage.

The final chapter provides conclusions and a critique of the work carried out during this investigation into the importance of contributions from hillslopes bordering a floodplain reach. Suggestions are also made for further work.

Chapter Eight
CONCLUSIONS

8.1 INTRODUCTION

This research has examined two-dimensional floodplain inundation models. These were originally developed for civil engineering applications and have been developed to a high level of sophistication. These developments have also enabled the application of such models to other fields including hydrology, geomorphology and ecology. Two-dimensional finite element models provide a very powerful tool for investigations in these fields and may be considered as a platform for further developments which incorporate specific processes occurring within the floodplain environment. In the case of hydrological applications, a problem has been identified in that these models do not currently consider catchment hydrology. The hydrological interaction which occurs between the floodplain and bordering hillslopes involves many complex and inter-related processes. A complete examination of these was obviously not possible within the scope of this investigation. It was therefore decided to further examine two-dimensional hydraulic floodplain flow and to develop methods of relaxing the current zero flux at the floodplain/hillslope interface as a starting point.

The first part of this chapter discusses the results of this investigation in light of the aims set out in Chapter One. Following this, suggestions for further work are made.

8.2 REALISATION OF THE AIMS

Hillslope inflows may be an important additional input under some circumstances. The model used in this investigation was the two-dimensional finite element model, RMA-2 which was applied to a 14 km reach of the River Culm in Devon. The starting point for this investigation was to examine the effect of applying inflows, at a constant rate with respect to time, to selected elements along a 1 km test reach. This made use of the 'side inflow capability' which is a feature of RMA-2. The feature had previously been implemented in order to enable additional inputs to selected elements and been used to simulate rainfall inputs and tributary inflows, although it had never been used to apply hillslope inflows. The results of this pilot investigation were presented in Chapter Three. Hillslope inflows were observed to have an appreciable localised effect

on depth predictions and flow field behaviour predictions. This effect was attenuated away from the point of application. From this it was concluded that hillslope inflows were likely to have a significant localised effect on floodplain inundation under certain circumstances.

A coupled hillslope hydrology - floodplain inundation modelling scheme has been configured: A hillslope hydrology model, VSAS3, has been set up for a section of the hillslopes bordering the study reach, using the hillslope topography as a geometric template. The rainfall input used was for gauges sited close to the hillslope and for the same events used as an input to RMA-2. The set up of this model was described in Chapter Four. At each time step, the outflow predicted by VSAS3 is spatially averaged by dividing the total discharge produced by the slope width. This spatially averaged flow is then applied to all the elements along the edge of the RMA-2 finite element mesh. The inflow applied to each element is weighted by the element length.

A very simple, yet functional, coupling mechanism has been adopted and was described in detail in Chapter Five. This utilises the RMA-2 side inflow capability and, at each time step, the appropriate volume of water is simply applied over the surface of each element at the edge of the RMA-2 FEM. Thus all the water which is generated at the base of the hillslope during time period of the coupled simulation is applied to the floodplain.

A sensitivity analysis has been carried out to identify some of the environments where inflows may be significant: It was obviously not possible to examine all the parameters necessary to provide a comprehensive analysis of the complete range of hillslope-floodplain environments where inflows should be considered as an additional model input. It was thus decided to examine the effect of inflows produced by different hillslope types. Five parameters were selected and a sensitivity analysis was carried out, altering each parameter through three different values whilst keeping the other parameters constant. The results of this sensitivity analysis were presented in Chapter Six. It was found that, of those parameters examined, the coupled model was most sensitive to changes in:

1) Rainfall volume
2) Initial moisture conditions
3) Soil depth
4) Slope angle
5) Hydraulic conductivity

As discussed in Chapters Five and Six, it was also possible to examine the effect of the relative timing of the hillslope inflow and input hydrograph applied at the upstream end of the reach. In the original sensitivity analysis, the timing of the hillslope contribution relative to the upstream input was such that the sensitivity of the coupled scheme to the recession limb of the inflows hydrographs was considered. In order to observe the effect of relative timing, the time base of the hillslope hydrograph was shifted. This enabled the sensitivity of the coupled model to be re-assessed by examining the sensitivity to the rising limb and peak of the inflows hydrograph. The results showed that, although the relative sensitivity to the selected parameters was not affected, there was an appreciable effect on the predicted hydrographs as well as localised changes. In addition, the timing of the downstream hydrograph peak was advanced in most cases. The relative timing of the floodplain and hillslope input hydrographs has been shown to be an important factor.

An examination was made of the results of the sensitivity analysis in more generalised terms. The effect of adding different inflow *volumes* was considered. While the same upstream input hydrograph was applied, it was found that increasing volumetric inputs resulted in a greater total output volume. The predicted hydrograph peak was also increased in magnitude when an increasing inflows volume was used. Localised effects were also observed, both in terms of changes in depth and inundation extent. Changes in depth were greatest for the narrowest parts of the reach while differences in inundation extent were most noticeable over the wider parts of the reach. These findings were reported in Chapter Six.

This additional input has an effect on the calibration of the floodplain model: A major issue which was investigated was the effect on model calibration made by relaxing the boundary condition at the hillslope / floodplain interface. RMA-2 was originally calibrated for a reach to which no inflows were applied. Inflows have been observed to have a significant effect on model predictions. Chapter Seven describes how the calibration issue was examined. The floodplain model was re-calibrated for selected coupled simulations to examine the degree of re-calibration required in each case. It was found that re-calibration was necessary for all the events examined during this part of the investigation.

8.3 RECOMMENDATIONS FOR FUTURE RESEARCH

8.3.1 To carry out additional sensitivity analyses to further identify the range of environments where inflows are important

It is possible that all the following factors could affect the relative contribution of hillslope inflows to a floodplain reach:

- Hillslope response
- The location of the reach within the catchment
- The length of the reach under consideration
- The effect of water delivery mechanisms and the importance of the coupling mechanisms used to represent them

It was obviously beyond the scope of this investigation to examine all of these, and it was only possible to consider the effect of a small number of hillslope parameters. This has provided a valuable insight into some of the issues concerned with coupling a hillslope hydrology model to a floodplain inundation model, although only some of the hillslope-floodplain environments where hillslope inflows may be important could be identified. In order to identify the full range of circumstances where hillslope inflows should be used as an additional input, it would be necessary to carry out many more sensitivity analyses. The ultimate aim would be to produce a matrix showing threshold values for the most significant factors affecting the relative importance of hillslope inflows. From this it would be feasible to identify whether hillslope inflows should be modelled for a given application to a particular floodplain. The floodplain environment is very complex and there are a considerable number of inter-relationships. It is unlikely that it would be possible to identify clear thresholds. This point is illustrated in Figure 8.1. Three hypothetical parameters, A, B and C are represented. The unshaded area represents the zone where inflows are 'insignificant' and the shaded area indicates where inflows would be 'significant'. Between these two zones is a grey area which indicates the 'zone of uncertainty' which would probably exist. It is also probable that beyond the 'significant' zone, there will be a further threshold beyond which it is not possible to apply two-dimensional floodplain hydraulic models.

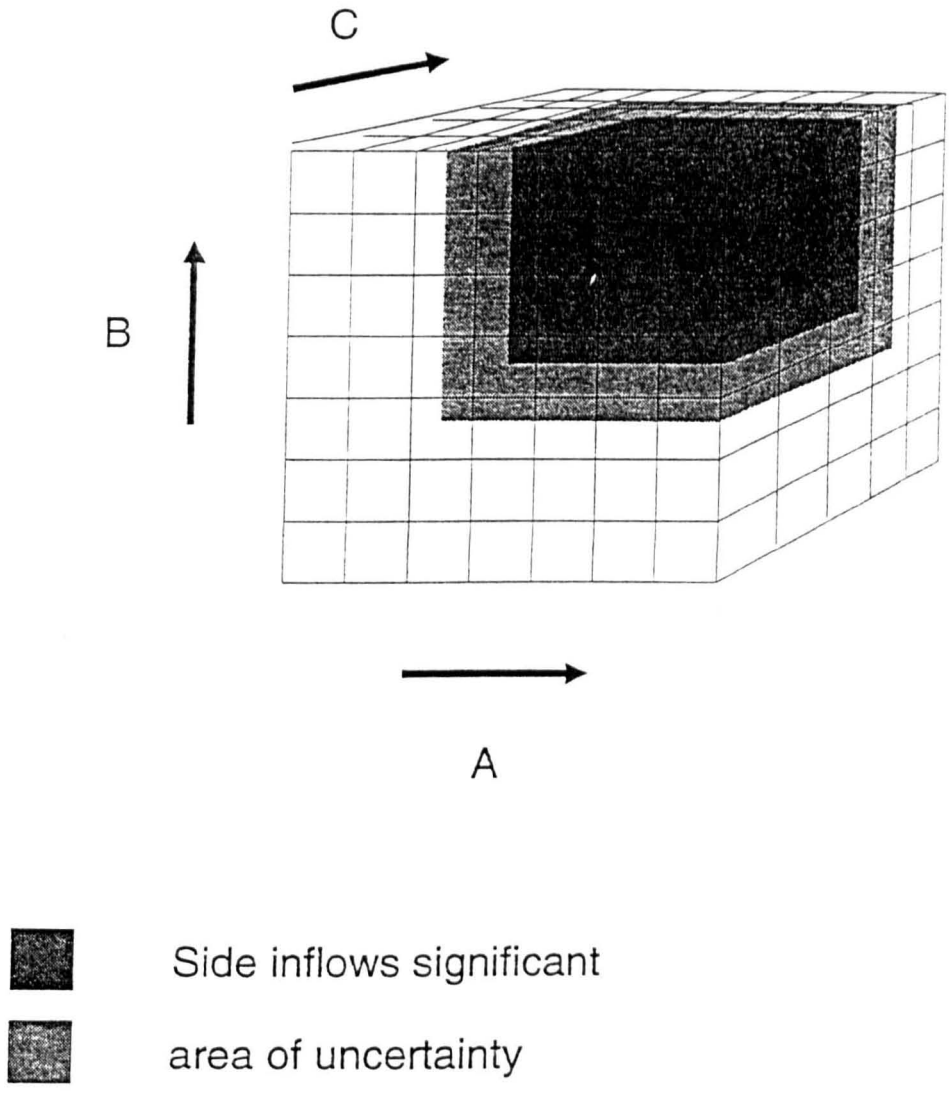

Figure 8.1: Illustration of the areas of 'significance', 'insignificance' and the 'area of uncertainty' relating to the importance of using hilislope inflows as an additional input to a floodplain hydraulic model for three hypothetical parameters, A, B and C

8.3.2 *To identify the most appropriate type of hillslope model to use in the coupled scheme*

The semi-theoretical approach used in the investigation meant that although a process based distributed hydrology model was used, the input parameter values were 'typical' values obtained from the literature. Were the coupled scheme to be applied to simulate the processes occurring in a particular catchment, it would be necessary to consider the issues connected with the parameterisation of distributed models such as the most appropriate sampling strategy to use and the quantity of data required. It is therefore proposed that there is a need to determine the most appropriate type of hillslope hydrology model to use in the scheme; for example, if spatially varied inflows do not make a significant difference to model predictions compared to spatially averaged inflow, it might not be justifiable to use a fully distributed hillslope model in terms of the additional data and computing requirements. A catchment model using a lumped approach might be more appropriate.

8.3.3 *The issue of coupling*

Another major issue concerns the coupling mechanism used. It has been shown that the relative timing of the hillslope and upstream input hydrographs has a significant effect on the model predictions. The coupling mechanism used to represent the transfer of water from the hillslopes to the floodplain is likely to have a major influence on this relative timing. In this first pass investigation, a relatively crude method has been used to effect the transfer of water from the hillslopes to the floodplain. Although this might be representative for narrow floodplains adjoining hillslopes dominated by surface flow, for systems dominated by ground water it is clearly inappropriate. It is therefore necessary to develop a more physically representative coupling mechanism.

This could also have implications in determining the range of environments where inflows are important. For example, if under some circumstances the hillslope contribution is made mainly to the baseflow component of the flow in the channel, after the period of the coupled simulation, it would not be necessary to consider the hillslope contribution.

Two-dimensional models of floodplain hydraulics are a very powerful tool and can be seen as a platform for developing integrated systems to carry out research into a number of fields, through adding new components to increase process representation. The research in this thesis has sought to begin this development process.

REFERENCES

Abbott, M.B., Bathurst, J.C., Cunge, J.A., O'Connell, P.E. and Rasmussen, J. (1986) An introduction to the European Hydrological System - Systeme Hydrologique European, "SHE", 2: structure of a physically based distributed modelling system. *Journal of Hydrology*, 87, 61-77

Anderson, M.G. and Burt, T.P. (1978) The role of topography in controlling through flow generation. *Earth Surface Processes and Landforms*, vol.3, 331-344

Akanbi, A.A. and Katopodes, N.D. (1988) Model for flow propagation on initially dry land. *Journal of the hydraulics division, ASCE*, 114, 689-706

Arya, L. M. and Paris, J. F. (1981) A physicoempirical model to predict the soil moisture characteristic from particle size distribution and bulk density data. *Soil Sci. Am. Jnl.*, 45, 1023-1030

Atkinson, T.C. (1978) Techniques for measuring subsurface flow on hillslopes. Chapter 3 in *Hillslope Hydrology*, (ed. M.J. Kirkby). John Wiley & Sons, pp. 73-120

Baird and Anderson (1990) Flood Inundation Modelling. (Vol. 1). User Manual. Final Technical Report. US Corps of Engineers

Bates, P.D., Anderson, M.G., Baird, L., Walling, D.E. and Simm, D. (1992) Modelling floodplain flows using a two-dimensional finite element model. *Earth Surface Processes and Landforms*, 17

Bates, P.D., (1993) Unpublished Ph.D. thesis, University of Bristol

Bathurst, J.C. (1986a) Physically based distributed modelling of an upland catchment using the Systeme Hydrologique European. *J. of Hydrology*. 87, 79-102

Bathurst, J.C. (1986b) Sensitivity analysis of the Systeme Hydroqique European for an Upland catchment. *J. of Hydrology*. 87, 103-23

Bathurst, J.C. (1988) Flow processes and data provision for channel flow models, in Anderson, M.G. (ed.), *Modelling Geomorphological Systems*, John Wiley, Chichester, pp. 127-152

Bathurst, J.C. (1993) Flow resistance through the channel network. In Channel Network Hydrology. Ed. K. Beven and M.J. Kirkby. Wiley, Chichester. 319pp

Bernier, P.Y. (1985) Variable source areas and stormflow generation, an update of the concept and a simulation effort. *Journal of hydrology*, 79, 195-213

Bernier, P.Y. (1982) VSAS2: A revised source area simulator for small forested basins. Unpublished PhD dissertation, University of Georgia, Athens, Georgia

Betson, R. P. (1964) What is watershed runoff?. *Jnl. Geophys. Research*, 69, 1541-52

Betson and Mauris (1969) Source areas of storm runoff. *Water Resource Research*. 5(3), 574-582

Beven, K.J. (1977a) The hydrological response of headwater and sideslope areas. *Hydrol. Sci. Bull.* 23, 419-37

Beven, K.J. and Kirkby, M.J. (1979) A physically based variable contributing area model of basin hydrology. *Hydrological sciences bulletin*, 24, 43-69

Beven, K.J., Kirkby, M.J., Schoffield, N. and Tagg, A. (1984) Testing a physically based flood forecasting model TOPMODEL for three U.K. catchments. *Journal of hydrology*, 69, 119-143

Beven, K.J. (1985) Distributed models. In Anderson, M.G. and Burt, T.P. (eds.), *Hydrological Forecasting*, John Wiley, Chichester, 405-435

Beven, K,J. (1986) Runoff production and flood frequency in catchments of order n: an alternative approach. In *Water Resources Research* 8. In Gupa, G.K., Rodriguez, I. and Wood, E.F. (eds.), *Scale Problems in Hydrology*. Reidel, Dordrecht, pp. 107-132

Beven, K. J. (1987) Towards the use of catchment geomorphology in flood frequency predictions. *Earth Surface Processes and Landforms*, 12, 69-82

Beven, K. J. (1989) Changing ideas in hydrology - the case of physically based models. *Jnl. of Hydrology*, 105, 139-157

Beven, K.J. and Wood, E.F. (1993) Flow routing and the hydrological response of channel networks. In Channel Network Hydrology. Ed. K. Beven and M.J. Kirkby. Wiley, Chichester. 319pp

Bhowmick, N.G. and Demissie, A.M. (1982) Carrying Capacity of Flood Plains. *Journal of the Hydraulics Division, Proceedings of the American Society of Civil Engineers.* Vol 108, No. HY3

Brakenseik, D.L. and Rawls, W.J. (1983) Use of infiltration procedures for estimating runoff. Paper presented to *Soil Cons. Workshop*, Tempe, Arizona

Calver, A. (1988) Calibration, sensitivity and validation of a physically-based rainfall-runoff model. *Journal of Hydrology*, 103, 103-115

Campbell, G.S. (1974) A simple method for determining unsaturated conductivity form moisture retention data. *Soil Sci.*, 117, 364-371

Chen and Chow (1968) Hydrodynamics of mathematically simulated surface runoff. *Hydraul. Eng. Ser.* 18, 132 pp., Univ. of Ill., Urbana, 1968

Childs, E.C. (1940) The use of moisture characteristics in soil studies. *Soil Sci.* 50, 239-252

Childs, E.C., and Collis-George, N. (1950) The permeability of porous materials. *Proc. Roy. Soc.*, 201A, 392-405

Chow, Ven Te. (1959) Open Channel Hydraulics. McGraw-Hill, New York, USA, 680 pp.

Cooper, H.H.,Jr., and Rorabaugh, M.I. (1963) Groundwater movementsand bank storage due to flood stages in surface streams. *U.S. Geol. Surv. Water-Supply Paper*, 1536-J

Cunge, J.A., Holly, F.M. and Verway, A. (1980) Practical aspects of computational river hydraulics. Pitman, London

Davie, T.W. (1992) Unpublished Ph.D. thesis. University of Bristol

Dunne, T. (1969) Runoff production in a humid area. Unpublished Ph.D. thesis. The John Hopkins University

Einstein, H.A. and Shen, H.W. (1964) A study of the meandering in straight alluvial channels. *J. of Geophysical Research.* 69, 5239-5247

Erivine, D.A. and Ellis, J. (1987) Experimental and computational aspects of overbank floodplain flow. *Transactions of the Royal society of Edinburgh, Earth Sciences*, 78, 315-325

Fawcett K,R., Anderson, M.G., Bates, P.D. Jordan, J-P and Bathurst, J.C. (1994) The importance of internal validation in the assessment of physical based distributed models. *Trans. Inst. Br. Geographers.* 20, 248-265

Feldhaus R. et al. (1992) Finite element simulation of flow and pollution transport applied to part of the River Rhine. In Flcolner, R.A., Shiona, K. and Matthews R.G.S. (eds.), *Hydraulic and Environmental Modelling; Esturine and River Waters*, Ashgate Publishing, Aldershot, pp. 323-334

Fread, D.L. (1976) Flood routing in meandering rivers with floodplains. Symposium in Inland Waterways for Navigation Flood control and Water Divisions, *Proceedings of the American Society of Civil Engineers*, 16-35

Fread, D.L. (Anderson, M.G. and Burt, T.P. (eds.)) Channel routing, in *Hydrological forecasting*. John Wiley, Chichester, 1985, 437-503

Freeze, R.A. (1971) Three dimensional transient, saturated - unstaturated flow in a groundwater basin. *Water Resources Research*. 7, 347-366

Freeze, R.A. (1972a) Role of subsurface flow in generating surface runoff. 1. Baseflow contributions to channel flow. *Water Resources Research*. 8(3), 609-623

Freeze, R.A. (1972b) Role of subsurface flow in generating surface runoff. 2. Upstream source areas. *Water Resources Research*. 8(5), 1272-1283

Gee, D.M., Anderson, M.G. and Baird, L. (1990) Large-scale floodplain modelling. *Earth Surface Processes and Landforms*, 15, 513-523

Gee, D.M. and Wilcox, D.B. (1985) Use of a two dimentional flow model to quantify aquatic habitat. *Proc. Am. Soc. Civ. Eng. Spec. Conf. on Computer Applications in Water Resources*, Buffalo, New York

Hall, D.G.M., Reeve, M.J., Thomasson, A.J. and Wright, V.F. (1977) Water retention, porosity and density of field soils. *Soil Survey Technical Monograph 9*, Soil Survey of England and Wales, Harpenden

Hervouiet J.M. and Janin, J.M. (1994) Finite element algorithms for modelling flood propagation. In Molinaro, P. and Natale, L. (eds.), Modelling of flood propagation over initially dry areas. *Proceedings of the speciality conference*, co-sponsored by ASCE-CNR/GNDCI-ENEL spa 102-113

Hervouet, J.M. (1993) Validating the numerical simulation of dam breaks and floods. *Proc. Int. Conf. in Hydroscience and Engineering*, Washington

Hey, R.D and Thorne, C.R (1975) Secondary flows in river channels. *Area 7*, 191-195

Hewlett, J.D. and Hibbert, A.R. (1963) Moisture and energy conditions within a sloping soil mass during drainage. *Jnl. Geophys. Research*, 68, 1081-7

Hewlett, J.D. and Hibbert, A.R. (1967) Factors affecting the response of small watersheds to precipitation in humid areas, in *Forest Hydrology*, W.E Sopper and H.W. Lull (eds.), Pergamon, Oxford, pp.276-90

Hewlett, J.D and Nutter, W.L. (1970) The varying source area of streamflow from upland basins, in *Proceedings of Symposium on Watershed Management*, American Society of Civil Engineers, New York, pp.65-83

Hewlett, J.D. and Troendle, C.A (1975) Non-point and diffused water sources: a variable source area problem, in *Proceedings of Symposium on Watershed Management*, American Society of Civil Engineers, New York, pp.21-46

Hillel, D. (1980) *Applications in soil physics.* Academic Press, New York

Hollinrake, P.G. (1987) The structure of flow in open channels - a literature search. Report SR 96 Jan 1987 Hydrauilics Research, Wallingford

Horton, R.E. (1933) The role of infiltration in the hydrolic cycle. *Trans. AGU*, 14, 446-60

Hursh, C.R. (1944) Report to the sub-committee on substance flow. *Trans. AGU*, 25, 743-6

Jackson, R.D. (1972) On the calculation of hydraulic conductivity. *Soil science Society of American Proceedings*. 36, 380-382

Jones, J.A.A. (1986) Some limitations to the a/s index for predicting basin-wide patterns of soil water drainage. *Zeitschrift Geomorphologie, N.F.* 60, 7-20

Jones, J.A.A. (1987) The effects of soil piping on contributing areas and erosion patterns. *Earth Surf. Proc. and Landforms*, 12, 229-48

Keller, E.A. and Melhorn, W. (1973) Bedforms and fluvial processes in alluvial stream channels: selected observations. In Morisawa, M. (ed.) *Fluvial Geomorphology*, SUNY Binghampton, Publications in Geomorphology, pp.253-83

Keppel, R.V. and Renard, K.G. (1962) Transmission losses in ephemeral stream beds, *Journal of the Hydraulics Division, American Society of Civil Engineers.*, v.88, no. HY3, pp. 59-68

King, I.P. and Norton, W.R. (1978) Recent Applications of RMA's finite element models for two-dimensional hydrodynamics and water quality. *Proc. Second Int. Conf. on Finite Elements in Water Resources*, Pentech Press, London, 1978, 81-99

King, I.P. (1985) Finite-element modelling of stratified flow in estuaries and reservoirs. *International Journal for Numerical Methods in Fluids*. 5(11). 943-955.

King, I.P. and Roig, L.C. (1988) Two-dimensional finite element model for floodplains and tidal flats. In Niki, K. and Kawahara, M. (eds.) *Computational Methods in flow analysis, Proceedings of the International Associations of Hydraulics Research*, 12(1), 43-63

Kirkby, M.J. and Chorley, R.J. (1967) Throughflow, overland flow and erosion. *Int. Assoc. Hydrol. Sci. Bull.*, 12, 5-21

Knight, D.W. (1989) Hydraulics of flood channels, in Beven, K. and Carling, P. (eds), *Floods: hydrological, sedimentological and geomorphological implications*, John Wiley, Chichester, 83-105

Knight, D.W., Demetriou, J.D. and Hamed, M.E. (1984) Stage discharge relationships for compound channels. In Smith, K.V.H (ed.), *Proceedings of the First International Conference on Hydraulic Design in Water Resources Engineering, Channels and Channel Control Structures*, University of Southampton, Southampton

Knight, D.W. and Patel, H.S. (1985a) Boundary shear in smooth rectangular ducts. *J. of Hydraulic Engineering, ASCE.* 111(1), 29-47

Knight, D.W., Demetriou, J.D. and Hamed, M.E. (1984) Stage discharge relationships for compound channels. *Proc. 1st International Conference on Channels and Channel Control Structures* (ed. K.V.H. Smith), pp.4.21-4.35. Springer

Knight, D.W. and Lai, C.J. (1985) Turbulent flow in compound channels and ducts. *International Symposium on Refined Flow Modelling and Turbulence Measurements.* Iowa, USA.

Knighton, D. (1984) Fluvial forms and processes. Arnold, 218pp

Kunze, R.J., Nnehava, G. and Graham, K. (1968) Factors important in the calculation of hydraulic conductivity. *Proc. Soil Sci. Soc. Am.*, 31, 451-454

Marriot, P. (1992) Textural analysis and modelling of floodplain deposit: River Severn. Uk *ESPL* 17, 687-697

Meyer, O.H. (1941) Simplified flood routing. *Civil Engineering*, 11(5) , 306-307

Millington, R.J. and Quirk, J.P.(1961) Permeability of porous solids. *Transactions of the Faraday Society.* 57, 1200-1207

Morris, E.M., Blyth, K. and Clark, R.T. (1980) Watershed and river characteristics and their use in a mathematical model to predict flood hydrographs. In Fraysee, G. (ed.), *Remote sensing Apllication in Agriculture and Hydrology.* Balkema, Rotterdam, 431-446

Naot, D. and Rodi, W. (1982) Calculations of secondary currents in channel flow. *Journal of the Hydraulic Division*. ASCE, 108(HY8), 948-68

Natural Environment Research Council (1975) *Flood Studies Report*, 5 volumes

Niemeyer, G. (1979) Efficient simulation of non-linear steady flow. *J. Hyd. Div. Am. Soc. Cov. Eng.*, 105, 185-196

Norton, W.R., King, I.P. and Orlob, G.T. (1973) A finite element model for Lower Granite Reservoir. Water Resources Engineers, California

O'Brien, J.S. Julien, P.Y. and Fullerton, W.T. (1993) Two-dimentional water flood and mudflow simulation. *Journal of Hydraulic Engineering*. 119(2), 244-61

Odgaard, A.J. (1984) Shear-induced secondary currents in channel flows. *Journal of Hydraulic Engineering*, ASCE, 110(7), July, 996-1004

Pearce, A.J., Stewart, M.K. and Sklash, M.G. (1987) Storm runoff generation in humid headwater catchments. *Water Resour. Res.* 22, 1263-72

Philip, J.R. (1969) Theory of infiltration. *Advances in Hydroscience*. 5, 216-296

Preissmann, A. and Zaoui, J. (1979) La module "ecoulement de surface" du Systeme Hydrologique Europeen (SHE). *Proc 18th Congress International Association for Hydraulic Research*, Cagliari. 5, 193-199

Radojkovic, V. (1976) Mathematical modelling of rivers with floodplains. Symposium of Inland Waterways for Navigatiuonal Flood Control and Water Divisions, *Proceedings of the American Socirty of Civil Engineers*, 1, 56-64

Rajaratnam, N. and Ahmadi, R. (1981) Hydraulics of channels with floodplains. *Journal of Hydraulic Research*, 19, 43-60

Richards, K. (1982) *Rivers: Form and Process in Alluvial Channels*. Methuen, New York, 361 pp

Robson, A., Beven, K. and Neal, C. (1992) 'Towards identifying sources of subsurface flow: A comparison of components identified by a physically based runoff model and those determined by chemical mixing techniques. *Hydrological processes*, vol.6, 199-214

Samuels, P.G. (1985) Modelling of river and flood plain flow using the finite elemnt method. Hydraulics research ltd, Technical Report SR61, Wallingford, Oxford

Samuels, P.G. (1990) (White WR (ed.)), Cross section location in one dimensional models. *Int conf. on river flood hydraulics*. John Wiley, Chichester, 339-350

Sellin, R.H.J. (1964) A laboratory investigation into the interaction between flow in the channel of a river and that over its floodplain. *La Houille Blanche*, 7

Shaw, E.M. (1988) Hydrology in practice. McGraw Hill. 539pp.

Shiono, K. and Knight, D.W. (1988) Two dimensional analytical solution for a compound channel. *Proc. 7th.Intl. Symp. on Turbulent ShearFlows. Stanford. USA. August.* pp 28.1.1-28.1.6

Shiono, K. and Knight, D.W. (1991) 'Turbulent open channel flows with variable depth across the channel. *Journal of Fluid Mechanics*, 222, 617-646

Sklash, M.G., Stewart, M.K. and Pearce, A.J. (1986) Storm runoff generation in humid headwater catchments, II. A case study of hillslope and low order stream response. *WRR*, 22, 1273-82

Su, T.Y. et. al. (1980) Depth averaged models of river flows. *Proc Third Int. Conf. on Finite Elements in Water Resources*, University of Mississippi, Mississippi

Thompson, A. (1985) Secondary flows and the pool-riffle unit: a case study of the processes of meander development. *Earth Surface Processes and Landforms*, vol.11, 631-641

Todd, D.K. (1955) Ground-water in relation to a flooding stream. Proc. Amer. Soc. Civil Engrs. 81, pp. 1-20, 628

Tracy, H.J. (1965) Turbulant flow in a three-dimentional channel. *Journal of the Hydraulics Division*, ASCE. 91(HY6), 9-35

Troendle, C.A. (1979) A variable source area model for storm flow prediction on first order forested watersheds. *Unpublished PhD Thesis.* University of Georgia

Troendle, C.A. (1985) Variable source area models. In Anderson, M.G. and Burt, T.P. (eds.), *Hydrological Forecasting*, John Wiley, Chichester, 349-403

Tseng, M.T. (1975) Evaluation of flood risk factors in the design of highwater stream crossings. Finite Element Model for Bridge Backwater Computation. *Office of Research and Development, Federal Highway Administration*, Report No. FHWA-RD-75-53 Vol. III, Washington D.C.

Walling, D.E. and Peart, M.R. (1986) Fingerprinting sediment sources: the example of a drainage basin in Devon, U.K. In (ed.) Hadley, R.F. *Drainage basin sediment delivery.* IAHS Publication 159

Walling, D.E. and Bradley, S.B. (1989) Rates and patterns of contemporary floodplain sedimentation: A case study of the River Culm, Devon, U.K. *Geojournal*, 19, 53-62

Walling, D.E., Quine,T.A. and He, Q. (1991) Investigating contemporary rates of floodplain sedimentation. In Petts, G.E. and Carling, P.A. (eds.), *Lowland Floodplain Rivers: a Geomorphological Perspective*, John Wiley, Chichester

Walling, D.E., Quinne, T.A. and He, Q. (1992) Investigating contemporary rates of floodplain sedimentation. In (eds.). Carling, P.A. and Petts, G.E. *Lowland Floodplain Rivers: Geomorphic perspectives*. John Wiley and Sons Ltd.

Ward, R.C. (1984.) On the response of headwater streams in humid areas. *Journal of Hydrology*. 74, 171-189

Whitelaw, A.S. (1988) Hydrological modellling using variable source areas. Unpublished Ph.D. thesis, University of Bristol

Williams, J. R. and Hann , R.H. (1973) HYMO: a problem orientated computer language for hydrological modelling - user's manual. *Agricultural Research Service, Southern Region Report* ARS-S-9

Wilson, E.M. (1990) *Engineering Hydrology*. 348 pp. Macmillan Education, Basingstoke

Wooding, R.A. (1965) A hydraulic model f or the catchment stream problem: I Kinematic wave theory. *Journal of Hydrology*. 3, 254-267; II Numerical Solutions. *Journal of Hydrology*. 3, 268-282; III Comparison with runoff observations. *Journal of Hydrology*. 4, 21-37

Wright R.R. and Carstens, H.R. (1970) Linear momentum flux to overbank sections. *Journal of the Hydraulics Division, Proceedingd of the American Society of Civil Engineers*, 96(hy9), 1781-1794

Zeike W. and Urban W. (1981) 2-d modelling of rivers with flood plains. Numerical modelling of river channel overland flow for water resources and Environmental applications, *IAHR*

Zheleznyakov, G.V. (1965) Relative dedict of mean velocity of unstable river flow; kinematic effect in river bend with floodplains. *Proceedings of the Eleventh Congress of the International Association for Hydraulics Research*, Lenigrad, USSR.

Zheleznyakov, G.V. (1971) Two-dimensional modelling of rivers with floodplains. *Proceedings of the Fourteenth Congress of the International Association for Hydraulics Research*, Paris, France

APPENDICES

Notes on input for INPUT.SEG

Names of variables are shown in italics

LINE 1: Number of segments (*MNO*), Title of run (*NAME*)
01 TRIAL RUN

LINE 2: *NOTE*: Notes on run
Hypothetical segment

LINE 3: No. of coarse scale iterations (*KREP*), No. of fine scale iterations (*LREP*), Output control for segment geometry (*NOUTA*) (default is not to print it), Option for calculation of 100 and 75% saturated area (*NTMP*), No. of soil types per segment (*NOST*)
6 5 0 0 1

LINE 4: No. of segment (*ISGNO*), No. of subsegments (*KNO*), No. of layers (*JNO*), No. of soil types (*STNO*); routing delay (minutes) (*IROUT*)
1 1 3 0

LINE 5: Stone content of each layer (unit%) (*STONEC*)
0

LINE 6: No. of increments upslope (*NLIMK*(k),k=1,*KNO*)
10

LINE 7: Elevation of each increment (metres) (*DEPMAX*(k,n),n=1,nn) (nn=*NLIMK*)
822.7 824.8 825.6 827.8 832.4 837.5 840.3 844.1 848.4 854.9

LINE 8: Depth of each increment (metres) (*DEPMAX*(k,n),n=1,nn)
2.0 2.0 2.0 2.0 2.0 2.0 2.0 2.0 2.0 2.0

LINE 9: Distance from stream of each increment (metres) (*XI*(k,n),n=1,nn)
1.70 8.48 22.04 42.38 69.50 103.40 144.08 191.54 245.78 306.80

LINE 10: Width of segment at channel (*XWIDTH*(k,1)), Width of segment at watershed (*XWIDTH*(k,2)), Length of upstream side of segment (*HORIZ*(k,1), Length of downstream side of watershed (*HORIZ*(k,2)) (all given in metres)
98 96 328 350

LINE 11: Depth of top layer (metres) (*A1*), Proportion of each layer in remaining depth (unit %) (*BDEPTH*(i)i=2,*JNO*)
0.5 0.5 0.5

LINE 12: Area of stream (metres^2) (*A1*), Area of impervious surfaces linked to channel (metres^2) (*A2*), Offset for flow beween elements in skewed segments (*ROFFST*(k),k=1,*KNO*-1)
0.0 0.0

LINE 13: Position along slope of different hydrological properties (unit %) (*POS*(k), k=1,*NOST*), mean length of segment (metres) (*HLEN*(k), k=1,*KNO*)
1.0 336.0

LINE 14: END OF INPUT
0199999999999999999999999999999999999999999

Notes on input for INPUT.SMC

Variable names are shown in italics

LINE 1: Number of points on suction moisture curve (*NSMC*), standard deviation of moisture contents on suction moisture curve (*SDX*)
6 0.0

LINE 2: Moisture contents ((*AX*(i),i=1,*NSMC*))
.265 .290 .310 .340 .355 .484

LINE 3: Suctions ((*Y*(i),i=1,*NSMC*))
-10. -5.08 -3.35 -1.98 -1.05 -0.001

LINE 4: Saturated moisture content (*ASR1*), standard deviation of saturated moisture content (*SDSR*)
.485 0.0

LINE 5: Saturated conductivity (m s^{-1}) (*ASTCON*), standard deviation of saturated conductivity (*SDSAT*)
.00000165 .0

The number of lines in this file is dependent upon
i) The number of segments (MNO)
ii) The number of soil layers in each segment (JNO)

In this case there is one segment which has three layers. Each line represents the percentage moisture contents for each element from the channel to the watershed. These are listed from left to right.

1.000 1.000 1.000 1.000 1.000 1.000 1.000 1.000 1.000 1.000
1.000 1.000 1.000 1.000 1.000 1.000 1.000 1.000 1.000 1.000
1.000 1.000 1.000 1.000 1.000 1.000 1.000 1.000 1.000 1.000

LINE 1: Date of event
100788

Each of the following lines contains 8 hourly rainfall values
0.00 0.00 0.05 0.05 0.10 0.10 0.10 0.10
0.10 0.20 0.60 1.40 0.00 0.00 0.00 0.00

END OF DATA
9.0

```
      program edgefinder
c
      integer icontab(4000,6)
      real coords(4000,3)
      integer nodes(4000,12),ncheck(4000,8),ielems(4000,3)
      real elems(4000),leng
      character*80 line1
      integer ncount,elem1,elem2
c
open(7,file='v10culm.dat')
c     open(7,file='test2.dat')
c
c       open(7,file='test1.dat')
     open(8,file='results.rac')
c
c ... Skip first 3 lines of file
      do 10 i=1,3
       read(7,11) line1
 11   format (a80)
 10   continue

c ... Read in each line, keeping a count of the total number of lines
c ... into an array, icontab (connection table).

      dowhile(iel.ne.9999)
       read(7,12) iel,n1,n2,n3,n4,mann
 12   format(i5,i4,6x,i4,6x,i4,6x,i4,6x,i1)
        if(iel.ne.9999) then
       icontab(ncount+1,1)=iel
       icontab(ncount+1,2)=n1
          icontab(ncount+1,3)=n2
          icontab(ncount+1,4)=n3
          nodes(n1,1)=n1
          nodes(n1,2)=nodes(n1,2)+1
          nodes(n1,(2+nodes(n1,2)))=iel
          nodes(n2,1)=n2
          nodes(n2,2)=nodes(n2,2)+1
          nodes(n2,(2+nodes(n2,2)))=iel
          nodes(n3,1)=n3
          nodes(n3,2)=nodes(n3,2)+1
          nodes(n3,(2+nodes(n3,2)))=iel
       if(n4.gt.0) then
           icontab(ncount+1,5)=n4
           nodes(n4,1)=n4
           nodes(n4,2)=nodes(n4,2)+1
           nodes(n4,(2+nodes(n4,2)))=iel
       endif
        icontab(ncount+1,6)=mann
       ncount=ncount+1
       endif
      enddo

c ... Read in x and y co-ordinates for nodes
```

```
      do 20 j=1,ncount
       read(7,13) node,x,y
       coords(j,1)=node
       coords(j,2)=x
       coords(j,3)=y
 13   format(5x,i4,4x,f5.1,5x,f5.1)
 20   continue


c ... Find out which nodes only appear 2 times in nodes array. Then look
c ... at icontab to see which elements and adjoining edge nodes correspond.
c ... 1) get elements
c ... 2) get nodes
c ... we know which is the 'central' node so it is a simple matter of
c ... Pythagoras to get the lengths of those two elements. List elements
c ... so they can be checked so this calculation isn't performed > once.


      do 100 j=1,4000
       node = nodes(j,1)
       locc = nodes(j,2)
       lel1 = nodes(j,3)
       lel2 = nodes(j,4)
       if(node.gt.0 .and. locc.le.2) then
        n1=0
        n2=0
        n1found=0
        n2found=0
        do 200 k=1,4000
         if(k.ne.j) then
          knode = nodes(k,1)
          kocc = nodes(k,2)
          kel1 = nodes(k,3)
          kel2 = nodes(k,4)
          if(knode.gt.0 .and. kocc.eq.2) then
              if(lel1.eq.kel1 .or. lel1.eq.kel2
     &       .or. lel2.eq.kel1 .or. lel2.eq.kel2) then
               if(n1found.eq.0) then
                n1=knode
              n1found=1
                if(lel1.eq.kel1 .or. lel1.eq.kel2) then
                    iel1=lel1
                else if(lel2.eq.kel1 .or. lel2.eq.kel2) then
                    iel1=lel2
                endif
               else
                n2=knode
                n2found=1
             endif
              endif
           endif
          endif
 200    continue
      endif
      if(n1found.eq.0) n1=9999
```

```
          if(n2found.eq.0) n2=9999
          if(node.gt.0 .and. locc.le.2) then
           ncheck(j,1)=node
           ncheck(j,2)=n1
           ncheck(j,3)=n2
          endif
        node=0
          knode=0
        n1=0
        n2=0
          locc=0
        n1found=0
        n2found=0
  100  continue

c ... We now have a list of nodes and the nodes to which they are connected
c ... if that element from whence the node came has only 2 nodes. For the
c ... more complicated cases, we go through again.

      do 291 kj=1,5
        do 201 jk=1,4000
         if(nodes(jk,2).eq.2) then
          if(ncheck(jk,3).eq.9999 .and. ncheck(jk,2).ne.9999) then
           n2=0
           node=ncheck(jk,1)
           n1=ncheck(jk,2)
           do 202 kk=1,4000
              np=0
              n1p=0
            do 203 kl=2,5
c ... find the 2 elements which contain 1)node and n1 2) node and the
c ... therefore undiscovered node, n2
               if(icontab(kk,kl).eq.node) then
                np=kl
               else if(icontab(kk,kl).eq.n1) then
                n1p=kl
               endif
  203        continue
             if(np.ne.0) then
               if(n1p.ne.0) then
                jelem1=kk
                je1n1=icontab(kk,2)
                je1n2=icontab(kk,3)
                je1n3=icontab(kk,4)
                je1n4=icontab(kk,5)
                npos=np
                n1pos=n1p
               else if(n1p.eq.0) then
                jelem2=kk
                je2n1=icontab(kk,2)
                je2n2=icontab(kk,3)
                je2n3=icontab(kk,4)
                je2n4=icontab(kk,5)
                npose2=np
               endif
             endif
```

```
202     continue

        if(icontab(jelem1,5).eq.0) then
            if(npos.eq.2) then
              locn1adj=4
              locn2adj=3
            else if(npos.eq.3) then
              locn1adj=2
              locn2adj=4
            else if(npos.eq.4) then
              locn1adj=3
              locn2adj=2
            endif
        else
            if(npos.gt.2) then
              locn1adj=npos-1
            else if(npos.eq.2) then
              locn1adj=5
         endif
            if(npos.lt.5) then
              locn2adj=npos+1
            else if(npos.eq.5) then
              locn2adj=2
            endif
        endif
        n1adj=icontab(jelem1,locn1adj)
        n2adj=icontab(jelem1,locn2adj)
        write(8,*)'n1adj,n2adj',node,n1adj,n2adj

        if(icontab(jelem2,5).eq.0) then
            if(npose2.eq.2) then
              locn3adj=4
              locn4adj=3
            else if(npose2.eq.3) then
              locn3adj=2
              locn4adj=4
            else if(npose2.eq.4) then
              locn3adj=3
              locn4adj=2
            endif
        else
            if(npose2.gt.2) then
              locn3adj=npose2-1
            else if(npose2.eq.2) then
              locn3adj=5
            endif
            if(npose2.lt.5) then
              locn4adj=npose2+1
            else if(npose2.eq.5) then
              locn4adj=2
            endif
        endif
            write(8,*)'locn3adj,locn4adj',locn3adj,locn4adj
            n3adj=icontab(jelem2,locn3adj)
            n4adj=icontab(jelem2,locn4adj)
```

```
            if(n1adj.eq.n3adj .or.n2adj.eq.n3adj) then
             n2=n4adj
            else if(n1adj.eq.n4adj .or. n2adj.eq.n4adj) then
             n2=n3adj
            endif




c ... write to array ncheck
        if(n2.ne.0) then

           if(ncheck(n2,1).eq.0 .and. n2.eq.9999) then
               ncheck(n2,1)=n2
            ncheck(n2,2)=node
            ncheck(n2,3)=9999
           else
               ncheck(jk,3)=n2
           endif

               endif
          endif
         endif

 201  continue
 291  continue

        do 875 ih=1,4000
         if(ncheck(ih,1).ne.0) then
          write(8,26) ncheck(ih,1),ncheck(ih,2),ncheck(ih,3)
 26       format(5(1x,i4))
         endif
 875    continue


c ... Now write to a new array with the element numbers, lengths

      do 131 kj=1,4000

         node=ncheck(kj,1)
         n1=ncheck(kj,2)
         n2=ncheck(kj,3)
       if(node.ne.0 .and. n1.ne.9999) then
          do 133 lj=1,4000
           nflag1=0
           nflag2=0
           do 134 lk=2,5
               if(icontab(lj,lk).eq.node) nflag1=1
               if(icontab(lj,lk).eq.n1) nflag2=1
 134       continue
           if(nflag1.eq.1 .and. nflag2.eq.1) then
               elem1=icontab(lj,1)
               ncheck(kj,4)=elem1
           endif
 133      continue
```

```
          endif
          if(node.ne.0 .and. n2.ne.9999) then
           do 135 jj=1,4000
            nflag1=0
            nflag2=0
            do 136 jk=2,5
                if(icontab(jj,jk).eq.node) nflag1=1
                if(icontab(jj,jk).eq.n2) nflag2=1
 136        continue
            if(nflag1.eq.1 .and. nflag2.eq.1) then
                elem2=icontab(jj,1)
                ncheck(kj,5)=elem2
            endif
 135      continue

          endif

 131   continue

c ... write to the array ielems with element number and 2 nodes
c .. and do the Pythagoras bit.

          do 371 ko=1,4000
           if(ncheck(ko,4).ne.0) then
            if(icontab(ncheck(ko,4),6).ne.1) then
             ielno=ncheck(ko,4)
           if(ielems(ielno,1).eq.0) then
                ielems(ielno,1)=ncheck(ko,4)
                ielems(ielno,2)=ncheck(ko,1)
                ielems(ielno,3)=ncheck(ko,2)
                x1=coords(ielems(ielno,2),2)
                y1=coords(ielems(ielno,2),3)
                x2=coords(ielems(ielno,3),2)
                y2=coords(ielems(ielno,3),3)
                a2=(y2-y1)**2
                b2=(x2-x1)**2
                leng=sqrt(a2+b2)
                elems(ielno)=leng
c    endif
           endif
           if(ncheck(ko,5).ne.0) then
            if(icontab(ncheck(ko,5),6).ne.1) then
             ielno=ncheck(ko,5)
c     If(ielems(ielno,1).eq.0) then
                ielems(ielno,1)=ncheck(ko,5)
                ielems(ielno,2)=ncheck(ko,1)
                ielems(ielno,3)=ncheck(ko,3)
                x1=coords(ielems(ielno,2),2)
                y1=coords(ielems(ielno,2),3)
                x2=coords(ielems(ielno,3),2)
                y2=coords(ielems(ielno,3),3)
                a2=(y1-y2)**2
                b2=(x1-x2)**2
                leng=sqrt(a2+b2)
                elems(ielno)=leng
               endif
```

```
        endif
          endif
        endif

371     continue

        do 98 jj=1,4000
         if(elems(jj).ne.0) then
          write(8,*) 'elem,length',ielems(jj,1),elems(jj)
         endif
98    continue


        stop
        end
```

```
      open(unit=7,file='ncheck.dat')
        open(unit=8,file='newchk.dat')
        do 10 j=1,4000
         read(7,5) node,n1,n2
 5       format(3(1x,i4))
         if(node.ne.0) then
          write(8,6) node,n1
          write(8,6) node,n2
 6      format(2(1x,i4))
         endif
10      continue
        stop
        end
```

```
      program finedge
c
      integer icontab(4000,6)
      real coords(4000,3)
      integer nodes(4000,12),ncheck(4000,8),ielems(4000,3)
      real elems(4000),leng
      character*80 line1
      integer ncount,elem1,elem2
c
     open(7,file='v10culm.dat',status='old')
c     open(7,file='test2.dat')
c
c        open(7,file='test1.dat')
     open(8,file='results.ncheckro')
        open(9,file='endchk.dat',status='old')
c
c
c ... Skip first 3 lines of file
        do 10 i=1,3
         read(7,11) line1
  11   format (a80)
  10  continue

c ... Read in each line, keeping a count of the total number of lines
c ... into an array, icontab (connection table).

        dowhile(iel.ne.9999)
         read(7,12) iel,n1,n2,n3,n4,mann
  12   format(i5,i4,6x,i4,6x,i4,6x,i4,6x,i1)
          if(iel.ne.9999) then
        icontab(ncount+1,1)=iel
        icontab(ncount+2,2)=n1
           icontab(ncount+1,3)=n2
           icontab(ncount+1,4)=n3
           nodes(n1,1)=n1
           nodes(n1,2)=nodes(n1,2)+1
           nodes(n1,(2+nodes(n1,2)))=iel
           nodes(n2,1)=n2
           nodes(n2,2)=nodes(n2,2)+1
           nodes(n2,(2+nodes(n2,2)))=iel
           nodes(n3,1)=n3
           nodes(n3,2)=nodes(n3,2)+1
           nodes(n3,(2+nodes(n3,2)))=iel
        if(n4.gt.0) then
            icontab(ncount+1,5)=n4
            nodes(n4,1)=n4
            nodes(n4,2)=nodes(n4,2)+1
            nodes(n4,(2+nodes(n4,2)))=iel
        endif
          icontab(ncount+1,6)=mann
         ncount=ncount+1
         endif
        enddo
```

```
c ... Read in x and y co-ordinates for nodes

      dowhile(nflag2.ne.1)
       read(7,13) node,x,y
       if(node.eq.1405) then
        write(6,*)'something sarcastic'
       endif
       if(node.eq.9999) nflag2=1
     if(nflag2.ne.1) then
        coords(node,1)=node
        coords(node,2)=x
        coords(node,3)=y
 13    format(5x,i4,4x,f5.1,5x,f5.1)
       endif
     enddo


c ... read in the ncheck data from file endchk.dat

      do 370 jo=1,262
       read(9,22) ncheck(jo,1),ncheck(jo,2)
 22    format(2(1x,i4))
370  continue

c ... find elements corresponding to the nodes

      do 372 m=1,4000
       node=ncheck(m,1)
       n1=ncheck(m,2)
       if(node.ne.0) then
        do 373 j=1,4000
         do 374 k=2,5
          if(icontab(j,k).eq.node) nflag1=1
          if(icontab(j,k).eq.n1) nflag2=1
374      continue
         if(nflag1.eq.1 .and. nflag2.eq.1) then
          ncheck(m,3)=icontab(j,1)
         endif
         nflag1=0
         nflag2=0
373      continue
       endif
     write(8,*)(ncheck(m,kl),kl=1,3)
372  continue

c ... write to the array ielems with element number and 2 nodes
c ..  and use Pythagoras to calculate the length of each element edge.

      do 18 jg=1,4000
       write(8,*) coords(jg,1),coords(jg,2),coords(jg,3)
 18  continue

      do 371 ko=1,4000
       write(6,*) ko

         if(ncheck(ko,1).ne.0) then
```

```
            ielno=ncheck(ko,3)
            n1=ncheck(ko,1)
               n2=ncheck(ko,2)
               x1=coords(n1,2)
               y1=coords(n1,3)
               x2=coords(n2,2)
               y2=coords(n2,3)
               a2=(y2-y1)**2
               b2=(x2-x1)**2
               leng=sqrt(a2+b2)
               lcount=lcount+1
               elems(ielno)=leng
            endif

371    continue

       do 98 jj=1,4000
        iel=ncheck(jj,3)
        if(iel.ne.0) then
         write(8,*) iel,elems(iel)
        endif
98   continue

     write(6,*)'lcount',lcount



       stop
       end
```

```
      program filemake

      real elems(300,3)
      integer nelems(300)
      character*80 line
      character*20 fname1,fname2
      character*3 inf


      write(6,*)'Enter inflows file'
      read(5,5) fname1
      write(6,*)'Enter new rma-2 input file'
      read(5,5) fname2
 5  format(a20)

      open(unit=7,file='hyd1_g10.in',status='old')
      open(unit=8,file='elenarea.dat',status='old')
      open(unit=9,file=fname1,status='old')
      open(unit=10,file=fname2)

      inf='262'

c ... read elenarea.dat into an array

      do 50 l=1,262
       read(8,11) nelems(l),elems(l,1),elems(l,2)
 11   format(1x,i4,7x,f7.2,4x,f10.2)
 50   continue

c ... read in first 33 lines from rma-2 input file
c ... and write these to the new rma-2 input file
      do 10 j=1,33
       read(7,6) line
  6   format(a80)
       write(10,6) line
 10   continue

c ... read in 34th line and change number of inflows
c ... the write this to the new rma-2 input file


      read(7,6) line
      write(line(12:14),19) inf
 19   format(a3)
      write(10,6) line

c ... now read in first inflow value from the inflows file

      read(9,7) flow
  7   format(5x,e12.2)

c ... and read in each element number, length and area
c ... multiply flow by length and divide by area of
c ... element and write to new rma-2 file
```

```
      do 20 j=1,262
       flowk=flow*elems(j,1)
       flowk=flowk/elems(j,2)
       sumflo=sumflo+flowk
       write(10,12) nelems(j),flowk
12    format(1x,i4,5x,e9.2)
20    continue

c ... now read in 3 lines for each time step (42 tsteps)
c ... changing the 3rd one for nsid and writing out
c ... inflows for each element in the same way as above

      do 60 k=1,41
       do 70 j=1,3
        read(7,6) line
        if(j.eq.3) then
       write(line(12:14),19) inf
         write(10,6) line

c ... write to line and write out line
          read(9,7) flow
          do 80 i=1,262
              flowk=flow*elems(i,1)
              sumflo=sumflo+flowk
              flowk=flowk/elems(i,2)
        write(10,12) nelems(i),flowk
80      continue
        else
         write(10,6) line
      endif
70     continue
60    continue
       write(6,*) 'sumflo=', sumflo
       stop
       end
```

```
      program hydsum

c ... A program to add the inflows for each VSAS time step, to
c ... obtain the total runoff for an event.

c ... the data are in the VSAS output file which has the outflow
c ... for each segment listed consecutively

      real flow(7,500),hydro(100)
      real sum
      integer ntstep,flag,start,rmaend
      character*20 fname1,fname2

      write(6,*) 'Enter vsas.out filename'
      read(5,2) fname1
      write(6,*) 'Enter inflows filename'
      read(5,2) fname2
      write(6,*) 'Enter event return period'
      read(5,*) ievent
      write(6,*) 'Enter RMA start time'
      read(5,*) start
 2    format(a20)

      open(8,file=fname1,status='old')
      open(9,file=fname2)

      conver=35.3147
      width=4902.43
      totlen=92068.98
      if(ievent.eq.1) then
       rmaend=start+13
      else if(ievent.eq.5) then
       rmaend=start+49
      else if(ievent.eq.12) then
       rmaend=start+21
      endif

c ... loop through the segments to read in data

      do 10 i=1,7
       flag=0
       ntstep=0
       dowhile(flag.eq.0)
        read(8,5) q,rf
 5      format(11x,f7.1,6x,f4.1)
        if(rf.eq.90.0) flag=1
        if(flag.eq.0) then
         ntstep=ntstep+1
         flow(i,ntstep)=q
        endif
       enddo
 10   continue

c ... Sum inflows for each timestep then divide by template
```

```
          ncount=ncount+1
         else
          write(9,18) nt,sum
          write(9,18) nt+1,sum
          nt=nt+2
          ncount=ncount+1
         endif
18       format(1x,i3,1x,e12.2)
30    continue
        write(10,*)'totsl volume contributedum',totsum
        suminf=suminf*2
      write(10,19) suminf
19    format(1x,e12.2)

        stop
        end
```